DEVELOPING BIOACTIVE MATERIALS FOR DENTAL APPLICATIONS

EDITED BY: Mary Anne Sampaio Melo, Fabricio Mezzomo Collares and Salvatore Sauro

PUBLISHED IN: Frontiers in Materials

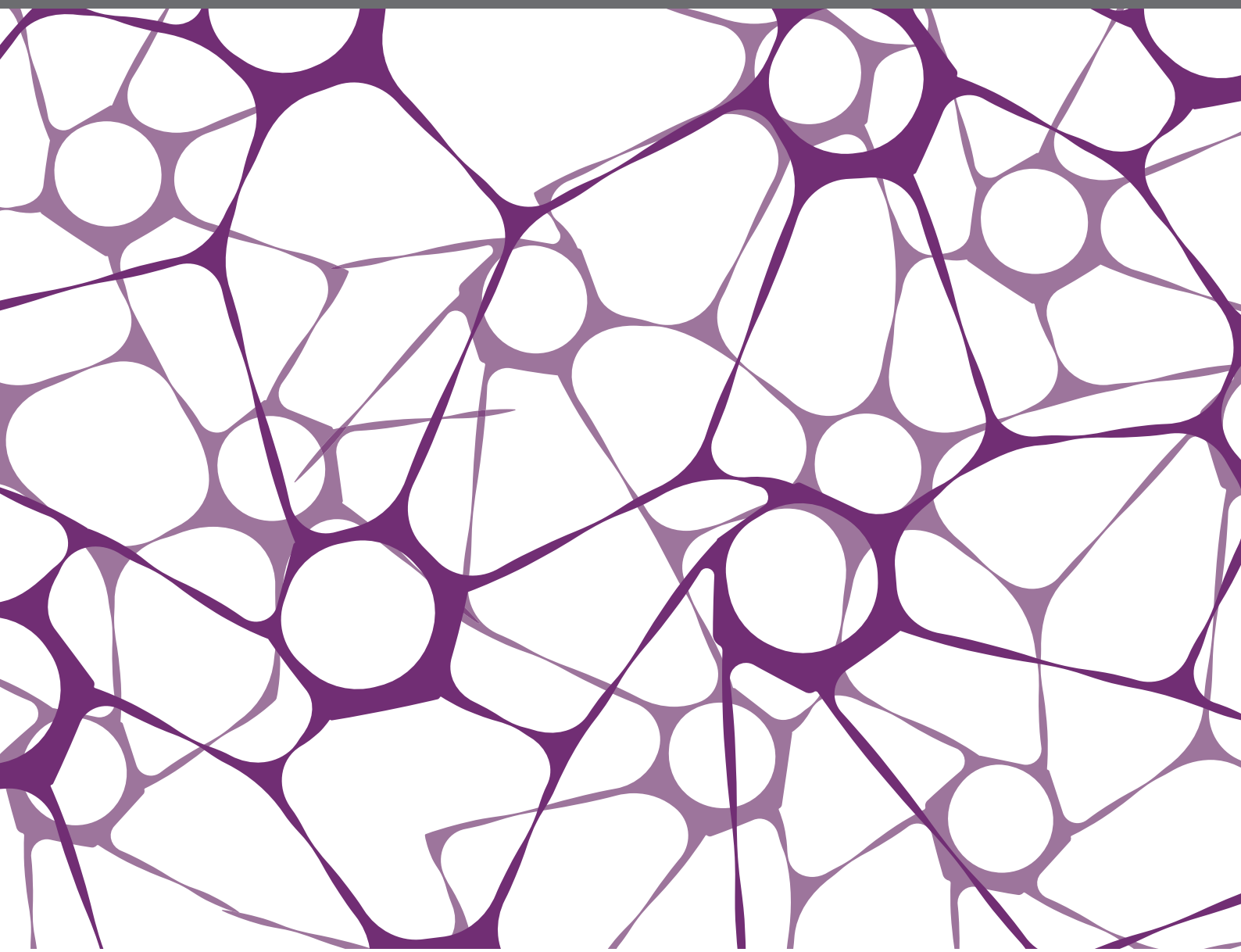

frontiers Research Topics

frontiers

ISSN 1664-8714
ISBN 978-2-88971-458-2
DOI 10.3389/978-2-88971-458-2

About Frontiers

Frontiers is more than just an open-access publisher of scholarly articles: it is a pioneering approach to the world of academia, radically improving the way scholarly research is managed. The grand vision of Frontiers is a world where all people have an equal opportunity to seek, share and generate knowledge. Frontiers provides immediate and permanent online open access to all its publications, but this alone is not enough to realize our grand goals.

Frontiers Journal Series

The Frontiers Journal Series is a multi-tier and interdisciplinary set of open-access, online journals, promising a paradigm shift from the current review, selection and dissemination processes in academic publishing. All Frontiers journals are driven by researchers for researchers; therefore, they constitute a service to the scholarly community. At the same time, the Frontiers Journal Series operates on a revolutionary invention, the tiered publishing system, initially addressing specific communities of scholars, and gradually climbing up to broader public understanding, thus serving the interests of the lay society, too.

Dedication to Quality

Each Frontiers article is a landmark of the highest quality, thanks to genuinely collaborative interactions between authors and review editors, who include some of the world's best academicians. Research must be certified by peers before entering a stream of knowledge that may eventually reach the public - and shape society; therefore, Frontiers only applies the most rigorous and unbiased reviews.
Frontiers revolutionizes research publishing by freely delivering the most outstanding research, evaluated with no bias from both the academic and social point of view. By applying the most advanced information technologies, Frontiers is catapulting scholarly publishing into a new generation.

What are Frontiers Research Topics?

Frontiers Research Topics are very popular trademarks of the Frontiers Journals Series: they are collections of at least ten articles, all centered on a particular subject. With their unique mix of varied contributions from Original Research to Review Articles, Frontiers Research Topics unify the most influential researchers, the latest key findings and historical advances in a hot research area! Find out more on how to host your own Frontiers Research Topic or contribute to one as an author by contacting the Frontiers Editorial Office: frontiersin.org/about/contact

DEVELOPING BIOACTIVE MATERIALS FOR DENTAL APPLICATIONS

Topic Editors:
Mary Anne Sampaio Melo, University of Maryland, United States
Fabricio Mezzomo Collares, Federal University of Rio Grande do Sul, Brazil
Salvatore Sauro, Universidad CEU Cardenal Herrera, Spain

Citation: Melo, M. A. S., Collares, F. M., Sauro, S., eds. (2021). Developing Bioactive Materials for Dental Applications. Lausanne: Frontiers Media SA.
doi: 10.3389/978-2-88971-458-2

Table of Contents

frontiers in Materials

EDITORIAL
published: 18 August 2021
doi: 10.3389/fmats.2021.751618

Editorial: Developing Bioactive Materials for Dental Applications

Mary Anne Melo[1,2]*, *Fabricio Collares*[3] *and Salvatore Sauro*[4,5]

[1]Division of Operative Dentistry, Department of General Dentistry, University of Maryland School of Dentistry, Baltimore, MD, United States, [2]Dental Biomedical Science PhD Program, University of Maryland School of Dentistry, Baltimore, MD, United States, [3]Dental Materials Laboratory, Department of Conservative Dentistry, School of Dentistry, Federal University of Rio Grande do Sul, Porto Alegre, Brazil, [4]Dental Biomaterials and Minimally Invasive Dentistry, Department of Dentistry, Cardenal Herrera-CEU University, CEU Universities, Valencia, Spain, [5]Department of Therapeutic Dentistry, I. M. Sechenov First Moscow State Medical University, Moscow, Russia

Keywords: dental (restorative) composites, biofilm, bioactive, nanotecehnology, biomaterial

Editorial on the Research Topic

Developing Bioactive Materials for Dental Applications

Bioactive biomaterials for managing tissue loss due to congenital or acquired diseases as dental caries, periodontitis, and bone defects have gained significant relevance in the last decades. New materials currently being introduced, under development are expected to be bioactive in that they will be intended to interact in some positive way with the oral environment. These materials will provide a wide range of diverse functions, including the inhibition of bacterial biofilm formation, remineralization of mineral loss in dental hard tissues as dentin and enamel, and the regeneration of diseased pulp, bone soft tissues.

The mouth is a dynamic environment, so dental materials regularly experience changes that alter performance, and this highlights the profound need for methods to allow tracking of its performance in physiologically complex.

Generally, dental materials provide core functions, such as mechanical support to masticatory loads (e.g., dental crowns) or optical properties to display a pleasant and natural appearance (e.g., resin composites). This approach has led to the successful design of numerous clinically used materials over the years, such as sealants, orthodontic adhesives, luting cement, hybrids materials for computer-assisted design/computer-assisted manufacturing (CAD/CAM)-based restorative dentistry.

Still, advances in material design and polymer chemistry have recently allowed us to incorporate dynamic features into biomaterials. This approach ranges from the design of materials that hold low polymerization shrinkage to eliminate internal stresses and stresses at the restoration's margins to those with stimuli-responsive and interactive properties, where chemical or biological signals can trigger a response in dental material properties or release drugs on-demand. Thus, giving to the material a feature associated with being "biointeractive."

Our increased understanding of native tissue architecture and cell-material interactions and the development of processing methods and chemical syntheses have driven the design of new bioactive agents and, consequently, new biointeractive or bioactive dental materials.

Nanotechnology can provide new solutions in developing dental materials by including bioactive compounds without affecting the functional, aesthetic performance, and other core properties.

Dentistry has an ongoing interest in creating bioactivity for dental materials. Currently, limited dental materials present bioactivity—releasing ions, including those present in tooth minerals. Therefore, the capability of a dental material to positively affect its biological surroundings seems like an avenue for improving the longevity and clinical service inside the mouth.

OPEN ACCESS

Edited and reviewed by:
Hasan Uludag,
University of Alberta, Canada

***Correspondence:**
Mary Anne Melo
mmelo@umaryland.edu

Specialty section:
This article was submitted to Biomaterials, a section of the journal Frontiers in Materials

Received: *01 August 2021*
Accepted: *06 August 2021*
Published: *18 August 2021*

Citation:
Melo MA, Collares F and Sauro S (2021) Editorial: Developing Bioactive Materials for Dental Applications. Front. Mater. 8:751618. doi: 10.3389/fmats.2021.751618

The use of bioactive materials, in which either the material itself or a released factor elicits an effect, increases the chances of local regeneration while decreasing the likelihood of adverse effects elsewhere.

Over the years, numerous natural or synthetic nano-to microscale agents have been assessed for bioactivity in the oral environment to be delivered by dental materials in multiple clinical indications. Data to date clearly illustrate that biomaterials for use in the maintenance of oral health are developing at a rapid pace.

In the Research Topic "*Developing Bioactive Materials for Dental Applications*," inspiring findings on natural and synthetic biomimetic, bioinspired, and bioactive agents and materials developed with its incorporation over different length scales and their capacity to modulate bacterial cell functions and to deliver in localized and sustained fashion various therapeutics were discussed.

As acidogenic bacteria grow over the dental materials used for dental fillings, the tooth–material interface degrades by bacterial acidsleading to increasing premature failure of tooth filling Balhaddad et al. investigated the application of polymerizable antibacterial monomers based on quaternary ammonium compounds as an antibacterial strategy against root caries from high caries risk patients. Feitosa et al. also looked for anti-caries strategies via experimental adhesives containing tailored fluoridated calcium phosphate fillers.

Looking for strategies to enhance the adhesive's interface performance, Spencer et al. develop a molecular-level understanding of a peptide-functionalized adhesive/collagen hybrid biomaterial using Raman spectroscopy combined with a chemometrics approach. An engineered hydroxyapatite-binding peptide (HABP) was copolymerized in dentin adhesive, and dentin was demineralized to provide collagen matrices that were partially infiltrated with the peptide-functionalized adhesive.

Garcia et al. have shown the promising role of niobium pentoxide filler incorporated into dental adhesives providing good mechanical properties, improved resistance against solvents, and increased radiopacity, without changing the degree of conversion.

Cui et al. explored the polymer-infiltrated ceramic network composites (PICNs) to understand the relationship between surface roughness and flexural strength for CAD-CAM materials. In this work, a novel dental restorative composite was fabricated *via* infiltrating mixtures of Bis-GMA/TEGDMA and UDMA/TEGDMA into partially sintered porous sodium aluminum silicate blocks and curing.

The pursuit of odontogenic and pulp regeneration approaches has led researchers to investigate different synthesis routes and formulations with combined agents. Jayash et al. revealed the supporting activity in bone healing as a result of the combination of chitosan with different bio-active materials. Chitosan-based gel scaffold and osteoprotegerin-chitosan gel scaffold demonstrated a significant bone quantity and quality compared to unfilled surgical defects in this animal study. Huang et al. highlight the design of mesoporous BG-nanoparticles by a well-established sol-gel method and suggest an odontogenic and acidic-pH neutralizing potential for application in pulp-dentin regeneration under a pathophysiologically challenged acidic environment.

Nassar et al. review the ongoing studies on identifying a cariostatic ability by reducing enamel dissolution of Inositol hexaphosphate (IP6). Inositol is abundant in nature and an essential molecule for different biological functions. In addition, IP6 has a unique structure granting it distinctive properties; a high negative charge density provides IP6 with enormous chelating ability and valuable antioxidant properties. Finally, Jeevanandam et al. presented an outline of recent nanobiomaterials that are extensively investigated for dental implant applications.

As we observe an increasing number of investigations addressing hard dental tissues in the last decade, many efforts are also directed to soft tissues repairs. Canciani et al. analyze the effects of polycaprolactone (PCL) nanofibers enriched with hyaluronic acid and vitamin E vs nude nanofibers on gingival fibroblasts activity an innovative graft for periodontal soft tissue regeneration purposes. Bermudez et al. looked over the combined use of scaffolds, cells, and bioactive molecules such as peptides are considered the best approach to achieve tissue regeneration. These peptides can induce diverse cellular processes as they can influence cell behavior and modify scaffold properties, giving; as a result, the enhancement of cell adhesion, proliferation, migration, differentiation, and biomineralization that are required given the complex nature of oral tissues.

We hope that this work set will stimulate further research on the development of bioactive materials for dental applications by providing an overview of the latest and most exciting advances in emerging approaches for bioactivity. In addition, this book may help readers to understand the basics and latest developments in this field.

AUTHOR CONTRIBUTIONS

MM contributed to the writing of the manuscript. FC and SS contributed to the critical review of the manuscript. All authors have read and agreed to the published version of the manuscript.

Conflict of Interest: The authors declare that the research was conducted in the absence of any commercial or financial relationships that could be construed as a potential conflict of interest.

frontiers in Materials

ORIGINAL RESEARCH
published: 06 August 2020
doi: 10.3389/fmats.2020.00241

Mesoporous Bioactive Glass Nanoparticles Promote Odontogenesis and Neutralize Pathophysiological Acidic pH

Wenyan Huang[1†], Jingjing Yang[1†], Qiong Feng[1], Yan Shu[1,2], Cong Liu[3], Shihan Zeng[3], Hongbing Guan[1], Lihong Ge[1,4], Janak L. Pathak[1]* and Sujuan Zeng[1]**

[1] Guangzhou Key Laboratory of Basic and Applied Research in Oral Regenerative Medicine, Affiliated Stomatology Hospital of Guangzhou Medical University, Institute of Oral Disease, Guangzhou Medical University, Guangzhou, China, [2] Department of Pharmaceutical Sciences, School of Pharmacy, University of Maryland, Baltimore, MD, United States, [3] National Engineering Research Center for Tissue Restoration and Reconstruction, South China University of Technology, Guangzhou, China, [4] Department of Pediatric Dentistry, Peking University Hospital of Stomatology, Beijing, China

OPEN ACCESS

Edited by:
Mary Anne Sampaio Melo, University of Maryland, Baltimore, United States

Reviewed by:
Monica Yamauti, Hokkaido University, Japan
Tissiana Bortolotto, Université de Genève, Switzerland

***Correspondence:**
Lihong Ge
gelh0919@163.com;
gelh0919@126.com
Janak L. Pathak
j.pathak@gzhmu.edu.cn
Sujuan Zeng
13922265473@163.com

[†] These authors have contributed equally to this work and share first authorship

Specialty section:
This article was submitted to Biomaterials, a section of the journal Frontiers in Materials

Received: 25 May 2020
Accepted: 01 July 2020
Published: 06 August 2020

Citation:
Huang W, Yang J, Feng Q, Shu Y, Liu C, Zeng S, Guan H, Ge L, Pathak JL and Zeng S (2020) Mesoporous Bioactive Glass Nanoparticles Promote Odontogenesis and Neutralize Pathophysiological Acidic pH. Front. Mater. 7:241. doi: 10.3389/fmats.2020.00241

Pathophysiological acidic-pH hinders the dental biomaterial-based pulp-dentin regeneration. Bioactive glass (BG) synthesized by sol-gel methods had shown odontogenic and pulp regeneration potential. However, the pathophysiological acidic-pH neutralizing potential of BG has not been tested yet. In this study, we aimed to design mesoporous BG-nanoparticles by a well-established sol-gel method and test its odontogenic and acidic-pH neutralizing potential. BG-nanoparticles were synthesized and further characterized by SEM, EDS, XRD, and FTIR. Mono-dispersed and spherical mesoporous BG-nanoparticles with size 300–500 nm were successfully fabricated. Effect of BG ionic extraction in DMEM with 0.1–2.5 g/L BG concentrations on proliferation and odontogenic differentiation of stem cells from human exfoliated deciduous teeth (SHED) was analyzed. All the BG ionic extractions did not affect SHEDs proliferation at early time points (day 1 and 3). BG ionic extraction 0.5 g/L robustly enhanced odontogenic differentiation of SHEDs, as shown by the expression pattern of ALP, Col1, DSPP, and matrix mineralization results. The chemical composition of the BG ionic extraction-induced mineralized matrix resembled natural dentin. BG-nanoparticles/alginate paste neutralized the butyric acid solution (pH 5.4) and buffered within pH 8.3 for a month. Our findings showed the odontogenic and pathophysiological acidic-pH neutralizing potential of BG-nanoparticles, indicating its possible application in pulp-dentin regeneration under pathophysiologically challenged acidic environment.

Keywords: bioactive glass nanoparticles, odontogenic differentiation, pulp-dentin regeneration, acidic pH, odontogenesis

INTRODUCTION

Dentin and pulp tissue damage are mainly caused by bacterial activity, chemical erosion, and trauma. Dentin and pulp tissue damage are among the most common dental problems that substantially impact patient oral health and quality of life (Shah et al., 2020). After the introduction of restorative mineral trioxide aggregate (MTA) as a sealing agent in the early 1990s, pulpotomy

to protect the damaged tooth entered a new era (Lee et al., 1993). The conventional calcium hydroxide-based biomaterials are still the primary choice for dental caries repair and pulp capping (Parirokh et al., 2018). However, calcium hydroxide-based biomaterials, including MTA, have numbers of limitations, such as long solidification time, poor handling performance, toxicity, postoperative tooth discoloration, and high cost (Parirokh and Torabinejad, 2010; Parirokh et al., 2018). Therefore, novel cost-effective biomaterials for dentin and pulp tissue repair are still in high demand.

With recent advances in biomaterials design, researchers around the world are focused on developing novel dental biomaterials with dentin and pulp tissue restorative and regenerative properties. Bioactive glass (BG) is a highly biocompatible and osteoinductive silicate biomaterial (Rahaman et al., 2011). Ionic dissolution products from BG (e.g., Si, Ca, and P) are closely related to its biological and physiochemical activities (Hench and Polak, 2002; Hench and Jones, 2015). BG ionic dissolution products develop a hydroxycarbonate apatite (HCA) layer that promotes tissue regeneration. The HCA layer creates a strong bond between BG and hard tissues. BG-based biomaterials are biocompatible, angiogenic, immunomodulatory, antibacterial, and anti-inflammatory (Kargozar et al., 2018; Zeng et al., 2018; Zhou et al., 2018; Lin et al., 2019). Since BG is relatively low cost biomaterial, it possesses the potential to be the cost effective biomaterial for pulp-dental regeneration. BG is analogous to MTA, except the MTA has crystalline calcium phosphates structure, and BG has silicon-oxygen inorganic networks containing amorphous structure with robust biological activity. Dentin and pulp tissue regeneration are complex biological processes, involving odontogenesis, angiogenesis, immunomodulation, inflammation, and neuronal signaling (Shah et al., 2020). BG biomaterials had shown promising potential to regenerate various tissue, including bone, cartilage, skin, nerve, and periodontal tissue (Marquardt et al., 2014; Yu et al., 2016; Barbeck et al., 2017; Farano et al., 2019; Gomez-Cerezo et al., 2019). BG had been reported to enhance the odontogenic differentiation of precursor cells (Gong et al., 2014; Wang et al., 2014). Therefore, BG-based biomaterials hold potential for dentin/pulp tissue restoration/regeneration.

Mesoporous BG nanoparticles had been reported to enhance antimicrobial and tissue regenerative potential (Vichery and Nedelec, 2016). The sol-gel method is a widely accepted method of mesoporous BG nanoparticle fabrication for biomedical applications (Hu et al., 2018). Excessive bacterial localization-induced acidic pH in the decayed tooth is a key hurdle during the dentin and pulp tissue regeneration. The bacterial and inflammatory milieu with acidic pH in the decayed tooth affects the physicochemical properties of restorative/regenerative sealing materials (Elnaghy, 2014). Moreover, acidic pH impairs cell viability and tissue-specific differentiation of precursor cells. The sealing materials with the potential to neutralize the acidic pH in the affected tooth and pulp tissue have not been reported so far. Therefore, it is wise to design the bioactive restorative/regenerative dental materials that could neutralize the acidic pH and maintain the physicochemical properties of biomaterials and cellular activity.

In this study, we aimed to fabricate mesoporous BG nanoparticles by well-established sol-gel method and analyze its acidic pH neutralizing and odontogenic potential. The mesoporous BG nanoparticles were successfully synthesized and characterized. The release of Si, Ca, and P ions in neutral pH and acidic pH, as well as in regular cell culture medium, were analyzed. The effect of BG nanoparticles ionic extract on stem cells from human exfoliated deciduous teeth (SHEDs) proliferation, odontogenic differentiation, and dentin like matrix mineralization was analyzed. The acidic pH simulating the pathophysiological pH during dental erosion and pulp damage was neutralized by mesoporous BG nanoparticles/alginate paste for 30 days *in vitro*. The BG ionic extract robustly enhanced odontogenic differentiation of SHEDs and dentin-like matrix mineralization, indicating its application in pulp-dentin regeneration of decayed teeth with pathophysiologically challenged acidic pH.

MATERIALS AND METHODS

Preparation of Mesoporous BG Nanoparticles

Mesoporous BG nanoparticles were synthesized by the sol-gel method as described previously (Li et al., 2017; Hu et al., 2018), with a slight modification in the contents of SiO_2, CaO, and P_2O_5 (wt %) used. Briefly, the procedure was designed to use the molar composition of 58% SiO_2 (mass fraction), 33% CaO, and 9% P_2O_5. Dodecylamine (DDA, Aladdin) was used as a catalyst and template. DDA (4 g) was dissolved in 25 mL of deionized water (DW) and 80 mL of absolute ethanol (EtOH, Guanghua Chemical). Then, 16 mL of tetraethyl orthosilicate (TEOS, Guanghua Chemical) was added to the DDA solution and stirred for 1 h. 1.21 ml triethyl phosphate (TEP, Aladdin) and 3.32 g calcium nitrate tetrahydrate (CN, Guanghua Chemical) were added subsequently in 30 min interval under magnetic stirring at 40°C. The resulting solution was vigorously stirred for another 3 h. The white precipitate was collected by three times filtration and rinsing with absolute ethanol and deionized water. The filtrate was freeze-dried for 24 h. The BG nanoparticles were obtained by removing the templates and organic components by sintering at 650°C for 3 h (2°C/min).

Physicochemical Characterization of BG Nanoparticles

The morphology and elemental composition of BG nanoparticles were characterized by scanning electron microscope equipped with an energy-dispersive X-ray spectrometer (SEM-EDX, Hitachi S-3400N II, Model 550i, Japan). The phase composition analysis was assessed by X-ray diffraction (XRD, Bruker D8 AVANCE equipped with a LYNXEYE detector, Bruker AXS, Karlsruhe, Germany). Chemical structure analysis was performed by Fourier transform infrared spectroscopy (FTIR, Thermo Nicolet IS10, United States) with a wavenumber range from 500 to 4000 cm^{-1}.

BG Ionic Extraction Preparation for *in vitro* Cell Culture

The BG nanoparticles ionic extraction was prepared by incubating BG nanoparticles in DMEM (Gibco, United States) at the concentration of 10 g/L at 37°C and 120 rpm/min for 24 h, as described previously (Gong et al., 2014). BG-DMEM solution 10 g/L was further diluted to 0.1, 0.5, and 2.5 g/L. Particulates were removed by filtration through a 0.22 μm filter (Millipore, United States). The elementary content of silicon (Si), calcium (Ca), and phosphorus (P) ions in BG ionic extraction was determined by ICP-OES analysis (Agilent, United States). All BG ionic extraction in DMEM with 0.1, 0.5, and 2.5 g/L of BG were supplemented with 10% fetal bovine serum (Gibco, United States), 100 mg/mL streptomycin, and 100 U/mL penicillin and used for cell culture.

Isolation and Characterization of SHEDs

The deciduous teeth (6 incisors) were all collected from the 6–8 years old patients visiting the Pediatric Dentistry Department of Affiliated Stomatology Hospital of Guangzhou Medical University. The written informed consents were obtained from the patients' parent. The Research Ethics Committee of Guangzhou Medical University approved this study (KY2019008). The inclusion criteria for the primary tooth were: lower deciduous tooth, root resorption less than 1/3, no dental cavities, and no periapical disease. There was no history of systemic and hereditary diseases in these patients.

The deciduous tooth and the peripheral area were thoroughly disinfected with 1% tincture iodine before extraction. After extraction, the tooth was washed with saline for 2 times, put in 4°C DEME medium containing 5 times penicillin/streptomycin for up to 4 h before SHEDs isolation. SHEDs were isolated, as described previously (Miura et al., 2003). The SHEDs of the third passage were labeled with fluorescein isothiocyanate-conjugated or phycoerythrin-conjugated antibodies and analyzed with flow cytometry. Cell aliquots (2.0×10^6 cells) were incubated for 0.5 h at 4°C with monoclonal antibodies specific for human CD45, CD34, CD19, CD105, CD90, and CD73 (BD Biosciences), or isotype-matched control IgGs (Southern Biotechnology Associates). After the cells were washed with stain buffer for 2 times, the cells were incubated with a secondary antibody at 4℃ for another 30 min. The expression profiles for the cell surface markers were analyzed by flow cytometry (Calibur, BD Biosciences).

Cell Proliferation Assay

SHEDs (passage 5) were seeded at a density of 2.0×10^3 cells/well into 96-well plates with routine DEME contained with 10% fetal bovine serum, 100 mg/mL streptomycin, and 100 U/mL penicillin. After 24 h, the culture medium was replaced with fresh medium containing the above-mentioned BG ionic extractions (0, 0.1, 0.5, and 2.5 g/L). The fresh BG ionic extraction medium was changed every 2 days. At days 1, 3, 5, and 7, cell proliferation was analyzed by using the CCK8 assay (Dojindo, Japan) as described previously (Wang et al., 2020).

Alkaline Phosphatase (ALP) Activity and ALP Staining

Alkaline phosphatase (ALP) is a marker of odontogenic differentiation of precursor cells. SHEDs (passage 5) were seeded at a density of 2.0×10^4 cells/well into 48-well plates with routine DMEM. After 24 h, the culture medium was replaced with fresh BG ionic extraction medium. The fresh BG ionic extraction medium was changed in every 2 days. At 4 and 7 days, the ALP and total protein content in SHEDs' cultures were detected using an alkaline phosphatase assay kit and BCA quantitative detection kit (JianCheng Co., Nanjing, China), respectively, as described previously (Wang et al., 2020). The quantitative value of ALP activity was normalized with the total protein content. For ALP staining, at days 4 and 7, culture plates of SHEDs were fixed with a 4% paraformaldehyde solution and then stained with AKP kit (Beyotime, Shanghai, China).

Odontogenic Gene Expression Analysis

The expression of odontogenic markers, including ALP, collagen type I (COLI), and dentin sialophosphoprotein (DSPP), were detected by qRT-PCR. SHEDs (passage 5) were seeded at a density of 2.0×10^5 cells/well into 6-well plates with routine DMEM. After 24 h, the culture medium was replaced with fresh BG ionic extraction medium. The fresh BG ionic extraction medium was changed every 2 days. At 3, 7, and 10 days, the total RNA was extracted using a Trizol reagent (Invitrogen, Carlsbad, CA) according to the manufacturer's instructions. Two μg total RNA was reverse transcribed using cDNA kit (Invitrogen, Carlsbad, CA). Real-time (RT)-qPCR was performed using the SYBR Green qPCR kit (Qiagen, Germany) in iCycler IQMulti-color, Real time PCR Detection System. GADPH was used as a housekeeping gene. The following gene-specific primer sequences were used: ALP forward primer, 5′-GGACCATTCCCACGTCTTCAC-3′, and reverse primer, 5′-CCTTGTAGCCAGGCCCATTG-3′; COLI forward primer, 5′- CAGTGGTAGGTGATGTTCTGGGAG-3′, and reverse primer, 5′-CAAGAGGCATGTCTGGTTCGG-3′; DSPP forward primer, 5′-ATATTGAGGGCTGGAATGGGGA-3′, and reverse primer, 5′-TTTGTGGCTCCAGCATTGTCA-3'; GAPDH, 5'-GGACCTGACCTGCCGTCT AG-3', and reverse primer, 5'-GTAGCC CAGGATGCCCTTGA-3'.

Western Blot Analysis

After 1 and 3 days, the cultures were rinsed with PBS for 2 times. The cells were trypsinized and lysed. Proteins were quantitated with the bicinchoninic acid assay (BestBio, China). Total of 30 μg protein was separated by 10% sodium dodecyl sulfate-polyacrylamide gel electrophoresis and transferred to polyvinylidene fluoride (PVDF) membrane. The PVDF membrane was blocked with 5% skim milk at room temperature for 1 h and incubated with rabbit monoclonal anti-GAPDH (Abcam, United Kingdom) or human anti-DSPP (Bioss, China) primary antibody (1:1000 dilution) overnight at 4°C. Then PVDF membranes were incubated with HRP-conjugated goat anti-rabbit IgG (Abcam, United Kingdom)

secondary antibody (1:3000 dilution) 1 h at room temperature. The immunoblots were detected using a chemiluminescence kit (Millipore, United States) and photographed. ImageJ.1x (NIH. MD, United States) software was used to quantify band intensity.

In vitro Matrix Mineralization Assay

SHEDs (passage 5) were seeded at a density of 2.0×10^4 cells/well into 48-well plates with routine DEME. After 24 h, the culture medium was replaced with fresh BG ionic extraction medium. When the cells become 80% confluence, the cultures were supplemented with 50 μg/ml ascorbic acid, 5 mM β-Glycerophosphate, and 10 nM dexamethasone for odontogenic differentiation. For dentin mineralization assay, the cultures (day 14) were fixed with 70% ethanol and stained with 2% alizarin red (Sigma-Aldrich). Odontogenesis was determined by cellular accumulation of alizarin red-stained mineralized matrix. The mineralized matrix in different culture conditions was quantified as described previously (Yu et al., 2019).

Raman Spectroscopy for Native Dentin and *in vitro* Mineralized Matrix

After pulp tissue extraction, the deciduous tooth was stored in 1% chloramine T solution (Solarbio, China) at 4°C and polished with #320, 800, 1200, and 3000 mesh sandpaper in running water to expose the dentin. The deciduous tooth dentin and mineralized matrix in 0.5 g/L BG extraction treated culture were analyzed by a Raman Spectroscopy (LabRAM HR Evolution, HORIBA JY, France) operated with a diode laser of 785 nm wavelengths, a 2 cm^{-1} resolution and nominal laser power of 50 mW, for 20 s and 5 co-additions. The range of analysis was 200–2000 cm^{-1}. The data collection was controlled by the WINWIEW software. The fluorescence from the 48 average spectra was removed with a polynomial fitting of varying degrees using the OriginPro 2018 (OriginLab Corporation, MA, United States). Overall mean and standard deviation (SD) for peaks at 960, 1070, 1660 cm^{-1}, and ratios of 1070/960, 960/1660 were calculated based on 5 evaluations from each test layer of the 3 specimens (He et al., 2017). The peaks heights and ratios among the different dentin layers were compared. Mean mineral-to-matrix ratio values were calculated for native dental tissues and mineralized matrix in the BG ionic extraction treated SHEDs. Mineral-to-matrix ratio was calculated by dividing the area under the ∼960-cm^{-1} peak by the area under the Amide I peak at ∼1,660 cm^{-1} (Schwartz et al., 2012). The carbonate-to-phosphate ratio indicated carbonate substitution for phosphate and was calculated by dividing the area under the ∼1070-cm^{-1} peak by the area under the ∼960 cm^{-1} peak.

Acidic pH Neutralizing Capacity of Mesoporous BG Nanoparticles Paste

The BG nanoparticles were mixed with a phosphate buffer solution containing 1 wt% sodium alginate on a glass plate. The nanoparticles-to-solution ratio was ∼1.5 g/mL (Wang et al., 2014). The paste mixture was obtained by stirring and then filled to a sterile PTFE plastic ring (diameter 10 mm, height 3 mm). All the plastic rings were incubated at 37°C temperature and 5% CO_2 concentration for 12 h. Then BG/alginate paste was immersed in 10 mL aseptic PBS (pH = 7.4) or butyric acid (0.025% in PBS, pH = 5.4) and incubated on shaker at 37°C temperature and constant speed of 120 rpm/min for 5, 30 min, 1, 2, 4, 8, and 12 h, and 1, 2, 3, 4, 5, 6, 7, 14, 21, and 30 days. At each time point, the pH was determined using a twin pH meter (Mattler Toledo, Switzerland). On day 5, BG extractions were collected and filtered through a 0.45-mm microfiltration membrane. The elementary content of Si, Ca, and P ion in the solution was determined by ICP-OES analysis (Agilent, United States).

Statistical Analysis

All statistical calculations were performed with SPSSv.20.0 (SPSS Inc., Chicago, IL, United States) software. All data are expressed as mean ± standard deviation (SD). Differences between groups were analyzed using analysis of variance (ANOVA) followed by *Bonferroni* test. P value of <0.05 was considered statistically significant.

RESULTS

BG Nanoparticles Were Successfully Fabricated and Characterized

SEM images showed that mesoporous BG nanoparticles were formed with a regular spherical shape, mono dispersion, nanostructure, and size range 300–500 nm (**Figures 1A,B**). The EDX spectroscopy showed that BG nanoparticles are composed of silicon (84.19 wt%), calcium (14.56 wt%), and phosphorus (1.25 wt%) (**Figure 1C**).

The XRD results of BG nanoparticles showed the characteristic diffraction peaks of amorphous silicate materials in 15–30°, indicating the amorphous nature of BG nanoparticles (**Figure 1D**). The FTIR absorption spectrum of BG nanoparticles showed characteristic absorption peaks at 1090, 800, and 475 cm^{-1}, which in turn corresponds to typical Si-O-Si non-telescopic vibration peak, Si-O symmetrical expansion vibration peak, and Si-O-Si symmetrical bending vibration peak (**Figure 1E**).

Mesoporous BG Ionic Extraction in DMEM Showed the Dissolved Si, Ca, and P Ions

The concentration of Si in 0, 0.1, 0.5, and 2.5 g/L DMEM BG extractions-group was 1.84 ± 0.12, 15.46 ± 0.77, 54.64 ± 4.42, and 92.75 ± 2.49 mM, respectively (**Table 1**). The concentration of Si was very low in routine DMEM medium. The concentration of Si ion gradually increases in the groups with the increase of BG nanoparticles' concentration dissolved in DMEM. The ionic concentration of Ca in BG extractions was slightly higher than that in routine DMEM medium. The ionic concentrations of P in BG extractions were lower than that in routine DMEM medium,

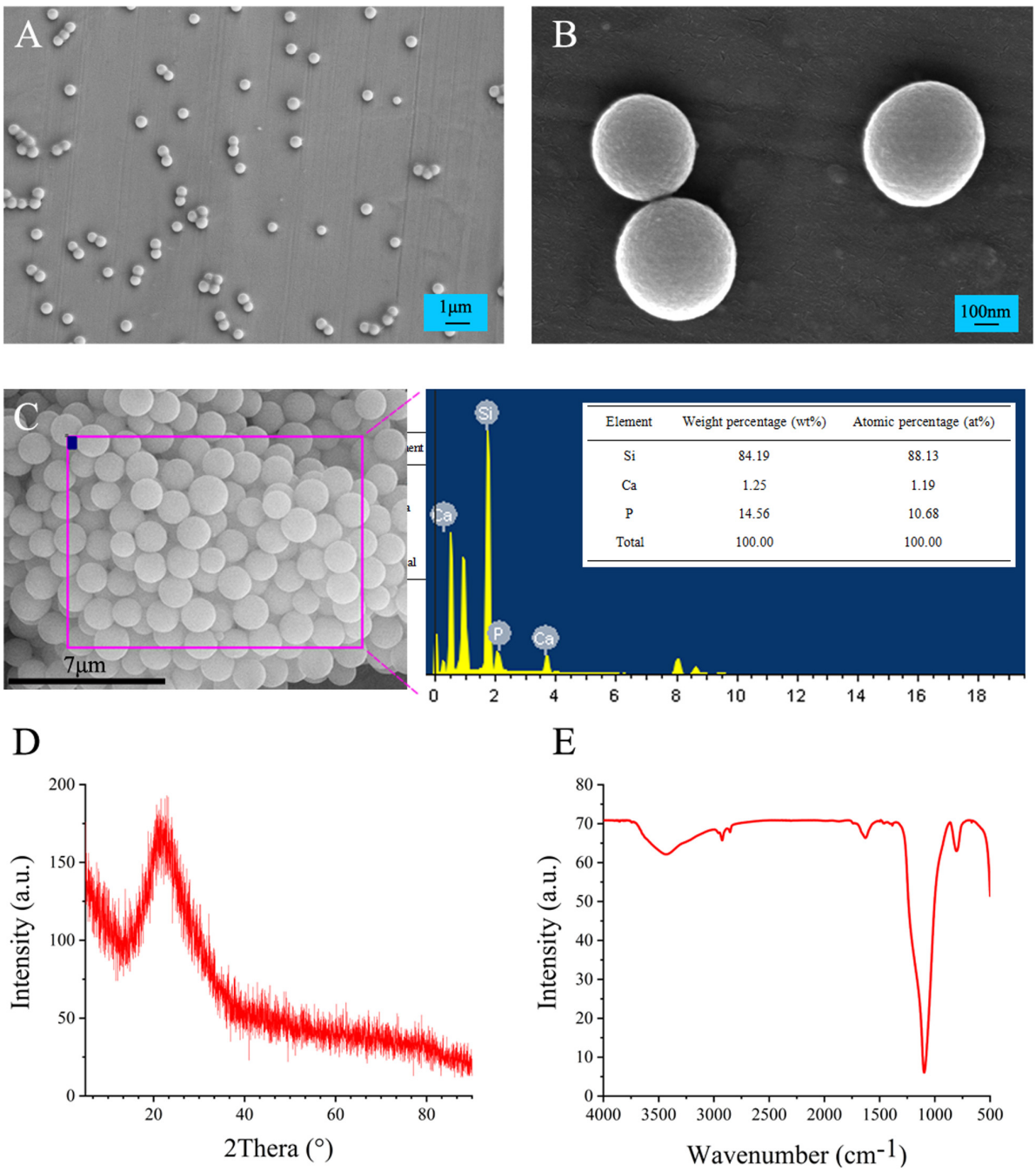

FIGURE 1 | Physicochemical characterization of mesoporous BG nanoparticles. **(A,B)** SEM micrographs, **(C)** EDX elemental composition analysis, **(D)** XRD patterns, and **(E)** functional analysis by FTIR.

which may be related to the formation of hydroxyapatite carbonate on BG surface.

SHEDs Were Successfully Isolated From Deciduous Teeth and Characterized

The isolated SHEDs were photorefractive and adherent to the wall. After one week of culture, the cell population around the tissue explants increased gradually, forming the appearance of cell colonies (**Figure 2A**). The cell morphology resembled to the fibroblasts (**Figure 2A**). The cells were polygonal or fusiform and adherent to the culture plate. The cells were stably cultured for up to 8 passages with consistent morphology and proliferation.

The FACs' results indicated that the MSCs' surface markers CD73, CD90, and CD105 were highly expressed in SHEDs, with an expression rate of ≥95% (**Figure 2B**). In

TABLE 1 | Si, Ca, and P ion concentration in BG ionic extraction in DMEM.

Group	Si (mg/L)	Ca (mg/L)	P (mg/L)
DMEM	1.84 ± 0.12	63.83 ± 0.47	30.4 ± 1.15
0.1 g/L BG-DMEM	15.46 ± 0.77	73.77 ± 1.20	25.45 ± 0.62
0.5 g/L BG-DMEM	54.64 ± 4.42	74.10 ± 1.28	25.13 ± 1.55
2.5 g/L BG-DMEM	92.75 ± 2.49	80.21 ± 1.49	22.44 ± 1.22

The data are presented as mean ± SD from 3 independent experiments (n = 3).

contrast, SHEDs did not show significant expression (≤2%) of hematopoietic/endothelial origin stem cell markers, i.e., CD19, CD34, and CD45 (**Figure 3B**).

BG Ionic Extraction From Higher Concentration of BG Inhibited SHEDs Proliferation at Day 5 and 7

All the concentrations of BG ionic extraction treated (0.1, 0.5, and 2.5 g/L-group) did not affect SHEDs proliferation at days 1 and 3 (**Figure 3A**). BG ionic extraction (0.5 and 2.5 g/L-group) inhibited SHEDs proliferation at days 5 and 7 (**Figure 3A**). BG extractions 2.5 g/L-group showed higher inhibition on SHEDs proliferation at days 5 and 7 compared to BG extractions 0.5 g/L-group (**Figure 3A**).

BG Ionic Extraction 0.5 g/L-Group Induced the Highest Odontogenic Differentiation of SHEDs

BG ionic extraction 0.1 and 2.5 g/L-group did not affect, but 0.5 g/L-group enhanced ALP activity at day 4 by 1.4-fold compared to the control group (**Figure 3B**). Interestingly, BG ionic extraction 0.1, 0.5, and 2.5 g/L-group enhanced ALP activity at day 7 by 1. 7-, 2. 2-, and 1.9-fold, respectively, compared to the control group (**Figure 3B**). ALP protein expression at day 4 did not show noticeable differences between the control and BG ionic extraction treatment groups (**Figure 3C**). However, 0.1, 0.5, and 2.5 g/L-group showed higher ALP protein expression at day 7 compared to the control group, and 0.5 g/L-group showed the highest expression of ALP protein at day 7 compared to the other groups (**Figure 3C**). DSPP is another established marker of odontogenic differentiation. Protein level expression of DSPP was analyzed by western blot assay. All the BG ionic extraction groups tested in this study upregulated DSPP expression in SHEDs at day 1 and day 3 (**Figures 3D,E**).

We further analyzed the mRNA expression of odontogenic differentiation markers ALP, Col1, and DSPP in BG ionic extractions treated SHEDs at days 3, 7, and 10. The 0.1 g/L-group enhanced ALP expression at days 3 and 7, COL1 at day 7, and DSPP at day 3 (**Figure 4**). Interestingly, 0.5 g/L-group robustly upregulated the expression of ALP, COl1, and DSPP expression at days 3 and 7. However, 2.5 g/L-group did not affect ALP, COl1, and DSPP expression at days 3 and 7. All the treatment did not affect ALP, COl1, and DSPP expression at day 10 (**Figures 4A–C**).

BG Ionic Extraction 0.5 g/L-Group Induced the Highest Matrix Mineralization in SHEDs Culture

Alizarin red staining revealed that more matrix-mineralized nodules were generated in the BG extraction groups than in the control group after 2 weeks of culture (**Figure 5A**). BG extraction 0.5 g/L-group showed the most intense alizarin red staining compared to other groups (**Figure 5A**). Quantitative analysis of alizarin red staining showed that BG extraction 0.1 and 0.5 g/L-group showed 1.44- and 1.67-fold, higher matrix mineralization, compared to control group, respectively (**Figure 5B**).

Mineral Contents in the Mineralized Matrix Resemble to Natural Dentin

As shown in **Figure 6**, the mineralized matrix showed a strong peak related to PO_4^{3-} vibration at 960 cm^{-1} band. As shown in **Figure 6** and **Table 2**, the mineralized matrix and natural dentin had similar spectral characteristics between 200–2000 cm^{-1} band and mineral/matrix ratio. Mineralized matrix showed slightly lower carbonate substitution and peak intensity of phosphate 960 cm^{-1} band, indicating that the calcium phosphate content of mineralized matrix *in vitro* was lower than that of the natural dentin. Besides, the characteristic peaks of organic components, including Amide III and Amide I, varied in the mineralized matrix.

The Ionic Release and Acidic pH Neutralization by BG Nanoparticles Paste

The Si and Ca ions concentrations in the solutions were increased while P ion concentration was decreased ($P < 0.05$), which may be related to the consumption of P in the process of hydroxyapatite formation. A low Si ion concentration was observed in butyric acid solution (pH 5.4) than in PBS (pH of 7.4) (**Figure 7**).

BG nanoparticles/alginate paste increased the pH value in both butyric acid solution (pH 5.4) and PBS (pH 7.4). In BG nanoparticles/alginate paste immersed PBS, the pH values increased slowly within the first 48 h, then tended to be stable (pH 9.32 ± 0.07). This result suggests the alkaline nature of BG ionic extraction. In BG nanoparticles/alginate paste immersed butyric acid solution, the pH value reached 7.13 at 24 h, then showed a slow continuous increase in pH and reached up to pH 8.34 on day 30. This result suggests that the BG ionic release could neutralize butyric acid solution (pH 7.4) and buffer it below pH 8.3 for a month. Under the acidic condition, the silicon hydroxyl groups are formed on the surface of BG and further create a silica gel membrane, which could hinder the ion exchange reaction and slows down the Si ion release. Such a porous gel membrane could allow the inner layer of BG to exchange slowly with the surrounding solution to form an alkaline environment (**Figure 8**).

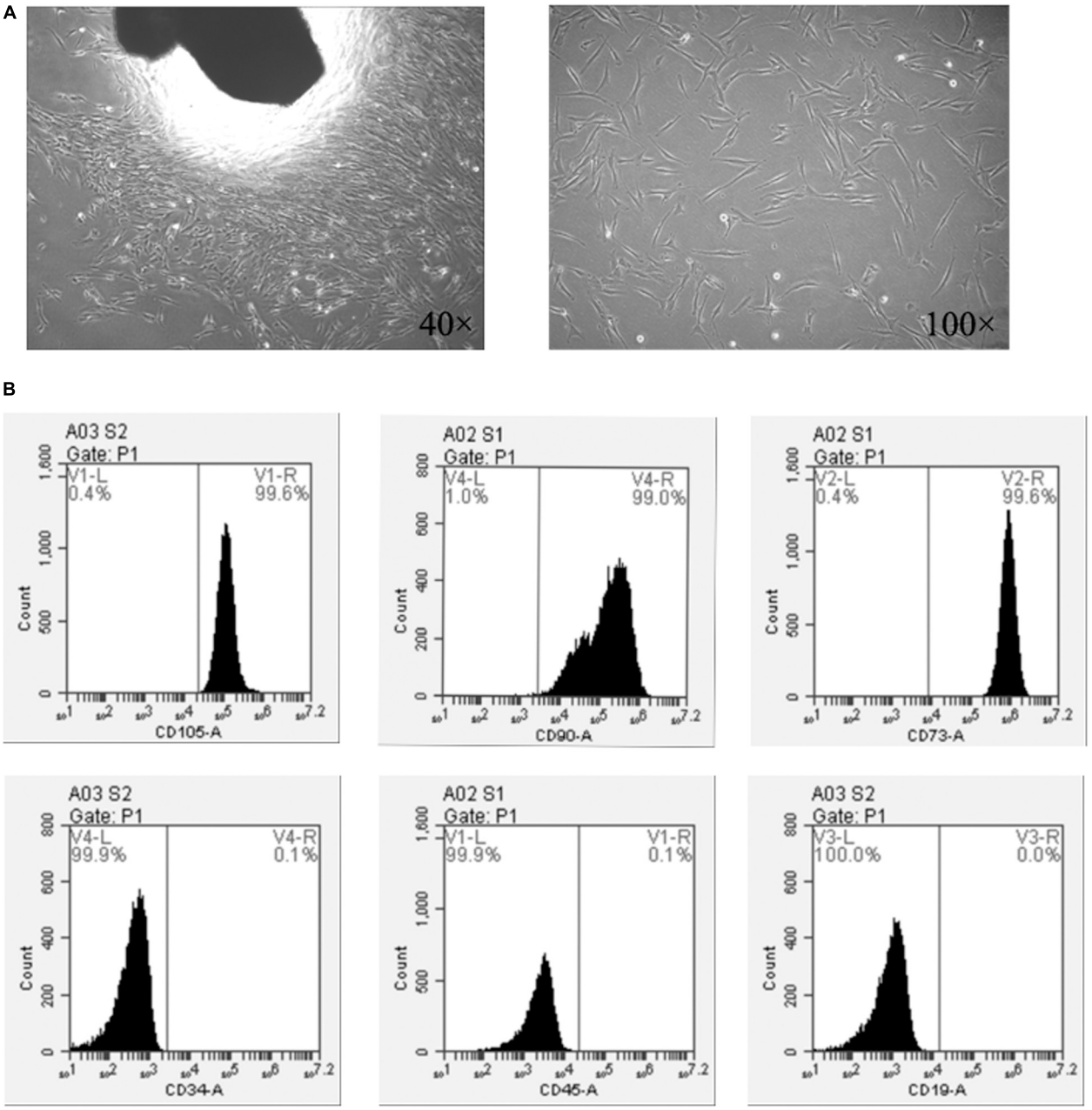

FIGURE 2 | SHEDs isolation and characterization. **(A)** Cell morphology at passage 0, and **(B)** expression of MSC surface markers on SHEDs as determined by flow cytometry.

DISCUSSION

In clinical applications such as direct pulp capping and root canal lateral puncture repair, the pulp capping material directly contacts the tissue fluid and is exposed to local metabolic acidic environment caused by bacteria or inflammation. Anaerobic bacteria are dominant bacteria in pulp infection, and butyric acid, as one of the metabolic byproducts of anaerobic bacteria, is often used in the laboratory to simulate infectious acidic environments. Bacterial localization and pulpal/periapical inflammation-mediated acidic pH (pH ∼5.5) hinders pulp-dentin regeneration (Loesche, 1996; Azuma, 2006; Hirose et al., 2016). Acidic pH in tooth lesions affects the physicochemical properties of the biomaterials and hinders the sealing potential, and inhibits cellular activity (Pushpa et al., 2018). Butyric acid is one of the bacterial byproducts causing acidic pH in and affecting dental/periodontal health and treatments (Niederman et al., 1997). Therefore, neutralizing the butyric acid-mediated acidic pH in dental and periodontal milieu could facilitate the treatment of dental/periodontal diseases. However, the dental

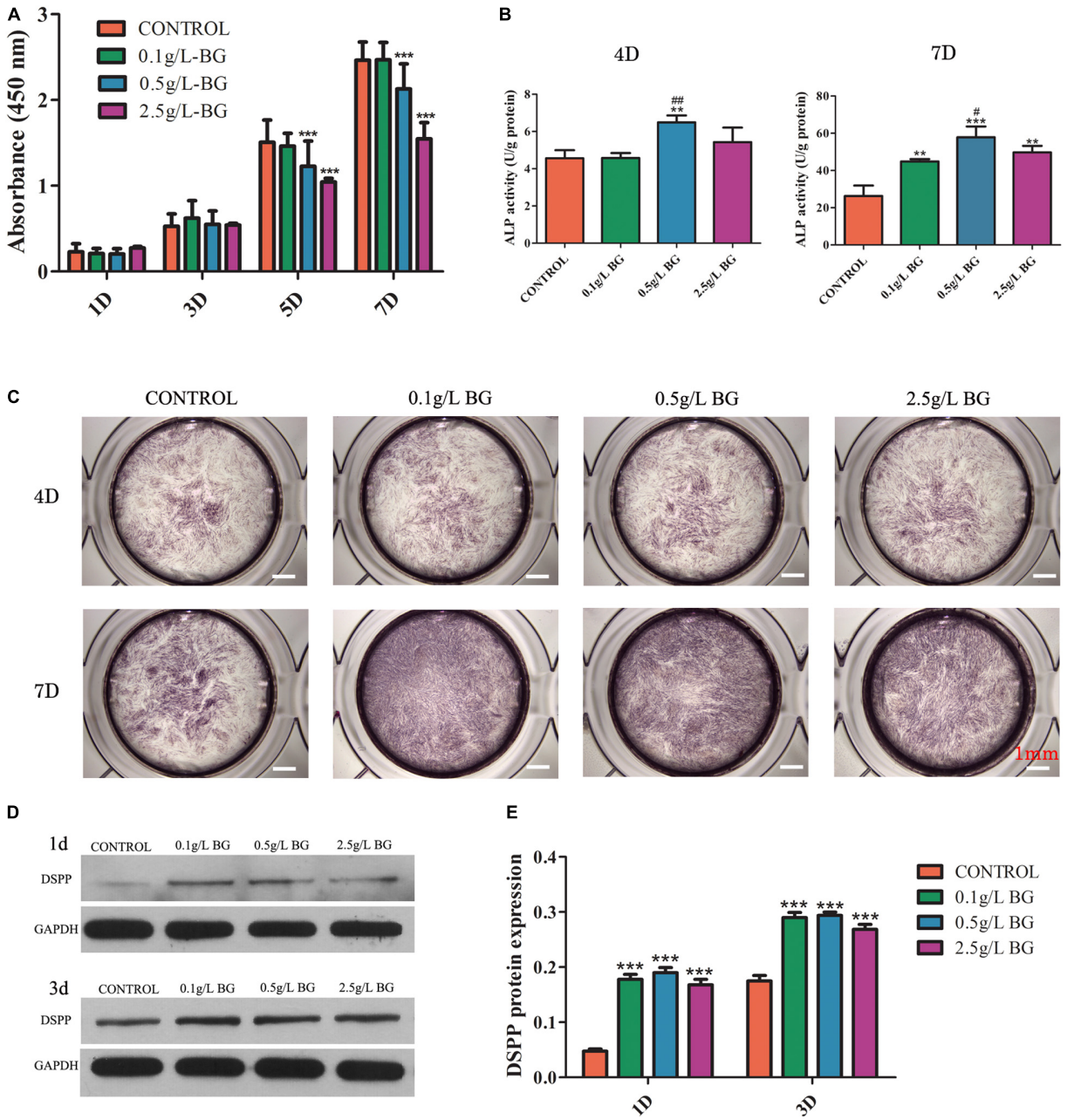

FIGURE 3 | Effect of BG ionic extraction on SHEDs proliferation and odontogenic differentiation. **(A)** CCK8 assay, **(B)** ALP activity, **(C)** ALP staining (scale bars: 1 mm), **(D)** Western blot assay, and **(E)** Quantitative analysis of western blots. The data are presented as mean ± SD from independent experiments ($n = 3$). Significant effect of treatment: compared to control, $^{*}P < 0.05$, $^{**}P < 0.01$, $^{***}P < 0.001$; compared to 0.1 g/L-group, $^{\#}P < 0.05$, $^{\#\#}P < 0.01$. D: Day.

biomaterials that can neutralize the acidic pH and promotes pulp-dentin regeneration have not been reported yet. In this study, we fabricated the mesoporous BG nanoparticles with dentin regeneration and acidic pH neutralization potential. Butyric acid is the main metabolic byproduct of the anaerobic bacteria, which are predominantly localized in tooth lesions and infected dental pulp (Loesche, 1996). BG nanoparticles/alginate paste increases the pH 5.4 of butyric acid solution to pH 7.12 within 24 hrs. BG nanoparticles ionic extraction robustly enhanced odontogenic differentiation of SHEDs and dentin like matrix mineralization in SHEDs culture. Our finding suggests the possible application of mesoporous BG nanoparticles in pulp-dentin regeneration under acidic pathophysiological environment. BG has shown robust potential for hard and soft tissue regeneration, including bone and skin (Hench and Polak, 2002; Hench and Jones, 2015). In recent years, scientific community is focused on developing various BG-based materials for various tissue regeneration applications. In

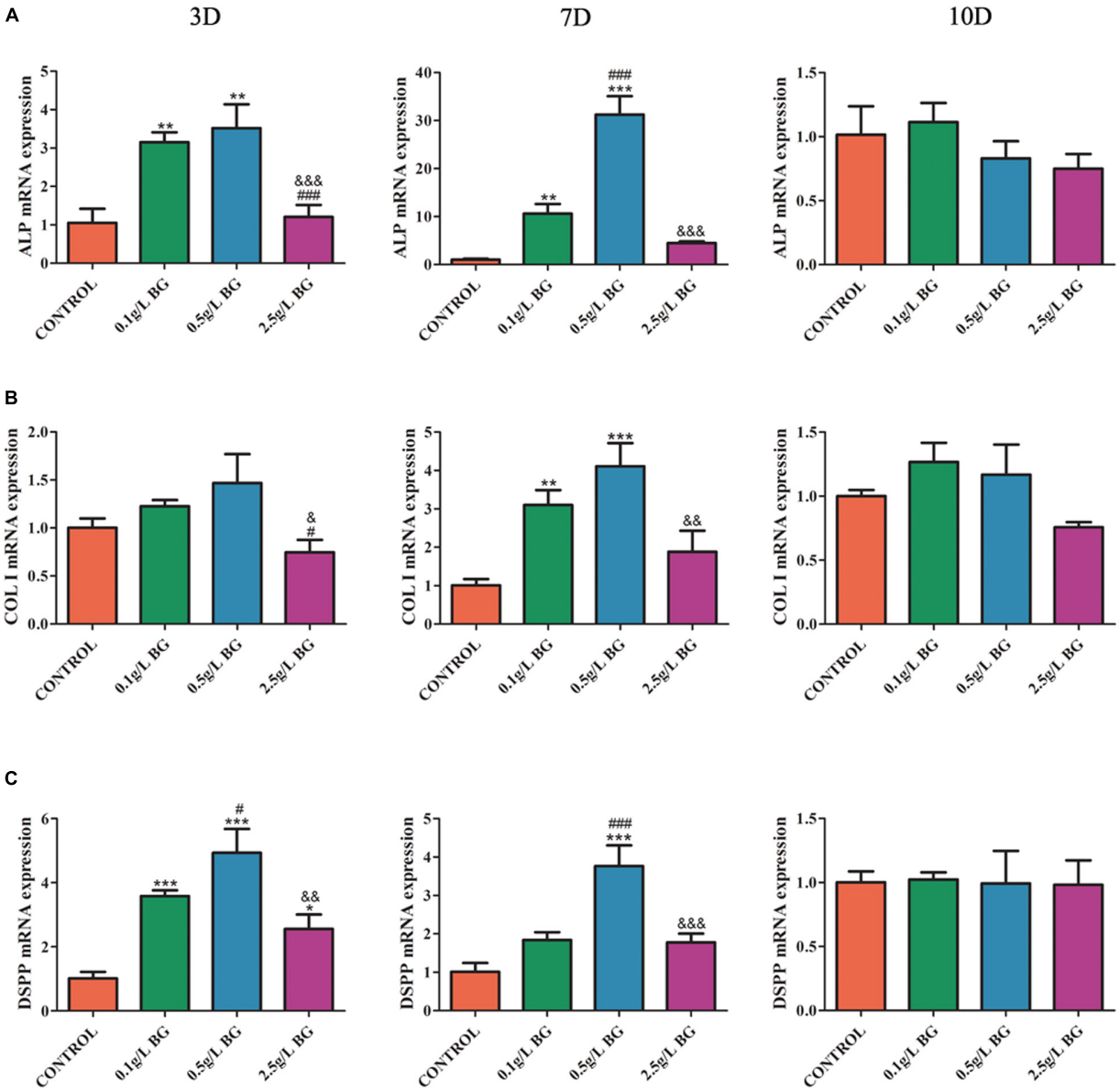

FIGURE 4 | Odontogenic gene expression analysis. **(A)** ALP, **(B)** COLI, and **(C)** DSPP at days 3, 7, and 10. The data are presented as mean ± SD from 3 independent experiments ($n = 3$). Significant effect of treatment: compared to control, $^{*}P < 0.05$, $^{**}P < 0.01$, $^{***}P < 0.001$; compared to 0.1 g/L-group, $^{\#}P < 0.05$, $^{\#\#\#}P < 0.001$; compared to 0.5 g/L-group, $^{\&}P < 0.05$, $^{\&\&}P < 0.01$, $^{\&\&\&}P < 0.001$. D: Day.

dentistry, BG has been applied to treat periodontal disease, maxillofacial bone defect, dentin hypersensitivity, and dental defects in the form of a composite substrate material (Schepers et al., 1991; Lovelace et al., 1998; Skallevold et al., 2019). Most commonly used BG-based materials in dental clinics are prepared by the traditional melting method (Skallevold et al., 2019). The sol-gel-derived BG had shown superior bioactivity compared to the melting-derived BG (Li et al., 1991; Lei et al., 2012). This effect is mainly achieved by micro/mesoporous structure, uniform micron/submicron particle size, and large specific surface area. Moreover, sol-gel-derived BG quickly forms HCA increasing the bonding with bone or dentin (Hu et al., 2018). The sol-gel method allows us to fabricate BG with micro to nanoscale size (Hu et al., 2018). Nanoscale biomaterials have shown a robust effect on cellular activity and tissue regenerative potential compared to macro/micro-scale biomaterials (Lei et al., 2012; Zhu et al., 2020). Mesoporous BG nanoparticles provide a large surface area and porosity that not only increases its bioactivity but also provides drugs carrier platform. In this study, we fabricated mono-dispersed mesoporous BG nanoparticles by slight modification in the previously described sol-gel method for BG preparation (Hu et al., 2018). The spherical and mono-dispersed mesoporous BG nanoparticles (300–500 nm diameter) were successfully

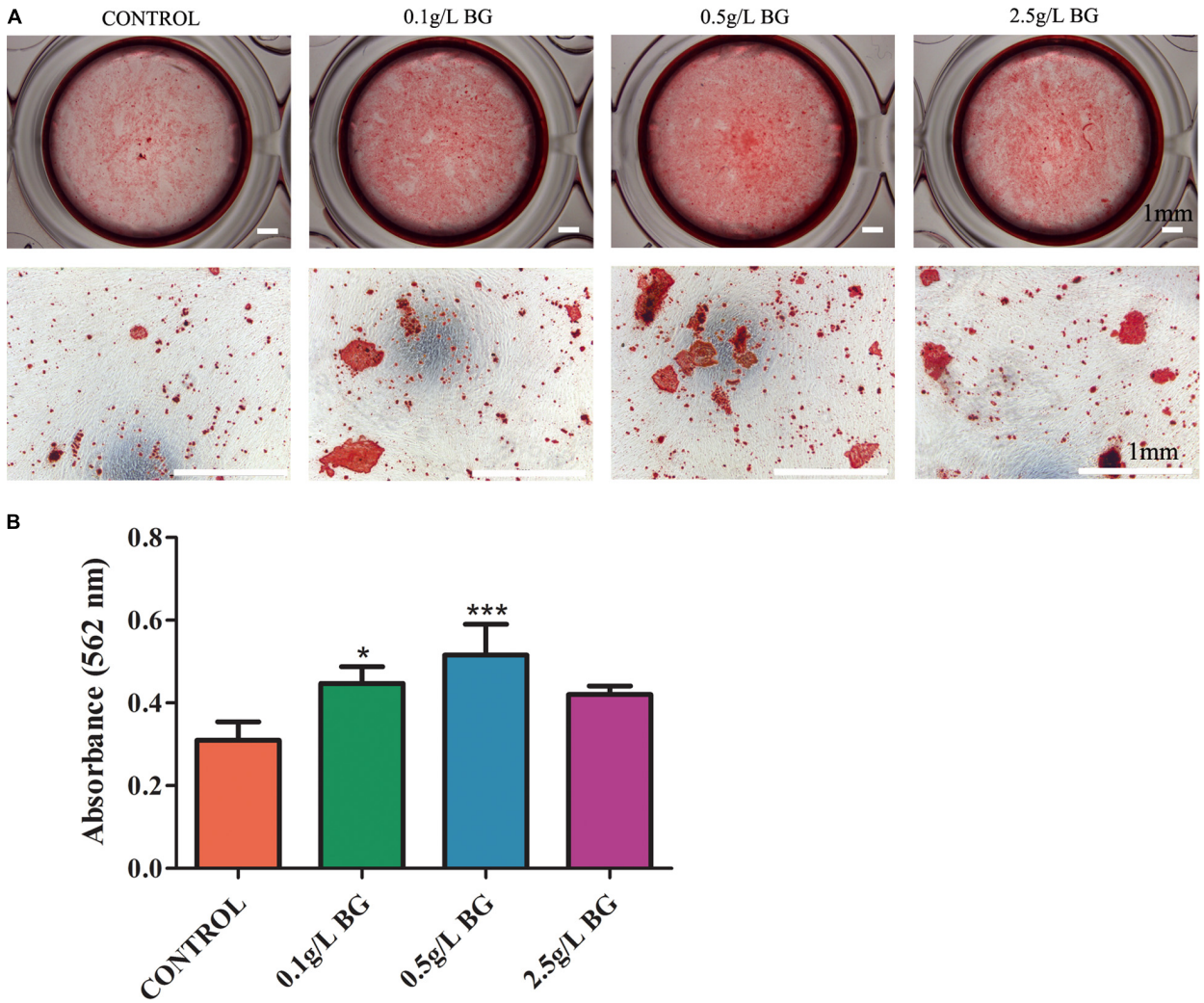

FIGURE 5 | Alizarin red staining for mineralized matrix in SHEDs cultures at day 14. **(A)** Representative images of alizarin red-stained mineralized matrix (scale bars: 1 mm). **(B)** Quantitative analysis of mineralized matrix. The data are presented as mean ± SD from 3 independent experiments ($n = 3$). Significant effect of treatment compared to control, $^{*}P < 0.05$, $^{***}P < 0.001$.

synthesized and characterized. Hu et al. (2014) previously reported the synthesis of bioactive mesoporous BG nanoparticles with a size range of 256–716 nm diameter using the sol-gel technique.

Among the various dental stem cells, SHEDs have a higher degree of stemness and are conveniently available from the pediatric dental clinic (Akpinar et al., 2014). Therefore, this study used SHEDs as a stem cell model for dentin regeneration. We successfully isolated and characterized SHEDs using established protocol (Miura et al., 2003). Biocompatibility of the biomaterials is vital for dentin and pulp regeneration therapy. We found that BG ionic extraction from 0.1–2.5 g/L BG did not affect the SHEDs viability at early time points (days 1 and 3). However, the BG ionic extracts from 0.5 and 2.5 g/L BG inhibited SHEDs' proliferation at days 5 and 7. This effect could be caused by the more prolonged incubation of SHEDs with a high concentration of Si. High levels of Si had shown an inhibitory effect on cell growth and proliferation (Rismanchian et al., 2013; Zhou et al., 2013). Similarly, Gong et al. (2014) had reported an inhibitory effect of BG ionic extractions from 1 g/L BG on the proliferation of adult human dental pulp stem cells (hDPSCs). Our findings and reports from the literature suggest that the optimization of BG concentration is crucial to eliminate the cytotoxicity during BG-mediated pulp-dentin regeneration.

Dentin protects the dental pulp, and odontogenic differentiation of dental pulp stem cells is crucial for the maintenance and regeneration of dentin (Shah et al., 2020). Therefore, the biomaterials used for pulp-dentin revitalization should have odontogenic potential. Nanoscale BG had shown higher odontogenic potential compared to microscale BG (Gong et al., 2014; Wang et al., 2014). Ionic extractions from 1 g/L nano BG (10–100 nm) robustly enhance odontogenic differentiation of hDPSCs compared to ionic extractions from micro-scale BG (Gong et al., 2014). Similarly, 0.1 and 0.5 g/L of

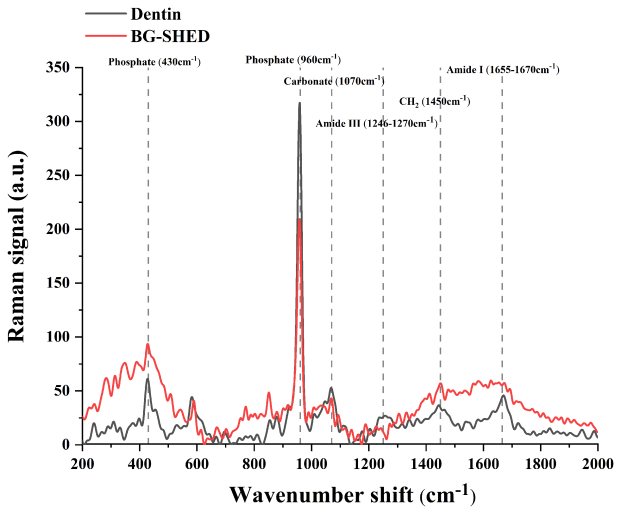

FIGURE 6 | Representative Raman spectrum of mineral components in the mineralized matrix and native dentin. The red line represents the Raman spectrum of mineralized matrix in SHEDs. The black line represents the Raman spectrum of the native dentin of deciduous teeth.

TABLE 2 | Normalized spectra intensity of mineral components.

Group	Phosphate peak (960 cm^{-1})	Mineral-to-matrix ratio	Carbonate-to-phosphate ratio
Native dentin	313.27 ± 5.05	10.12 ± 1.04	0.16 ± 0.01
Mineral matrix	207.47 ± 4.21	7.51 ± 2.72	0.20 ± 0.01

The data are presented as mean ± SD from 3 independent experiments (n = 3).

BG nanoparticles (20 nm) enhance odontogenic differentiation of hDPSCs in dose-dependent manner (Wang et al., 2014). In this study, the ionic extraction from 0.5 g/L mesoporous BG showed the highest effect on the upregulation of odontogenic differentiation of SHEDs. BG ionic extraction from 0.5 g/L BG induced the higher expression of odontogenic markers and matrix mineralization in SHEDs culture compared to 0.1 and 2.5 g/L BG. This inhibitory effect of the BG ionic extraction from 2.5 g/L BG could be associated with the higher dose of Si induced cytotoxicity. Si concentration in BG ionic extract from 2.5 g/L BG was 1.7-fold higher than in BG ionic extract from 0.5 g/L BG. Our results rule out the dose-dependent anabolic effect of BG on odontogenesis, suggesting the importance of the optimal dose of BG in dentin-pulp regeneration. The difference between native dentin and mineralized matrix in SHEDs cultured with BG ionic extraction has not been investigated yet. We analyzed the mineral and organic contents in the BG-induced mineralized matrix in SHEDs culture. The most intense peak at 960 cm^{-1} was assigned to the dentin mineral phosphate, and the peak at 1070 cm^{-1} was assigned to the mineral carbonate (CO_3^{2-}). The peaks at 1246–1270, 1450, and 1655–1667 cm^{-1} were assigned to Amide III, CH_2, and Amide I, respectively, that are related to the organic composition in hard tissue (Wang et al., 2014). We confirmed for the first time that the chemical characteristics of the mineralized matrix in SHEDs cultured with BG ionic extraction resembled native dentine. This result indicates the dentin regenerative potential of mesoporous BG nanoparticles.

Butyric acid and lactic acid are the main acidic byproducts of localized bacteria in the dental cavity (Hojo et al., 1994; Loesche, 1996), which could drop the pH below 5.5 in the decayed tooth cavity and affect pulp tissue homeostasis. Acidic pH not only affects the physicochemical biomaterial used but also impairs cell viability and activity (Hirose et al., 2016; Pushpa et al., 2018). Moreover, acidic pH also amplifies the inflammation in pulp tissue. Although mild inflammation is necessary for dentin-pulp tissue regeneration, the chronic and higher degree of inflammation will cause detrimental effects. Mesoporous BG nanoparticles not only have antimicrobial properties but also provides the nano-platform for antimicrobial strategies (Kargozar et al., 2018). In this study, we showed the butyric acid pH 5.4 neutralizing potential of mesoporous BG nanoparticles/alginate paste. BG/alginate paste was able to buffer pH of the butyric acid solution and PBS within pH 8.3 and 9.3, respectively. Neutral to pH 8.3 favors pH cell growth and activity. BG showed a markedly slower release of Si at a pH of 5.4 than at a pH of 7.4. Our findings suggest mesoporous BG nanoparticles as a potent biomaterial with pH buffering capacity, indicating its application in pulp-dentin regeneration in acidic pathophysiological environment.

Bacterial infection, inflammation, acidic pH, and immune reaction are the main factors affecting pulp-dentin regeneration (Schmalz and Smith, 2014; Jung et al., 2019; Shah et al., 2020). Synergistic activity of immune cells, mesenchymal stem cells, angiogenic, and neurogenic processes are involved in pulp-dentin restoration (Shah et al., 2020). BG had shown potential for immunomodulation, inflammation mitigation, odontogenesis, angiogenesis, neuron regeneration, and inhibition of microbial growth (Marquardt et al., 2014; Drago et al., 2015; Yu et al., 2016; Barbeck et al., 2017; Zhao et al., 2018; Farano et al., 2019; Gomez-Cerezo et al., 2019). We believe that the mesoporous BG nanoparticles designed in this study might have above-mentioned potentials, and could be used for various oral tissue regeneration, including pulp-dentin. Moreover, mesoporous BG nanoparticles could be the carrier of growth factors and antimicrobial agents needed during pulp-dentin regeneration.

In this study, we used the well-established sol-gel method to fabricate mesoporous BG nanoparticles. In comparison to BG nanoparticles, mesoporous BG nanoparticles have small size with higher specific surface area that enhances the bioactivity (Hu et al., 2014). Moreover, the mesoporous BG nanoparticles provide higher specific surface area to load desired drugs, proteins, and doping metal ions. The BG nanoparticles were well characterized, and the release of Si, Ca, and P ions from BG in a regular cell culture medium, acidic solution, and PBS were analyzed. Pulp/dentin regeneration of the hopeless tooth is still a challenge. Combination therapy of suitable biomaterial and stem cells could have the potential to regenerate the damaged pulp-dentin tissue. SHEDs have promising pulp-dentin regenerative potential and could be more easily harvested from deciduous teeth using a minimally invasive procedure compared to stem cells from permanent tooth pulp tissue. In

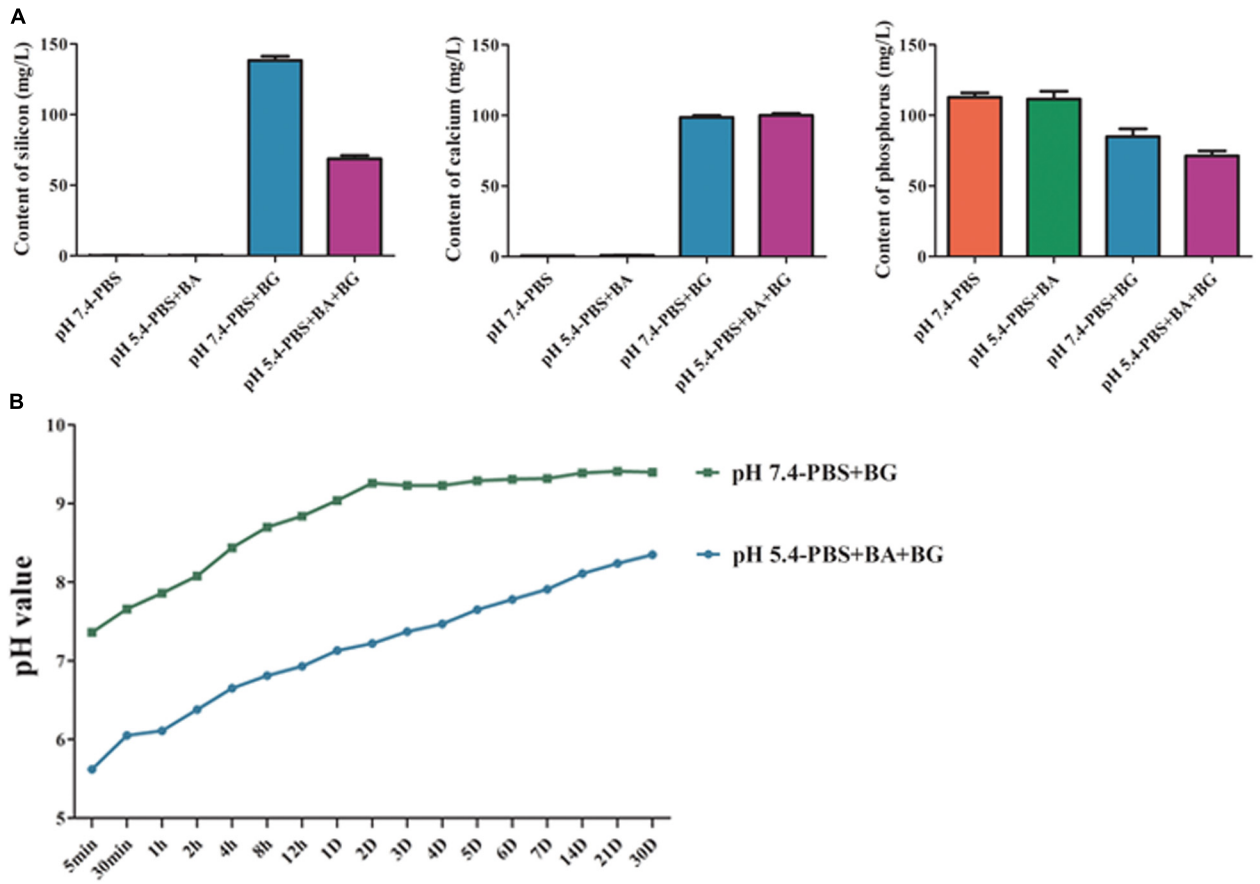

FIGURE 7 | (A) The Si, Ca, and P ion release from BG nanoparticles/alginate paste. **(B)** Change in pH of BG nanoparticles/alginate paste immersed PBS (pH 7.4) and butyric acid solution (pH 5.4). The data are presented as mean ± SD from 3 independent experiments (n = 3). BA: Butyric Acid; BG: BG nanoparticles/alginate paste; D: Day.

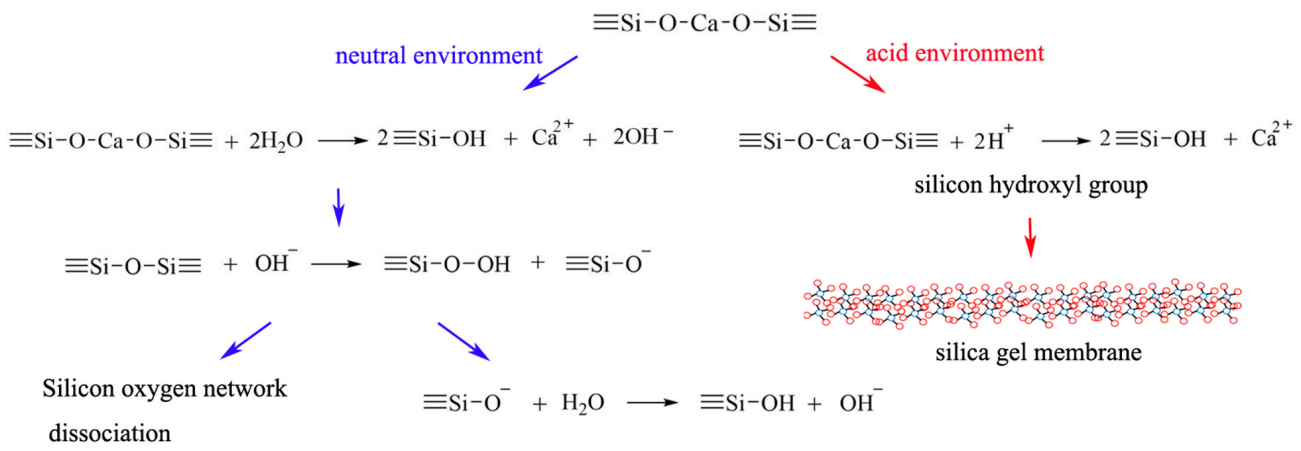

FIGURE 8 | Scheme of the ionic reaction of BG nanoparticles in a neutral or acidic environment.

this study, we used SHEDs as a source of stem cells to get insights on the possible use of mesoporous BG nanoparticles and SHEDs for pulp dentin regeneration. Dentin like mineralized matrix regenerative potential of BG nanoparticles in SHEDs culture was analyzed by comparing the chemical properties with native dentin using Raman spectroscopy. BG/alginate paste was fabricated, and the acidic pH neutralizing potential for one month was tested. A limitation of this study is that we did

not analyze the dentin regeneration of acidic pH neutralizing potential using *in vivo* set up. Future studies on pulp-dentin regeneration using mesoporous BG nanoparticles containing tooth sealing materials are strongly recommended. Moreover, the chemical, molecular, and cellular mechanism of BG-mediated pulp-dentin regeneration needs to be elucidated for the possible clinical applications.

CONCLUSION

In this study, spherical and mono-dispersed mesoporous BG nanoparticles were successfully fabricated and characterized. The BG nanoparticles showed odontogenic and dentin regenerative potential *in vitro*. Moreover, the BG nanoparticles/alginate paste neutralized the acidic pH 5.4 and buffered within pH 8.3 for a month. The concentration of Si ion release from BG in butyric acid solution (pH 5.4) was reduced by half compared to in PBS (pH 7.4). The findings of this study indicate the potential application of BG nanoparticles alone or in combination with SHEDs for pulp-dentin regeneration in pathophysiological acidic environment.

DATA AVAILABILITY STATEMENT

The raw data supporting the conclusions of this article will be made available by the authors, without undue reservation.

ETHICS STATEMENT

The studies involving human participants were reviewed and approved by The Research Ethics Committee of Guangzhou Medical University. Written informed consent to participate in this study was provided by the participants' legal guardian/next of kin.

AUTHOR CONTRIBUTIONS

WH, LG, JP, and SZ conceptualized and designed the study and reviewed the final manuscript. WH, JY, QF, YS, and HG acquired the data, analyzed the data, and wrote the manuscript. WH and JY performed *in vitro* experiments. CL and SZ prepared and characterized BG nanoparticles. All authors read and approved the submitted version.

FUNDING

This work was supported by project of Guangdong Science and Technology Department (2017A020215141), Project of Guangzhou Science Technology and Innovation Commission (201707010026), and High-Level University Construction Talents of Guangzhou Medical University (B185006003014 and B195002003017). The funder had no role in the study design and collection, analysis, and interpretation of the results.

REFERENCES

Akpinar, G., Kasap, M., Aksoy, A., Duruksu, G., Gacar, G., and Karaoz, E. (2014). Phenotypic and proteomic characteristics of human dental pulp derived mesenchymal stem cells from a natal, an exfoliated deciduous, and an impacted third molar tooth. *Stem Cells Int.* 2014:457059. doi: 10.1155/2014/457059

Azuma, M. (2006). Fundamental mechanisms of host immune responses to infection. *J. Periodont. Res.* 41, 361–373. doi: 10.1111/j.1600-0765.2006.00896.x

Barbeck, M., Serra, T., Booms, P., Stojanovic, S., Najman, S., Engel, E., et al. (2017). Analysis of the in vitro degradation and the in vivo tissue response to bi-layered 3D-printed scaffolds combining PLA and biphasic PLA/bioglass components - Guidance of the inflammatory response as basis for osteochondral regeneration. *Bioact. Mater.* 2, 208–223. doi: 10.1016/j.bioactmat.2017.06.001

Drago, L., De Vecchi, E., Bortolin, M., Toscano, M., Mattina, R., and Romano, C. L. (2015). Antimicrobial activity and resistance selection of different bioglass S53P4 formulations against multidrug resistant strains. *Future Microbiol.* 10, 1293–1299. doi: 10.2217/FMB.15.57

Elnaghy, A. M. (2014). Influence of acidic environment on properties of biodentine and white mineral trioxide aggregate: a comparative study. *J. Endod.* 40, 953–957. doi: 10.1016/j.joen.2013.11.007

Farano, V., Maurin, J. C., Attik, N., Jackson, P., Grosgogeat, B., and Gritsch, K. (2019). Sol-gel bioglasses in dental and periodontal regeneration: a systematic review. *J. Biomed. Mater. Res. B Appl. Biomater.* 107, 1210–1227. doi: 10.1002/jbm.b.34214

Gomez-Cerezo, N., Casarrubios, L., Saiz-Pardo, M., Ortega, L., de Pablo, D., Diaz-Guemes, I., et al. (2019). Mesoporous bioactive glass/varepsilon-polycaprolactone scaffolds promote bone regeneration in osteoporotic sheep. *Acta Biomater.* 90, 393–402. doi: 10.1016/j.actbio.2019.04.019

Gong, W., Huang, Z., Dong, Y., Gan, Y., Li, S., Gao, X., et al. (2014). Ionic extraction of a novel nano-sized bioactive glass enhances differentiation and mineralization of human dental pulp cells. *J. Endod.* 40, 83–88. doi: 10.1016/j.joen.2013.08.018

He, Z., Chen, L., Hu, X., Shimada, Y., Otsuki, M., Tagami, J., et al. (2017). Mechanical properties and molecular structure analysis of subsurface dentin after Er:YAG laser irradiation. *J. Mech. Behav. Biomed. Mater* 74, 274–282. doi: 10.1016/j.jmbbm.2017.05.036

Hench, L. L., and Jones, J. R. (2015). Bioactive glasses: frontiers and challenges. *Front. Bioeng. Biotechnol.* 3:194. doi: 10.3389/fbioe.2015.00194

Hench, L. L., and Polak, J. M. (2002). Third-generation biomedical materials. *Science* 295, 1014–1017. doi: 10.1126/science.1067404

Hirose, Y., Yamaguchi, M., Kawabata, S., Murakami, M., Nakashima, M., Gotoh, M., et al. (2016). Effects of extracellular pH on dental pulp cells in vitro. *J. Endod.* 42, 735–741. doi: 10.1016/j.joen.2016.01.019

Hojo, S., Komatsu, M., Okuda, R., Takahashi, N., and Yamada, T. (1994). Acid profiles and pH of carious dentin in active and arrested lesions. *J. Dent. Res.* 73, 1853–1857. doi: 10.1177/00220345940730121001

Hu, Q., Jiang, W. H., Li, Y. L., Chen, X. F., Liu, J. M., Chen, T., et al. (2018). The effects of morphology on physicochemical properties, bioactivity and biocompatibility of micro-/nano-bioactive glasses. *Adv. Powder Technol.* 29, 1812–1819. doi: 10.1016/j.apt.2018.04.017

Hu, Q., Li, Y. L., Miao, G. H., Zhao, N. R., and Chen, X. F. (2014). Size control and biological properties of monodispersed mesoporous bioactive glass submicron spheres. *RSC Adv.* 4, 22678–22687. doi: 10.1039/c4ra01276c

Jung, C., Kim, S., Sun, T., Cho, Y. B., and Song, M. (2019). Pulp-dentin regeneration: current approaches and challenges. *J. Tissue Eng.* 10:2041731418819263. doi: 10.1177/2041731418819263

Kargozar, S., Montazerian, M., Hamzehlou, S., Kim, H. W., and Baino, F. (2018). Mesoporous bioactive glasses: promising platforms for antibacterial strategies. *Acta Biomater.* 81, 1–19. doi: 10.1016/j.actbio.2018.09.052

Lee, S. J., Monsef, M., and Torabinejad, M. (1993). Sealing ability of a mineral trioxide aggregate for repair of lateral root perforations. *J. Endod.* 19, 541–544. doi: 10.1016/S0099-2399(06)81282-3

Lei, B., Chen, X. F., Han, X., and Zhou, J. A. (2012). Versatile fabrication of nanoscale sol-gel bioactive glass particles for efficient bone tissue regeneration. *J. Mater. Chem.* 22, 16906–16913. doi: 10.1039/c2jm31384g

Li, R., Clark, A. E., and Hench, L. L. (1991). An investigation of bioactive glass powders by sol-gel processing. *J. Appl. Biomater.* 2, 231–239. doi: 10.1002/jab.770020403

Li, Y. L., Liang, Q. M., Lin, C., Li, X., Chen, X. F., and Hu, Q. (2017). Facile synthesis and characterization of novel rapid-setting spherical sub-micron bioactive glasses cements and their biocompatibility in vitro. *Mater. Sci. Eng. C Mater. Biol. Appl.* 75, 646–652. doi: 10.1016/j.msec.2017.02.095

Lin, R., Deng, C., Li, X., Liu, Y., Zhang, M., Qin, C., et al. (2019). Copper-incorporated bioactive glass-ceramics inducing anti-inflammatory phenotype and regeneration of cartilage/bone interface. *Theranostics* 9, 6300–6313. doi: 10.7150/thno.36120

Loesche, W. J. (1996). "Microbiology of dental decay and periodontal disease," in *Medical Microbiology*, ed. S. Baron (Galveston, TX: University of Texas Medical Branch).

Lovelace, T. B., Mellonig, J. T., Meffert, R. M., Jones, A. A., Nummikoski, P. V., and Cochran, D. L. (1998). Clinical evaluation of bioactive glass in the treatment of periodontal osseous defects in humans. *J. Periodontol.* 69, 1027–1035. doi: 10.1902/jop.1998.69.9.1027

Marquardt, L. M., Day, D., Sakiyama-Elbert, S. E., and Harkins, A. B. (2014). Effects of borate-based bioactive glass on neuron viability and neurite extension. *J. Biomed. Mater. Res. A* 102, 2767–2775. doi: 10.1002/jbm.a.34944

Miura, M., Gronthos, S., Zhao, M., Lu, B., Fisher, L. W., Robey, P. G., et al. (2003). SHED: stem cells from human exfoliated deciduous teeth. *Proc. Natl. Acad. Sci. U.S.A.* 100, 5807–5812. doi: 10.1073/pnas.0937635100

Niederman, R., Buyle-Bodin, Y., Lu, B. Y., Robinson, P., and Naleway, C. (1997). Short-chain carboxylic acid concentration in human gingival crevicular fluid. *J. Dent. Res.* 76, 575–579. doi: 10.1177/00220345970760010801

Parirokh, M., and Torabinejad, M. (2010). Mineral trioxide aggregate: a comprehensive literature review–Part III: clinical applications, drawbacks, and mechanism of action. *J. Endod.* 36, 400–413. doi: 10.1016/j.joen.2009.09.009

Parirokh, M., Torabinejad, M., and Dummer, P. M. H. (2018). Mineral trioxide aggregate and other bioactive endodontic cements: an updated overview - part I: vital pulp therapy. *Int. Endod. J.* 51, 177–205. doi: 10.1111/iej.12841

Pushpa, S., Maheshwari, C., Maheshwari, G., Sridevi, N., Duggal, P., and Ahuja, P. (2018). Effect of pH on solubility of white mineral trioxide aggregate and biodentine: an in vitro study. *J. Dent. Res. Dent. Clin. Dent. Prospects* 12, 201–207. doi: 10.15171/joddd.2018.031

Rahaman, M. N., Day, D. E., Bal, B. S., Fu, Q., Jung, S. B., Bonewald, L. F., et al. (2011). Bioactive glass in tissue engineering. *Acta Biomater.* 7, 2355–2373. doi: 10.1016/j.actbio.2011.03.016

Rismanchian, M., Khodaeian, N., Bahramian, L., Fathi, M., and Sadeghi-Aliabadi, H. (2013). In-vitro comparison of cytotoxicity of two bioactive glasses in micropowder and nanopowder forms. *Iran J. Pharm. Res.* 12, 437–443.

Schepers, E., Declercq, M., Ducheyne, P., and Kempeneers, R. (1991). Bioactive glass particulate material as a filler for bone-lesions. *J. Oral Rehabil.* 18, 439–452. doi: 10.1111/j.1365-2842.1991.tb01689.x

Schmalz, G., and Smith, A. J. (2014). Pulp development, repair, and regeneration: challenges of the transition from traditional dentistry to biologically based therapies. *J. Endod.* 40(4 Suppl.), S2–S5. doi: 10.1016/j.joen.2014.01.018

Schwartz, A. G., Pasteris, J. D., Genin, G. M., Daulton, T. L., and Thomopoulos, S. (2012). Mineral distributions at the developing tendon enthesis. *PLoS One* 7:e48630. doi: 10.1371/journal.pone.0048630

Shah, D., Lynd, T., Ho, D., Chen, J., Vines, J., Jung, H. D., et al. (2020). Pulp-dentin tissue healing response: a discussion of current biomedical approaches. *J. Clin. Med.* 9:434. doi: 10.3390/jcm9020434

Skallevold, H. E., Rokaya, D., Khurshid, Z., and Zafar, M. S. (2019). Bioactive glass applications in dentistry. *Int. J. Mol. Sci.* 20:960. doi: 10.3390/ijms20235960

Vichery, C., and Nedelec, J. M. (2016). Bioactive glass nanoparticles: from synthesis to materials design for biomedical applications. *Materials* 9:288. doi: 10.3390/ma9040288

Wang, L., Pathak, J. L., Liang, D., Zhong, N., Guan, H., Wan, M., et al. (2020). Fabrication and characterization of strontium-hydroxyapatite/silk fibroin biocomposite nanospheres for bone-tissue engineering applications. *Int. J. Biol. Macromol.* 142, 366–375. doi: 10.1016/j.ijbiomac.2019.09.107

Wang, S., Gao, X., Gong, W., Zhang, Z., Chen, X., and Dong, Y. (2014). Odontogenic differentiation and dentin formation of dental pulp cells under nanobioactive glass induction. *Acta Biomater.* 10, 2792–2803. doi: 10.1016/j.actbio.2014.02.013

Yu, H., Peng, J., Xu, Y., Chang, J., and Li, H. (2016). Bioglass activated skin tissue engineering constructs for wound healing. *ACS Appl. Mater. Interf.* 8, 703–715. doi: 10.1021/acsami.5b09853

Yu, X., Wan, Q., Ye, X., Cheng, Y., Pathak, J. L., and Li, Z. (2019). Cellular hypoxia promotes osteogenic differentiation of mesenchymal stem cells and bone defect healing via STAT3 signaling. *Cell Mol. Biol. Lett.* 24:64. doi: 10.1186/s11658-019-0191-8

Zeng, D., Zhang, X., Wang, X., Huang, Q., Wen, J., Miao, X., et al. (2018). The osteoimmunomodulatory properties of MBG scaffold coated with amino functional groups. *Artif. Cells Nanomed. Biotechnol.* 46, 1425–1435. doi: 10.1080/21691401.2017.1369428

Zhao, F., Xie, W., Zhang, W., Fu, X., Gao, W., Lei, B., et al. (2018). 3D printing nanoscale bioactive glass scaffolds enhance osteoblast migration and extramembranous osteogenesis through stimulating immunomodulation. *Adv. Healthc. Mater.* 7:e1800361. doi: 10.1002/adhm.201800361

Zhou, H. M., Shen, Y., Wang, Z. J., Li, L., Zheng, Y. F., Hakkinen, L., et al. (2013). In vitro cytotoxicity evaluation of a novel root repair material. *J. Endod.* 39, 478–483. doi: 10.1016/j.joen.2012.11.026

Zhou, Y., Han, S., Xiao, L., Han, P., Wang, S., He, J., et al. (2018). Accelerated host angiogenesis and immune responses by ion release from mesoporous bioactive glass. *J. Mater. Chem. B* 6, 3274–3284. doi: 10.1039/c8tb00683k

Zhu, L., Luo, D., and Liu, Y. (2020). Effect of the nano/microscale structure of biomaterial scaffolds on bone regeneration. *Int. J. Oral Sci.* 12:6. doi: 10.1038/s41368-020-0073-y

Conflict of Interest: The authors declare that the research was conducted in the absence of any commercial or financial relationships that could be construed as a potential conflict of interest.

frontiers in Materials

ORIGINAL RESEARCH
published: 15 October 2020
doi: 10.3389/fmats.2020.582395

Physicochemical Properties of Experimental Resin-Based Materials Containing Fluoridated Calcium Phosphates

*Victor P. Feitosa[1], Levy S. Pinheiro[2], Maria Elisa M. Moura[2], Diego M. De-Paula[1], Adyson H. Alves[1], Lidiany Karla Rodrigues[2] and Salvatore Sauro[3]**

[1] Paulo Picanço School of Dentistry, Fortaleza, Brazil, [2] Post-Graduate Program in Dentistry, Department of Restorative Dentistry, Federal University of Ceará, Fortaleza, Brazil, [3] Dental Biomaterials, Departamento de Odontologia, Facultad de Ciencias de la Salud, CEU-Cardenal Herrera University, Valencia, Spain

The aim of this study was to evaluate the physicochemical properties of experimental adhesives containing tailored fluoridated calcium phosphate fillers. Five experimental resins were formulated, one contained no calcium phosphate filler (Control) and the other four resins contained 40 wt% of calcium phosphate fillers doped with increasing concentrations of fluoride: adhesives CaP (no fluoride), CaP-2F (2 wt% F), CaP-4F (4 wt% F), and CaP-8F (8 wt% F). Resin specimens were prepared for a three-point bending test to evaluate the elastic modulus (E) and flexural strength (FS) at 24 h and after 2 months of water storage. Disk-shaped specimens were prepared to analyze the water sorption (Ws) according to ISO 4049. The degree of conversion (DC) of the tested resins was also assessed through FTIR. Statistical analysis was performed with ANOVA and Tukey's test ($p < 0.05$). The addition of F-CaP particles at 0 and 2 wt% fluoride had no effect on the DC ($p > 0.05$) compared to the filler-free resin. However, these same experimental resins showed the highest E after water storage. All resins had a significant reduction of the FS after water storage ($p < 0.001$), but at a lower percentage rate for those experimental resins containing fluoride-free CaP or fluoride-doped CaP-2F. These latter experimental resins achieved similar Ws to control the filler-free resin. Conversely, those resins containing 4 or 8 wt% fluoride-doped CaP had a significant Ws increase ($p < 0.05$). In conclusion, the incorporation of calcium phosphate particles without fluoride or with 2 wt% fluoride may represent a promising strategy to generate adhesive resins with specific physicochemical properties. Fluoride incorporation in CaP fillers for dental resin adhesive should be performed at low concentrations in order to avoid excessive water sorption and a decrease of polymerization.

Keywords: fluoride, calcium phosphate, polymerization, water sorption, resin systems, mechanical properties, dental materials

OPEN ACCESS

Edited by:
Luis Alberto Loureiro Dos Santos, Federal University of Rio Grande do Sul, Brazil

Reviewed by:
Vicente Leitune, Federal University of Rio Grande do Sul, Brazil
Joanna Mystkowska, Bialystok University of Technology, Poland

****Correspondence:***
Salvatore Sauro
salvatore.sauro@uchceu.es

Specialty section:
This article was submitted to Biomaterials, a section of the journal Frontiers in Materials

Received: *11 July 2020*
Accepted: *13 August 2020*
Published: *15 October 2020*

Citation:
Feitosa VP, Pinheiro LS, Moura MEM, De-Paula DM, Alves AH, Rodrigues LK and Sauro S (2020) Physicochemical Properties of Experimental Resin-Based Materials Containing Fluoridated Calcium Phosphates. Front. Mater. 7:582395. doi: 10.3389/fmats.2020.582395

INTRODUCTION

Resin composite restorations are the foremost procedure in modern restorative dentistry as such materials present optimal esthetics and appropriate mechanical properties to replace those dental hard tissues that were lost for different causes (e.g., caries and tooth wear). Such a restorative approach allows for more conservative cavity preparations as resin composites can be bonded

directly onto dentin and enamel through the use of adhesive systems (Palaniappan et al., 2011; Van Meerbeek et al., 2020). Nevertheless, the bond between the adhesive and dentin is still characterized by issues related to the longevity of simplified adhesives (Hashimoto, 2010; Feitosa et al., 2014); the main cause for frequent failure/replacement of restorations (Ferracane, 2011; Demarco et al., 2017, Feitosa et al., 2019).

The dentin substrate is a highly heterogeneous dental tissue (overall 30 vol% organic components), characterized by differences in wetness and morphology/physiology, depending on its location and/or proximity to the pulp tissue (Marshall et al., 1997; Bertassoni et al., 2012). Bonding to dentin is still an important challenge due to the presence of dentinal tubules as well as the pulpal fluid, which make the use of hydrophilic monomers necessary to accomplish proper resin hybridization (Van Landuyt et al., 2008; Sauro et al., 2009, Van Meerbeek et al., 2020). Such hydrophilic components, if present in high concentration, can decrease the mechanical properties of adhesive resins (Ito et al., 2005), and increase water sorption (Feitosa et al., 2014), permeability (Sauro et al., 2009; Feitosa et al., 2019), and hydrolytic degradation (Ferracane, 2006; Sauro et al., 2019).

Severe degradation of the resin-dentin bonds occurs quite rapidly as it relies on the hydrolysis of unprotected collagen fibrils, principally when the bonding procedures were performed using simplified etch-and-rinse adhesives (Carrilho et al., 2007). In this regard, after finishing a composite restoration, the demineralized collagen that was not perfectly enveloped by the resin polymers of the adhesives is prone to hydrolytic degradation (Sauro and Pashley, 2016). Furthermore, the collagen breakdown might be accelerated by the activation of host-derived matrix metalloproteinases (MMPs) and cysteine cathepsins (Scaffa et al., 2012), thereby promoting significant resin-dentin degradation within a period of a few months after completing the composite restoration (Carrilho et al., 2007).

Although several enzyme inhibitors may be employed in order to increase the durability of dentin bonds (Scaffa et al., 2012; Van Meerbeek et al., 2020), one of the most promising strategies to decrease the degradation of the dentin collagen is based on a biomimetic remineralization of the dentine substrate (Tay and Pashley, 2008; Brackett et al., 2011, Sauro and Pashley, 2016). Such a technique may restore demineralized dentin collagen fibrils back to their natural (mineralized) stage through the deposition of nanophases of amorphous calcium phosphate (ACP) (Tay and Pashley, 2008; Sauro and Pashley, 2016). Several ion-releasing fillers have been incorporated to adhesive resins for this purpose, such as modified Portland cement (Profeta et al., 2012), bioactive glass (Sauro et al., 2012), and calcium silicate/polycarboxylate (Sauro and Pashley, 2016). Nevertheless, none of these fillers are able to form an acid-resistant fluoride-containing calcium phosphate (Xu et al., 2010). It has been advocated that the addition of fluoride may improve the anti-caries properties, thereby avoiding or reducing the incidence of secondary caries; it is one of the major reasons for the replacement of composite restorations (Andrade Neto et al., 2016).

The aim of this study was to evaluate some specific physicochemical properties, such as degree of conversion, water sorption, elastic modulus, and flexural strength of experimental resin adhesives containing tailored calcium phosphate fillers doped with fluoride at different concentrations (F-CaP). The hypothesis tested was that the incorporation of the experimental fillers tested in this study would not interfere with the physicochemical properties of the experimental resin adhesives.

MATERIALS AND METHODS

Experimental Adhesive and Inorganic Particles

A resin blend (control) was prepared by mixing bisphenol-A-glycidyl-dimethacrylate (BisGMA 20 wt%), urethane-dimethacrylate (UDMA, 27 wt%), triethylene-glycol-dimethacrylate (TEGDMA 25 wt%), hydroxy-ethyl-methacrylate (HEMA 5 wt%), and 20 wt% ethanol. After the mixture of monomers and solvent, a ternary photoinitiator system was dissolved comprising 0.5 wt% camphorquinone (photosensitizer), 1 wt% ethyl-dimethylamine-benzoate (coinitiator), and 1.5 wt% diphenyliodonium hexafluorophophate (accelerator). All reagents were mixed in a dark room at 25 °C and ultrasonicated for 10 min at the end to warrant adequate homogeneity to the blend.

The inorganic filler (CaP-F) was obtained by a specific reaction as previously reported (Sauro and Feitosa, 2019), which is a precursor of fluorapatite. In brief, a 1:1 molar ratio of beta-tricalcium phosphate (β-TCP) and monocalcium phosphate monohydrate (MCPM) were mixed with a 1:1 weight ratio of calcium and sodium fluorides in final concentrations of 5, 10, or 20%, to attain fillers with increasing concentration of fluoride. Four different micro fillers were incorporated (40 wt%) into the resin blend to create four experimental resins to obtain the materials with compositions that had different final concentrations of fluoride (0, 2, 4, 8 wt%) except for the control filler-free adhesive (Control). The calcium phosphate mixture without fluoride addition (CaP) was also tested. Fluoride containing groups were designated as CaP-2F, CaP-4F, and CaP-8F, according to the final concentration of fluoride (**Table 1**). All reagents were purchased from Sigma Aldrich Chemicals (Milwaukee, United States).

Degree of Conversion

The polymerization of each resin was assessed by means of a Fourier-transform infrared spectroscopy (FTIR Bruker

TABLE 1 | Spreading of groups and materials' compositions.

	Resin	CaP	(NaF + CaF_2)
Control	100%	_	_
CaP	60%	40%	_
CaP-2F	60%	38%	2%
CaP-4F	60%	36%	4%
CaP-8F	60%	32%	8%

Spectrometer, Bruker, Bremen, Germany), equipped with a crystal of attenuated total reflectance (ATR). The distance between the light-curing tip and the adhesive drop was standardized at 2 mm. Each drop (0.3 μL) was dispensed directly onto the ATR crystal, providing a similar height of adhesive resin and the spectra (1580–1660 cm^{-1}) of uncured resins were detected at 4 cm^{-1} resolution and 32 scans. After light-curing using a LED unit (DB 685, Dabi Atlante, São Paulo, Brazil) for 40 s at 1100 mW/cm^2 irradiance, the spectra of the polymerized adhesives were also evaluated. Each material (Control, CaP, CaP-2F, CaP-4F, and CaP-8F) was surveyed in triplicate. The degree of conversion was obtained by calculating the ratio between the peak (height) 1635 cm^{-1} (aliphatic C = C double bond) and 1608 cm^{-1} (aromatic C = C double bond as internal reference) (Andrade Neto et al., 2016). Data were statistically analyzed by a Shapiro-Wilk normality test ($p > 0.05$) and after the normalization of the data was confirmed, these were analyzed by one-way ANOVA and Tukey's test ($p < 0.05$).

Specimens Preparation

Bar-shaped specimens (2 mm width, 1 mm thickness, and 7 mm length) were prepared for a three-point bending test, whilst disk-shaped specimens (1 mm thickness and 7 mm diameter) were prepared for the assessment of the water sorption of the tested materials. All specimens were dispensed in pre-fabricated silicone molds following the indication of ISO 4049, except for the dimensions of the specimens (Lopes et al., 2009). Each specimen was light-cured for 40 s using the LED curing system (DB 685, Dabi Atlante). All specimens were carefully removed from the molds and checked for defects using a stereomicroscope; those that presented voids, bubbles, or structural defects were discarded. Eight specimens per group ($n = 8$) were prepared for each test. They were kept dried for 24 h at 37°C to ensure a proper polymerization reaction.

Three-Point Bending Test

After 24 h storage at 37°C, the flexural strength and modulus of the experimental bar-shaped specimens were obtained by three-point bending (5 mm distance between the supports) in a universal testing machine (Instron 3345, Canton, United States) using a 500 N load cell. The test was monitored by the Bluehill 2 software (Instron), which generated a stress/strain graph that allowed for the detection of an elastic (flexural) modulus and maximum flexural strength. Specimens were prepared and tested after 24 h (dried) and further specimens were immersed for 2 months in distilled water and tested as described earlier after water storage. Data attained were statistically analyzed by a Shapiro-Wilk normality test and after confirming the normalization of the data, a two-way ANOVA as well as a Tukey's test was performed ($\alpha = 5\%$).

Water Sorption

The protocol for water sorption assessment was in accordance with the ISO 4049. Disk-shaped specimens were measured using a digital caliper and the volume of each specimen was calculated. Thereafter, they were dehydrated in a vacuum chamber with silica gel. They were weighed daily in a precision balance (0.01 mg, Mitutoyo, Tokyo, Japan) until the weight stabilized with no change within the next 6 days. This initial weight (M1) was established and the specimens were individually immersed in 1.5 mL of distilled water at 37°C for one week. The weight after immersion (M2) was rapidly detected avoiding dehydration. Following, the specimens were kept again in the drying chamber for a period of approximately three weeks until stabilization of the weight (M3). The water sorption results were obtained using the formula (M2-M3)/V. Data were statistically analyzed by a Shapiro-Wilk normality test. After normal data was confirmed, the results were analyzed by a one-way ANOVA and a Tukey's test ($p < 0.05$).

RESULTS

The results of the degree of conversion (DC) are presented in **Figure 1A**. The highest DC was attained with the adhesive resin containing no filler (78.1%), and it was significantly different ($p < 0.001$) compared to CaP-4F and CaP-8F; these latter two materials attained the lowest degree of conversion. The adhesive resin containing the fluoride-free calcium phosphates (CaP) and that doped with 2 wt% fluoride (CaP-2F) achieved similar DC values to the control filler-free resin ($p = 0.439$ and $p = 0.596$, respectively). The results of maximum flexural strength are presented in **Table 2**. The statistical interaction between factors was significant ($p < 0.001$). After water storage, the flexural strength of all adhesive resins presented a significant reduction ($p < 0.001$). However, a lower reduction (%) was observed in the groups CaP and CaP-2F, while a greater reduction was observed in the control group (filler-free adhesive resin) (**Table 2**). Regarding the initial flexural strength, the incorporation of calcium phosphate fillers with and without fluoride induced an overall decrease compared to the control filler-free resin ($p < 0.05$). In particular, there was a greater reduction in the resins with fillers containing fluoride, rather than the resin containing the fluoride-free calcium phosphate fillers (CaP). Moreover, after prolonged water storage, the highest flexural strength was detected with the resin containing fluoride-free CaP (52.4 MPa), while the lowest values were observed in the group CaP-8F (27.3 MPa).

The results of the flexural modulus are presented in **Table 3**. The interaction between factors was statistically significant ($p < 0.001$). All the tested adhesive resins, except the specimens in group CaP-8F ($p = 0.139$), depicted an increase in the elastic modulus after prolonged water storage ($p < 0.001$). Moreover, an increase (%) of the modulus was evident in those experimental resins containing CaP-2F and CaP (**Table 3**). The initial highest flexural modulus was attained with the resin CaP-8F (513.2 MPa), whilst the lowest was observed with the 2 wt% resin (201.2 MPa). After water storage, the highest modulus was detected in the CaP group, followed by the specimens in group CaP-2F.

The outcomes of water sorption are depicted in **Figure 1B**. Higher water sorption was observed in the resin adhesive CaP-8F (111.3 $\mu g/mm^3$), followed by the resin CaP-4F; both presented values significantly higher than the control filler-free resin, CaP, and CaP-2F ($p = 0.0154$, $p = 0.0308$, and $p = 0.0127$,

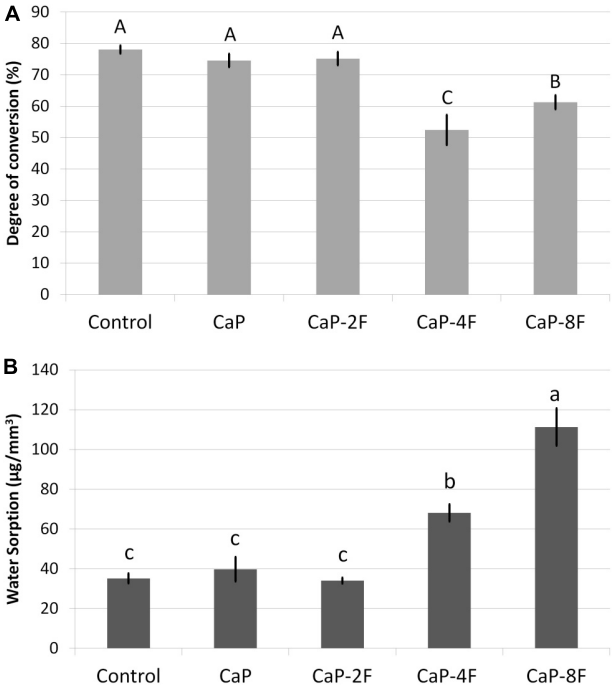

FIGURE 1 | Means (standard deviations) of the degree of conversion (%) in **(A)** and water sorption ($\mu g/mm^3$) in **(B)**. Different letters indicate statistical difference ($p < 0.05$).

TABLE 2 | Means (standard deviations) of maximum flexural strength (MPa).

Flexural strength	24 h	2 months	% Variation
Control	117.9 (10.1) A, a	35.3 (5.6) BC, b	−70.1
CaP	70.9 (4.7) B, a	52.4 (5.2) A, b	−26.1
CaP-2F	50.8 (7.7) C, a	36.3 (4.6) B, b	−28.6
CaP-4F	51.8 (5.6) C, a	32.8 (5.7) BC, b	−36.7
CaP-8F	57.3 (4.8) C, a	27.3 (3.5) C, b	−52.3

Different capital letters in column and different lower case letters in row indicate statistical difference ($p < 0.05$).

TABLE 3 | Means (standard deviations) of elastic modulus (MPa).

Elastic modulus (MPa)	24 h	2 months	% Variation
Control	267.5 (28.7) BC, a	464.5 (44.4) D, b	+ 73.6
CaP	314.4 (64.8) B, a	904.3 (104.6) A, b	+ 187.6
CaP-2F	201.2 (47.0) C, a	757.4 (79.8) B, b	+ 276.4
CaP-4F	261.9 (41.3) BC, a	604.5 (85.1) C, b	+ 130.7
CaP-8F	513.2 (41.7) A, a	464.8 (68.5) D, a	−9.4

Different capital letters in column and different lower case letters in row indicate statistical difference ($p < 0.05$).

respectively). The incorporation of calcium phosphate fillers (CaP) and those with only 2 wt% fluoride had no influence on the water sorption compared to the filler-free control resin ($p = 0.693$ and $p = 0.915$, respectively).

DISCUSSION

An optimal degree of conversion is essential for dental resins to obtain adequate mechanical properties as well as chemical stability. Several properties such as compressive strength, wear resistance, fracture toughness, water sorption, and solubility may be affected by "poor" polymerization; this can also affect the clinical longevity of resin-based restorative materials (Calheiros et al., 2008). In the present study, experimental adhesives containing bioactive fillers with high concentrations of fluoride (CaP-4F and CaP-8F) presented a lower degree of conversion in comparison with those containing a filler with a lower concentration of fluoride (CaP-2F, CaP) and the control filler-free adhesive. These findings are in agreement with those of Shinohara et al. (2009) who demonstrated a similar degree of conversion between the fluoride-containing Clearfil Protect Bond and the fluoride-free Clearfil SE Bond. Both adhesives possess very similar chemical compositions, but the Protect Bond releases fluoride (from inorganic particles) and contains an antibacterial monomer. Indeed, the outcomes reported by Shinohara et al. (2009) showed a significant reduction of the degree of conversion between the adhesive resin containing fluoride (DC: 50-60%) and the fluoride-free adhesive, which achieved a degree of conversion of 70-80%.

Fluorine is a well-known highly electronegative chemical element; in other words, fluoride has a great potential to attract electrons. In this regard, during the polymerization reaction, fluoride ions may promote a certain inhibition (Tjaderhane et al., 2013) on the free-radical polymerization reaction due to partial inactivation of unpaired electrons. Based on the present results, it was observed that only fluoride concentrations higher than 2 wt% were able to induce significant inhibition of the polymerization in the experimental adhesives tested in this study (**Figure 1A**).

Flexural strength is comprised of a wide variety of tensions such as compression, shear, and tensile. The clinical relevance of this mechanical property relies on different tensions that dental materials undergo during chewing. The results of the current investigation demonstrated a decrease in flexural strength after 2 months of water storage for all the resin-based materials tested in this study. However, such a degradation rate was notably lower for those resins containing fluoride-free calcium phosphates (CaP) or 2 wt% fluoride (CaP-2F). Conversely, the greatest degradation was observed in the control filler-free resin and the resin containing calcium phosphates with 8 wt% fluoride (CaP-8F) (**Table 2**). The initial high flexural strength of CaP-8F, even with a lower degree of conversion, may be related to the high strength of fillers containing high amount of fluoride. Nevertheless, after water storage and a loss of fluoride from these fillers, the drop in flexural strength was expected, as the fillers become more porous.

A possible explanation to justify the reduction in the flexural strength of the tested materials might be in part related to the DC of the polymeric chain, as well as to the hydrolytic degradation of polymers (Ferracane, 2006; Feitosa et al., 2013, 2019) due to breakdown of ester bonds in methacrylate monomers. Such a situation may have been caused by water uptake, which is usually triggered by the presence

of hydrophilic monomers such as hydroxyl-ethyl-methacrylate (HEMA) (Van Landuyt et al., 2008; Van Meerbeek et al., 2020). However, the inorganic chemical reaction between the water and the bioactive calcium phosphate fillers may have reduced the polymer degradation. The rationale behind this hypothesis is that the water may have been absorbed by the filler for a successive bioactive reaction [$Ca(H_2PO_4)_2.H_2O + Ca_3(PO_4)_2 + 7H_2O -> 4\ CaHPO_4.2H_2O$], rather than leaving it available for polymer chains breakdown (Sauro et al., 2012).

In this study, we intentionally added small amounts of HEMA to promote water uptake and demonstrate the protective effect of the calcium phosphate particles. Nevertheless, with the addition of a high percentage of fluoride (i.e., 8 wt%) a higher release of this ion might be expected, but with a concomitant intense drop in mechanical properties (**Table 2**).

Regarding the elastic (flexural) modulus, only the resin with calcium phosphates and 8 wt% fluoride (CaP-8F) presented a reduction after two-month water storage. We speculate that such a situation may have been caused by high solubility of those specific resins, which in turn may have jeopardized the mechanical properties of the experimental resins (**Table 3**). Conversely, the increase of the elastic modulus observed in the other tested resin-based materials could be due to the fact that the fillers used in those materials transformed into more complex forms of calcium phosphates such as fluorapatite and hydroxyapatite (Sauro and Feitosa, 2019). Such a crystallization process may have contributed to the increase of the elastic modulus after water storage; this was significantly higher for CaP and CaP-2F than the control filler-free resin (**Table 3**).

Moreover, it was also found in a previous investigation (Ito et al., 2005) that the leaching of unreacted monomers and water uptake may provide the formation of hydrogen bonds, particularly with BisGMA (Stansbury, 2012), leading to higher rigidity of the polymer after water storage.

Water sorption in resin composites is a process of water diffusion principally through the organic resin matrix (Ferracane, 2006). Although water sorption is characterized by a multifactorial process, water uptake occurs mostly due to the hydrophilic nature of monomeric units (Ito et al., 2005; Sauro et al., 2019; Van Meerbeek et al., 2020). When one analyzes the results in **Figure 1**, it is possible to note that the higher the degree of conversion, the lower the water sorption. Therefore, also in this case, the extent of polymerization may play an important role on the water sorption of an adhesive resin. Control resin, CaP, and CaP-2F presented the highest degree of conversion (**Figure 1A**) and, consequently, they depicted the lowest water sorption (**Figure 1B**). Even though control, CaP, and CaP-2F demonstrated similar water sorption ($p < 0.05$), adhesives containing calcium phosphate particles did uptake more water due to the aforementioned inorganic reaction. Conversely, the water absorbed by the control group is the actual water sorption that might induce degradation and jeopardize mechanical properties. Thus, although the measured water sorption was similar, lower degradation and reduction on mechanical properties could be expected with the addition of these particular calcium phosphate fillers, with or without fluoride (**Tables 2**, **3**). Since higher concentrations of fluoride (8 wt%) were detrimental to the physicochemical properties of experimental adhesives, the study hypothesis needs to be rejected.

CONCLUSION

Calcium phosphate fillers without fluoride and with 2 wt% fluoride may attain the best physicochemical property outcomes for experimental adhesives. These particles present a lower reduction in flexural strength after water storage, did not interfere on the degree of conversion, and presented the best elastic modulus and similar water sorption to the control filler-free resin. Therefore, within the limitations of this investigation, we can affirm that our calcium phosphate fillers with low concentrations of fluoride may be the ideal choice to create a bioactive adhesive system, without impairing the physicochemical properties of the resin-based material.

DATA AVAILABILITY STATEMENT

The raw data supporting the conclusions of this article will be made available by the authors, without undue reservation.

AUTHOR CONTRIBUTIONS

VF performed project supervision, funding acquisition, formal analysis, and drafting the manuscript. LP performed experiments and drafted the manuscript. MM performed investigation, methodology, and data analysis. DD-P performed methodology and degree of conversion investigation. AA performed funding acquisition and experimental analyses. LR wrote and reviewed and edited the manuscript. SS performed project administration, writing up, and review and editing. All authors contributed to the article and approved the submitted version.

REFERENCES

Andrade Neto, D. M., Carvalho, E. V., Rodrigues, E. A., Feitosa, V. P., Sauro, S., Mele, G., et al. (2016). Novel hydroxyapatite nanorods improve anti-caries efficacy of enamel infiltrants. *Dent. Mater.* 32, 784–793. doi: 10.1016/j.dental.2016.03.026

Bertassoni, L. E., Orgel, J. P., Antipova, O., and Swain, M. V. (2012). The dentin organic matrix - limitations of restorative dentistry hidden on the nanometer scale. *Acta Biomater.* 8, 2419–2433. doi: 10.1016/j.actbio.2012.02.022

Brackett, M. G., Li, N., Brackett, W. W., Sword, R. J., Qi, Y. P., Niu, L. N., et al. (2011). The critical barrier to progress in dentin bonding with the etch-and-rinse technique. *J. Dent.* 2011, 238–248. doi: 10.1016/j.jdent.2010.12.009

Calheiros, F. C., Daronch, M., Rueggeberg, F. A., and Braga, R. R. (2008). Degree of conversion and mechanical properties of a BisGMA:TEGDMA composite as a function of the applied radiant exposure. *J. Biomed. Mater. Res. B. Appl. Biomater.* 84, 503–509. doi: 10.1002/jbm.b.30897

Carrilho, M. R., Geraldeli, S., Tay, F. R., Goes, M. F., Carvalho, R. M., Tjaderhane, L., et al. (2007). In vivo preservation of the hybrid layer by chlorhexidine. *J. Dent. Res.* 86, 529–533. doi: 10.1177/154405910708600608

Demarco, F. F., Collares, K., Correa, M. B., Cenci, M. S., Moraes, R. R., and Opdam, N. J. (2017). Should my composite restorations last forever? Why are they failing?. *Braz. Oral. Res.* 31(Suppl. 1):e56. doi: 10.1590/1807-3107BOR-2017.vol31.0056

Demarco, F. F., Corrêa, M. B., Cenci, M. S., Moraes, R. R., and Opdam, N. J. (2012). Longevity of posterior composite restorations: not only a matter of materials. *Dent. Mater.* 28, 87–101. doi: 10.1016/j.dental.2011.09.003

Feitosa, V. P., Bazzocchi, M. G., Putignano, A., Orsini, G., Luzi, A. L., Sinhoreti, M. A. C., et al. (2013). Dicalcium phosphate (CaHPO4·2H2O) precipitation through ortho- or meta-phosphoric acid-etching: effects on the durability and nanoleakage/ultra-morphology of resin-dentine interfaces. *J. Dent.* 41, 1068–1080. doi: 10.1016/j.jdent.2013.08.014

Feitosa, V. P., Sauro, S., Ogliari, F. A., Stansbury, J. W., Carpenter, G. H., Watson, T. F., et al. (2014). The role of spacer carbon chain in acidic functional monomers on the physicochemical properties of self-etch dental adhesives. *J. Dent.* 42, 565–574. doi: 10.1016/j.jdent.2014.02.009

Feitosa, V. P., Sauro, S., Zenobi, W., Silva, J. C., Abuna, G., Van Meerbeek, B., et al. (2019). Degradation of adhesive-dentin interfaces created using different bonding strategies after five-year simulated pulpal pressure. *J. Adhes. Dent.* 21, 199–207. doi: 10.3290/j.jad.a42510

Ferracane, J. L. (2006). Hygroscopic and hydrolytic effects in dental polymer networks. *Dent. Mater.* 22, 211–22. doi: 10.1016/j.dental.2005.05.005

Ferracane, J. L. (2011). Resin composite – State of the art. *Dent. Mater.* 27, 29–38. doi: 10.1016/j.dental.2010.10.020

Hashimoto, M. (2010). A review: micromorphological evidence of degradation in resin-dentin bonds and potential preventional solutions. *J. Biomed. Mater. Res. B. Appl. Biomater.* 92, 268–280. doi: 10.1002/jbm.b.31535

Ito, S., Hashimoto, M., Wadgaonkar, B., Svizero, N., Carvalho, R. M., Yiu, C., et al. (2005). Effects of resin hydrophilicity on water sorption and changes in modulus of elasticity. *Biomaterials* 26, 6449–6459. doi: 10.1016/j.biomaterials.2005.04.052

Lopes, M. B., Moraes, R. R., Gonini-Junior, A., and Piva, E. (2009). Impact of curing protocol on the selected properties of a model bis-GMA/TEGDMA dental resin composite. *Biomed. Mater.* 4:025014. doi: 10.1088/1748-6041/4/2/025014

Marshall, G. W., Marshall, S. J., Kinney, J. H., and Salooch, M. (1997). The dentin substrate: structure and properties related to bonding. *J. Dent.* 25, 441–458. doi: 10.1016/s0300-5712(96)00065-6

Palaniappan, S., Bharadwaj, D., Mattar, D. L., Peumans, M., Van Meerbeek, B., and Lambrechts, P. (2011). Nanofilled and microhybrid composite restorations: Five-year clinical wear performances. *Dent. Mater.* 27, 692–700. doi: 10.1016/j.dental.2011.03.012

Profeta, A. C., Mannocci, F., Foxton, R. M., Thompson, I., Watson, T. F., and Sauro, S. (2012). Bioactive effects of a calcium/sodium phosphosilicate on the resin-dentin interface: a microtensile bond strength, scanning electron microscopy, and confocal microscopy study. *Eur. J. Oral Sci.* 120, 353–362. doi: 10.1111/j.1600-0722.2012.00974.x

Sauro, S., and Feitosa, V. P. (2019). *Preparation, Composition and Application of a Bioactive Fluoride-Doped Calcium Phosphate Able to Induce Controlled Deposition of Fluorapatite*. W.O. Patent No 2019/243592 A1. Geneva: World Intellectual Property Organization.

Sauro, S., Makeeva, I., Faus-Matoses, V., Foschi, F., Giovarruscio, M., Pires, P. M., et al. (2019). Effects of ions-releasing restorative materials on the dentine bonding longevity of modern universal adhesives after load-cycle and prolonged artificial saliva aging. *Materials* 12:722. doi: 10.3390/ma12050722

Sauro, S., Mannocci, F., Toledano, M., Osorio, R., Thompson, I., and Watson, T. F. (2009). Influence of the hydrostatic pulpal pressure on droplets formation in current etch-and-rinse and self-etch adhesives: a video rate/TSM microscopy and fluid filtration study. *Dent. Mater.* 25, 1392–1402. doi: 10.1016/j.dental.2009.06.010

Sauro, S., Osorio, R., Watson, T. F., and Toledano, M. (2012). Therapeutic effects of novel resin bonding systems containing bioactive glasses on mineral-depleted areas within the bonded-dentin interface. *J. Mater. Sci. Mater. Med.* 23, 1521–1532. doi: 10.1007/s10856-012-4606-6

Sauro, S., and Pashley, D. H. (2016). Strategies to stabilise dentine-bonded interfaces through remineralising operative approaches – State of the art. *Int. J. Adhesion Adhes.* 69, 39–57. doi: 10.1016/j.ijadhadh.2016.03.014

Scaffa, P. M., Vidal, C. M., Barros, N., Gesteira, T. F., Carmona, A. K., Breschi, L., et al. (2012). Chlorhexidine inhibits the activity of dental cysteine cathepsins. *J. Dent. Res.* 91, 420–425. doi: 10.1177/0022034511435329

Shinohara, M. S., De Goes, M. F., Schneider, L. F., Ferracane, J. L., Pereira, P. N., Di Hipólito, V., et al. (2009). Fluoride-containing adhesive: durability on dentin bonding. *Dent. Mater.* 25, 1383–1391. doi: 10.1016/j.dental.2009.06.011

Stansbury, J. W. (2012). Dimethacrylate network formation and polymer property evolution as determined by the selection of monomers and curing conditions. *Dent. Mater.* 28, 13–22. doi: 10.1016/j.dental.2011.09.005

Tay, F. R., and Pashley, D. H. (2008). Guided tissue remineralisation of partially demineralised human dentin. *Biomaterials* 29, 1127–1137. doi: 10.1016/j.biomaterials.2007.11.001

Tjaderhane, L., Nascimento, F. D., Breschi, L., Mazzoni, A., Tersariol, I. L., Geraldeli, S., et al. (2013). Optimizing dentin bond durability: control of collagen degradation by matrix metalloproteinases and cysteine. *Dent. Mater.* 29, 116–135. doi: 10.1016/j.dental.2012.08.004

Van Landuyt, K. L., Snauwaert, J., Peumans, M., De Munck, J., Lambrechts, P., and Van Meerbeek, B. (2008). The role of HEMA in one-step self-etch adhesives. *Dent. Mater.* 24, 1412–1419. doi: 10.1016/j.dental.2008.02.018

Van Meerbeek, B., Yoshihara, K., Van Landuyt, K., Yoshida, Y., and Peumans, M. (2020). From Buonocore's pioneering acid-etch technique to self-adhering restoratives. a status perspective of rapidly advancing dental adhesive technology. *J. Adhes. Dent.* 22, 7–34. doi: 10.3290/j.jad.a43994

Xu, H. H., Weir, M. D., Sun, L., Moreau, J. L., Takagi, S., and Chow, L. C. (2010). Strong nanocomposites with Ca, PO4 and F release for caries inhibition. *J. Dent. Res.* 89, 19–28. doi: 10.1177/0022034509351969

Conflict of Interest: The authors declare that the research was conducted in the absence of any commercial or financial relationships that could be construed as a potential conflict of interest.

frontiers in Materials

ORIGINAL RESEARCH
published: 23 November 2020
doi: 10.3389/fmats.2020.583861

Pronounced Effect of Antibacterial Bioactive Dental Composite on Microcosm Biofilms Derived From Patients With Root Carious Lesions

Abdulrahman A. Balhaddad[1,2], *Maria S. Ibrahim*[1,3], *Isadora M. Garcia*[1,4], *Fabrício M. Collares*[4], *Michael D. Weir*[1,5], *Hockin H. Xu*[1,5]* *and Mary Anne S. Melo*[1,6]*

[1]*Ph.D. Program in Biomedical Sciences, University of Maryland School of Dentistry, Baltimore, MD, United States,* [2]*Department of Restorative Dental Sciences, Imam Abdulrahman Bin Faisal University, College of Dentistry, Dammam, Saudi Arabia,* [3]*Department of Preventive Dental Sciences, Imam Abdulrahman Bin Faisal University, College of Dentistry, Dammam, Saudi Arabia,* [4]*Department of Dental Materials, School of Dentistry, Federal University of Rio Grande do Sul, Porto Alegre, Brazil,* [5]*Biomaterials and Tissue Engineering Division, Department of Advanced Oral Sciences and Therapeutics, University of Maryland School of Dentistry, Baltimore, MD, United States,* [6]*Division of Operative Dentistry, Department of General Dentistry, University of Maryland School of Dentistry, Baltimore, MD, United States*

OPEN ACCESS

Edited by:
Hae-Won Kim,
Institute of Tissue Regeneration Engineering (ITREN), South Korea

Reviewed by:
Sergey V. Dorozhkin,
Independent Researcher, Moscow, Russia
Joanna Mystkowska,
Bialystok University of Technology, Poland

***Correspondence:**
Mary Anne S. Melo
mmelo@umaryland.edu
Hockin H. Xu
HXu@umaryland.edu

Specialty section:
This article was submitted to Biomaterials, a section of the journal Frontiers in Materials

Received: *15 July 2020*
Accepted: *28 October 2020*
Published: *23 November 2020*

Citation:
Balhaddad AA, Ibrahim MS, Garcia IM, Collares FM, Weir MD, Xu HH and Melo MAS (2020) Pronounced Effect of Antibacterial Bioactive Dental Composite on Microcosm Biofilms Derived From Patients With Root Carious Lesions. Front. Mater. 7:583861. doi: 10.3389/fmats.2020.583861

Resin composites are the material of choice for dental restorative treatment in oral health care. However, the inherent composition of this class of material commonly results in microbial adherence and colonization, which carries the potential risk of recurrent carious lesions around dental restorations. The high risk of resin composites failure complicates the treatment of root caries, defined as the onset of tooth decay over the prone root surface of a tooth. The restorative treatment of root caries among high caries risk individuals, especially for senior patients, is a challenging, painful, and costly. The dysbiotic microbiota colonizes the composite's surfaces and forms polymicrobial biofilms that are difficult to be dislodged by regular tooth brushing. This study assesses the antibiofilm performance of a surface contact killing antibacterial dental resin composites on the growth of microcosm biofilms using dental plaque sampled from patients with active root carious lesions as an inoculum. The designed formulations contain dimethylaminohexadecyl methacrylate (DMAHDM), a tailored quaternary ammonium monomer with an alkyl chain length of 16, at 3–5 wt.% in a base resin with and without 20 wt.% nanoparticles of amorphous calcium phosphate (NACP). Biofilms were grown on the tested resin composites using a 48 h plaque-derived microcosm biofilm model. Dental plaque collected from active root carious lesions was used as an inoculum to emulate the microbiota present in those lesions. The biofilm growth was assessed via the colony-forming unit (CFU) counts in four culture media, metabolic behavior, lactic acid production, and confocal microscopy. The percentage of reacted double bonds of the formulations was also investigated. The dental resin composites formulated with 3–5 wt.% DMAHDM and 20 wt.% NACP were effective at eradicating surface-attached biofilms from the total microbial load and each relevant cariogenic group: total *streptococci*, *mutans streptococci,* and *lactobacilli.* The metabolic activities and lactic acid production of the plaque-derived microcosm biofilms were reduced by 80–95%, respectively. Fewer viable microorganisms were observed over resin composites containing DMAHDM and NACP. Besides, all the experimental

formulations demonstrated an acceptable degree of conversion values. This new strategy fits with ongoing dental caries preventive and minimally invasive approaches by preventing biofilm growth over-restored carious root lesions and improving the lifespan of dental restorations.

Keywords: amorphous calcium phosphate, antibacterial agents, dental caries, polymerization, quaternary ammonium compounds, Amorphous calcium, Biomaterials, Antibacterial

INTRODUCTION

Dysbiotic biofilm-triggered mineral loss causes tooth cavitation, and it is the primary reason for the loss of tooth structure (Takahashi and Nyvad, 2016; Damé-Teixeira et al., 2017). When it is located at the root of a tooth, noted as "*root caries*," the onset of carious lesions could be accelerated due to multiple risk factors (Takahashi and Nyvad, 2016; Damé-Teixeira et al., 2017). Root caries is a preventable dental disease that affects a growing number of adults. The annual incidence of root caries ranged from 10.1 to 40.6%, with the highest-burden observed among elderly patients (Hayes et al., 2017a).

Root surfaces are at higher risk of biofilm-triggered mineral loss compared to enamel, as the cement and dentin, constituents of the root, hold lower mineral contents compared to the enamel. As a result, microorganisms involved in root caries are less dependent on carbohydrates, and less amount of pH drop is required to induce demineralization (Takahashi and Nyvad, 2016; Damé-Teixeira et al., 2017). Moreover, the location of the root surface close to the gingival margin and cementoenamel junction is considered a plaque-stagnation area, making it more difficult to be cleaned by brushing (Vandana and Haneet, 2014). As the present demographic shifts, the population of the United States over the age of 65 years is projected to increase from 13.5 to 20% in 2030 (The United States census bureau, 2019). Therefore, there is a demographic and oral health imperative to understand how to better care for senior dental patients who are at high risk of root caries (Gati and Vieira, 2011; Tonetti et al., 2017).

Currently, the standard of care on the management of root caries cavitation relies on restorative treatment by placing a circumferential "dental filling" to replace the missing root structure (Tan et al., 2017). Resin composite restorations can perform better in restoring root surfaces compared to glass ionomer and resin-modified glass ionomer restorations (Meyer-Lueckel et al., 2019). However, the survival rate of resin composite restorations in replacing the root surface is poor, as the annual failure rates reach 15% (Meyer-Lueckel et al., 2019).

One of the main reasons for restoration failure is secondary caries, especially around resin composite surfaces, which are more susceptible to plaque accumulation (Bourbia and Finer, 2018). Biofilms have specialized physiology where cells aggregate together and become encased in a self-produced polysaccharide and protein matrix that protects the cells from several oral environmental conditions (Khatoon et al., 2018). Resin composite restorations have no bioactivity and undergo several degradative effects caused by bacterial acids as well as salivary esterase (Delaviz et al., 2014). It is no longer sufficient for dental restorations to simply repair esthetics and function without providing protection against microorganisms and their associated biofilms. In this sense, dentists and dental material researchers worldwide have been perseveringly searching for restorative approaches that can contribute to the longevity of root caries restorative treatment (Gavriilidou and Belibasakis, 2019).

There is currently no approved dental composite that can effectively contribute to the protection of restorations against biofilm accumulation. However, several investigations were conducted to design a bioactive resin composite with antibacterial or ion-releasing properties (Cheng et al., 2012). The use of quaternary ammonium methacrylate, such as 12-methacryloyloxydodecylpyridinium bromide (MDPB) or bis(2-methacryloyloxyethyl) dimethylammonium bromide (QADM) was associated with slightly reduced growth of total microorganisms and caries-related pathogens (Melo et al., 2018). This class of monomers has a positive-charge surface that can interact with the negatively charged bacterial membrane causing cell wall disturbance and lysis (Zubris et al., 2017).

Importantly, these antibacterial monomers can copolymerize with other dental monomers to provide a long-lasting effect with no leaching adverse effects (Yuan et al., 2013). Holding the contact killing property based on bacterial membrane interactions, the recently developed antibacterial monomer, DMAHDM, had its synthesis tailored with a 16-alkyl chain to allow robust antibacterial action against cariogenic biofilms (Ibrahim et al., 2019); covalent bond with the commonly used Bis-GMA/TEGDMA dental resin system (Liang et al., 2014) and high surface charge density (Balhaddad et al., 2020).

In the course of investigating anti-caries approaches via dental materials, the understanding of caries as a dynamic process that shifts toward de- or remineralization has encouraged the incorporation of a potential resource for ion-depleted tooth surfaces around dental restorations (Melo et al., 2017). Nano-sized amorphous calcium phosphate (NACP) fillers may provide the release of calcium and phosphate ions under acidic pH as ion-enriched source incorporated in the dental material resulting in buffering capacity and remineralization effect (Weir et al., 2012).

Clinically, patients with active root carious lesions are assessed at a severely high risk of caries (Hayes et al., 2017b). They very often present several risk-indicators, such as hyposalivation, gingival recession, high cariogenic diet intake, and low fluoride exposure (Ritter et al., 2010). In view of the intended use for root restorations, the developed bioactive resin composite must present maximum anti-biofilm performance to confront high

FIGURE 1 | Clinical appearance of the carious root lesions showing a massive plaque build-up over exposed root surfaces. The lesions are presented as discoloration and loss of surface continuity or cavitation below the cementoenamel junction **(A)**. Root carious lesions are mainly located on the root surface of a tooth, usually close to or below the gingival margin **(B)**. The activity of such lesion can be determined based on the texture (smooth, rough), appearance (shiny or matte), and location in a plaque-stagnation area **(C)**.

plaque build-up inside the mouth. Considering the bacterial diversity within the biofilms, it would be conceivably preferable to use natural inoculum to facilitate the development of *in vitro* biofilms to more broadly resemble the *in vivo* community for testing new antibiofilm biomaterials (Signori et al., 2016). Plaque-derived inoculum can represent the environmental diversity related to the root surface in a site-dependent and niche-dependent manner, making the inoculum more clinically relevant for *in vitro* models testing new antibacterial compounds (Marsh, 2006; Fontana et al., 2009)

In this study, we examined for the first time the antibiofilm performance of a surface contact killing antibacterial dental resin composites on the growth of microcosm biofilms using dental plaque sampled from patients with active root carious lesions as an inoculum. It was hypothesized that: 1) The DMAHDM -NACP composites would substantially reduce biofilm activities, including colony-forming units (CFU), metabolic activity, and acid production, and 2) Adding DMAHDM and NACP into composite would not compromise the degree of conversion (DC).

MATERIAL AND METHODS

Participants Selection and Plaque Collection

Ethical Considerations

The participants were ongoing patients who visited university dental clinics for regular dental treatment. All participants consented to donate samples of dental plaque after getting comprehensive information about the study. The study protocol and written informed consent from all participants were approved by The University of Maryland Baltimore Institutional Review Board (HP-00083485).

Participants

Each participant had at least one exposed root with a primary active root carious lesion in order to collect the plaque. The average years of age of the participants were 56.8 ± 22.6 (N = 10; 40% female; 60% male). Ten adult volunteers presenting active root carious lesions at clinical oral examination, as shown in **Figure 1**, were recruited for the plaque collection. The lesions are presented as discoloration and loss of surface continuity or cavitation below the cement-enamel junction (**Figures 1A**). They were located on the root surface of a tooth, usually close to or below the gingival margin (**Figures 1B**). The activity of root caries was determined based on the texture (smooth, rough), appearance (shiny or glossy, matte or non-glossy), and location in a plaque-stagnation area (**Figures 1C**). The inclusion and exclusion criteria of the participants are described in **Table 1**.

Plaque sampling from patients with active root carious lesions.

The plaque sampling was undertaken at carious root sites. To assure proper sampling, the teeth presenting the lesions were isolated with cotton rolls and slightly air-dried. The dental plaque (supragingival biofilm) was removed using a sterile ultrafine micro-brush applicator (head size: 0.5 mm; MUT400; Microbrush international, Grafton, WI, United States) with a circular motion parallel to the gingival margin, as illustrated in **Figure 2** by the sequential images (2A-C). The samples were

TABLE 1 | The inclusion and exclusion criteria for the participant's selection for this study.

Inclusion Criteria	Exclusion Criteria
Adult patients over the age of 30	Patients under the age of 30
Patients should have active root carious lesions	Patient with no or inactive root carious lesions
No history of antibiotics in the last 6 months	Patients with a history of antibiotics in the last 6 months
No active periodontal treatment in the last 6 months	Patients with active periodontal treatment in the last 6 months
No systematic disease that may affect the oral environment	Patients with a systematic disease known to affect the oral environment
Patients should not be pregnant/lactating, or tobacco user	Tobacco users and pregnant/lactating patients

FIGURE 2 | (A) Clinical photographic images illustrating how the plaque was scraped and collected from the carious root lesions; **(B)** The dental plaque (supragingival biofilm) was removed using a sterile ultrafine micro-brush applicator; and **(C)** with a circular motion parallel to the gingival margin.

placed inside a liquid dental transport medium composed of a buffered mineral salt-based liquid medium with reducing agents (Anaerobe System, Morgan Hill, CA, United States) and transferred to the laboratory settings.

The collected plaque samples were mixed, stored in a solution of brain heart infusion, and glycerol at the ratio of 7:3, and stored at −80°C for further plaque-derived microcosm biofilm assays. The addition of glycerol stabilizes the frozen bacteria, preventing damage to the cell membranes and keeping the cells alive (Fontana et al., 2009).

Experimental Design

An *in vitro* study was conducted using a validated plaque-derived microcosm assay model (Melo et al., 2013). For the purpose of studying the antibacterial activity and DC of the designed formulations, a flowchart of the experimental process was intended, as shown in **Figure 3**. The factors under study were the DMAHDM concentration at three levels (0, 3, and 5%) and incorporation of NACP at two levels [absence and presence of 20% NACP], generating six groups as described in **Table 2**. For microbiological analyses derived from *in vitro* biofilms, four independent experiments were carried out, and the data were statistically analyzed according to the design of this study, considering the biofilm grown over the composite disk as a statistical unit ($n = 4 \times 3$ replicates). The dependent variables were: 1) CFUs counting for total microorganisms, 2) total *streptococci*, 3) *mutans streptococci*, and 4) total *lactobacilli*, 5) metabolic activity, 6) and lactic acid production. For DC, the statistical unit was the cured composite samples ($n = 5$).

Synthesizing the Dimethylaminohexadecyl Methacrylate Monomer and Nano-Sized Amorphous Calcium Phosphate Fillers

A modified Menschutkin reaction was performed to synthesize DMAHDM following previous studies (Zhou et al., 2013). Briefly, 10 mmol of 2-(dimethylamino)ethyl methacrylate (DMAEMA; Sigma-Aldrich, St. Louis, MO, United States), 10 mmol of 1-bromohexadecane (BHD, TCI America, Portland, OR, United States), and 3 g of ethanol were placed in a 20 ml-scintillation vial and mixed very well and stirred at 70°C for 24 h. Then, the solvent was evaporated, and DMAHDM was obtained.

The NACP fillers were synthesized by a spray-drying technique, as reported previously (Xu et al., 2011). The final molar ratio of Ca/P was 1.5, the same as that for ACP [$Ca_3(PO_4)_2$]. The full characterization of the NACP particles, including transmission electron microscopy and X-ray diffraction patterns, was described by previous study (Xu et al., 2011).

Resin Composite Formulations

At a mass ratio of 1:1, bisphenol glycidyl dimethacrylate (BisGMA; Esstech, Essington, PA, United States) and TEGDMA (Esstech, Essington, PA, United States) were mixed (referred to as "BT resin"). 0.2 wt.% camphorquinone, and 0.8 wt.% ethyl 4-N, N- dimethylaminobenzoate photoinitiators were added as photoinitiators. In the base formulation, the resin matrix mass to the fillers was designed at the ratio of 35:65 with BT as a resin matrix, and barium boroaluminosilicate glass particles with a median size of 1.4 μm (Caulk/Dentsply; Milford, DE, United States) silanized with

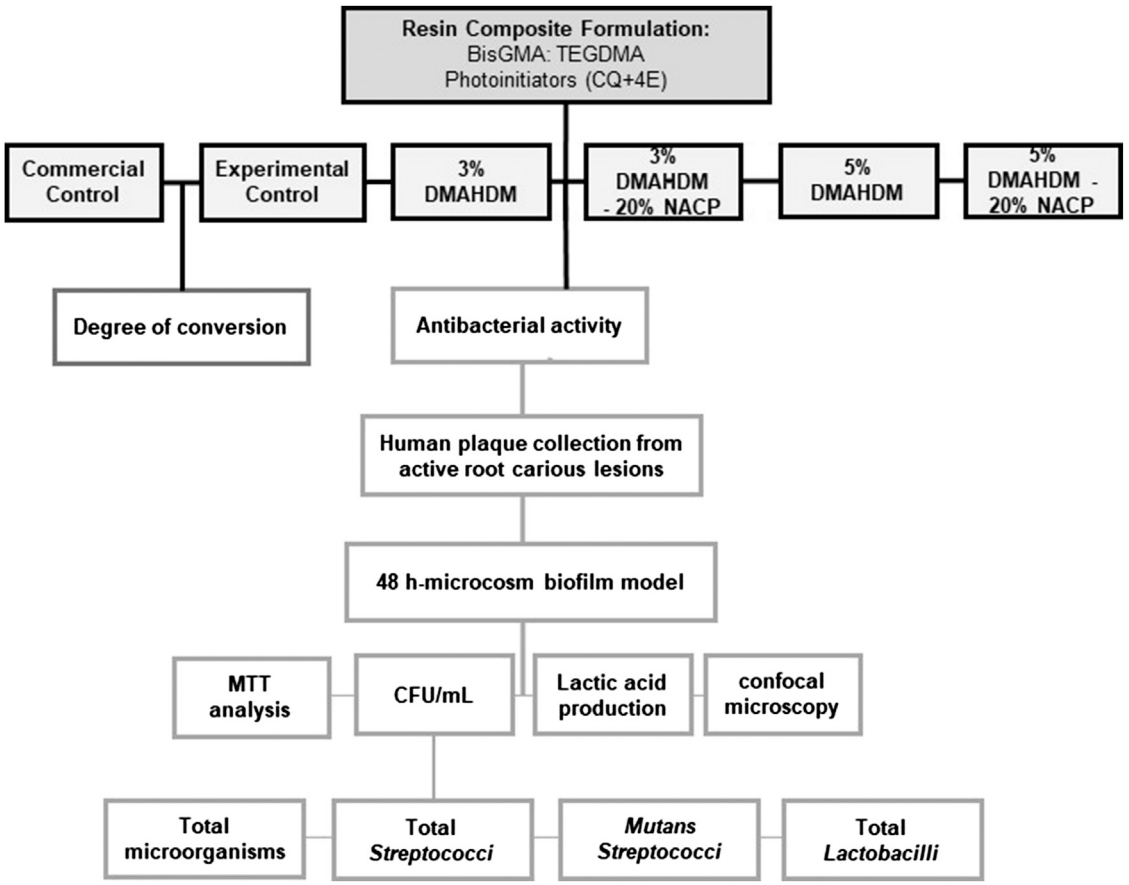

FIGURE 3 | Schematic drawing showing the design of the study. Antibacterial resin composite formulations were optimized containing the different mass fraction of DMAHDM with and without NACP. Microbiological analysis and the degree of conversion of the designed formulations were assessed.

TABLE 2 | Description of the components used to design the resin composite formulations.

Group	Manufacturer/Experimental formulation
Commercial control	Heliomolar, ivoclar vivadent, schaan, Liechtenstein
Experimental control	35% BT + 65% glass
3% DMAHDM	32% BT + 3% DMAHDM +65% glass
3% DMAHDM + 20% NACP	32% BT + 3% DMAHDM +20% NACP +45% glass
5%DMAHDM	30% BT + 5% DMAHDM +65% glass
5%DMAHDM-20%NACP	30% BT + 5% DMAHDM +20% NACP +45% glass

4 wt.% three- methacryloxypropyltrimethoxysilane as fillers. For the experimental formulations, DMAHDM was introduced to achieve the final mass fractions of 3 wt.% and 5 wt.% in the dental composite with and without 20 wt.% of NACP. All the investigated formulations are described in **Table 2**.

Plaque-Derived Microcosm Biofilm Assays

Sample Preparation

Circular molds with a diameter of 8 mm and a thickness of 1 mm were used to fabricate resin composite discs. The samples were cured (60 s; 1,000 mW/cm^2; VALO Cordless, Ultradent Products, South Jordan, UT, United States) and kept in a dry incubator for 24 h at 37°C followed by 1 h stirring in distilled water at 100 rpm to remove uncured monomers. Ethylene oxide (AnproleneAN 74i; Andersen, Haw River, NC, United States) gas was used to sterilize the samples, followed by seven days of de-gassing to assure the release of entrapped ethylene oxide (Farrugia et al., 2015).

Preparation of the Plaque-Derived Microcosm Assay

A McBain artificial saliva growth medium was prepared as the following: mucin (Type II, porcine, gastric), 2.5 g/L; bacteriological peptone, 2.0 g/L; tryptone, 2.0 g/L; yeast extract, 1.0 g/L; NaCl, 0.35 g/L, KCl, 0.2 g/L; $CaCl_2$, 0.2 g/L; 50 mM pipes, 15 g/L; hemin, 0.001 g/L; vitamin K_1, 0.0002 g/L, at pH 7. 0.2% sucrose was added to this medium (McBain et al., 2003). The plaque-brain heart infusion-glycerol solution containing the dispersed bacteria was added into the McBain artificial saliva growth medium to have approximately 1.5×10^6 cells/ml in each well of the 24-well plate (Fontana et al., 2009) containing the resin composite samples.

The plates containing the samples were incubated at 37°C supplemented with 5% CO_2. Fresh McBain medium supplemented with 0.2% of sucrose was added after 8 and 24 h of the incubation. At a total of 48 h incubation, the samples were transferred to conduct the CFUs count, metabolic activity assay, lactic acid measurement, or confocal laser scanning microscopy.

Biofilm Disruption Procedure

To quantify bacterial viability in biofilms grown over the composite, each specimen (n = 12) containing 2-day-old microcosm biofilms was washed and transferred to a vial containing 1 ml of cysteine peptone water. The sessile cells were harvested from the composites by sonication (Branson 3510, Branson Ultrasonics Corp., Danbury, CT) (5 min; 1x) followed by two rounds of 30 s vortexing (900 rpm, Vortex-Genie 2, Scientific Inc., Bohemia, NY). The volume of each disrupted biofilm was ten-fold serially diluted using buffered peptone water.

CFU counts of biofilms on resin composites.

The suspensions of the bacterial biofilms (10 µl) were plated in triplicate onto each agar plate using the drop-counting technique. The agar plates were incubated at 37°C in 5% CO_2 for 48 h, except for rogosa plates, which were incubated for 96 h. The number of CFU per ml of disrupted biofilm over each disk was determined by counting the colonies grown in the media. The colonies on plates were enumerated using a colony counter (Quebec Darkfield 3328; American Optical Corp, New York, United States). The detection limit with the methods used was 100 CFU/ml of disrupted biofilm. Four solid culture media, including non-selective and selective agar growth media, were used for selective isolation of the cariogenic bacteria (Wan et al., 2002):

(1) Tryptic soy blood agar (TSA) plates to estimate the biofilm growth of the total microorganisms.
(2) Mitis salivarius agar plates containing 15% sucrose to estimate the biofilm growth of total *streptococci*. Potassium tellurite at 1% was added to the agar to inhibit most gram-negative bacilli and most gram-positive bacteria.
(3) Mitis salivarius agar culture plates with the addition of 0.2 units of bacitracin per ml (MSB) were used to estimate the biofilm growth *mutans streptococci.*
(4) Rogosa agar culture plates to determine the growth of *lactobacilli.* Sodium acetate and ammonium citrate at a low pH were added at a high level to allow only the total *lactobacilli* to grow.

The number of CFU/specimen was calculated and converted to $\log_{10}$ for the statistical analysis.

MTT Assay for Quantification of Metabolic Activity of Biofilms

A colorimetric assay was performed to evaluate the enzymatic reduction of MTT (3-[4,5-dimethylthiazol-2-yl]-2,5-diphenyltetrazolium bromide) as previously described (Melo et al., 2013). Briefly, resin composite samples (n = 4 × 3 replicates) subjected to the 48-h plaque-derived biofilm were washed with phosphate-buffered saline (PBS) and immersed with 1 ml of tetrazolium dye. The plate was incubated at 37°C in 5% CO_2 for 1 h. Then, the samples were soaked with 1 ml of dimethyl sulfoxide in the dark for 20 min. The absorbance of the dimethyl sulfoxide at 540 nm was measured using a microplate reader (SpectraMax M5; Molecular Devices, Sunnyvale, CA, United States).

Lactic Acid Production by Biofilms

The lactic acid production was determined via an enzymatic (lactate dehydrogenase) method following a previous study (Balhaddad et al., 2020). Resin composite discs (n = 4 × 3 replicates) subjected to 48 h biofilms were washed with cysteine peptone water solution, immersed with 1.5 ml of buffered-peptone water plus 0.2% sucrose, and incubated for 3 h to allow the biofilms to produce acid. 1 M of glycine and 0.8 M of hydrazine sulfate were mixed at a ratio of 1:1. 170 µl of this mix was placed inside the wells of a 96-well plate followed by 20 µl of 26 mM of ß-nicotinamide adenine dinucleotide and 10 µl of each sample. The microplate reader (SpectraMax M5; Molecular Devices, Sunnyvale, CA, United States) was used to measure the absorbance of the buffered-peptone water solution of each well at 340 nm (optical density OD_{340}) before and after the addition of 10 µl of L-lactic dehydrogenase bovine heart (1,000 units/ml; Sigma-Aldrich, St. Louis, MO, United States). The standard curve was created using a lactic acid standard (Sigma-Aldrich, St. Louis, MO, United States).

Confocal Laser Scanning Microscopy

Confocal laser scanning microscopy was used to visualize the biofilm organization using BacLight live/dead kit (Molecular Probes, Eugene, OR, United States), and the images were three-dimensional reconstructed as previously described (Ibrahim et al., 2020c). Three random areas were selected and scanned using a ×20 air objective. To obtain the Z-series, vertical optical sectioning with a thickness of 1 µm was utilized. The images were processed using ZEN Black 2.3 SP1 (Bitplane, Zürich, Switzerland).

Degree of Conversion

Fourier-transform infrared spectroscopy with attenuated total reflectance device (FTIR-ATR) was used to investigate the DC of the resin composite formulations, as previously described (Collares et al., 2013; Monteiro et al., 2020). Briefly, resin composites (n = 5) were placed inside a mold of polyvinylsiloxane mold over the ATR crystal (Nicolet 6700; Thermo Fisher Scientific, Waltham, MA, United States) to standardize the thickness of each sample (thickness = 1 mm). A polyester strip was used to cover the resin composites. Then, a light-curing tip (VALO Cordless; Ultradent Products, South Jordan, UT, United States) was placed as close as possible to the sample to achieve photoactivation of 20 s with a radiant emittance of 1,000 mW/cm^2.

The spectra of each sample were captured before and after the light-curing procedure. OMNIC Series Software (Thermo Fisher Scientific), from 4,000 to 400 cm^{-1}, with 32 scans and 4 cm^{-1}

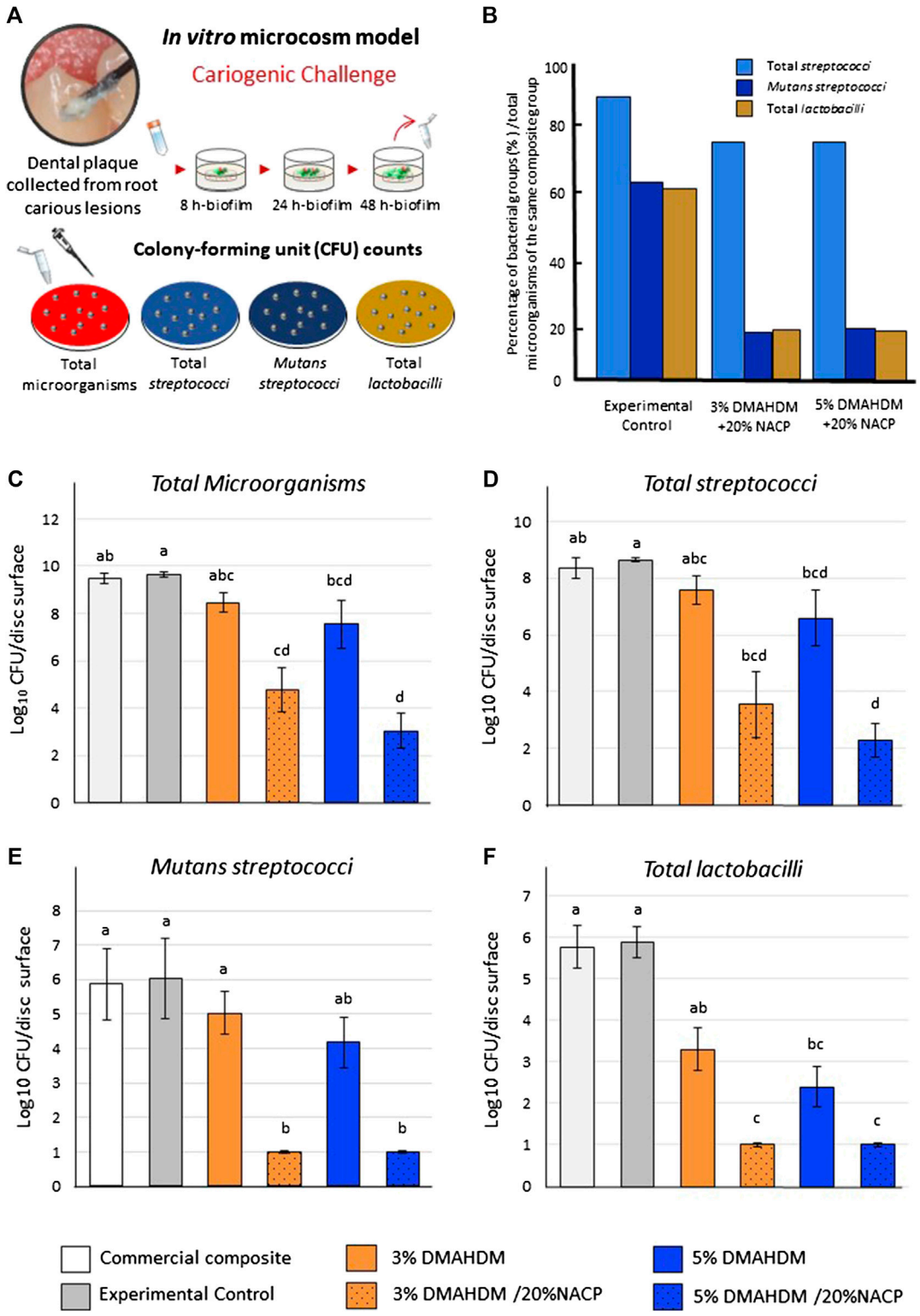

FIGURE 4 | Colony-forming unit (CFU) counts for biofilms grown over the resin composite discs. **(A)** The plaque samples isolated from active root carious lesions were used to initiate plaque-derived microcosm biofilms *in vitro*. **(B)** The percentage of the bacterial groups after biofilm inhibition, compared to total microorganisms, quantified over the same resin composite disk. the experimental control. **(C)** Total microorganisms, **(D)** total *streptococci*, **(E)** *mutans streptococci*, and **(F)** total *lactobacilli*. Values indicated by different letters are statistically different from each other ($p < 0.05$).

resolution, was used to evaluate the recorded data. The intensity of the aliphatic carbon-carbon double bond (1,638 cm^{-1}) and the aromatic carbon-carbon double bond (1,608 cm^{-1}) from the resin composite samples were studied before and after the curing to estimate the DC percentage using the equation:

$$DC(\%) = 100 \times \left(\frac{\text{peak height of cured aliphatic C = C/peak height of cured aromatic C = C}}{\text{peak height of uncured aliphatic C = C/peak height of uncured aromatic C = C}} \right)$$

Statistical Analysis

Data normality and distribution were evaluated via the Shapiro-Wilk test. Data were analyzed using one-way ANOVA and Tukey's post hoc test. All tests were conducted using the statistical software package Sigma Plot 12.0 (SYSTAT, Chicago, IL, United States), and the statistical significance was set at $p < 0.05$.

RESULTS

Colony-forming Unit Counts of the Plaque-Derived Microcosm Assay

Figure 4 summarizes the CFU results for the plaque-derived microcosm assays. Overall, all the experimental resin composites resulted in a significant bacterial reduction. **Figures 4A** illustrates the dental plaque-derived microcosm biofilm model and the respective agar media used in the study. **Figures 4B** displays the percentage of the cariogenic bacterial groups (in Log_{10}) in relation to the total microorganisms grown over the same surface containing DMAHDM and NACP. Compared to the experimental control, incorporating DMAHDM and NACP in the resin composite formulation reduced the prevalence of cariogenic species involved in root caries.

In **Figures 4C,** the growth of total microorganisms was significantly different among the tested groups ($p < 0.001$; power of analysis = 100%). The massive amount of reduction was observed with the DMAHDM-NACP resin composites where the CFU counts were reduced by around five and 6.5-log in the 3% DMAHDM-20% NACP and 5% DMAHDM-20% NACP resin composites, respectively, compared to the controls ($p < 0.001$). For the total *streptococci* biofilms (**Figures 4D**), the combinatorial addition of 3 and 5 wt.% of DMAHDM and 20% NACP reduced the growth by approximately 5 to 6-log ($p < 0.001$; power of analysis = 100%).

Figures 4E displays the counts for *mutans streptococci* in a selective agar medium. Adding 3 wt.% and 5 wt.% of DMAHDM to the resin composite formulations reduced the growth of *mutans streptococci* by around 1 and 2-log, respectively. The NACP-DMAHDM resin composites significantly reduced the *mutans streptococci* biofilms by 5-log compared to the control groups ($p < 0.001$; power of analysis = 100%). Resin composite with 3 wt.% of DMAHDM inhibited the CFU growth of the total *lactobacilli* by around 2.5-log, and by increasing the concentration to 5 wt.%, 3.5-log reduction was observed ($p < 0.05$). The NACP-DMAHDM resin composites significantly inhibited the *lactobacilli* biofilm growth ($p < 0.001$; power of analysis = 100%), resulting in 5-log reduction compared to the commercial and experimental controls (**Figures 4F**).

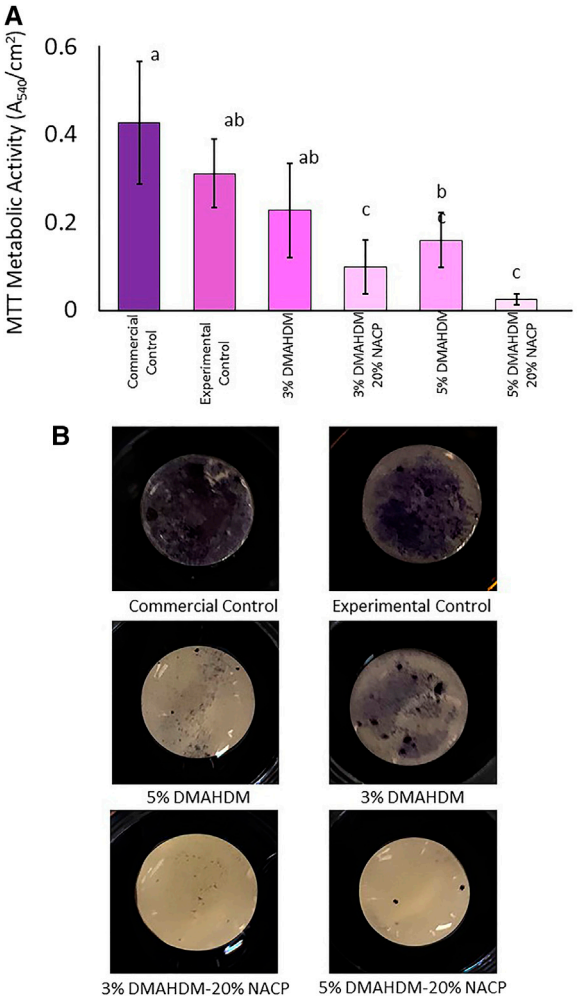

FIGURE 5 | (A) Metabolic activities absorbance values, higher absorbance values are associated with higher metabolic activities. Values indicated by different letters are statistically different from each other ($p < 0.05$). **(B)** Several resin composite discs showing high adherence of tetrazolium dye to the control groups indicate highly metabolic microorganisms. Resin composite with DMAHDM and NACP were associated with low adherence indicating a lower quantity of highly metabolic microorganisms.

Metabolic Activities

Resin composites containing 3 wt.% DMAHDM did not significantly reduce the metabolic activities of the biofilms compared to the commercial (0.43 ± 0.14) and experimental (0.31 ± 0.08) control samples ($p > 0.05$; power of analysis = 100). However, incorporating 5 wt.% DMAHDM into the base formulation resulted in significant inhibition (0.16 ± 0.06) (**Figures 5A**). Formulations containing 20 wt.% NACP with 3 wt.% or 5 wt.% of DMAHDM significantly reduced the metabolic activities compared to the control groups ($p < 0.001$).

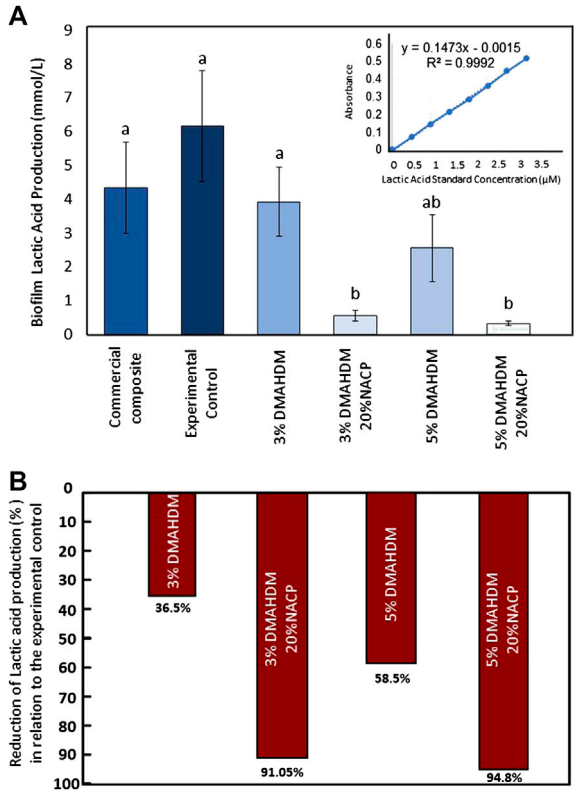

FIGURE 6 | (A) Lactic acid production values, higher readings are associated with higher lactic acid production. Values indicated by different letters are statistically different from each other ($p < 0.05$). **(B)** The percentages of lactic acid reduction among the experimental groups compared to the experimental control.

In **Figures 5B**, commercial and experimental control discs are associated with the most substantial stains indicating a noticeable bond between the tetrazolium dye and a considerable amount of highly metabolic microorganisms. The addition of 3 wt.% and 5 wt.% of DMAHDM resulted in reduced staining. The least amount of staining can be observed among the NACP-DMAHDM resin composites as the surfaces look shiny with a small extent of the stain.

Lactic Acid Production

The concentration of lactic acid production in (mmol/L) was calculated among resin composite samples (**Figures 6A**). The incorporation of 3 wt.% and 5 wt.% of DMAHDM into the resin composite formulations did not significantly reduce the lactic acid production compared to the controls ($p > 0.05$). However, the addition of NACP to DMAHDM resulted in a significant reduction ($p < 0.001$; power of analysis = 100%). In this assay, a commercially obtained lactic acid standard was used to validate the L-lactic dehydrogenase solution and create the standard curve using different lactic acid concentrations. As shown in **Figures 5**, **6**, DMAHDM alone prevented lactic acid production by 36.5–58.5%. However, the combination of NACP and DMAHDM in the resin composite formulations reduced the production by more than 90% compared to the experimental control.

Confocal Laser Scanning Microscopy

Representative live/dead images using a confocal microscope are shown in **Figures 7A–C**. A high visualization of viable microorganisms with thick biofilm was observed over the commercial control resin composite. The incorporation of 3 wt.% and 5 wt.% of DMAHDM resulted in less viable microorganisms. In the 3% DMAHDM-20% NACP samples, a reduced quantification of viable microorganisms and a considerable amount of dead colonies were observed (**Figures 7D–F**). Almost no viable microorganisms were observed over the 5% DMAHDM-20% NACP resin composites (**Figures 7G–I**).

Degree of Conversion

Figure 8 exhibits the results for the monomer conversion of the formulations. **Figures 8A** illustrates the chemical composition of the monomers and photoinitiators used in the tested formulations. **Figures 8B** illustrates the representative image of the FTIR spectra of monomer and polymer during the DC analysis. The DC was determined by the variation of peaks corresponding to aliphatic (1,638 cm^{-1}) and aromatic (1,608 cm^{-1}) C=C bonds of the monomer and polymer. All the experimental formulations demonstrated a higher DC compared to the commercial control ($p < 0.001$; power of analysis = 100%).

In **Figures 8C**, the radial chart displays the percentage of monomer conversion for each formulation. The addition of 3% wt.% and 5% wt.% of DMAHDM led to values of 59.9 ± (1.3) % and 60.5 ± (1.2) %. Likewise, the addition of 20% wt.% of NACP to the formulation did not compromise the DC (p= >0.05), as the values were 60.2 ± (1.0)% and 62.3 ± (2.6)% in the 3% DMAHDM-20%NACP and 5%DMAHDM-20%NACP resin composites, respectively.

DISCUSSION

There is currently a great need to develop effective antibacterial dental restorative material that can be used in the clinical setting. Since root caries is a significant and growing oral health concern. It is anticipated that root caries increases in prevalence and severity with the increased rate of aging globally. In this study, we tested the ability of a resin composite formulated with an antibacterial monomer and remineralizing fillers to modulate bacterial pathogens isolated from carious root lesions.

Often, secondary caries around root caries restorations is a burden for patients and a source of frustration for dentists in routine dental practice (Askar et al., 2020). In geriatric patients, the survival rate of composites due to secondary caries is at a low level (Meyer-Lueckel et al., 2019). Patients with prevailing risk factors such as hyposalivation, mental and physical disabilities, and areas of root surface exposure are at a high risk of developing the disease. Considering that the dentin located at the root is more susceptible to caries progression than enamel, managing these lesions at the root surfaces is even more complicated. As a

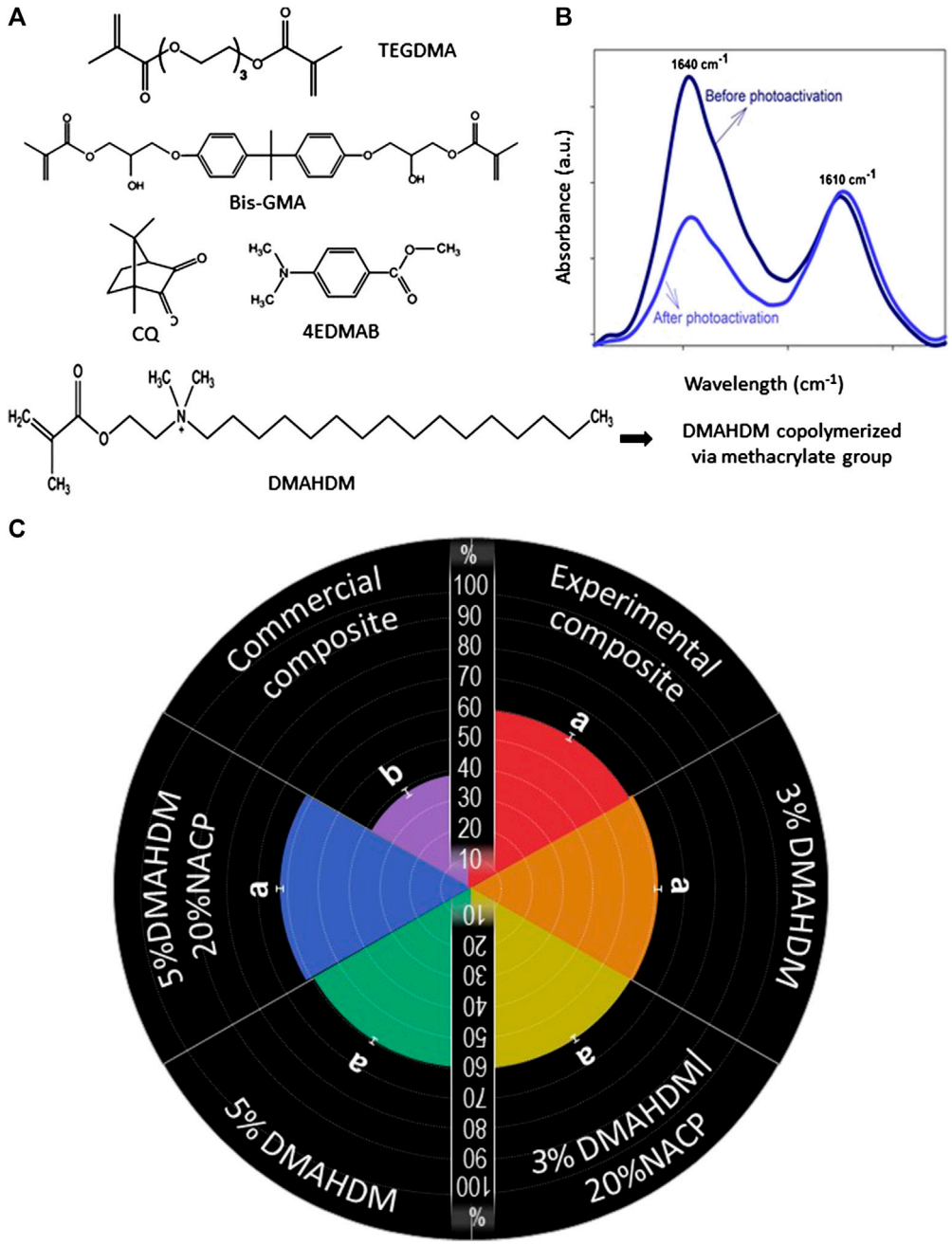

FIGURE 7 | (A) The chemical structures of the monomers used in the study to formulate the base resin, the antibacterial monomer, and photoinitiators. **(B)** A schematic illustration showing the spectra of FTIR of uncured and cured resin, evidencing that the peak of C=C in the aliphatic chain (1,640 cm^{-1}) decreases after the photoactivation. **(C)** Degree of conversion of the composite resins. Values indicated by different letters are statistically different from each other ($p < 0.05$).

result, the newly developed bioactive resin composites discussed, if successfully translated to the dental clinics, could assist the survival rate of root caries restorations.

In the current work, we assessed for the first time the new dental material using biofilm models that most closely resemble *in vivo* microbial communities by applying inoculum harvested from root lesions with whole ecosystem diversity. Previous studies have investigated the potential antibiofilm performance using *in vitro* biofilm models inoculated only with saliva from healthy patients (Balhaddad et al., 2020). Here, we carefully screened patients who presented active carious root lesions to improve microbial representativity of intraoral challenges faced by the restorative material applied on root carious lesions. It is well established that under planktonic growth, individual bacterium behavior dramatically differs from its behavior within complex or multi-species oral biofilms (Fernández et al., 2017).

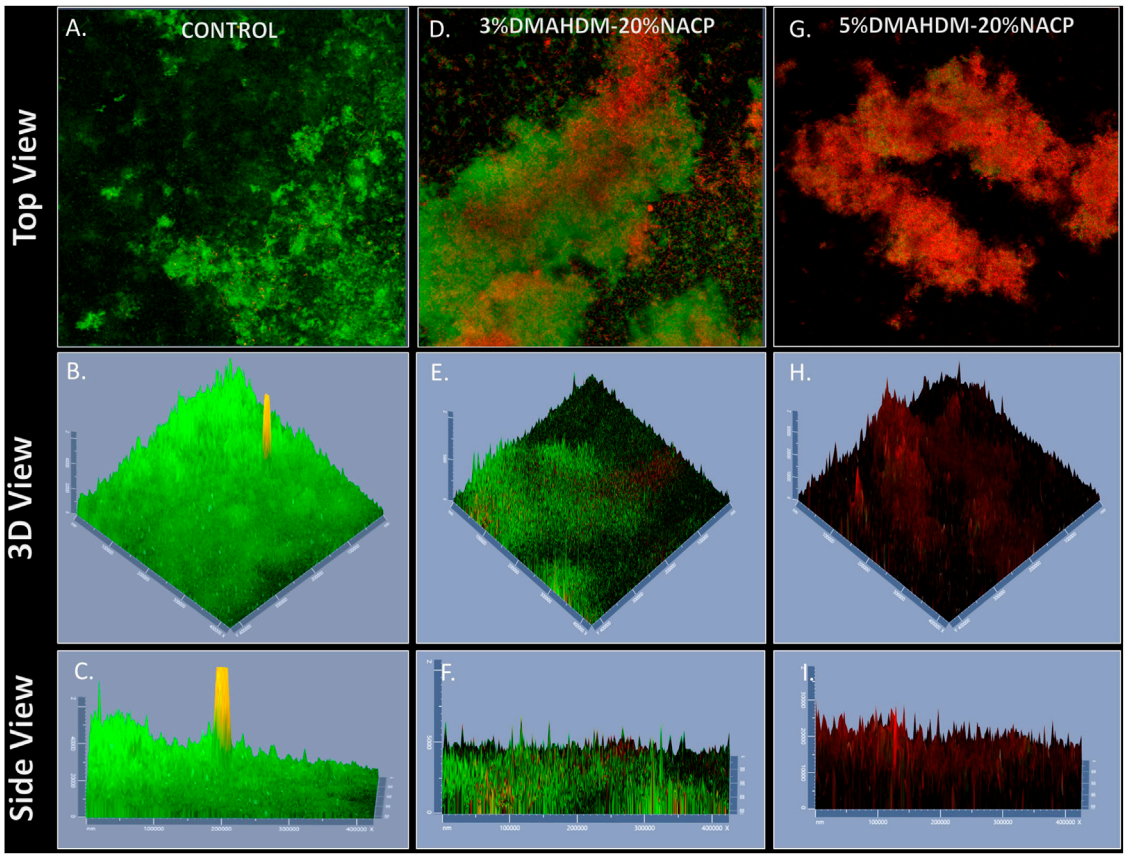

FIGURE 8 | Representative live/dead staining images of biofilms using confocal microscopy; **(A–C)** commercial control, **(D–F)** 3%DMAHDM-20%NACP%, **(G–I)** 5%DMAHDM-20%NACP%. Live bacteria were stained green, and compromised bacteria were stained red.

The assessment of the new bioactive materials may reveal different antibacterial performance, depending on the susceptibilities of the bacteria/biofilm target used for the evaluation (Ibrahim et al., 2020b). The survival mechanisms of clinically relevant microorganisms grown in biofilm inside the mouth are known to be highly resistant to antibacterial therapy delivered by dental products (Sharma et al., 2019). Besides, bacterial species isolated from plaque are quantitatively different from saliva (Georgios et al., 2015; Ruparell et al., 2020). Also, the location where the dental plaque has grown matters. A highly diverse microbial species can be isolated from plaque grown over the lesions compared to other oral niches found inside the mouth (Ruparell et al., 2020). More aciduric and cariogenic species can also be isolated from caries-active individuals than their caries-free counterparts (Georgios et al., 2015; Johansson et al., 2016; Zhou et al., 2016). Highly cariogenic species are often associated with a thicker exopolysaccharide matrix and increased lactic acid production (Wu et al., 2018).

In this study, we have demonstrated the ability of DMAHDM-NACP resin composites to inhibit the growth and activities of plaque-derived microcosm biofilms. The clinically accepted standard of bacterial reduction by an antimicrobial agent is at least a 3-log reduction in cell numbers (Pankey and Sabath, 2004). However, there is no evidence that a somewhat more or less stringent number might not be equally useful in predicting clinical use. Here, the DMAHDM-NACP resin composite reduced the CFUs of highly cariogenic plaque-derived biofilms by around 4-6-log (**Figure 4**), two to three times higher than what have has reported previously against non-cariogenic inoculum. The DMAHDM-NACP significantly decreased the metabolic activities and lactic acid production compared to DMAHDM solely and control groups (**Figures 5**, **6**).

Additionally, the confocal microscope revealed less and thinner biofilms growing over the DMAHDM-NACP resin composite (**Figure 7**). The great antibacterial action of our formulations could be attributed to the increased DMAHDM concentration and the use of NACP to convey a multifunctional approach to target dental pathogens. When the DMAHDM concentration was increased up to 5%, an additional reduction was achieved, indicating the ability of DMAHDM to kill pathogens in a dose-dependent manner.

Increasing the DMAHDM concentration up to 5% reveals significant challenges as increasing the concentration may compromise structural stability and low mechanical properties. Our previous report demonstrated the capability of designing and optimizing a resin composite formulation containing 5%

DMAHDM and 20% NACP with acceptable mechanical properties, high surface-charge density, and clinically acceptable surface roughness (Balhaddad et al., 2020).

The dimethylaminohexadecyl methacrylate is an antibacterial monomer with a contact-killing mechanism. The positively-charged quaternary ammonium embedded within its structure can interact with microorganisms composed of negatively charged-membrane (Ibrahim et al., 2020c). Short-chain quaternary ammonium induces antibacterial killing solely through the quaternary ammonium by disrupting the bacterial membrane and compromising the balance of some essential ions such as K^+, Na^+, Ca^{2+}, and Mg^{2+} (Cheng et al., 2017). Therefore, the antibacterial properties of the synthesized antibacterial monomers are indeed influenced by their alkyl chain length, as suggested by published literature (Li et al., 2013; Ibrahim et al., 2019)

While several other additives were found to impart bioactivity to resin composite formulations, some additives had a disappointing long-term performance for promoting limited or lack of action after depleting ion release (Young, 2010). Opposingly, the use of quaternary ammonium monomers affords a long-lasting effect without leaching or release (Zhang et al., 2018).

In developing bioactive dental materials, the combinatorial approach aims to incorporate agents to target multiple risk factors for disease development. Many researchers, including our group, have sequentially investigated the addition of calcium/fluoride-ions source fillers into an antibacterial resin blend to combine remineralizing and antibacterial actions in one formulation. Several reports support the ability of NACP fillers in resin-based materials to release calcium and phosphate ions under low pH acidic challenge (Melo et al., 2017; Ibrahim et al., 2020a). With a combinatorial approach of antibacterial and bioactivity responses, the resin composite intended to restore root caries lesions could afford different functionality against acidic biofilm attack. The DMAHDM-NACP resin composites could be a promising strategy to assist in preventing secondary caries around root restorations.

Even though we are facing here exciting results, more studies are needed to understand better what signals trigger biofilm development over the dental materials *in vivo* and to learn how to extrapolate these signals to the *in vitro* environment (Velsko and Shaddox, 2018). As limitations, many of the influencing factors for the robust growth of patient's isolates derived biofilms are difficult to control in the laboratory setting (Papadimitriou et al., 2016; Cattò and Cappitelli, 2019). As we have done here, researchers often characterize dental plaque-derived microcosm biofilms and make the assumption that they are representative of the entire microbiome of the root caries. It should also be noted that quantitation of *in vitro* biofilms suffers from inherent flaws since methodological steps such as sonication that only removes a proportion of bound cells from the composite disk or the sucrose concentration and frequency used in the models can lead to an inadequate translation of microbial profiling (Luo et al., 2015; Williams et al., 2019).

Other expressive findings in this study were the achievement of a suitable percentage of conversion of C=C to C-C in the aliphatic chains during the polymerization reaction for the tested formulations. Studies found that resin composite materials usually accept a DC from 40 to 80% (Noronha Filho et al., 2010). Materials with a low DC are expected to have poor mechanical properties with subsequent high susceptibility to degradation and release of residual unreacted monomers, that may induce toxic reaction to the surrounding tissues and stimulate the biofilm growth (Drummond, 2008; Collares et al., 2013; Maktabi et al., 2018; Fujioka-Kobayashi et al., 2019). Therefore, it is essential when designing a new formulation to assess this chemical property once the monomer conversion can control several properties of the cured material, including mechanical strength, polymerization shrinkage, wear behavior and monomer release (Fujioka-Kobayashi et al., 2019).

In our work, the degrees of conversion for the designed bioactive formulations were comparable to commercially available resin composites. Neither the addition of NACP nor DMAHDM had negatively affected this property. The lack of high rates of uncured monomers may indicate that these formulations are biocompatible and can achieve the required amount of polymerization, enhancing the long-term performance of these restorations. Future studies may involve long-term evaluation of the mechanical and antibacterial properties of the DMAHDM-NACP resin composites. Moreover, investigations on the DMAHDM-NACP composites using a translational model of dental caries can provide evidence of efficacy and the bases for clinical trials.

CONCLUSION

In summary, we demonstrated, for the first time, a pronounced anti-biofilm performance of DMAHDM-NACP resin composites against plaque-derived microcosm biofilms from carious root lesions. An antibacterial action was imparted in the newly designed bioactive formulations without adversely affecting the monomer conversion. This study presents a practicable strategy to assist in the preventive measures against the onset of secondary caries at the tooth-restoration interface, especially in a highly challenging clinical situation as restoring carious root lesions in high caries-risk patients.

DATA AVAILABILITY STATEMENT

All datasets presented in this study are included in the article/ supplementary material.

ETHICS STATEMENT

The studies involving human participants were reviewed and approved by The University of Maryland Baltimore Institutional

Review Board (HP-00083485). The patients/participants provided their written informed consent to participate in this study.

AUTHOR CONTRIBUTIONS

AB, MI, FC, and IG contributed to the design and the writing of the manuscript. MW, HX, and MM contributed to the critical review of the manuscript. All authors have read and agreed to the published version of the manuscript.

FUNDING

This work was supported by the award of the University of Maryland, Baltimore, Institute for Clinical and Translational Research (ICTR) (MM), and the University of Maryland School of Dentistry departmental funds (MM, HX).

ACKNOWLEDGMENTS

The authors are grateful to the volunteers for their participation in this study. The authors thank the faculty and staff of the Department of General Dentistry at the University of Maryland School of Dentistry for their assistance and use of their clinical facilities. We are grateful to Esstech (Essington, PA) for kindly donating the BisGMA and TEGDMA monomers. MM acknowledges the award support of the University of Maryland, Baltimore, Institute for Clinical & Translational Research (ICTR); the Research Center for Innovative Biomedical Resources (CIBR)-Confocal Microscopy Facility on behalf Mauban for the assistance with confocal microscopy. AB and MI acknowledge the scholarship during their Ph.D. studies from the Imam AbdulRahman bin Faisal University, Dammam, Saudi Arabia, and the Saudi Arabia Cultural Mission. IG acknowledge the scholarship during their Ph.D. studies from the Coordenação de Aperfeiçoamento de Pessoal de Nível Superior - Brasil (CAPES) - Finance Code 001 – scholarship.

REFERENCES

Askar, H., Krois, J., Göstemeyer, G., Bottenberg, P., Zero, D., Banerjee, A., et al. (2020). Secondary caries: what is it, and how it can be controlled, detected, and managed? *Clin Oral Invest.* 24, 1869–1876. doi:10.1007/s00784-020-03268-7

Bourbia, M., and Finer, Y. (2018). Biochemical stability and interactions of dental resin composites and adhesives with host and bacteria in the oral cavity: a review. *J. Can. Dent. Assoc.* 84, i1

Cattò, C., and Cappitelli, F. (2019). Testing anti-biofilm polymeric surfaces: where to start? *Int. J. Mol. Sci.* 20, 2–60. doi:10.3390/ijms20153794

Cheng, L., Weir, M. D., Zhang, K., Xu, S. M., Chen, Q., Zhou, X., et al. (2012). Antibacterial nanocomposite with calcium phosphate and quaternary ammonium. *J. Dent. Res.* 91, 460–466. doi:10.1177/0022034512440579

Cheng, L., Zhang, K., Zhang, N., Melo, M. A. S., Weir, M. D., Zhou, X. D., et al. (2017). Developing a new generation of antimicrobial and bioactive dental resins. *J. Dent. Res.* 96, 855–863. doi:10.1177/0022034517709739

Collares, F. M., Portella, F. F., Leitune, V. C. B., and Samuel, S. M. W. (2013). Discrepancies in degree of conversion measurements by FTIR. *Braz. Oral Res.* 27, 453–454. doi:10.1590/S1806-83242013000600002

Damé-Teixeira, N., Parolo, C. C. F., and Maltz, M. (2017). Specificities of caries on root surface. *Monogr. Oral Sci.* 26, 15–25. doi:10.1159/000479303

Delaviz, Y., Finer, Y., and Santerre, J. P. (2014). Biodegradation of resin composites and adhesives by oral bacteria and saliva: a rationale for new material designs that consider the clinical environment and treatment challenges. *Dent. Mater.* 30, 16–32. doi:10.1016/j.dental.2013.08.201

Drummond, J. L. (2008). Degradation, fatigue, and failure of resin dental composite materials. *J. Dent. Res.* 87, 710–719. doi:10.1177/154405910808700802

Farrugia, C., Cassar, G., Valdramidis, V., and Camilleri, J. (2015). Effect of sterilization techniques prior to antimicrobial testing on physical properties of dental restorative materials. *J. Dent.* 43, 703–714. doi:10.1016/j.jdent.2015.03.012

Fernández, C. E., Aspiras, M. B., Dodds, M. W., González-Cabezas, C., and Rickard, A. H. (2017). The effect of inoculum source and fluid shear force on the development of *in vitro* oral multispecies biofilms. *J. Appl. Microbiol.* 122, 796–808. doi:10.1111/jam.13376

Fontana, C. R., Abernethy, A. D., Som, S., Ruggiero, K., Doucette, S., Marcantonio, R. C., et al. (2009). The antibacterial effect of photodynamic therapy in dental plaque-derived biofilms. *J. Periodont. Res.* 44, 751–759. doi:10.1111/j.1600-0765.2008.01187.x

Fujioka-Kobayashi, M., Miron, R. J., Lussi, A., Gruber, R., Ilie, N., Price, R. B., et al. (2019). Effect of the degree of conversion of resin-based composites on cytotoxicity, cell attachment, and gene expression. *Dent. Mater.* 35, 1173–1193. doi:10.1016/j.dental.2019.05.015

Gati, D., and Vieira, A. R. (2011). Elderly at greater risk for root caries: a look at the multifactorial risks with emphasis on genetics susceptibility. *Int J Dent.* 2011, 647168. doi:10.1155/2011/647168

Gavriilidou, N. N., and Belibasakis, G. N. (2019). Root caries: the intersection between periodontal disease and dental caries in the course of ageing. *Br. Dent. J.* 227, 1063–1067. doi:10.1038/s41415-019-0973-4

Georgios, A., Vassiliki, T., and Sotirios, K. (2015). Acidogenicity and acidurance of dental plaque and saliva sediment from adults in relation to caries activity and chlorhexidine exposure. *J. Oral Microbiol.* 7, 26197. doi:10.3402/jom.v7.26197

Hayes, M., Burke, F., and Allen, P. F. (2017a). Incidence, prevalence and global distribution of root caries. *Monogr. Oral Sci.* 26, 1–8. doi:10.1159/000479301

Hayes, M., Da Mata, C., McKenna, G., Burke, F. M., and Allen, P. F. (2017b). Evaluation of the Cariogram for root caries prediction. *J. Dent.* 62, 25–30. doi:10.1016/j.jdent.2017.04.010

Ibrahim, M. S., Balhaddad, A. A., Garcia, I. M., Collares, F. M., Weir, M. D., Xu, H. H. K., et al. (2020a). pH-responsive calcium and phosphate-ion releasing antibacterial sealants on carious enamel lesions *in vitro*. *J. Dent.* 97, 103323. doi:10.1016/j.jdent.2020.103323

Ibrahim, M. S., Garcia, I. M., Kensara, A., Balhaddad, A., Collares, F. M., Williams, M. A., et al. (2020b). How we are assessing the developing antibacterial resin-based dental materials? A scoping review. *J. Dent.* 99, 103369. doi:10.1016/j.jdent.2020.103369

Ibrahim, M. S., Garcia, I. M., Vila, T., Balhaddad, A. A., Collares, F. M., Weir, M. D., et al. (2020c). Multifunctional antibacterial dental sealants suppress biofilms derived from children at high risk of caries. *Biomater. Sci.* 8 (Suppl. 18). doi:10.1039/D0BM00370K

Ibrahim, M. S., Ibrahim, A. S., Balhaddad, A. A., Weir, M. D., Lin, N. J., Tay, F. R., et al. (2019). A novel dental sealant containing dimethylaminohexadecyl methacrylate suppresses the cariogenic pathogenicity of Streptococcus mutans biofilms. *Int. J. Mol. Sci.* 20 (14), 3491. doi:10.3390/ijms20143491

Johansson, I., Witkowska, E., Kaveh, B., Lif Holgerson, P., and Tanner, A. C. R. (2016). The microbiome in populations with a low and high prevalence of caries. *J. Dent. Res.* 95, 80–86. doi:10.1177/0022034515609554

Khatoon, Z., McTiernan, C. D., Suuronen, E. J., Mah, T.-F., and Alarcon, E. I. (2018). Bacterial biofilm formation on implantable devices and approaches to its treatment and prevention. *Heliyon.* 4, e01067. doi:10.1016/j.heliyon.2018.e01067

Li, F., Weir, M. D., and Xu, H. H. K. (2013). Effects of quaternary ammonium chain length on antibacterial bonding agents. *J. Dent. Res.* 92, 932–938. doi:10.1177/0022034513502053

Liang, X., Söderling, E., Liu, F., He, J., Lassila, L. V. J., and Vallittu, P. K. (2014). Optimizing the concentration of quaternary ammonium dimethacrylate

monomer in bis-GMA/TEGDMA dental resin system for antibacterial activity and mechanical properties. *J. Mater. Sci. Mater. Med.* 25, 1387–1393. doi:10.1007/s10856-014-5156-x

Luo, X., Jellison, K. L., Huynh, K., and Widmer, G. (2015). Impact of bioreactor environment and recovery method on the profile of bacterial populations from water distribution systems. *PloS One.* 10, e0133427. doi:10.1371/journal.pone.0133427.

Maktabi, H., Balhaddad, A. A., Alkhubaizi, Q., Strassler, H., and Melo, M. A. S. (2018). Factors influencing success of radiant exposure in light-curing posterior dental composite in the clinical setting. *Am. J. Dent.* 31, 320–328

Marsh, P. D. (2006). Dental plaque as a biofilm and a microbial community – implications for health and disease. *BMC Oral Health.* 6, S14. doi:10.1186/1472-6831-6-S1-S14.

McBain, A. J., Bartolo, R. G., Catrenich, C. E., Charbonneau, D., Ledder, R. G., and Gilbert, P. (2003). Growth and molecular characterization of dental plaque microcosms. *J. Appl. Microbiol.* 94, 655–664. doi:10.1046/j.1365-2672.2003.01876.x.

Melo, M. A. S., Cheng, L., Zhang, K., Weir, M. D., Rodrigues, L. K. A., and Xu, H. H. K. (2013). Novel dental adhesives containing nanoparticles of silver and amorphous calcium phosphate. *Dent. Mater.* 29, 199–210. doi:10.1016/j.dental.2012.10.005.

Melo, M. A. S., Weir, M. D., Passos, V. F., Powers, M., and Xu, H. H. K. (2017). Ph-activated nano-amorphous calcium phosphate-based cement to reduce dental enamel demineralization. *Artif. Cells Nanomed. Biotechnol.* 45, 1778–1785. doi:10.1080/21691401.2017.1290644.

Melo, M. A. S., Weir, M. D., Passos, V. F., Rolim, J. P. M., Lynch, C. D., Rodrigues, L. K. A., et al. (2018). Human in situ study of the effect of bis(2-methacryloyloxyethyl) dimethylammonium bromide immobilized in dental composite on controlling mature cariogenic biofilm. *Int. J. Mol. Sci.* 19 (11), 3443. doi:10.3390/ijms19113443

Meyer-Lueckel, H., Machiulskiene, V., and Giacaman, R. A. (2019). How to intervene in the root caries process? Systematic review and meta-analyses. *Caries Res.* 53, 599–608. doi:10.1159/000501588

Monteiro, J. C., Stürmer, M., Garcia, I. M., Melo, M. A., Sauro, S., Leitune, V. C. B., et al. (2020). Dental sealant empowered by 1,3,5-tri acryloyl hexahydro-1,3,5-triazine and α-tricalcium phosphate for anti-caries application. *Polymers (Basel).* 12 (4), 895. doi:10.3390/polym12040895

Noronha Filho, J. D., Brandão, N. L., Poskus, L. T., Guimarães, J. G. A., and Silva, E. M. (2010). A critical analysis of the degree of conversion of resin-based luting cements. *J. Appl. Oral Sci.* 18, 442–446. doi:10.1590/s1678-77572010000500003

Pankey, G. A., and Sabath, L. D. (2004). Clinical relevance of bacteriostatic versus bactericidal mechanisms of action in the treatment of Gram-positive bacterial infections. *Clin. Infect. Dis.* 38, 864–870. doi:10.1086/381972

Papadimitriou, K., Alegría, Á., Bron, P. A., de Angelis, M., Gobbetti, M., Kleerebezem, M., et al. (2016). Stress physiology of lactic acid bacteria. *Microbiol. Mol. Biol. Rev.* 80, 837–890. doi:10.1128/MMBR.00076-15

Ritter, A. V., Shugars, D. A., and Bader, J. D. (2010). Root caries risk indicators: a systematic review of risk models. *Community Dent. Oral Epidemiol.* 38, 383–397. doi:10.1111/j.1600-0528.2010.00551.x

Ruparell, A., Inui, T., Staunton, R., Wallis, C., Deusch, O., and Holcombe, L. J. (2020). The canine oral microbiome: variation in bacterial populations across different niches. *BMC Microbiol.* 20, 42. doi:10.1186/s12866-020-1704-3

Sharma, D., Misba, L., and Khan, A. U. (2019). Antibiotics versus biofilm: an emerging battleground in microbial communities. *Antimicrob. Resist. Infect. Contr.* 8, 76. doi:10.1186/s13756-019-0533-3

Signori, C., van de Sande, F. H., Maske, T. T., de Oliveira, E. F., and Cenci, M. S. (2016). Influence of the inoculum source on the cariogenicity of *in vitro* microcosm biofilms. *Caries Res.* 50, 97–103. doi:10.1159/000443537

Takahashi, N., and Nyvad, B. (2016). Ecological hypothesis of dentin and root caries. *Caries Res.* 50, 422–431. doi:10.1159/000447309

Tan, H., Richards, L., Walsh, T., Worthington, H. V., Clarkson, J. E., Wang, L., et al. (2017). Interventions for managing root caries. *Cochrane Database Syst. Rev.* 2017 (8). doi:10.1002/14651858.CD012750

The United States census bureau (2019). By 2030, All baby boomers will Be age 65 or older. Available at: https://www.census.gov/library/stories/2019/12/by-2030-all-baby-boomers-will-be-age-65-or-older.html (Accessed June 1, 2020).

Tonetti, M. S., Bottenberg, P., Conrads, G., Eickholz, P., Heasman, P., Huysmans, M.-C., et al. (2017). Dental caries and periodontal diseases in the ageing population: call to action to protect and enhance oral health and well-being as an essential component of healthy ageing - consensus report of group 4 of the joint EFP/ORCA workshop on the boundaries between caries and periodontal diseases. *J. Clin. Periodontol.* 44 (Suppl. 18), S135–S144. doi:10.1111/jcpe.12681

Vandana, K. L., and Haneet, R. K. (2014). Cementoenamel junction: an insight. *J. Indian Soc. Periodontol.* 18, 549–554. doi:10.4103/0972-124X.142437

Velsko, I. M., and Shaddox, L. M. (2018). Consistent and reproducible long-term *in vitro* growth of health and disease-associated oral subgingival biofilms. *BMC Microbiol.* 18 (1), 70. doi:10.1186/s12866-018-1212-x

Wan, A. K. L., Seow, W. K., Walsh, L. J., and Bird, P. S. (2002). Comparison of five selective media for the growth and enumeration of Streptococcus mutans. *Aust. Dent. J.* 47, 21–26. doi:10.1111/j.1834-7819.2002.tb00298.x

Weir, M. D., Moreau, J. L., Levine, E. D., Strassler, H. D., Chow, L. C., and Xu, H. H. K. (2012). Nanocomposite containing CaF2 nanoparticles: thermal cycling, wear and long-term water-aging. *Dent. Mater.* 28, 642–652. doi:10.1016/j.dental.2012.02.007

Williams, D. L., Smith, S. R., Peterson, B. R., Allyn, G., Cadenas, L., Epperson, R. T., et al. (2019). Growth substrate may influence biofilm susceptibility to antibiotics. *PLoS One.* 14, e0206774. doi:10.1371/journal.pone.0206774

Wu, H., Zeng, B., Li, B., Ren, B., Zhao, J., Li, M., et al. (2018). Research on oral microbiota of monozygotic twins with discordant caries experience - *in vitro* and *in vivo* study. *Sci. Rep.* 8, 7267. doi:10.1038/s41598-018-25636-w

Young, A. M. (2010). "11 - antibacterial releasing dental restorative materials," in *Drug-device combination products woodhead publishing series in biomaterials*. Editos A. Lewis (Cambridge, UK: Woodhead Publishing), 246–279

Yuan, Y., Sun, F., Zhang, F., Ren, H., Guo, M., Cai, K., et al. (2013). Targeted synthesis of porous aromatic frameworks and their composites for versatile, facile, efficacious, and durable antibacterial polymer coatings. *Adv. Mater.* 25, 6619–6624. doi:10.1002/adma.201301955

Zhang, N., Zhang, K., Xie, X., Dai, Z., Zhao, Z., Imazato, S., et al. (2018). Nanostructured polymeric materials with protein-repellent and anti-caries properties for dental applications. *Nanomaterials (Basel).* 8 (6),393. doi:10.3390/nano8060393

Zhou, C., Weir, M. D., Zhang, K., Deng, D., Cheng, L., and Xu, H. H. K. (2013). Synthesis of new antibacterial quaternary ammonium monomer for incorporation into CaP nanocomposite. *Dent. Mater.* 29, 859–870. doi:10.1016/j.dental.2013.05.005

Zhou, J., Jiang, N., Wang, S., Hu, X., Jiao, K., He, X., et al. (2016). Exploration of human salivary microbiomes--insights into the novel characteristics of microbial community structure in caries and caries-free subjects. *PLoS One.* 11, e0147039. doi:10.1371/journal.pone.0147039

Zubris, D. L., Minbiole, K. P. C., and Wuest, W. M. (2017). Polymeric quaternary ammonium compounds: versatile antimicrobial materials. *Curr. Top. Med. Chem.* 17, 305–318. doi:10.2174/1568026616666160829155805

Conflicts of Interest: The authors HX and MW have patents (US20150299345A1; US8889196B2) for the manufacture and use of antibacterial monomers and amorphous calcium phosphate used in this study. The funders had no role in the design of the study; nanoparticles in the collection, analyses, or interpretation of data; in the writing of the manuscript, or in the decision to publish the results.

frontiers in Materials

ORIGINAL RESEARCH
published: 02 February 2021
doi: 10.3389/fmats.2020.601078

Physicochemical Effects of Niobic Acid Addition Into Dental Adhesives

Isadora Martini Garcia[1†], Vicente Castelo Branco Leitune[1†], Gabrielade Souza Balbinot[1†], AbdulRahman A. Balhaddad[2,3†], Mary Anne S. Melo[4,5†], Susana Maria Werner Samuel[1†] and Fabrício Mezzomo Collares[1†]*

[1]Department of Dental Materials, School of Dentistry, Federal University of Rio Grande do Sul, Porto Alegre, Brazil, [2]Ph.D. Program in Biomedical Sciences, University of Maryland School of Dentistry, Baltimore, MD, United States, [3]Department of Restorative Dental Sciences, Imam Abdulrahman Bin Faisal University, College of Dentistry, Dammam, Saudi Arabia, [4]Division of Operative Dentistry, Department of General Dentistry, University of Maryland School of Dentistry, Baltimore, MD, United States, [5]Ph.D. Program in Biomedical Sciences, University of Maryland School of Dentistry, Baltimore, MD, United States

The incorporation of metallic oxides in dental adhesives has been a strategy to confer improved radiopacity and physicochemical properties for polymers. Tailoring the structure of these fillers could contribute to their application in therapeutic strategies for dental restorations. The aim of this study was to evaluate the incorporation of niobic acid into experimental dental adhesives, and compare these adhesives to niobium pentoxide containing adhesives. A control group without $Nb_2O_5{\cdot}n\ H_2O$ or Nb_2O_5 was also used for comparison. Niobium-based particles have been used as a feasible approach, mainly because of their bioactivity. In this study, hydrated niobium pentoxide, also called niobic acid ($Nb_2O_5{\cdot}n\ H_2O$), was incorporated into an experimental dental adhesive as a potential catalyst for monomer conversion. A base resin for dental adhesive was formulated with methacrylate monomers and photoinitiators. Two types of oxides were tested as filler for this adhesive: $Nb_2O_5{\cdot}n\ H_2O$ or niobium pentoxide (Nb_2O_5). Both fillers were added separately into the experimental adhesive at 0, 2.5, 5, and 10 wt.%. One group without $Nb_2O_5{\cdot}n\ H_2O$ or Nb_2O_5 (0 wt.% of filler addition) was used as a control group. The formulated materials were analyzed for radiopacity according to the ISO 4049 and used FTIR analysis to assess the degree of conversion (DC) and the maximum polymerization rate (RP_{max}). Mechanical properties were analyzed by ultimate tensile strength (UTS) in a testing machine. Softening in solvent was conducted by measuring Knoop microhardness before and after immersion of samples in ethanol. Normality of data was assessed with Shapiro-Wilk, and comparisons between factors were conducted with two-way ANOVA and Tukey at 5% of significance. Both fillers, Nb_2O_5 or $Nb_2O_5{\cdot}n\ H_2O$, increased the radiopacity of dental adhesives in comparison to the unfilled adhesive ($p < 0.05$). There were no differences among groups for the ultimate tensile strength ($p > 0.05$), and all groups containing Nb_2O_5 or $Nb_2O_5{\cdot}n\ H_2O$ improved the resistance against softening in solvent ($p < 0.05$). The groups with 5 and 10 wt% addition of Nb_2O_5 showed decreased DC compared to the control group ($p < 0.05$), while the addition of $Nb_2O_5{\cdot}nH_2O$ up to 10 wt% did not alter the DC ($p > 0.05$). The polymerization rate did not change among groups ($p > 0.05$). In conclusion, $Nb_2O_5{\cdot}n\ H_2O$ is a promising filler to be incorporated into dental adhesives providing proper mechanical properties, improved resistance against solvents, and increased radiopacity, without changing the DC.

Keywords: niobium, dentin-bonding agents, polymerization, mechanical phenomena, dental materials

OPEN ACCESS

Edited by:
Masoud Mozafari,
University of Toronto, Canada

Reviewed by:
Matej Par,
University of Zagreb, Brazil
Victor Pinheiro,
Feitosa, Faculdade Paulo Picanço, Brazil

***Correspondence:**
Fabrício Mezzomo Collares
fabricio.collares@ufrgs.br

†ORCID:
Isadora Martini Garcia
https://orcid.org/0000-0002-7388-0200
Vicente Castelo Branco Leitune
https://orcid.org/0000-0002-5415-1731
Gabriela de Souza Balbinot
https://orcid.org/0000-0001-9076-2460
AbdulRahman A. Balhaddad
https://orcid.org/0000-0001-6678-7940
Mary Anne S. Melo
https://orcid.org/0000-0002-0007-2966
Susana Maria Werner Samuel
https://orcid.org/0000-0001-5467-2636
Fabrício Mezzomo Collares
https://orcid.org/0000-0002-1382-0150

Specialty section:
This article was submitted to Biomaterials, a section of the journal Frontiers in Materials

Received: *31 August 2020*
Accepted: *21 December 2020*
Published: *02 February 2021*

Citation:
Garcia IM, Leitune VCB, Balbinot GS, Balhaddad AA, Melo MAS, Samuel SMW and Collares FM (2021) Physicochemical Effects of Niobic Acid Addition Into Dental Adhesives. Front. Mater. 7:601078. doi: 10.3389/fmats.2020.601078

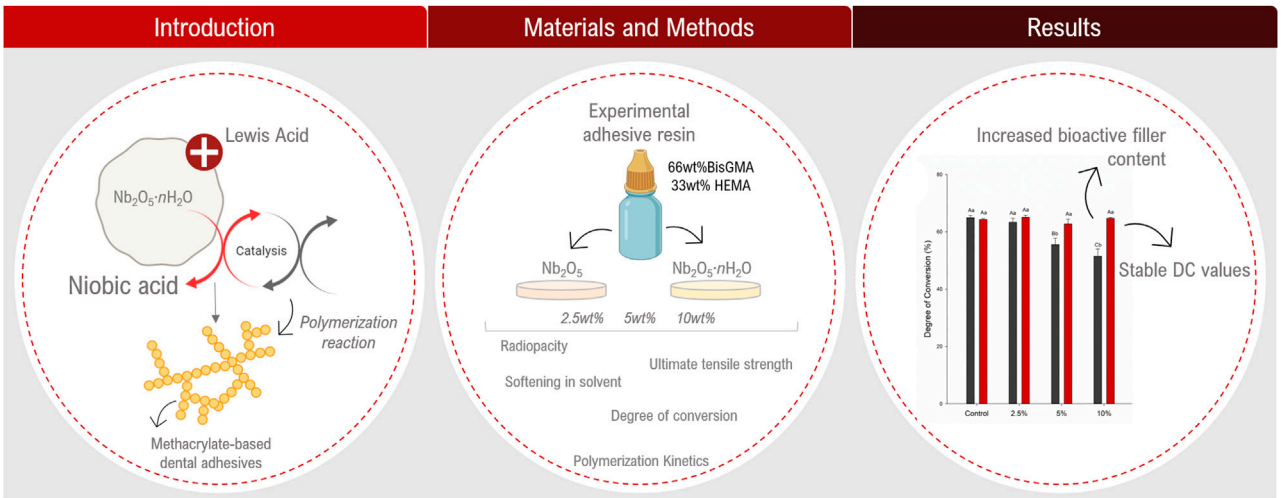

GRAPHICAL ABSTARACT

INTRODUCTION

Adhesive systems for dental restoration have undergone several modifications so that their physical and chemical properties could be improved, supporting long-lasting restorative treatments. Inorganic fillers have been incorporated into dental adhesives aiming to reduce polymeric degradation via increasing hydrolytic stability (Münchow and Bottino, 2017). Furthermore, these particles have been tuning in adhesives formulation to improve polymers' radiopacity (Garcia et al., 2020a) and mechanical properties (Lohbauer et al., 2010; Belli et al., 2014). Inorganic fillers have also been proposed to improve the therapeutic activity of resin-based materials. Bioactive particles have been used to assist in tooth remineralization (Balhaddad et al., 2019; Braga and Fronza, 2020), making bioactive resin-based dental materials to be feasible approaches to prevent dental demineralization and to provide the recovery of hard dental tissues affected by caries (Garcia et al., 2017; Ibrahim et al., 2020a; Ibrahim et al., 2020b). Calcium phosphates (Garcia et al., 2017; Braga and Fronza, 2020), calcium silicates (Profeta, 2014), bioactive glasses (Balbinot et al., 2020a; Yao et al., 2020), and zinc-based particles (Toledano et al., 2016) were already tested and showed mineral deposition or remineralization effect on dental hard tissues. Recently, niobium-based particles have been highlighted due to their interesting properties for dentistry, such as high radiopacity and bioactivity (Marins et al., 2018).

Niobium pentoxide (Nb_2O_5) has been proposed as a stable bioactive inorganic compound that has been used in different biomaterials in the biomedical field (Obata et al., 2012; Balbinot et al., 2018). The ability to promote deposition and growth of hydroxyapatite crystals on its surface when in contact with simulated body fluid (Karlinsey and Yi, 2008), artificial or natural saliva (Karlinsey et al., 2006) was explored in different materials in dentistry (Mazur et al., 2015) (Lopes et al., 2014; Altmann et al., 2017; Balbinot et al., 2018; Balbinot et al., 2019; Marins et al., 2019; Balbinot et al., 2020a; Balbinot et al., 2020b; Marins et al., 2020). Nb_2O_5 was studied in experimental adhesives (Leitune et al., 2013a; Collares et al., 2014; Marins et al., 2018), endodontic sealer (Leitune et al., 2013b), and glass ionomer cements (Garcia et al., 2016), improving their radiopacity (Leitune et al., 2013a; Leitune et al., 2013b; Garcia et al., 2016; Marins et al., 2018), physical properties (Leitune et al., 2013a; Leitune et al., 2013b) and inducing mineral deposition on adhesives surfaces (Collares et al., 2014). Increasing the Nb_2O_5 content into the polymeric matrix may lead to modifications to the properties of the material. The higher concentration is related to the reduction in the conversion of carbon-carbon double bonds (C=C) into single carbon-bonds (C-C) of methacrylate groups (Leitune et al., 2013a; Leitune et al., 2013b). This ineffective polymerization results in more residual monomers are available in the resin matrix, which may lead to higher cytotoxic effects (Salehi et al., 2015), greater sorption and solubility (Collares et al., 2011), lower bonding effectiveness to dentin (Hass et al., 2013), and lower mechanical properties (Ferracane, 1985). Balancing the potential bioactivity of Nb_2O_5 with adequate physicochemical and mechanical properties is essential for the application of these materials in a clinical scenario.

Among the oxides of niobium (Nb), Nb_2O_5 is the most stable. Nb can present a wide range of oxidation numbers from +5 to −3, with higher oxidation stated being more frequent to be found, mainly +5 states (Nowak and Ziolek, 1999). Due to the coordination numbers variability of Nb, this is a versatile element to develop novel materials, including organometallic structures. Among the different forms of niobium oxides, it is possible to synthesize hydrated niobium pentoxide, also called niobic acid ($Nb_2O_5{\cdot}nH_2O$), through the hydrolysis of niobium pentachloride ($NbCl_5$) or niobium ethoxide ($Nb(OC_2H_5)_5$) (Nakajima et al., 2011) or chemical reaction with acetophenones (Skrodczky et al., 2019). Niobic acid has been used in industry as a heterogeneous catalyst for chemical reactions due to its behavior as Lewis acid (Tanabe, 2003; Nakajima et al., 2011).

TABLE 1 | Description of the components used to design the dental adhesives according to the addition of filles by weight.

Group	Filler content
Control	No filler addition
2.5%	2.5 wt.% Nb_2O_5
	2.5 wt.% $Nb_2O_5.nH_2O$
5%	5 wt.% Nb_2O_5
	2.5 wt.% $Nb_2O_5.nH_2O$
10%	10 wt.% Nb_2O_5
	10 wt.% $Nb_2O_5.nH_2O$

$Nb_2O_5{\cdot}nH_2O$ has a high acid strength (H*o* −5.6~−8.2) and Lewis and Brønsted acid sites are available in the $Nb_2O_5{\cdot}nH_2O$ surface, making this oxide an efficient catalyst due to the reception of electrons (Lewis acid) or donation of protons (Brønsted acid) (Ziolek and Ziolek, 1999). As a heterogeneous catalyst, niobic acid may confer lower necessary energy to activate the chemical reactions (Nakajima et al., 2011). These differences in chemical structure may result in an optimized response of $Nb_2O_5{\cdot}nH_2O$ for dental applications. Although Nb_2O_5 was analyzed in dental adhesives previously (Leitune et al., 2013a; Marins et al., 2018), the potential effect of $Nb_2O_5{\cdot}nH_2O$ was not investigated so far. The aim of this study was to evaluate the incorporation of niobic acid into experimental dental adhesives and compare these adhesives to niobium pentoxide containing dental adhesives. A control group without $Nb_2O_5{\cdot}nH_2O$ or Nb_2O_5 was also used for comparison. The following physicochemical properties were analyzed: radiopacity, ultimate tensile strength, softening in solvent, degree of conversion, and polymerization rate.

MATERIALS AND METHODS

Dental Adhesives Formulation

The experimental dental adhesives were formulated by mixing 66.66 wt.% of bisphenol A glycerolate dimethacrylate (BisGMA) and 33.33 wt.% 2-hydroxyethyl methacrylate (HEMA). Camphorquinone and ethyl 4-dimethylaminobenzoate at 1 mol% and butylated hydroxytoluene at 0.01 wt.% were added to all groups as photoinitiator system. Niobium pentoxide (Nb2O5) and niobic acid ($Nb_2O_5{\cdot}nH_2O$) were incorporated at three different concentrations into this base resin: 2.5; 5 and 10 wt.%. As a control group, this base resin was used without Nb2O5 or $Nb_2O_5{\cdot}nH_2O$ addition in all tests. **Table 1** describes the components used to design the adhesives resin groups according to the addition of fillers by weight. The monomers and the photoinitiator materials were obtained from Aldrich Chemical Co. (Milwaukee, WI, USA) and used without further purification. The fillers were hand-mixed for 5 min, sonicated for 180 s, and hand-mixed again for 5 min. A light-emitting diode (LED) unit (Radii, SDI, Bayswater, VIC, Australia) with 1,200 mW/cm^2 was used to perform the photoactivation for all tests.

Dental Adhesives Evaluation

Radiopacity

The radiopacity of the dental adhesives was evaluated according to ISO 4049 [(ISO), 2009], using five samples per group (10.0 mm diameter and 1.0 mm thick, n = 5). The samples were prepared using a polyvinyl siloxane mold (ADSIL, Vigodent, Rio de Janeiro, RJ, Brazil), 20 s of photoactivation on each side, and stored in distilled water for 24 h at 37°C. An X-ray source (DabiAtlante model Spectro 70X) at 70 kV and 8 mA was used to expose the samples and acquire the X-ray images. Phosphorus plates (Digital System, VistaScan, Dürr Dental GmbH & Co. KG, Bietigheim-Bissingen, Baden-Württemberg, Germany) were used with 0.8 s of exposition and a focus-film distance of 400 mm. Each film was exposed with one sample per group together with an aluminum step-wedge (8 mm thick with 1 mm steps) in all images acquirement. The images were saved in TIFF format, and the mean and standard deviation values of gray for each sample and each aluminum millimeter were obtained (Photoshop software, Adobe Systems Incorporated, San Jose, CA, USA). The values were expressed as the equivalent thickness of aluminum in mm (Leitune et al., 2013a).

Ultimate Tensile Strength

Ten samples per group (n = 10) were prepared using a metallic mold with an hourglass shape (8 mm long, 2 mm wide, 1 mm thick, 1 mm^2 cross-sectional area). Each specimen was photoactivated for 20 s on each side, removed from the mold, and stored in distilled water at 37°C for 24 h. After this period, each sample had its constriction area measured with a digital caliper and fixed with a cyanoacrylate resin into metallic jigs. Each jig was positioned in a universal testing machine (EZ-SX Series, Shimadzu, Tokyo, Kantō, Japan). The upper part of the jig was tensile at a crosshead speed of 1 mm/min until the samples fracture. The values were recorded in Newtons (N), divided by the area of each sample (mm), and expressed in megapascals (MPa).

Softening in Solvent

Three samples per group (1 mm thick and 5 mm diameter, n = 3) (Garcia et al., 2019) were prepared with a polyvinyl siloxane (Express™ VPS Impression Material, 3 M ESPE, St. Paul, MN, USA) mold, 20 s of photoactivation on each side, and stored in distilled water for 24 h at 37°C. The samples were embedded in self-curing acrylic resin (Clássico, São Paulo, São Paulo, Brazil) and polished (Model 3v, Arotec, Cotia, SP, BR) with silicon carbide sandpapers (from 600 to 2000-grit, Klingspor, Pinhas, PR, Brazil) and felt disc sutured with alumina suspension (Alumina 1 µm, Fortel, São Paulo, SP, BR). The embedded samples were washed with running water and sonicated for 480 s (L100; Schuster, Santa Maria, RS, Brazil) with distilled water. After 24 h, the specimens were evaluated by three indentations at 10 g/5 s to obtain the initial Knoop hardness (KHN1) using a digital microhardness tester (HMV 2, Shimadzu, Tokyo, Kantō, Japan). The specimens were subjected to softening in ethanol for 2 h, and the hardness test was performed again (KHN2). The percentual hardness reduction was calculated for each sample and each group, according to **Eq. 1**:

$$\%\Delta KHN = 100 - ((KHN2 \times 100)/KHN1). \quad (1)$$

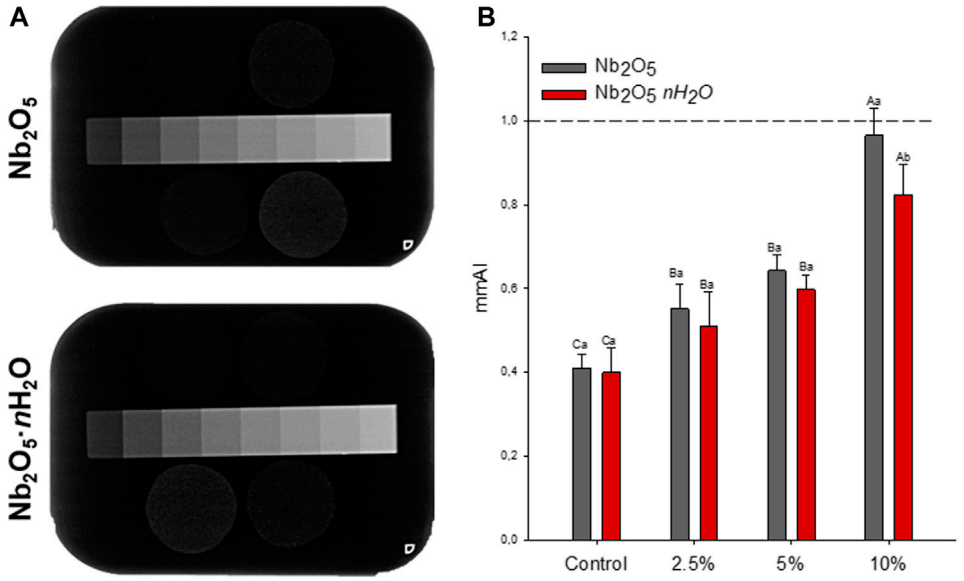

FIGURE 1 | Radiopacity of the formulates dental adhesives **(A)** Representative images of X-rays radiographs from the adhesives with different types of fillers (Nb_2O_5 or Nb_2O_5. nH_2O) and different concentrations (0, 2.5, 5, and 10 wt%). The aluminum scale bar was positioned close to the specimens to obtain mm Al values **(B)** Quantification of radiopacity in mm Al. The dotted line represents 1 mm Al, which is the same radiopacity of 1 mm of dentin. Different capital letters indicate a statistically significant difference among the concentrations (0, 2.5, 5, and 10 wt%) for the same type of filler (Nb_2O_5 or Nb_2O_5. nH_2O) ($p < 0.05$). Different lowercase letters indicate a statistically significant difference within the same concentration (0, 2.5, 5, or 10 wt%) comparing the different types of filler (Nb_2O_5 or Nb_2O_5. nH_2O) ($p < 0.05$).

Degree of Conversion

Three samples per group (n = 3) were evaluated by Fourier Transform Infrared Spectroscopy (FTIR) with a spectrometer (Vertex 70, Bruker Optics, Ettlingen, Baden-Württemberg, Germany) equipped with an attenuated total reflectance device (ATR). The uncured adhesives were dispensed onto the crystal using a polyvinyl siloxane mold of 1 mm thick and 5 mm diameter. The spectra from each sample were acquired using Opus 6.5 software (Bruker Optics, Ettlingen, Baden-Württemberg, Germany) with Blackman Haris 3-Term apodization, in the range from 400 to 4,000 cm^{-1}, with 64 scans and 4 cm^{-1} resolution. Then, the sample was light-cured for 20 s at a standardized distance of 1 mm between the tip of the LED unit and the top of the sample. Immediately after the light-curing process, the spectra of the cured adhesive samples were obtained. The degree of conversion (DC) was calculated according to previous studies using the peaks at 1,610 cm^{-1} (aromatic carbon-carbon double bonds) and 1,640 cm^{-1} (aliphatic carbon-carbon double bonds) (Collares et al., 2011; Collares et al., 2013; Garcia et al., 2018; Garcia et al., 2020b).

Polymerization Rate

The polymerization rate of three samples per group of dental adhesives (n = 3) were evaluated by differential scanning calorimetry (DSC, DSC-Q2000, TA Instrument Co., New Castle, DE, USA) with a photocalorimetric accessory (PCA) adjusted to 100 mW/cm^2. The uncured adhesives were photoactivated with PCA under a nitrogen flow rate of 50 ml/min. The maximum polymerization rate was determined according to a previous study (Rodrigues et al., 2015).

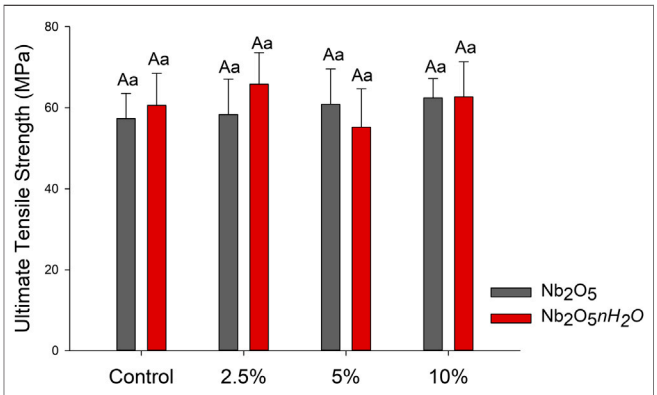

FIGURE 2 | Mean and standard deviation values of the ultimate tensile strength (UTS) of the dental adhesives in MPa. Different capital letters indicate a statistically significant difference among the concentrations (0, 2.5, 5, and 10 wt%) for the same type of filler (Nb_2O_5 or Nb_2O_5.nH_2O) ($p < 0.05$). Different lowercase letters indicate a statistically significant difference within the same concentration (0, 2.5, 5, or 10 wt%) comparing the different types of filler (Nb_2O_5 or Nb_2O_5. nH_2O) ($p < 0.05$).

Statistical Analysis

SigmaPlot software (version 12.0, Systat Software, San Jose, CA, USA) was used for the statistical analyses. Shapiro-Wilk test was used to analyze the data distribution. Radiopacity, DC, polymerization rate, UTS, and softening in solvent were evaluated using two-way ANOVA and Tukey post-hoc test considering the two factors: concentrations (0, 2.5, 5, or 10 wt.%) and filler (Nb_2O_5 or $Nb_2O_5 \cdot nH_2O$). A significance level of 0.05 was used to analyze the data statistically.

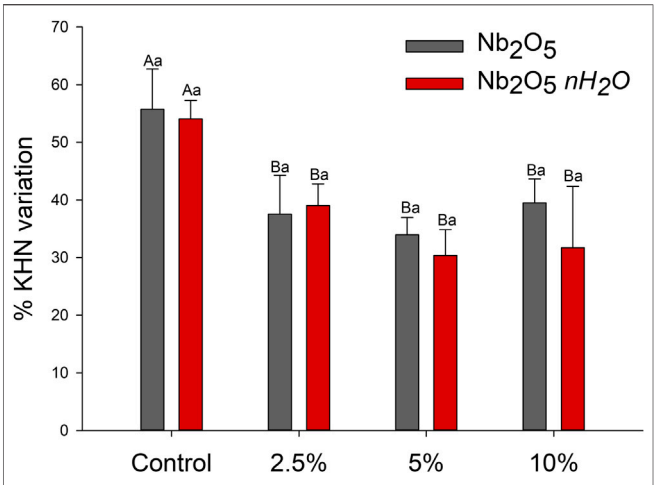

FIGURE 3 | Mean and standard deviation of softening in solvent after immersion in ethanolic solution in percentage of microhardness variation. Different capital letters indicate a statistically significant difference among the concentrations (0, 2.5, 5, and 10 wt%) for the same type of filler (Nb_2O_5 or $Nb_2O_5.nH_2O$) ($p < 0.05$). Different lowercase letters indicate a statistically significant difference within the same concentration (0, 2.5, 5, or 10 wt%) comparing the different types of filler (Nb_2O_5 or Nb_2O_5. nH_2O) ($p < 0.05$).

RESULTS

The results of the radiopacity evaluation of the dental adhesives are displayed in **Figure 1**. Representative x-ray images were shown in **Figure 1A** with an aluminum scale bar used as a comparison for mm Al calculation. With increasing the content of Nb_2O_5 or $Nb_2O_5{\cdot}nH_2O$, the radiopacity increased in contrast to the control group ($p < 0.05$). There were no differences between the groups with 2.5 or 5 wt.% of fillers regardless of its type (Nb_2O_5 or $Nb_2O_5{\cdot}nH_2O$) ($p > 0.05$). The group with 10 wt.% of Nb_2O_5 showed higher radiopacity in comparison to 10 wt% of $Nb_2O_5{\cdot}nH_2O$ ($p < 0.05$). However, within the same filler type, the incorporation of 10 wt% of Nb_2O_5 or $Nb_2O_5{\cdot}nH_2O$ showed the highest radiopacity ($p < 0.05$), with values close to 1 mm of aluminum.

The results from the mechanical evaluation of the dental adhesives are shown in **Figure 2**. Among all groups, the values ranged from 55.17 (±9.48) for 5 wt.% of $Nb_2O_5{\cdot}nH_2O$ to 65.80 (±7.79) for 2.5 wt.% of $Nb_2O_5{\cdot}nH_2O$. There were no statistically significant differences among groups regardless of the fillers' concentration or filler type ($p > 0.05$).

Figure 3 displays the results of softening in solvent. For Nb_2O_5 groups, the addition from 2.5 wt.% of this filler decreased the percentage of softening compared to the control group ($p < 0.05$), without statistically significant differences among 2.5, 5, and 10 wt.% ($p > 0.05$). The same behavior occurred for $Nb_2O_5{\cdot}nH_2O$ groups: the incorporation of any tested concentration of $Nb_2O_5{\cdot}nH_2O$ improved the resistance against softening in solvent in comparison to the unfilled adhesive ($p < 0.05$), and no changed were observed from 2.5 to 10 wt.% of $Nb_2O_5{\cdot}nH_2O$ ($p > 0.05$).

The DC and Rp_{max} are presented in **Figure 4**. For Nb_2O_5 groups, the DC ranged from 64.93 (±0.78) for the control to 51.49 (±2.55) for 10 wt.% ($p < 0.05$). From 5 wt.% of Nb_2O_5 addition, the DC decreased in comparison to 0 and 2.5 wt.% ($p < 0.05$), with lower DC result for the 10 wt.% Nb_2O_5 addition ($p < 0.05$). For $Nb_2O_5{\cdot}nH_2O$ groups, the DC ranged from 65.13 (±0.68) for 2.5 wt.% to 62.74 (±1.71) for 5 wt.% (**Figure 4A**). There were no statistically significant differences among groups with different

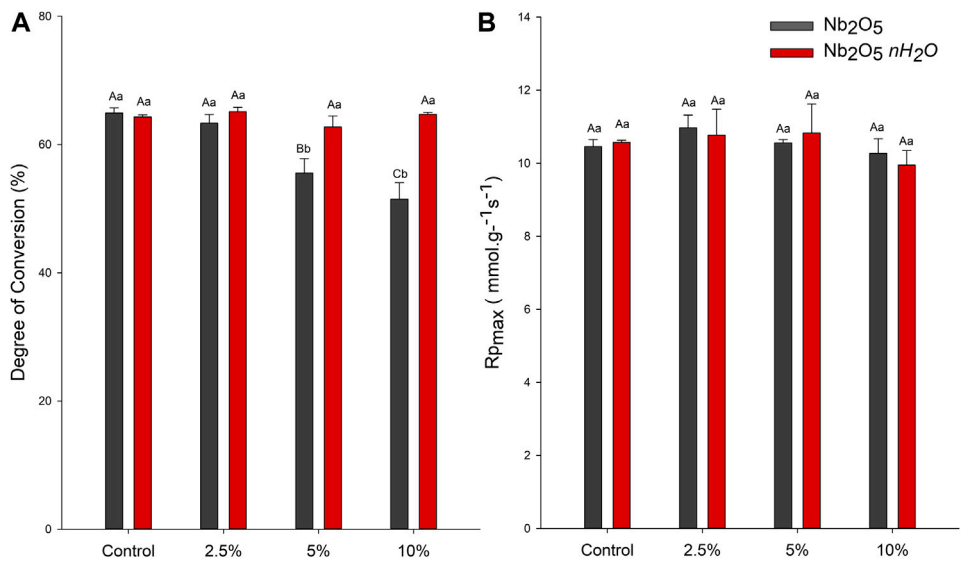

FIGURE 4 | Degree of conversion (DC) and maximum polymerization rate (RP_{max}) of dental adhesives **(A)** Percentage of converted carbon-carbon double bonds of the dental adhesives after photoactivation via FTIR-ATR **(B)** RP_{max} of the dental adhesives via DSC-PCA. Different capital letters indicate a statistically significant difference among the concentrations (0, 2.5, 5, and 10 wt%) for the same type of filler (Nb_2O_5 or Nb_2O_5. nH_2O) for the DC or RP_{max} evaluation ($p < 0.05$). Different lowercase letters indicate a statistically significant difference within the same concentration (0, 2.5, 5, or 10 wt%) comparing the different types of filler (Nb_2O_5 or Nb_2O_5. nH_2O) for the DC or RP_{max} evaluation ($p < 0.05$).

concentrations of $Nb_2O_5{\cdot}nH_2O$ ($p > 0.05$). The addition of five or 10 wt.% of $Nb_2O_5{\cdot}nH_2O$ induced higher DC in comparison to five or 10 wt% of Nb_2O_5. The Rp_{max} *via* DSC showed no difference among groups, neither between the two types of filler, neither among fillers concentration (**Figure 4B**).

DISCUSSION

Dental adhesives have been modified to present superior therapeutic and physicochemical properties (Profeta, 2014; Balbinot et al., 2020a; Bendary et al., 2020; Garcia et al., 2020b; Yao et al., 2020). In this context, bioactive fillers have been incorporated into dental adhesives (Profeta, 2014; Balbinot et al., 2020a; Bendary et al., 2020; Braga and Fronza, 2020; Yao et al., 2020). However, the effect of these fillers in the physicochemical properties of resin-based materials must be addressed to guarantee the proper behavior for dental adhesives. In the present study, niobic acid was studied as a potential catalyst bioactive inorganic filler into dental adhesives. The radiopacity, the resistance against softening in solvents, and the mechanical properties were maintained for niobic acid-containing adhesives when compared to niobium pentoxide filled materials. The highest concentrations of $Nb_2O_5{\cdot}nH_2O$ supported a high DC in comparison to the unfilled adhesive, with an increased percentage of conversion when compared to Nb_2O_5 in the same concentrations.

The life span of resin composite restorations is importantly affected by the recurrence of caries and the identification of marginal gaps, leading to the premature replacement of composites (Brouwer et al., 2016). Adhesives must be distinguishable from the adjacent tissues in the radiographic examination to assist in the proper diagnose of carious affected tissues (Brouwer et al., 2016; Mjor, 2005). The low radiopacity of adhesives hampers their distinguish from adjacent tissues and pathological processes, and as shown in **Figure 1A**, unfilled adhesives are difficult to be observed on X-ray radiographs. The International Organization for Standardization (ISO) established that polymer-based restorative materials must present radiopacity equal or superior to dentin (International Organisation for Standardization, 2009) and it is known that 1 mm of dentin has a radiopacity similar to 1 mmAl in the aluminum step-wedge (Mjor, 2005). Thus, reaching this value is the goal of the development of radiopaque materials. Neither particle reached a radiopacity average with this value, as shown in **Figure 1B**. However, both types of filler, Nb_2O_5, and $Nb_2O_5{\cdot}nH_2O$, provided dental adhesives with higher radiopacity than the unfilled material, which has a similar composition to a commercial widely used adhesive (Ogliari et al., 2006). Our results indicated that Nb_2O_5 or $Nb_2O_5{\cdot}nH_2O$ at 10 wt.% reached ~0.8–0.95 mm Al for the groups suggesting that, despite the potential bioactivity, these fillers could provide suitable radiopacity for the developed dental adhesives.

The main responsibility for the increased radiopacity is the higher atomic number of Nb (41) in comparison to the other components of the dental adhesive [carbon (6), hydrogen (1), nitrogen (7), oxygen (8)]. At 10 wt.% concentration, higher values were observed for Nb_2O_5 when compared to $Nb_2O_5{\cdot}nH_2O$ (**Figure 1**; $p < 0.05$). Differences in chemical composition between both particles may have led to the higher radiopacity of adhesives doped with Nb_2O_5 when 10 wt.% was added. The particles of $Nb_2O_5{\cdot}nH_2O$ are commonly derived from the hydrolysis of niobium pentachloride, forming $Nb_2O_5{\cdot}nH_2O$. In contrast, the particles of Nb_2O_5 are mostly composed of Nb, and O. Differences in the particle densities and, consequently, in the volume of filler incorporated, maybe was responsible for the radiopacity variation between the groups of adhesives with 10 wt.% of Nb_2O_5 or $Nb_2O_5{\cdot}nH_2O$.

The formulated dental adhesives were also analyzed for their mechanical properties *via* UTS and softening in solvent. The UTS shows the intrinsical resistance of materials against fractures when they are tensioned. Inorganic particles may act *via* toughening behavior such as crack deflection and increased elastic modulus (Lohbauer et al., 2010). In this study, we did not observe differences in the UTS (**Figure 2**; $p > 0.05$), while the softening in solvent for all groups containing a filler, regardless of its type, decreased in comparison to the control group (**Figure 3**). This test evaluates the ability of polymers to resist solvents. Therefore, the hydrophilicity and the crosslinking density of the polymers are involved in this process outcome.

When exposed to solvents, polymers are prone to swell because the forces among the polymer chains are surpassed by the attraction between polymer chains and molecule solvents (Schneider et al., 2008). Then, depending on the polymer network formation, the time of immersion, and the solubility parameter of the solution used, polymer chains maybe degrade via hydrolysis (Ferracane, 2006; Schneider et al., 2008). In this study, after the immersion in solvent, all groups presented lower Knoop hardness, corroborating with previous analyses (Schneider et al., 2008; Garcia et al., 2020b). Resins with inorganic fillers, such as the metallic oxides here tested, are less susceptible to suffer chemical degradation mainly because ionic bonding between atoms in oxides is more stable than covalent bonding within the organic matrix. Therefore, adhesives doped with inorganic fillers can present lower softening in solvent compared to unfilled adhesives (Stürmer et al., 2020). Irrespective of the concentration of Nb_2O_5 or $Nb_2O_5{\cdot}nH_2O$, both materials provided successful decreased softening for the dental adhesives. Therefore, the crosslinking density of the filled materials was superior to the control group, or the fillers were able to increase stability by reducing the amount of organic content.

The properties of Nb_2O_5 and $Nb_2O_5{\cdot}nH_2O$ particles, such as density, size, and volume, as well as their chemical composition, may affect the loading of these fillers into the dental adhesives. The ability to convert carbon-carbon double bonds into carbon-carbon single bonds highly depends on the availability of light through the polymer thickness since these materials are photoactivated (Par et al., 2020). By increasing metallic oxides content into adhesives, it is likely to observe a decreased DC (Leitune et al., 2013a; Garcia et al., 2018; Garcia et al., 2020a). This effect may be related to the higher opacity that filled adhesives may present in comparison to unfilled adhesives (Shortall, 2005). Moreover, it was suggested that the presence of oxides into the composition of unsilanized glasses could also jeopardize the

degree of conversion, depth of cure, and polymerization rate *via* "premature termination of free-radical-mediated polymerization" (Par et al., 2020). The results of the present study were in accordance with previous analyses when the addition of Nb_2O_5 decreased the DC of dental adhesives (Leitune et al., 2013a). While the addition of 5 wt.% of Nb_2O_5 was enough to reduce the DC in comparison to the control group, the use of $Nb_2O_5{\cdot}nH_2O$ did not change this property up to 10 wt.% (**Figure 2A**). The high DC, even with 10 wt.% of $Nb_2O_5{\cdot}nH_2O$, could be a result of the activity of this oxide within the resin during the polymerization reaction. The presence of Lewis and Brønsted acid sites in these particles may increase the reaction during the polymerization (Tanabe, 2003; Nakajima et al., 2011). In this way, even with possible lower light penetration through the filled adhesives, the catalyst activity of $Nb_2O_5{\cdot}nH_2O$ could minimize this effect and support the DC. Interestingly, there were no differences in the Rp_{max} to indicate the adhesive with $Nb_2O_5{\cdot}nH_2O$ decreased the energy required for the polymerization reaction (**Figure 2B**). However, the catalytic effect may also have shifted the chain mobility without altering the Rp_{max} and maintaining DC.

While the catalysis effect could explain the DC values, during the manipulation and polymerization process, differences in the optical properties between groups were observed. Nb_2O_5 is known to have a high refractive index (Leitune et al., 2013a), and the adhesives in this group presented an opaque white color, while $Nb_2O_5{\cdot}nH_2O$ containing materials were more translucent and yellowish. These differences could be observed in both uncured and cured adhesives, and this finding may be endorsed in the precursors of $Nb_2O_5{\cdot}nH_2O$ synthesis since $NbCl_5$ is a yellowish material. However, other features such as the refractive index difference between $Nb_2O_5{\cdot}nH_2O$ and Nb_2O_5, the density of the fillers, and the volume incorporated may lead to these color variations. Although color and translucency were not investigated in this study, with this exploratory tuning of both fillers was already possible to identify some interesting differences between $Nb_2O_5{\cdot}nH_2O$ and Nb_2O_5.

The balance between the bioactivity and the physicochemical properties is a demand in the study of bioactive dental materials. Niobium pentoxide was shown to induce mineral deposition by the formation of a phosphate-rich layer on 2.5 wt.% and 5 wt.% loaded dental adhesives (Collares et al., 2014). Increasing the quantity of bioactive fillers into the adhesives could lead to a higher release of niobium compounds that may induce higher mineral formation in the adhesive layer as the availability of ions could cause deposition of mineral as described previously (Obata et al., 2012). $Nb_2O_5{\cdot}nH_2O$ doped adhesives showed improved outcomes, such as higher radiopacity, maintenance of mechanical strength, and lower softening in solvent. With the incorporation of $Nb_2O_5{\cdot}nH_2O$ up to 10 wt.%, the DC was sustained, suggesting that the control of particle properties may be an alternative for the development of dental adhesives doped with mettalic oxides. It is a limitation of the present study to not have tested the mineral deposition capacity of the formulated adhesives. Future studies are encouraged to evaluate the possible bioactivity of $Nb_2O_5{\cdot}nH_2O$ doped adhesives.

CONCLUSION

In this study, we explored two niobium-based fillers for dental adhesives: niobium pentoxide (Nb_2O_5) and niobic acid (Nb_2O_5HY). These fillers were tested at 0, 2.5, 5, and 10 wt.%. Overall, Nb_2O_5 and Nb_2O_5HY doped adhesives showed improved outcomes, such as higher radiopacity, maintenance of mechanical strength, and lower softening in solvent. Through of addition of Nb_2O_5HY up to 10 wt.%, the DC was sustained as presented the unfilled adhesive. In conclusion, Nb_2O_5HY is a promising filler to be incorporated into dental adhesives providing proper mechanical properties, improved resistance against solvents, and increased radiopacity, without changing the DC.

DATA AVAILABILITY STATEMENT

The original contributions presented in the study are included in the article/Supplementary Material, further inquiries can be directed to the corresponding author.

AUTHOR CONTRIBUTIONS

IG: Investigation, Formal Analysis, Data Curation, Visualization, Writing—Original Draft. VL: Conceptualization, Formal Analysis, Resources, Writing—Review & Editing. GB: Visualization, Writing—Review & Editing. AB: Writing—Original Draft. MM:Writing—Original Draft. SS: Resources, Writing—Review & Editing. FC: Conceptualization, Resources, Writing—Review & Editing, Supervision, Funding acquisition.

FUNDING

This study was financed in part by the Coordenação de Aperfeiçoamento de Pessoal de Nível Superior—Brasil (CAPES)—Finance Code 001 (scholarship of IG and GB). There was no fund received for open access publication fees.

ACKNOWLEDGMENTS

AB acknowledge the scholarship during his Ph.D. studies from the Imam AbdulRahman bin Faisal University, Dammam, Saudi Arabia, and the Saudi Arabia Cultural Mission.

REFERENCES

Altmann, A. S. P., Collares, F. M., Balbinot, G. S., Leitune, V. C. B., Takimi, A. S., and Samuel, S. M. W. (2017). Niobium pentoxide phosphate invert glass as a mineralizing agent in an experimental orthodontic adhesive. *Angle Orthod.* 87, 759–765. doi:10.2319/122417-140.1

Balbinot, G. S., Collares, F. M., Herpich, T. L., Visioli, F., Samuel, S. M. W., and Leitune, V. C. B. (2020a). Niobium containing bioactive glasses as remineralizing filler for adhesive resins. *Dent. Mater.* 36, 221–228. doi:10.1016/j.dental.2019.11.014

Balbinot, G. S., Collares, F. M., Visioli, F., Soares, P. B. F., Takimi, A. S., Samuel, S. M. W., et al. (2018). Niobium addition to sol-gel derived bioactive glass powders and scaffolds: in vitro characterization and effect on pre-osteoblastic cell behavior. *Dent. Mater.* 34, 1449–1458. doi:10.1016/j.dental.2018.06.014

Balbinot, G. S., Leitune, V. C. B., Ogliari, F. A., and Collares, F. M. (2020b). Niobium silicate particles promote *in vitro* mineral deposition on dental adhesive resins. *J. Dent.* 101, 103449. doi:10.1016/j.jdent.2020.103449

Balbinot, G. S., Leitune, V. C. B., Ponzoni, D., and Collares, F. M. (2019). Bone healing with niobium-containing bioactive glass composition in rat femur model: a micro-CT study. *Dent. Mater.* 35, 1490–1497. doi:10.1016/j.dental.2019.07.012

Balhaddad, A. A., Kansara, A. A., Hidan, D., Weir, M. D., Xu, H. H. K., and Melo, M. A. S. (2019). Toward dental caries: exploring nanoparticle-based platforms and calcium phosphate compounds for dental restorative materials. *Bioact. Mater.* 4, 43–55. doi:10.1016/j.bioactmat.2018.12.002

Belli, R., Kreppel, S., Petschelt, A., Hornberger, H., Boccaccini, A. R., and Lohbauer, U. (2014). Strengthening of dental adhesives via particle reinforcement. *J Mech. Behav. Biomed. Mater.* 37, 100–108. doi:10.1016/j.jmbbm.2014.05.007

Bendary, I. M., Garcia, I. M., Collares, F. M., Takimi, A., Samuel, S. M. W., and Leitune, V. C. B. (2020). Wollastonite as filler of an experimental dental adhesive. *J. Dent.* 102, 103472. doi:10.1016/j.jdent.2020.103472

Braga, R. R., and Fronza, B. M. (2020). The use of bioactive particles and biomimetic analogues for increasing the longevity of resin-dentin interfaces: a literature review. *Dent. Mater. J.* 39, 62–68. doi:10.4012/dmj.2019-293

Brouwer, F., Askar, H., Paris, S., and Schwendicke, F. (2016). Detecting secondary caries lesions: a systematic review and meta-analysis. *J. Dent. Res.* 95, 143–151. doi:10.1177/0022034515611041

Collares, F. M., Ogliari, F. A., Zanchi, C. H., Petzhold, C. L., Piva, E., and Samuel, S. M. (2011). Influence of 2-hydroxyethyl methacrylate concentration on polymer network of adhesive resin. *J. Adhesive Dent.* 13, 125–129. doi:10.3290/j.jad.a18781

Collares, F. M., Portella, F. F., Leitune, V. C., and Samuel, S. M. (2013). Discrepancies in degree of conversion measurements by FTIR. *Braz. Oral Res.* 27, 453–454. doi:10.1590/S1806-83242013000600002

Collares, F. M., Portella, F. F., Fraga, G. C. S., Semeunka, S. M., Almeida, L. C. B., Santos, E. R., et al. (2014). Mineral deposition at dental adhesive resin containing niobium pentoxide. *Applied Adhesion Science* 2, 6. doi:10.1186/s40563-014-0022-0

Ferracane, J. L. (1985). Correlation between hardness and degree of conversion during the setting reaction of unfilled dental restorative resins. *Dent. Mater.* 1, 11–14. doi:10.1016/S0109-5641(85)80058-0

Ferracane, J. L. (2006). Hygroscopic and hydrolytic effects in dental polymer networks. *Dent. Mater.* 22, 211–222. doi:10.1016/j.dental.2005.05.005

Garcia, I. M., Leitune, V. C. B., Balbinot, G. S., Samuel, S. M. W., and Collares, F. M. (2016). Influence of niobium pentoxide addition on the properties of glass ionomer cements. *Acta Biomater. Odontol. Scand.* 2, 138–143. doi:10.1080/23337931.2016.1239182

Garcia, I. M., Leitune, V. C. B., Ferreira, C. J., and Collares, F. M. (2018). Tantalum oxide as filler for dental adhesive resin. *Dent. Mater. J.* 37, 897–903. doi:10.4012/dmj.2017-308

Garcia, I. M., Leitune, V. C. B., Samuel, S. M. W., and Collares, F. M. (2017). Influence of different calcium phosphates on an experimental adhesive resin. *J. Adhesive Dent.* 19, 1–6. doi:10.3290/j.jad.a38997

Garcia, I. M., Souza, V. S., Souza, J. D., Visioli, F., Leitune, V. C. B., Scholten, J. D., et al. (2020b). Zinc-based particle with ionic liquid as a hybrid filler for dental adhesive resin. *J. Dent.* 102, 103477. doi:10.1016/j.jdent.2020.103477

Garcia, I. M., Leitune, V. C. B., Takimi, A. S., Bergmann, C. P., Samuel, S. M. W., Melo, M. A., et al. (2020a). Cerium dioxide particles to tune radiopacity of dental adhesives: microstructural and physico-chemical evaluation. *J. Funct. Biomater.* 11. doi:10.3390/jfb11010007

Garcia, I. M., Souza, V. S., Hellriegel, C., Scholten, J. D., and Collares, F. M. (2019). Ionic liquid-stabilized titania quantum dots applied in adhesive resin. *J. Dent. Res.* 98, 682–688. doi:10.1177/0022034519835203

Hass, V., Dobrovolski, M., Zander-Grande, C., Martins, G. C., Gordillo, L. A., Rodrigues Accorinte, Mde. L., et al. (2013). Correlation between degree of conversion, resin-dentin bond strength and nanoleakage of simplified etch-and-rinse adhesives. *Dent. Mater.* 29, 921–928. doi:10.1016/j.dental.2013.05.001

Ibrahim, M. S., Balhaddad, A. A., Garcia, I. M., Collares, F. M., Weir, M. D., Xu, H. H. K., et al. (2020a). pH-responsive calcium and phosphate-ion releasing antibacterial sealants on carious enamel lesions *in vitro*. *J. Dent.* 97, 103323. doi:10.1016/j.jdent.2020.103323

Ibrahim, M. S., Balhaddad, A. A., Garcia, I. M., Hefni, E., Collares, F. M., Martinho, F. C., et al. (2020b). Tooth sealing formulation with bacteria-killing surface and on-demand ion release/recharge inhibits early childhood caries key pathogens. 108, 3217–3227. doi:10.1002/jbm.b.34659

International Organization for Standardization (2009). *ISO 4049: 2009—dentistry—Polymer-based restorative materials*. Geneva, Switzerland: International Organization for Standardization.

Karlinsey, R. L., Hara, A. T., Yi, K., and Duhn, C. W. (2006). Bioactivity of novel self-assembled crystalline Nb2O5 microstructures in simulated and human salivas. *Biomed. Mater.* 1, 16–23. doi:10.1088/1748-6041/1/1/003

Karlinsey, R. L., and Yi, K. (2008). Self-assembly and bioactive response of a crystalline metal oxide in a simulated blood fluid. *J. Mater. Sci. Mater. Med.* 19, 1349–1354. doi:10.1007/s10856-007-3164-9

Leitune, V. C., Collares, F. M., Takimi, A., de Lima, G. B., Petzhold, C. L., Bergmann, C. P., et al. (2013a). Niobium pentoxide as a novel filler for dental adhesive resin. *J. Dent.* 41, 106–113. doi:10.1016/j.jdent.2012.04.022

Leitune, V. C., Takimi, A., Collares, F. M., Santos, P. D., Provenzi, C., Bergmann, C. P., et al. (2013b). Niobium pentoxide as a new filler for methacrylate-based root canal sealers. *Int. Endod. J.* 46, 205–210. doi:10.1111/j.1365-2591.2012.02107.x

Lohbauer, U., Wagner, A., Belli, R., Stoetzel, C., Hilpert, A., Kurland, H. D., et al. (2010). Zirconia nanoparticles prepared by laser vaporization as fillers for dental adhesives. *Acta Biomater.* 6, 4539–4546. doi:10.1016/j.actbio.2010.07.002

Lopes, J. H., Magalhães, A., Mazali, I. O., and Bertran, C. A. (2014). Effect of niobium oxide on the structure and properties of melt-derived bioactive glasses. *J. Am. Ceram. Soc.* 97, 3843–3852. doi:10.1111/jace.13222

Marins, N. H., Lee, B. E. J., E Silva, R. M., Raghavan, A., Villarreal Carreño, N. L., and Grandfield, K. (2019). Niobium pentoxide and hydroxyapatite particle loaded electrospun polycaprolactone/gelatin membranes for bone tissue engineering. *Colloids Surf. B Biointerfaces* 182, 110386. doi:10.1016/j.colsurfb.2019.110386

Marins, N. H., Silva, R. M., Ferrua, C. P., Łukowiec, D., Barbosa, A. M., Ribeiro, J. S., et al. (2020). Fabrication of electrospun poly(lactic acid) nanoporous membrane loaded with niobium pentoxide nanoparticles as a potential scaffold for biomaterial applications. *J. Biomed. Mater. Res. B Appl. Biomater.* 108, 1559–1567. doi:10.1002/jbm.b.34503

Marins, N. H., Meereis, C. T. W., Silva, R. M., Ruas, C. P., Takimi, A. S., Carreño, N. L. V., et al. (2018). Radiopaque dental adhesive with addition of niobium pentoxide nanoparticles. *Polym. Bull.* 75, 2301–2314. doi:10.1007/s00289-017-2150-8

Mazur, M., Kalisz, M., Wojcieszak, D., Grobelny, M., Mazur, P., Kaczmarek, D., et al. (2015). Determination of structural, mechanical and corrosion properties of Nb2O5 and (NbyCu 1-y)Ox thin films deposited on Ti6Al4V alloy substrates for dental implant applications. *Mater. Sci. Eng. C. Mater. Biol. Appl.* 47, 211–221. doi:10.1016/j.msec.2014.11.047

Mjor, I. A. (2005). Clinical diagnosis of recurrent caries. *J. Am. Dent. Assoc.* 136, 1426–1433. doi:10.14219/jada.archive.2005.0057

Münchow, E. A., and Bottino, M. C. (2017). Recent advances in adhesive bonding: the role of biomolecules, nanocompounds, and bonding strategies in enhancing resin bonding to dental substrates. *Curr. Oral Health Rep.* 4, 215–227. doi:10.1007/s40496-017-0146-y

Nakajima, K., Baba, Y., Noma, R., Kitano, M., Kondo, J. N., Hayashi, S., et al. (2011). Nb2O5·nH2O as a heterogeneous catalyst with water-tolerant Lewis acid sites. *J. Am. Chem. Soc.* 133, 4224–4227. doi:10.1021/ja110482r

Nowak, I., and Ziolek, M. (1999). Niobium compounds: preparation, characterization, and application in heterogeneous catalysis. *Chem. Rev.* 99, 3603–3624. doi:10.1021/cr9800208

Obata, A., Takahashi, Y., Miyajima, T., Ueda, K., Narushima, T., and Kasuga, T. (2012). Effects of niobium ions released from calcium phosphate invert glasses containing Nb2O5 on osteoblast-like cell functions. *ACS Appl. Mater. Interfaces* 4, 5684–5690. doi:10.1021/am301614a

Ogliari, F. A., de Sordi, M. L., Ceschi, M. A., Petzhold, C. L., Demarco, F. F., and Piva, E. (2006). 2,3-Epithiopropyl methacrylate as functionalized monomer in a dental adhesive. *J. Dent.* 34, 472–477. doi:10.1016/j.jdent.2005.11.001

Par, M., Spanovic, N., Mohn, D., Attin, T., Tauböck, T. T., and Tarle, Z. (2020). Curing potential of experimental resin composites filled with bioactive glass: a comparison between Bis-EMA and UDMA based resin systems. *Dent. Mater.* 36, 711–723. doi:10.1016/j.dental.2020.03.015

Profeta, A. C. (2014). Dentine bonding agents comprising calcium-silicates to support proactive dental care: origins, development and future. *Dent. Mater. J.* 33, 443–452. doi:10.4012/dmj.2013-267

Rodrigues, S. B., Collares, F. M., Leitune, V. C., Schneider, L. F., Ogliari, F. A., Petzhold, C. L., et al. (2015). Influence of hydroxyethyl acrylamide addition to dental adhesive resin. *Dent. Mater.* 31, 1579–1586. doi:10.1016/j.dental.2015.10.005

Salehi, S., Gwinner, F., Mitchell, J. C., Pfeifer, C., and Ferracane, J. L. (2015). Cytotoxicity of resin composites containing bioactive glass fillers. *Dent. Mater.* 31, 195–203. doi:10.1016/j.dental.2014.12.004

Schneider, L. F., Moraes, R. R., Cavalcante, L. M., Sinhoreti, M. A., Correr-Sobrinho, L., and Consani, S. (2008). Cross-link density evaluation through softening tests: effect of ethanol concentration. *Dent. Mater.* 24, 199–203. doi:10.1016/j.dental.2007.03.010

Shortall, A. C. (2005). How light source and product shade influence cure depth for a contemporary composite. *J. Oral Rehabil.* 32, 906–911. doi:10.1111/j.1365-2842.2005.01523.x

Skrodczky, K., Antunes, M. M., Han, X., Santangelo, S., Scholz, G., Valente, A. A., et al. (2019). Niobium pentoxide nanomaterials with distorted structures as efficient acid catalysts. *Communications Chemistry* 2, 11–13. doi:10.1038/s42004-019-0231-3

Stürmer, M., Garcia, I. M., Souza, V. S., Visioli, F., Scholten, J. D., Samuel, S. M. W., et al. (2020). Titanium dioxide nanotubes with triazine-methacrylate monomer to improve physicochemical and biological properties of adhesives. *Dent. Mater.* doi:10.1016/j.dental.2020.11.004

Tanabe, K. (2003). Catalytic application of niobium compounds. *Catal. Today* 78, 65–77. doi:10.1016/s0920-5861(02)00343-7

Toledano, M., Osorio, R., Osorio, E., García-Godoy, F., Toledano-Osorio, M., and Aguilera, F. S. (2016). Advanced zinc-doped adhesives for high performance at the resin-carious dentin interface. *J. Mech. Behav. Biomed. Mater.* 62, 247–267. doi:10.1016/j.jmbbm.2016.05.013

Yao, C., Ahmed, M. H., Li, X., Nedeljkovic, I., Vandooren, J., Mercelis, B., et al. (2020). Zinc-calcium-fluoride bioglass-based innovative multifunctional dental adhesive with thick adhesive resin film thickness, *ACS Appl. Mater. Interfaces* 12, 30120–30135. doi:10.1021/acsami.0c06865

Ziolek, I., and Ziolek, M. (1999). Niobium compounds: preparation, characterization, and application in heterogeneous catalysis. *Chem. Rev.* 99, 3603–3624.

Conflict of Interest: The authors declare that the research was conducted in the absence of any commercial or financial relationships that could be construed as a potential conflict of interest.

frontiers in Materials

REVIEW
published: 17 March 2021
doi: 10.3389/fmats.2021.638909

Phytic Acid: Properties and Potential Applications in Dentistry

Mohannad Nassar[1]†, Rania Nassar[2,3]†, Husain Maki[4], Abdullah Al-Yagoob[5], Mahmood Hachim[2], Abiola Senok[2], David Williams[3] and Noriko Hiraishi[6]*

[1]Department of Preventive and Restorative Dentistry, College of Dental Medicine, University of Sharjah, Sharjah, United Arab Emirates, [2]College of Medicine, Mohammed Bin Rashid University of Medicine and Health Sciences, Dubai, United Arab Emirates, [3]Oral and Biomedical Sciences, School of Dentistry, College of Biomedical and Life Sciences, Cardiff University, Cardiff, United Kingdom, [4]Speciality Dental Residency Program, Ministry of Health, Juffair, Bahrain, [5]Ras Al Khaimah College of Dental Sciences, Ras Al Khaimah Medical and Health Sciences University, Ras Al Khaimah, United Arab Emirates, [6]Department of Cariology and Operative Dentistry, Graduate School of Medical and Dental Sciences, Tokyo Medical and Dental University, Tokyo, Japan

OPEN ACCESS

Edited by:
Mary Anne Sampaio Melo, University of Maryland, Baltimore, United States

Reviewed by:
Ingrid Mathias-Santamaria, University of Maryland, Baltimore, United States
Lamia Mokeem, University of Maryland, Baltimore, United States
Ivana Vucenik, Independent Researcher, Baltimore, MD, United States

***Correspondence:**
Mohannad Nassar
minassar@sharjah.ac.ae

†These authors have contributed equally to this work and share first authorship

Specialty section:
This article was submitted to Biomaterials, a section of the journal Frontiers in Materials

Received: 07 December 2020
Accepted: 20 January 2021
Published: 17 March 2021

Citation:
Nassar M, Nassar R, Maki H, Al-Yagoob A, Hachim M, Senok A, Williams D and Hiraishi N (2021) Phytic Acid: Properties and Potential Applications in Dentistry. Front. Mater. 8:638909. doi: 10.3389/fmats.2021.638909

Inositol hexaphosphate (IP6) is the most abundant inositol phosphate in nature and an essential molecule for different biological functions. IP6 has a unique structure granting it distinctive properties; a high negative charge density provides IP6 with an immense chelating ability and valuable antioxidant properties. IP6 is also simple and cost-effective to produce. These features have attracted researchers and entrepreneurs to further study IP6 for a wide variety of applications in areas such as pharmaceutical, food and chemical industries, medicine, pharmacy, nutrition, and dentistry. The interest in IP6 in the dental field unfolded many decades ago following identification of a cariostatic ability and a positive impact on reducing enamel dissolution. Subsequently, IP6's anti-plaque, anti-calculus and cement-forming properties have been investigated. Despite encouraging findings, there was a phase of decreased attention to IP6 which slowed down research progress. However, the potential use of IP6 has recently been revisited through several publications that provided deeper understanding into its mechanisms of action in the aforementioned applications. Studies have also explored new applications in endodontics, adhesive, preventive and regenerative dentistry, and IP6's role in improving the characteristics and performance of dental materials. Evidence of the merits of IP6 in dentistry is now substantial, and this narrative review presents and discusses the different applications proposed in the literature and gives insights of future use of IP6 in the fields of orthodontics, implant and pediatric dentistry.

Keywords: adhesive, application, cariostatic, cement, dentistry, inositol hexakisphosphate, oral, phytic acid

INTRODUCTION

Phytic acid, known as inositol hexakisphosphate (IP6), inositol polyphosphate, or phytate when in salt form, was first recognized by Pfeffer in 1872 (Pfeffer, 1872), and in 1903 the term "la phytine" was used by Posternak (Posternak, 1903). In 1914, the IP6 structure was described by Anderson (Anderson, 1914) and this was confirmed by Johnson and Tate in 1969 using nuclear magnetic resonance spectroscopy (Johnson and Tate, 1969).

IP6 is a saturated cyclic acid and the phosphate ester of inositol, with the formula $C_6H_{18}O_{24}P_6$ (**Figure 1**). It has a high density of negative charges due to its six phosphate groups that become partially ionized at physiological pH, where the negative charges are counterbalanced by cations,

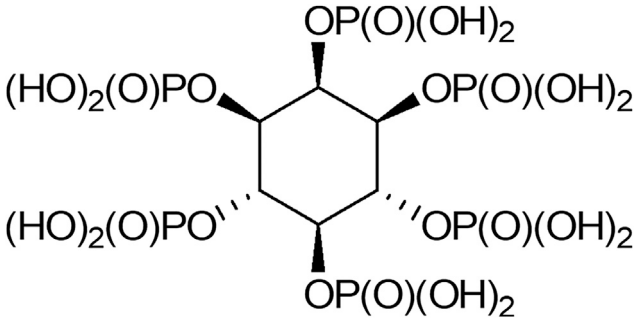

FIGURE 1 | Phytic acid structure.

mainly sodium ions. Throughout the present review, IP6 is used to refer to both phytic acid and phytic acid salt "phytate." IP6 is abundant in plants and has a significant nutritional role as the principal storage form of phosphorus in many plant tissues, especially bran and seeds. It is also considered a source of myoinositol, a cell wall precursor (Reddy et al., 1982; Schlemmer et al., 2009). In animal cells, myoinositol polyphosphates are ubiquitous, and IP6 is the most abundant form, with a concentration ranging from 10 to 100 μM in mammalian cells, depending on cell type and developmental stage (Szwergold et al., 1987; Sasakawa et al., 1995). The interaction of intracellular IP6 with specific intracellular proteins has been investigated *in vitro*, and these interactions result in the inhibition or potentiation of the physiological activities of proteins (Norris et al., 1995; Hanakahi et al., 2000). The evidence suggests an intracellular role for IP6 as a cofactor in DNA repair by non-homologous end-joining (Hanakahi et al., 2000). Other studies using yeast mutants, have also suggested that intracellular IP6 may be involved in mRNA export from the nucleus to the cytosol (York et al., 1999; Shears, 2001). IP6 has a potent anti-nutrient ability due to its strong binding affinity to crucial dietary minerals in their elemental form, including calcium, iron, and zinc; thus inhibiting their absorption (Schlemmer et al., 2009; Gupta et al., 2015). Studies have shown that there is a marked decrease of calcium absorption in the presence of IP6 and an enhanced availability after degradation. When iron or zinc binds to IP6, insoluble precipitates form, contributing to deficiencies of these elements in people whose diets rely on foods for their mineral intake (Hunt, 2002; Hurrell, 2003; Kancheva and Kasaikina, 2013). Thus, fortification of food, especially in developed countries, is seen as a desirable measure to achieve the recommended intakes of specific nutrients (FAO/IZiNCG, 2018).

The anti-nutrient effect of IP6 should not negate its health benefits (Nissar et al., 2017), and its ability to form insoluble complexes with calcium might also help decrease bone retention of heavy metals such as lead (Rose and Quarterman, 1984). IP6's strong iron chelating property has been found to have a protective effect in rat neuronal cells against apoptosis in iron-excess conditions, a finding of importance in patients with Parkinson's disease where disrupted iron homeostasis and iron overload in the brain is evident (Xu et al., 2008).

Studies have also shown that IP6 has an antioxidant effect indicating a role for IP6 in preventing free radical formation through chelation with iron that catalyses the generation of hydroxyl radicals (Graf, 1983; Graf et al., 1987; Graf and Eaton, 1990; Pallauf and Rimbach, 1997; Xu et al., 2008). The protective effect of IP6 against kidney stones and cancer has also been studied (Grases and Costa-Bauza, 1999; Grases et al., 2006; Shafie et al., 2013), and scientists have suggested that IP6 may partly explain why whole grains have been linked with a reduced risk of colon cancer (Aune et al., 2011). IP6's anti-cancer action has been demonstrated both *in vitro* and *in vivo* and it is claimed that there is enough evidence to legitimize the start of clinical trials in humans for its use as an anti-neoplastic agent (Fox and Eberl, 2002; Vucenik and Shamsuddin, 2006). IP6 has an inhibitory effect on osteoclastogenesis in human cell lines, suggesting it could play a role in reducing bone-mineral density loss and preventing osteoporosis (López-González et al., 2008; Arriero et al., 2012).

Due to its antioxidant properties, IP6 has been used as a food preservative to prevent spoilage and discoloration (Graf and Eaton, 1990). Adding IP6 to wine and other beverages would reduce the side effects and toxicity of high metal content (e.g. iron) in beverages (Trela, 2010). The pharmaceutical industry has also used IP6, to enhance drug efficacy and reduce undesired side effects. Adding IP6 to the drug content could improve drug absorption and increase oral bioavailability (Xie et al., 2014; Kim et al., 2016).

A finding that might be of interest to dental practitioners is the ability of IP6, in the presence of calcium, to inhibit fluoride bioavailability from the food matrix, thus attenuating the caries-preventive effect of fluoride (Cerklewski, 1992). In dentistry, IP6 gained attention in 1960 when McClure et al. tested its cariostatic effect on rats (McClure, 1960). In 1972, IP6's plaque-inhibiting effectiveness was examined (Nordbö and Rölla, 1972) and in 1975, Cole and Bowen tested its effect on microbial composition of animal dental plaque (Cole and Bowen, 1975). IP6 continued to generate a steady amount of interest due to its ability to bind to hydroxyapatite forming a monomolecular surface layer that limited both the growth and dissolution of hydroxyapatite crystals, thus inhibiting caries, plaque formation and enamel dissolution. These findings led to the development of several patented oral care regimes (Reddy et al., 1982; Graf, 1983; Kaufman, 1986; Sands et al., 1986; Reddy et al., 1989). IP6's cement forming properties were tested by Prosser et al., in 1983 (Prosser et al., 1983) where it was found to produce a fast setting and acid-resistant cement. Although the scholarly interest in IP6 furnished a number of intriguing findings regarding its application in dentistry, this interest reached a hiatus. Recently, interest in IP6 has been revitalized with several research papers exploring potential dental applications including its use in dentifrices and cements, and other new applications such as etchant in adhesive dentistry, chelating agent in endodontics or anti-staining agent added to dentifrices (Nassar et al., 2013; Nassar et al., 2015; Milleman et al., 2018; Parkinson et al., 2018; Uyanik et al., 2019). In 1983,

Ernst Graf was highly active in researching different features of IP6 and its potential in a vast array of applications. Graf was probably the first to give an in-depth description of the antioxidant and metal chelation properties. He stated that IP6 was an inexpensive, inert, non-toxic and abundant chemical that was easily obtained from different plant sources by relatively simple procedures. Despite all the encouraging data, limited efforts had been given to IP6's application for oral care and he believed that if enough funding and support were secured, novel oral health care products could have been developed (Graf, 1983). Based on the reviewed literature, it seems that IP6 possesses several properties that are valuable across a variety of dental fields. In the last 60 years, the use of IP6 has been evaluated in dentistry; this narrative literature review highlights the major potential applications of IP6 and presents insights into other future applications of this agent in dentistry.

POTENTIAL APPLICATIONS OF IP6 IN DENTISTRY

Cements

Dental cements are a mainstay in modern day dentistry where they are used in the restoration of prepared teeth for an indefinite or definite period, depending on the physical characteristics and projected longevity of the restoration (Hill, 2007). The requirements of an ideal cement include, but are not limited to, having sufficient working time and desired physical properties for its intended use, strong enough to resist functional forces and resistant to dissolution upon exposure to the oral environment (de la Macorra and Pradíes, 2002). Dental cements are also important for the success of fixed appliance-based orthodontic therapy, where they are needed to attach bands and brackets to tooth structure along with the ability to protect against dental caries during the treatment period (Millett et al., 2016). Nowadays, several varieties of dental cements are available and the development of new or improved dental cements is still ongoing; however, some have disappeared from the market.

Studies have shown that IP6 can drastically improve both the chemical and physical properties of dental cements when used as an additive. The notion of using IP6 was proposed in 1980, where its addition to aluminosilicate glass, resulted in a rapidly setting cement through an acid-base reaction. The resultant cement had low vulnerability to early attack by water and acid, as well as better adhesion to enamel compared with dentine, due to the lower mineral content of the latter (Prosser et al., 1983). Mechanical properties of zinc phosphate cements also improved with addition of IP6. Increasing the concentration of IP6 from 0 to 2% doubled the compressive strength. Replacing some of the phosphoric acid with 3–5% IP6 resulted in maximum compressive strength. When IP6 was added alone, the reaction was rapid and the setting time was short and controllable based on the ratio of IP6 and phosphoric acid or adjusting the water content to attain a more practical setting time. The leach from the resultant cement was reduced when some of the phosphoric acid was replaced with IP6, and this was explained by the higher stability of zinc phytate compared with zinc phosphate. This was considered the main advantage of using IP6. Applications where a large area of cement is exposed to saliva, such as in orthodontics might benefit most from this property. However, at high IP6 concentrations, the resultant cement was too viscous, with a high film thickness, thus rendering the cement unsuitable for dental application (Li et al., 1994).

Calcium silicate-based cements are commonly used in pulpal regeneration and hard tissue repair in endodontics along with mineral trioxide aggregate (MTA) and more recently, with Biodentine™. MTA exhibits a myriad of drawbacks such as a long setting time, poor handling characteristics and low washout resistance (Dawood et al., 2017). At a certain concentration, IP6 can effectively decrease the setting time of calcium silicate-based cements without altering their diametral tensile strength, and this effect was more pronounced with Biodentine™ compared with MTA (Uyanik et al., 2019). Acceleration of the setting time could be through the hydrophilic nature of IP6 having a synergistic effect with calcium silicate-based cements, which sets through a hydration reaction. It may also be explained by the highly negatively charged phosphate groups in IP6 that strongly bind to metallic ions within the cements (Hsieh et al., 2009; Silva and Bracarense, 2016). Furthermore, the abundance of negative charges in IP6 could play a role in the reaction process through chelation with calcium in the cement. High water: powder ratio increases porosity and solubility of the cement, thus compromising the mechanical properties of the set material (Li et al., 1994), and this is also applicable to MTA and Biodentine™ as a high water:powder ratio would adversely affect properties. The use of IP6 is thought to result in less water in the mixed cement; however, no improvement in the diametral tensile strength was detected (Uyanik et al., 2019).

Calcium phosphates occur in different forms, and have found their way into many dental applications, such as preventive dentistry (owing to high resemblance to natural enamel), periodontal therapy, restorative and implant dentistry, and pulp therapy (Al-Sanabani et al., 2013; Meyer et al., 2018). The brushite type of calcium phosphate is considered as a bone replacement material which possesses desirable properties, but also suffers several drawbacks such as short setting times, low mechanical strength and poor injectability, all of which limits the more inclusive clinical application of this cement, and trials to improve these properties are still ongoing (Gbureck et al., 2004). In 2017, Meininger et al. reported that IP6 was a setting retardant of di-calcium phosphate cements, an effect that was necessary to meet the clinical requirements of the handling time of cement that usually sets in less than 1 min in a retardant-free environment. IP6 is thought to exert this effect by adsorbing at the active growth sites of di-calcium phosphate crystals of the cement, thus delaying the crystal growth rate, which also decreases the maximum setting temperature. In the same study, the highest cement strength values were achieved using citric acid, the most commonly used retarder in brushite cements, followed by IP6, which led to higher values than those obtained with retardant-free cement. These results were correlated with the porosity of the set cement and confirmed some differences in the used retardants regarding the type and phase of the formed crystals in the set material. When IP6 was

used as a retarder, monetite was the predominant phase formed during setting, whereas citric acid resulted in the formation of a mixture of both brushite and monetite. Interestingly, cements with IP6 showed increased calcium concentration in the medium where the cement samples were immersed, while citric acid containing cement adsorbed calcium ions (Meininger et al., 2017). The increased availability of calcium ions might be advantageous in enhancing dentine formation in exposed dental pulps (Foreman and Barnes, 1990), which has possible implications in the field of regeneration as described later in this review. Cements that contained IP6 had significantly better cytocompatibility towards osteoblast cells compared with citric acid-containing cement (Meininger et al., 2017). In 2018, Hurle et al. studied the effect of IP6 on the hydration mechanism and setting kinetics of brushite cements (Hurle et al., 2018). Their findings were consistent with those obtained by Meininger et al. (Meininger et al., 2017), where controlled concentrations of IP6 acted as a retarder of the cement setting reaction, resulting in better mechanical performance and a cement that was composed of a monetite crystalline structure (Hurle et al., 2018). The latter finding was thought to be of clinical significance as this form of crystalline structure does not undergo phase conversion with aging in phosphate buffered saline (Sheikh et al., 2015). It was also observed that IP6 improved the injectability of the cement, due to the formation of a chelate complex between calcium ions and the phosphate groups of IP6, which led to a delayed rise in paste viscosity and a drastic retarding effect on cement hydration (Hurle et al., 2018). Weichhold et al. found similar effects on apatite cement and concluded that IP6 was a suitable additive for the development of calcium phosphate cement with superior properties (Weichhold et al., 2019).

Glass ionomer cement systems are versatile restorative and luting materials and essential in restorative and pediatric dentistry and orthodontics, because of their fluoride release and chemical adhesion to tooth structure. The literature supports their use in several clinical scenarios. These include cementation of crowns, bridges, inlays, onlays and orthodontic appliances, cavity base or liner, fissure sealant, tooth repair in atraumatic restorative treatment technique and restoration of certain cavity preparations in patients with high-caries risk and teeth that are difficult to isolate (Berg, 2002; Sidhu and Nicholson, 2016). Researchers are constantly striving to improve the performance of these cements as well as to develop new ones. Several chelating additives such as tartaric acid and citric acid have been described in the literature to enhance the characteristics of glass ionomer cements (Sidhu and Nicholson, 2016). It may also be interesting to see future studies on the impact of IP6 on these cements; to the best of our knowledge, such studies have not been performed yet.

Oral Care Products

Oral care products including dentifrices and mouthrinses are multifunctional, offering an array of advantages to combat an assortment of oral conditions e.g., caries, gingivitis, dentine hypersensitivity, teeth whitening, and halitosis. The addition of chemical agents to conventional products to augment their intended functions such as prevention of caries, plaque inhibition, or stain removal, represents an attractive field of study (Lippert, 2013; Cummins, 2016; Milleman et al., 2018).

Interest in the potential protective effects of different classes of phosphate compounds, including IP6, against caries is not new (Grenby, 1973). The concept of using IP6 as a cariostatic agent probably came from the speculative connection mentioned in earlier studies. These studies revealed an increased caries incidence with decreased intake of IP6 following changes in dietary habits and food processing and refinement (Jenkins et al., 1959a; Jenkins et al., 1959b; Jenkins, 1966). Several early studies showed a reduction of experimental caries in animals fed dietary IP6 (Taketa and Phillips, 1957; Buttner and Muhler, 1959; McClure, 1960; Madsen and Edmonds, 1962; Vogel et al., 1962; McClure, 1963; McClure, 1964; Dawes and Shaw, 1965; Englander and Keyes, 1970; Cole et al., 1980); however, these findings were not corroborated by other researchers, where IP6 had limited or no protective influence (Limbasuta et al., 1961; König and Grenby, 1965; Grenby, 1966; Lllienthal et al., 1966). The cariostatic mechanism of IP6 is not fully understood, although several pathways have been suggested. A local rather than a systemic effect is proposed by most researchers. IP6 rapidly adsorbs to hydroxyapatite forming a monomolecular layer on the crystal surface that leads to increased resistance of enamel to acid attack by acting as a diffusion barrier to ions (Magrill, 1973b) while at the same time limiting the growth of the hydroxyapatite (Koutsoukos et al., 1981; Grases et al., 2015). IP6 is mainly found at the surface of hydroxyapatite but it is too large to diffuse into the hydroxyapatite crystal. Another speculated mechanism is through the formation and precipitation of calcium-IP6 complexes on the crystal surface (Magrill, 1973b). IP6 content on the surface of hydroxyapatite was not significantly affected after washing with water or partial dissolution by acid, which indicated that IP6 was tightly bound to hydroxyapatite surfaces (Magrill, 1973b). The adsorption of IP6 to hydroxyapatite might also cause an alteration of the surface charge and free energy characteristics, thus impeding formation of plaque by negatively influencing the affinity of salivary proteins and bacteria to tooth surfaces (Napper and Smythe, 1966; Grenby, 1967a; Grenby, 1967b; Grenby, 1967c; Kaufman and Kleinberg, 1970; Pruitt et al., 1970; Nordbö and Rölla, 1972; Magrill, 1973b).

Recently, Fernández et al. showed that the adsorption energy to hydroxyapatite was the highest for IP6 when compared with other acids such as pyrophosphate, etidronate, and citrate. IP6 was able to form thirteen electrostatic interactions with hydroxyapatite surfaces. No hydrogen bond interaction was observed between IP6 and hydroxyapatite surfaces; however, the protonated oxygen atoms of IP6 formed hydrogen bonds with contiguous phosphate groups. In their study, there was a positive correlation between the adsorption energy with the number of functional groups and the total molecular negative charge of the acid that interacted with hydroxyapatite surface (Fernández et al., 2017).

The antimicrobial effect of IP6 on cariogenic bacteria is still questionable. However, there is some indication that oral streptococci and lactobacilli are sensitive to IP6 obtained from diet (Grenby, 1967b). There are similar characteristics between IP6 and linear condensed polyphosphates, and thus it might be

expected that the former may have an inhibitory effect on *Streptococcus mutans* by modifying certain portions of the glycolytic enzyme system (Handelman and Kreinces, 1973), or chelation of essential metabolites (Post et al., 1963; Elliott et al., 1964; Shibata and Morioka, 1982). Despite the promising potential of IP6 as a cariostatic agent, some researchers cast doubt on the clinical impact of caries control in humans (Grenby, 1967b). Importantly, bacteria with the ability to accumulate polyphosphate intracellularly can alter the chemical conditions of the oral environment and promote caries (Breiland et al., 2018).

Grases et al. showed that a mouthrinse containing IP6 retarded dental calculus formation (Grases et al., 2009). This effect was attributed to IP6 properties in altering protein binding to the tooth surface and concomitantly acting as an inhibitor of hydroxyapatite and brushite crystal formation (Grases et al., 2000). These actions were related to its structural similarity to pyrophosphate, the main polyphosphate used in inhibiting calculus (Cohen et al., 1994). This mechanism has found use in supplemented chewing gums which reduce calculus formation (Porciani et al., 2003). To our knowledge, there are no studies to date on the role of IP6 in chewing gum on removal of teeth stain or inhibition of calculus formation.

Despite these rather equivocal findings, there has been a reasonable endorsement to harness the cariostatic, anti-plaque and anti-calculus properties of IP6 by its inclusion in several oral care products that serve different dental and oral applications such as mouthrinses, dentifrices, dentures cleaners, teeth whitening and stain removal agents, and oral malodor rinses (Graf, 1983; Sands et al., 1986; Garlich et al., 1994; Kleinberg et al., 1998; Hoke et al., 2016; Nakauchi et al., 2017). Milleman et al. evaluated the efficacy of stain removal of 0.85% w/w IP6 incorporated into an experimental dentifrice, which was better for tooth stain removal than a reference control dentifrice. This provided further evidence that IP6 acted similarly to condensed polyphosphates in augmenting stain removal which was not accompanied with increased abrasivity of the dentifrice. This was considered highly important for people at risk of dentine hypersensitivity. The presence of IP6 in dentifrices is expected to not only remove stain, but also prevent new stain formation, and this effect is thought to be through binding to tooth structure surfaces. This, in turn, would disrupt protein binding to the surfaces through chelating with calcium, thus negatively affecting both the adhesion and the ionic crosslinking of pellicle and stain molecules. The other notable finding in their study was the usefulness of the experimental dentifrice for removing stains from inaccessible and difficult-to-reach areas, and surfaces of teeth that were typically missed during cleaning. The experimental dentifrice was also well-tolerated by the subjects, with no evidence of adverse effects in the oral cavity, at the IP6 level used (Milleman et al., 2018).

A study by Parkinson et al. tested the effect of increasing quantities of IP6 on fluoride ability to promote remineralization. No significant differences were encountered by addition of IP6 at 0.425% or 0.85% and there was no attenuation, or improvement in fluoride's caries prevention efficacy. Neither IP6 nor zinc ions within the dose range tested affected fluoride's ability to promote remineralization or prevent demineralization of enamel in the aforementioned model (Parkinson et al., 2018). Additional experiments by Creeth et al. demonstrated that, compared with fluoride-free controls, a dentifrice containing IP6 and sodium fluoride had beneficial effects on the dynamics of remineralization and demineralization for early enamel erosive lesions. However, due to reduced fluoride uptake in the presence of IP6, the remineralizing effect was inhibited. Thus, no benefits for including IP6 were perceived (Creeth et al., 2018), which contrasted with the results of Parkinson et al. (Parkinson et al., 2018). It was stated that this marked contrast was the result of using different models. Creeth et al. used a single-treatment model with plaque-free enamel surfaces (Creeth et al., 2018), whereas Parkinson et al. used plaque-covered surfaces which were clinically more relevant to developing caries lesions (Parkinson et al., 2018). Magrill reported an inhibition of mineralization in enamel specimens pre-treated with IP6 solution. However, the author was not concerned about similar *in vivo* effects as several animal experiments had already demonstrated the cariostatic properties of IP6 (Magrill, 1973a).

IP6's interaction with cations has received the most attention. However, IP6 also has the ability to interact with enzymes, starch and proteins. These less studied interactions might also be crucial in certain aspects of oral health including dental caries and the longevity of resin-based restorative material in adhesive dentistry, as described later. IP6 interacts with an array of enzymes such as α-amylase (Deshpande and Cheryan, 1984; Knuckles and Betschart, 1987), proteinases (pepsin, trypsin and chymotrypsin) (Singh and Krikorian, 1982; Inagawa, 1987; Deshpande and Damodaran, 1989), lipase (Knuckles, 1988), β-glucosidases, alcohol dehydrogenase, and polyphenol oxidase (Deshpande, 2002; Du et al., 2012). Interaction with these enzymes results in mostly inhibition of the activity, but some reported no effect or even a positive influence depending on the IP6:enzyme ratio (Deshpande, 2002; Greiner et al., 2006).

Salivary α-amylase is one of the major components of saliva and has a variety of biological functions requiring intact enzyme. The ability of salivary α-amylase to bind to bacteria leading to clearance might offer a protective effect (Scannapieco et al., 1993). Alternatively, its ability to bind to bacteria and adsorb to tooth enamel (Al-Hashimi and Levine, 1989; Scannapieco et al., 1994), its presence in enamel pellicle (Yao et al., 2001), and its ability to digest starch providing nutrients for cariogenic bacteria point towards α-amylase's role in promoting dental plaque and caries formation (Scannapieco et al., 1993). The inhibitory effect of IP6 on the activity of α-amylase is via chelation of calcium (Cawley and Mitchell, 1968), a cation necessary for activation and stabilization of α-amylase (Morris et al., 2011), or through the general complex-forming ability of IP6 with enzyme proteins (Sharma et al., 1978; Deshpande and Cheryan, 1984). Knuckles and Betschart confirmed an inhibitory effect of IP6 on α-amylase's ability to digest starch, and this effect was dependent on the degree of phosphorylation, IP6 concentration, pH and enzyme source (Knuckles and Betschart, 1987). The inhibitory effect was confirmed *in vivo* by the inverse relationship between the intake of dietary IP6 and the level of glucose in the blood (Yoon et al., 1983). Meanwhile,

Björck and Nyman showed IP6 had negligible influence on the activity of α-amylase (Björck and Nyman, 1987). The contrasting results reveal the complexity of IP6 interactions and many of the different findings may be due to experimental design, and the fact that *in vitro* studies may poorly reflect *in vivo* behaviour of IP6 (Björck and Nyman, 1987).

Starches are one of the predominant dietary carbohydrates in modern societies. The first step in the digestion of starch occurs in the oral cavity by salivary α-amylase leading to the formation of oligosaccharides, which may be fermented by oral microorganisms, thus contributing to the caries process (Touger-Decker and van Loveren, 2003; Butterworth et al., 2011). Taking into account the high level of salivary α-amylase in humans, Lingström concluded that food starches possess significant cariogenic potential, and it was premature to consider food starches as safe for teeth (Lingström et al., 2000). The authors of a recent systematic review stated that it was the intake of rapidly digestible starches and not total starch intake that was associated with increased risk of caries. As such it is recommended that dental health professionals encourage consumption of food containing slowly digestible starches such as whole grains, fruits, and vegetables (Halvorsrud et al., 2019). Starch digestion is negatively affected by direct IP6 binding with starch via hydrogen bond formation or indirect interaction of IP6 with the proteins (kafirin and glutelin) that bind to starch and are necessary for its digestion, or with α-amylase or calcium that is needed for α-amylase activity (Thompson and Yoon, 1984; Rickard and Thompson, 1997; Oatway et al., 2001; Selle et al., 2012). These interactions may modify the substrate leading to compensatory increases in outputs of α-amylase in order to digest starch (Selle et al., 2012). Thompson and Yoon studied the *in vitro* digestion of starch in human saliva. IP6 reduced digestibility by 28% or 60% at 1 h or 5 h of incubation, respectively (Thompson and Yoon, 1984).

Limited information is available about the *in vivo* interaction of IP6 with human saliva. In 2019, Delimont et al. were among the first to study salivary protein–IP6 interactions and explore the effect of IP6 supplementation on salivary proteins. In their study, proline-rich proteins did not bind to IP6, whilst IP6 formed weak complexes with a non-enzymatic salivary protein called cystatin SN (Delimont et al., 2019). The effect of IP6 on the functions and properties of cystatin SN is not yet understood. The main purpose of cystatin SN in the oral environment is inhibition of host cysteine proteases, which are involved in periodontal tissue destruction (Baron et al., 1999) and in protection against dental caries (Vitorino et al., 2006). Cystatin SN also adsorbs to enamel surfaces (Al-Hashimi and Levine, 1989; Johnsson et al., 1991) and has an effect on the sensitivity to bitter taste (Rodrigues et al., 2019). Delimont et al. suggested that repeated IP6 consumption might enhance basic proline-rich proteins production (Delimont et al., 2019), and this represented area of research that needs further exploration as this salivary component comprises about 70% of the total salivary proteins (Carlson, 1993) and is involved in several important functions that impact the oral health (Bennick, 1982; McArthur et al., 1995). Salivary mucins are glycoproteins that are responsible for several physical and chemical characteristics of mucus and play an important role in lubrication of hard and soft tissues of the oral cavity, modulation of oral microflora and formation of acquired enamel pellicle (Tabak, 1990). IP6 was reported to reduce the adsorption of native human whole salivary mucins to hydroxyapatite by 50% (Amerongen et al., 1988). However, deglycosylation of mucins increased their ability to compete with IP6 for hydroxyapatite surfaces (Amerongen et al., 1991).

The effect of IP6's interactions with dietary starch, proteins or salivary components such as enzymes on dental caries, pellicle formation and periodontal health is still unclear and the quantity of IP6 available from dietary sources to modify the functions of salivary components is still not known. However, in addition to the previously mentioned cariostatic mechanisms of IP6, we believe that the effect of IP6 on starch digestion and/or amylase activity has a role to play in the perceived anti-caries effect of IP6.

Etching Agent

Phosphoric acid at a concentration of 37% has been used in dentistry as an etching agent for enamel (Buonocore, 1955) and for dentine (Fusayama et al., 1979) since 1955 and 1979, respectively. The interaction of the etching agent with dentine is limited by the buffering effect of hydroxyapatite and other dentine components (Wang and Hume, 1988). However, it is believed that the depth of dentine demineralization also directly relates to the concentration of the applied acid (Chiba et al., 1989; Pashley, 1992). The acidic agent removes the smear layer and the superficial part of the dentine, opens the dentinal tubules, demineralizes the dentine surface, and increases the microporosity of the intertubular dentine (Van Meerbeek et al., 1992; Pashley et al., 1993; Sano et al., 1994). Although a definitely more effective enamel bonding is achieved through etching with phosphoric acid (Frankenberger et al., 2008), etching of dentine with phosphoric acid is now considered too aggressive (Van Meerbeek et al., 2011). Application of phosphoric acid to dentine results in exposure of collagen fibrils that are totally devoid of hydroxyapatite (Van Meerbeek et al., 1996; De Munck et al., 2003). These fragile collagen networks are susceptible to collapse, preventing optimal infiltration of resin (Prati et al., 1999; El Feninat et al., 2001), thus resulting in compromised bonding to dentine (Nakajima et al., 2002) and possible postoperative sensitivity (Chersoni et al., 2004). In addition, phosphoric acid regulates the activity of proteolytic enzymes in dentine (Tezvergil-Mutluay et al., 2013; DeVito-Moraes et al., 2016), thus jeopardizing the longevity of resin-based restorative materials (Pashley et al., 2004). Several approaches have been suggested to slow down the enzymatic activity associated with phosphoric acid on dentine, including evaluating other agents to replace phosphoric acid, such as maleic acid, citric acid, lactic acid or ethylenediaminetetraacetic acid (EDTA) (Breschi et al., 2002; Imbery et al., 2012; Trevelin et al., 2019). In addition, the use of crosslinking agents to strengthen the exposed collagen network has been proposed (Macedo et al., 2009).

In 2013, IP6 was evaluated as a dentine etching agent with results showing that upon etching with IP6, the bond strength of resin to dentine was significantly increased compared with phosphoric acid (Nassar et al., 2013). IP6 was shown to

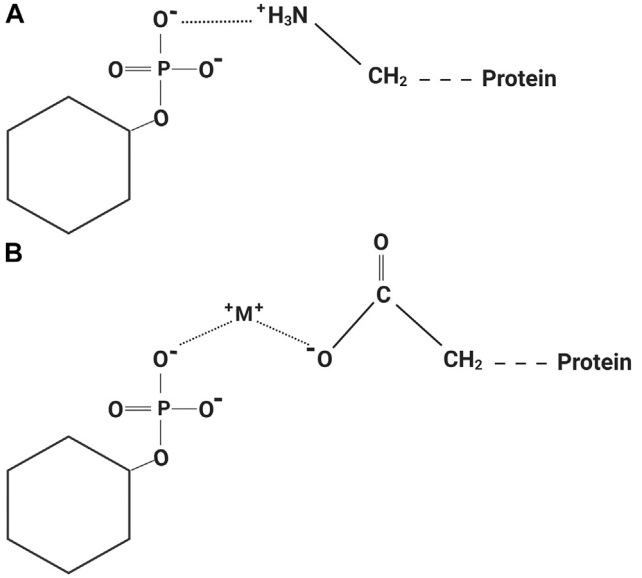

FIGURE 2 | (A) Binary protein-phytic acid complex at a pH below the isoelectric point of the protein. **(B)** Ternary protein-cation-phytic acid complex at a pH above the isoelectric point of the protein. This image was created using BioRender (https://app.biorender.com/).

effectively remove the dentinal smear layer at lower concentrations than phosphoric acid, and it also had less adverse effect on pulpal cells (Nassar et al., 2013). The speculated mechanism of action behind the increased resin-dentine bonding was attributed to two possible events. The first mechanism was due to IP6's ability to form insoluble complexes with calcium at a pH above 4 (Grynspan and Cheryan, 1983). As a result of the high dentine buffering capacity (Camps and Pashley, 2000), the pH of IP6 increases upon neutralization with dentine, and thus facilitated the formation of the insoluble complex, which might provide a certain level of stability for the exposed collagen. The second speculated mechanism was through the collagen crosslinking action of IP6 (Cheryan and Rackis, 1980; Lee et al., 2011; Ravichandran et al., 2013). The nature of IP6 protein interaction is governed by pH; at a pH below the isoelectric point of the protein, insoluble binary protein-IP6 complexes (**Figure 2A**) that dissolve only below pH 3.5 are formed by electrostatic interaction between the anionic phosphate groups of IP6 and the cationic groups of the protein. The binding sites for IP6 within the protein at low pH are the α-NH_2 terminal group, the ε-NH_2 of lysine, the imidazole group of histidine and guanidyl group of arginine. The stability of binary complexes is affected by the competitive action of multivalent cations (Cheryan and Rackis, 1980; Reddy and Salunkhe, 1981; Greiner et al., 2006; Selle et al., 2012). Dentinal collagen has a positive net charge after exposure to acidic solutions (Nezu and Winnik, 2000; Zhang et al., 2005) such as IP6, and thus we assume formation of a binary interaction between IP6 and dentinal collagen occurs. However, this interaction takes a different form at a pH above the isoelectric point, because both IP6 and the protein have a net negative charge at high pH. A soluble ternary protein-cation-IP6 complex (**Figure 2B**) is formed where cations such as calcium, bridges the IP6 to protein. In these types of complexes, the major binding sites are the non-protonated imidazole group of histidine and probably the ionized carboxyl group of the protein. The ternary protein-cation-IP6 complexes may be disrupted by high ionic strength, such as high pH (>10), and high concentrations of the chelating agents (Cheryan and Rackis, 1980; Reddy and Salunkhe, 1981; Greiner et al., 2006; Selle et al., 2012). Due to the buffering capacity of dentine (Camps and Pashley, 2000), this type of interaction might also occur between IP6 and dentinal collagen. A third more recent mechanism has been proposed for IP6-protein interaction, where IP6 acts as a Hofmeister anion through its six anionic groups that have marked kosmotropic effects resulting in stabilization and reduction of the solubility of proteins by interacting with water in the surrounding medium. However, this mechanism is a new concept that needs further investigation (Selle et al., 2012). Certain IP6-induced protein complexes result in decreased protein solubility and these complexes might be recalcitrant to enzymatic hydrolysis or require higher quantities of the enzymes to be degraded (Ravindran et al., 1995; Selle et al., 2012).

In a study done by Nassar et al., the increased number of mixed mode of failures at the adhesive–resin interface for the IP6-etched dentine reflected a strengthening effect of IP6 on the hybrid layer (Nassar et al., 2013). The reduced effect of IP6 on the used pulpal cells compared with phosphoric acid was attributed to the lower concentrations of IP6 used in the study (Nassar et al., 2013) and the ability of IP6 to reduce the level of oxidative stress through chelation with iron. This in turn, inhibits the ability of iron to catalyze the formation of hydroxyl radicals through the Fenton reaction (Xu et al., 2008). It is not only IP6, but also its intermediate products of hydrolysis that have iron chelating properties and are thus still effective in preventing iron ion-induced lipid peroxidation (Miyamoto et al., 2000). The effect of IP6 on dentinal collagen was later confirmed in a study that reported improved ultimate tensile strength of demineralized dentine upon treatment with IP6, which was comparable to results obtained with glutaraldehyde, a gold standard crosslinking agent used in dental research. Dentinal collagen exposed by IP6 was also less susceptible to collapse by air-drying and to collagenase degradation when compared with the fragile network of collagen attained by the use of phosphoric acid (Kong et al., 2015; Kong et al., 2017).

Wang et al. compared the use of IP6, glutaraldehyde and genipin for acellular animal-derived tissue fixation. It was postulated that IP6 with its strong electro-negativity reacts with –NH_2 on the tissues to form stable electrovalent bonds that could prevent degradation. To enhance biocompatibility, sodium hydroxide was used to elevate pH, which might also have resulted in the formation of hydrogen bonds between the negatively charged oxygen of phosphate anions and the protons on amino groups. These types of hydrogen bonds were said to far exceed ordinary hydrogen-bond interactions as the oxygen anions of IP6 possessed strong electro-negativity, and thus stable fixation was obtained. In their study, 5% IP6 was used for tissue fixation which resulted in a fixation index of 90%; no further enhancement occurred when

7.5% or 10% IP6 was used. The crosslinking rate for glutaraldehyde was quicker than IP6; however, the fixation index was comparable. Genipin had the lowest fixation index and rate. The microscopic porous structure was well preserved after crosslinking with IP6, which was similar to those of natural biological tissues and this intact structure plays an important role in the mechanical support and strength. IP6 resulted in samples with higher ultimate tensile strength compared with controls, indicating more effective crosslinking and formation of a compact intermolecular crosslinking network within collagen fibers. The enzymatic degradation of IP6-fixed tissue by subjecting the samples to collagenase was determined by measuring the relative weight loss of the tissue. At 24 h, control samples were 90.7% hydrolyzed compared with 49.2% for IP6-fixed tissues. The authors stated that IP6 introduced stable heteropolar bonds and hydrogen bonds through binding amino group, resulting in obstruction and protection of the cleavage site, blocking the action of the collagenase and reducing tissue degradability. In their study, glutaraldehyde resulted in the least relative weight loss indicating lower tissue degradation compared with IP6 and genipin. However, IP6 was more cytocompatible and enhanced secretion of angiogenic growth factors from human endothelial cells; a result that could increase cell proliferation and attachment and thus the process of angiogenesis (Wang et al., 2017). Tu et al. reported that the effect of IP6 on the self-assembly degree and kinetics of collagen isolated from bovine tendon was dose-dependent. Accelerated self-assembly kinetics and higher self-assembly degree were best at a 1:1 ratio of IP6 to collagen (Tu et al., 2018). These findings were attributed to the formation of hydrogen bonding between IP6 and amino group of collagen as described by Wang et al. (Wang et al., 2017). At higher IP6 concentrations, the self-assembly degree and kinetics were negatively affected compared with the control due to occupancy of hydrogen bonding sites on collagen by IP6 and the repulsion between IP6 absorbed on adjacent collagen molecules resulting in an inhibitory effect. The triple-helical conformation of collagen in the presence of IP6 was not altered; however, more slender and thinner morphology of the fibrils was observed than for IP6-free collagen. The thermal stability of collagen fibrils and the viscoelasticity of collagen were also enhanced by IP6 (Tu et al., 2018). The results of these studies are not only helpful to design future studies to optimize bonding to dentinal collagen, but they also provide insights into IP6's use in regenerative dentistry, as described later.

Matrix metalloproteinases play an important role in the degradation of the dentine organic matrix, which is mostly composed of collagen, thus leading to failure of resin-dentine bonding (Thompson et al., 2012) or progression of caries process (Toledano et al., 2012). In dentistry, use of matrix metalloproteinases inhibitors has gained much attention as a strategy to improve adhesive bonding to dentine, and currently there is intensive research towards their development (Nassar et al., 2014; Boelen and Boute, 2019). The mechanism of action of the first-generation of matrix metalloproteinases inhibitors is based on zinc and calcium ions chelation (Toledano et al., 2012); these ions are required to maintain optimum tertiary structures and functional active sites of matrix metalloproteinases (Visse and Nagase, 2003). EDTA has a significant inhibitory effect on matrix metalloproteinases through previously described mechanisms; however, EDTA can be rinsed off easily from dentine (Thompson et al., 2012; Toledano et al., 2012). In addition to IP6's excellent ability to chelate with calcium, it is also a potent chelator of zinc. The zinc-IP6 complex is stable and insoluble (Oatway et al., 2001), and these properties along with an ability to bind to collagen might make IP6 a potential inhibitor of dentinal matrix metalloproteinases.

Despite limited evidence, it seems that controlled concentrations of IP6 are not aggressive to dentine and create a stable collagen network which might be clinically translated to better longevity of resin-based restorations. However, more research is warranted on the effect of IP6 on dentinal matrix metalloproteinases and cysteine cathepsin which play important role in destruction of dentine organic matrix following etching of dentine by acidic agents. We also believe that IP6's interaction with dentinal collagen and metals merits thorough and comprehensive examination, and future studies could be directed to evaluating the stability and enzymatic degradation of IP6-treated dentinal collagen (Forgione et al., 2021).

Chelating Agent

The success of root canal therapy depends on both mechanical and chemical debridement. Mechanical debridement forms a smear layer inside the canal walls and is often associated with the incomplete seal and lack of adaptation of obturation materials to canal walls. Despite failure of reaching a consensus on whether to remove the smear layer or not, much of the literature seems to promote its removal (Violich and Chandler, 2010). Sodium hypochlorite is the most widely used intra-canal irrigant; however, it fails to fully remove the smear layer, which is the basic rationale behind use of chelating agents in endodontics (Haapasalo et al., 2014). Since 1957, EDTA at a concentration of 17% and an application time of 1–5 min has been the chemical of choice for smear layer removal (Nygaard-Ostby, 1957; Calt and Serper, 2002). EDTA is overused globally and is a major pollutant (Sillanpää, 1997). Furthermore, EDTA is not readily biodegradable and its extrusion into the periapical tissue needs to be avoided (Amaral et al., 2007). Thus, despite its popularity, a search for other chelating agents is ongoing. Solutions of chitosan, phosphoric acid, citric acid, and MTAD (mixture of doxycycline, citric acid and a detergent) have been studied as smear layer removal agents (Torabinejad et al., 2003; Machado-Silveiro et al., 2004; Prado et al., 2011; Silva et al., 2013). In 2015, Nassar et al. highlighted the potential of IP6 as an alternative root canal chelating agent (Nassar et al., 2015). The mechanism of the chelating action of IP6 stems from its multiple negative charges giving it a high affinity to calcium (Torres et al., 2005). Application of IP6 at concentrations lower than those used for EDTA removes the smear layer and widely opens dentinal tubules, whilst also being biocompatible to osteoblastic cells. The latter finding was based on the results of alkaline phosphatase activity and viability tests, when compared with EDTA, which might be reflected clinically as more rapid

wound healing in the periapical area in cases of extrusion (Nassar et al., 2015; Nassar et al., 2020). Milder effects on osteoblast cells may be explained by the lower concentration of IP6 needed to remove the inorganic component of the smear layer and its beneficial properties to protect the cells from iron-induced damage as described in the etchant section of this review. Eymirli et al. demonstrated that IP6 and EDTA produced similar results with regard to removing intracanal triple antibiotic paste and calcium hydroxide from root dentine (Eymirli et al., 2017). While Afshan et al. found that 1% IP6 had reduced erosive potential and smear layer removal ability compared with 17% EDTA, and this finding was in line with Jagzap et al. (Jagzap et al., 2017; Afshan et al., 2020).

When a new chemical is being evaluated as a smear layer removal agent, it is important to consider its effect on the chemical and physical characteristics of dentine by measurement of dentinal roughness and microhardness. The changes in roughness reflect altered topography and wettability of dentine, which might have an effect on the microbial and dental materials adhesion to dentine (Eick et al., 1972; Attal et al., 1994; Hu et al., 2010; Xu et al., 2019). A change in microhardness denotes an effect on the mineral content of dentine represented mainly by the calcium:phosphorus ratio (Hennequin et al., 1994; Doğan and Çalt, 2001). Decreased microhardness assists mechanical instrumentation of the canals (Cruz-Filho et al., 2002); however, a disproportionately heavy demineralization might weaken the tooth structure (Ulusoy and Görgül, 2013) and create a fragile collagen network which is susceptible to collapse, resulting in insufficient penetration of the adhesive or sealer, and suboptimal sealing ability (García-Godoy et al., 2005). The effect of IP6 on dentine roughness and microhardness has recently been studied and compared with EDTA. Nikhil et al. reported a higher reduction in dentine microhardness with 17% EDTA compared with 1% IP6, while, Muana et al., showed that 1% IP6 resulted in significantly higher roughness and lower microhardness compared with 17% EDTA (Nikhil et al., 2016; Muana et al., 2020). The equivocal results from studies comparing EDTA and IP6 on their effects on the smear layer, dentine microhardness and roughness, may be attributed to differences in pH, exposure time, and method of application of the tested agents (Muana et al., 2020). In addition, though IP6 is often solely referred to as IP6, commercial products of this solution often contain considerable amounts of impurities in the form of inositol with lesser degrees of phosphorylation, such as IP2, IP3, IP4, and IP5, and free orthophosphate. This will lead to different degrees of phosphorylation of the available products in the market (Hoke et al., 2016). The lower forms of IP6 are known to have reduced metal binding capacity (Persson et al., 1998), which is a function of the number of phosphate groups on the myo-inositol ring. The cation-myo-inositol phosphate complexes are also more soluble as the number of phosphate groups decreases (Greiner et al., 2006).

A characteristic of chelating agents is the ability to eradicate bacteria. *Enterococcus faecalis* is the most common microorganism associated with endodontic failure and persistent infections, and is known for its ability to resist several antibacterial agents (Stuart et al., 2006). The effect of IP6 on *E. faecalis* was recently assessed, where IP6 was found to be both bacteriostatic and bactericidal. The minimum inhibitory concentration (MIC) of IP6 was 0.156% while the minimum bactericidal concentration was 0.625%. In the same study, the MIC of EDTA was 0.14%; however, EDTA did not exhibit bactericidal activity. Further studies are needed to fully comprehend the mechanism of action of IP6 against endodontic pathogens (Nassar and Nassar, 2017). In general, the antimicrobial effect of IP6 has not been widely studied. Kim and Rhee stated that IP6's antimicrobial activity was expected to be different than the mechanism for other organic acids, which is the weak acid theory, and this is attributed to the unique structure of IP6 and its wide acidity range (Kim and Rhee, 2016). IP6 was found to be effective against some Gram-positive and Gram-negative bacteria (Zhou et al., 2019), and the proposed mechanism was by its chelating ability and cell membrane disruption (Kim and Rhee, 2016), thus causing excessive cell permeability, changes in cell morphology and reduction in intracellular ATP concentration (Zhou et al., 2019).

Implantology

Implantology is a rapidly growing dental field, where research aims to produce implants with superior properties (He et al., 2019). Osseointegration is the target of the implant industry, which is constantly modifying dental implant surfaces for improved direct structural and functional connection between the bone and the surface of the implant. The implant surface morphology, composition and the interaction with the surrounding tissues play key roles on the outcome of osseointegration (Bowers et al., 1992; Martin et al., 1995; Cochran et al., 1998; Pető et al., 2002). Conventionally, phosphoric acid has been used to treat the implant surfaces prior to its placement to increase surface porosity to promote healing and attachment (França et al., 2018). The use of chemical agents such as phosphoric acid is considered an integral part in the protocol of decontamination of implant surfaces during surgical peri-implantitis treatment (Hentenaar et al., 2017).

Recent studies tested IP6 as an alternative to conventional surface treating agents. Titanium surfaces can be covalently functionalized with IP6 through the direct reaction of phosphate groups of IP6 with titanium oxide without the need for a crosslinker. The resulting bioactive functionalized surfaces had an osteogenic effect that is thought to result in reduced progression of bone resorption and enhancement of osseointegration. There was also decreased adhesion of bacterial biofilm to the treated surfaces (Córdoba et al., 2016).

The success of dental implants is a function of several parameters, and the titanium oxide layer on the implant surface is one of them. Thus, several reports have sought to modify this oxide layer to enhance biological performance and attain best clinical results (Palmquist et al., 2010; de Souza et al., 2019; He et al., 2019). Use of IP6 to modify the titanium oxide layer was studied by Zhang et al. In their research, the liquid phase deposition of this layer was assisted by using an IP6 template that stimulated nucleation and promoted titanium oxide development, leading to a homogeneous and compact

film that displayed a notable hydrophilic behaviour and excellent bending strength (Zhang et al., 2016). Due to the chemical structure and properties of IP6, it is thought that IP6 can serve as a bridge between the titanium implant surfaces and calcium ions. This was the basis of the study conducted by Liu et al. in 2019, where calcium was successfully bound to implant surfaces via hydrothermal treatment with IP6 and this resulted in a continuous release of calcium over time. The research also reported the super-hydrophilicity of these modified surfaces, with increased cell adhesion and proliferation, and up-regulation of osteogenic-related genes (Liu et al., 2019).

Hydroxyapatite coatings have received a lot of attention from the dental implant industry as they are thought to facilitate an osteoconductive effect. However, enhanced susceptibility of hydroxyapatite to bacterial activity is a major concern (Pajor et al., 2019). To overcome this drawback, IP6 was used to incorporate ionic sliver into a hydroxyapatite coating using a low heat immersion process, thus granting the coating an antibacterial feature (Funao et al., 2016). A magnesium ion-integrated IP6 coating was also developed for improved corrosion resistance, reduced degradation rate and to heighten the osteocompatibility (Chen et al., 2014). Collectively, these findings might direct researchers' attention towards the use of IP6 to produce implants with superior quality and enhanced long-term clinical outcomes.

Regeneration

The potential for regenerative therapy in endodontics is rapidly gaining attention. The principle aim is to restore and maintain tooth vitality through biologically based procedures designed to replace damaged tooth structure such as dentine and the pulp-dentine complex (Murray et al., 2007; Kim et al., 2018). Both pulp and dentine play crucial roles in regenerative endodontics. The former has a population of dental stem cells with inherent differential propensity, which gives the pulp its regenerative capacity (Sloan and Smith, 2007; Govindasamy et al., 2010). The dentine matrix is a source of bio-active dentine matrix components that get released following tissue injury. Several bioactive molecules have been identified in dentine such bone morphogenetic proteins and growth factors, which are essential for the regenerative process (Cassidy et al., 1997; Smith, 2003; Mazzoni et al., 2015). Endodontic irrigants and materials have been used to induce release of dentine-bound bioactive molecules during regenerative procedures (Graham et al., 2006; Tomson et al., 2007; Galler et al., 2016; Smith et al., 2016; Alghilan et al., 2017). EDTA as an irrigant has gained particular attention and is considered the gold standard in regenerative endodontics (Duncan et al., 2018; Atesci et al., 2020) due to its ability to demineralize dentine and release growth factors from the dentine matrix (Yamauchi et al., 2011; Galler et al., 2015; Galler et al., 2016). EDTA also has a positive influence on dental pulp stem cell adhesion, their migration to dentinal walls, and differentiation to odontoblast-like cells (Sonoyama et al., 2008; Galler et al., 2016). Equivalent studies using IP6 are limited. In 2018, Deniz Sungur et al. compared the effect of 1% IP6, 17% EDTA and 9% etidronic acid on growth factor release, and dental pulp stem cell migration and viability. IP6 was found to promote release of transforming growth factor (TGF-β), which in turn influenced cellular activity and increased pulpal cell migration and proliferation. The amount of release was lower than for EDTA or etidronic acid. However, the differences were not statistically significant. Furthermore, EDTA and IP6 resulted in similar migration and proliferation of the cells after 24 h exposure. However, at this exposure time, EDTA resulted in a contracted and spherical morphology, while IP6-treated cells displayed a polygonal morphology that was more stretched out onto the dentine surface (Deniz Sungur et al., 2019). Recently, Atesci et al. studied the effect of 17% EDTA and 1% IP6 on the release of different types of growth factors and mesenchymal stem cell behaviour (Atesci et al., 2020). No adverse impacts of these agents on stem cell proliferation and attachment to root dentine were demonstrated. The amount of TGF-β or vascular endothelial growth factor released with either EDTA or IP6 was statistically similar. IP6 showed the highest release of bone morphogenetic protein 2 and fibroblast growth factor 2 in cell-free solutions that contained dentine discs. However, the difference did not reach the level of significance compared to EDTA (Atesci et al., 2020).

Bioactive glasses are involved in the regeneration of dental hard tissues through two different processes, namely *in situ* remineralization of enamel and dentine, and inducing odontogenic differentiation of dental pulp cells leading to tertiary dentine formation (Mocquot et al., 2020). The need for a bioactive glass with superior bioactivity and biodegradability has led to the use of IP6. The structure of IP6 and its extensive phosphorus component confer an ability to be a good candidate for the synthesis of bioactive glass with high phosphate content. Modifying the phosphate content allowed production of bioactive materials with bioactivity over a wider composition range and different degradation rates that suit the intended application. The bioactive glasses derived from IP6 also showed improved resistance to dissolution compared with other phosphorus precursors, and absence of calcium nitrate, a toxic material, thus expanding its application range. In the presence of IP6, calcium ions incorporate within the gel network without the need of further calcination treatments at higher temperature (Li and Qiu, 2011). Ren et al. compared the effect of three different phosphorus precursors on the bioactivity and structure of bioactive glass. It was found that the material prepared with IP6 remained amorphous with more phosphorus atoms present as orthophosphate, and also had more bioactivity compared with other phosphorus precursors (Ren et al., 2017).

In 2017, Cui et al. compared the effect of IP6-derived bioactive glass (PSC) and traditional bioactive glasses on the differentiation of dental pulp cells and formation of dentine. PSC promoted earlier hydroxycarbonate apatite precipitation, which could be of a clinical importance in establishing a rapid bond between the bioactive material and the soft and hard tissues of the pulp-dentine complex. This in turn would enhance regeneration and repair of the complex. PSC also exhibited better biocompatibility as it provided a stable pH and protected the pulpal cells from severe inflammation. The larger surface area of PSC resulted in the release of higher amounts of phosphorus and silicon which led to more effective cell proliferation and odontogenic

TABLE 1 | Summary of the potential applications of IP6 and the perceived benefits in dentistry.

IP6 potential dental application	Perceived benefits
Cement	Improving the chemical and physical characteristics of cements used in several applications in restorative, adhesive, preventive and pediatric dentistry, orthodontics and endodontics
Oral care products	Developing new oral care products and improving the efficiency of professionally applied or patient-applied products such as varnishes, mouthrinses, dentifrices, whitening products and chewing gum used for their cariostatic, anti-calculus, anti-plaque, anti-stain and anti-microbial effects
Etching agent	Used as an alternative to phosphoric acid to extend the longevity of restorations, enhance resin bonding to tooth structure, improve biocompatibility to pulpal cells and decrease post-operative sensitivity
Chelating agent	Used in root canal treatment to overcome drawbacks associated with EDTA, improve biocompatibility to osteoblast cells, enhance adhesion to root canal dentine and offer antimicrobial properties
Implantology	Used as implant surface treating agent to create a bioactive surface with enhanced osseointegration and decreased biofilm adhesion
Regeneration	Improving bioactivity, biocompatibility and chemical and physical characteristics of scaffolds and cements used in tissue regeneration and repair. Used in regenerative endodontics to release growth factors from root canal dentine

differentiation. Differences in up-regulation of certain genes for the bioactive materials were found to affect the quality of the formed dentine. Reparative dentine stimulated by PSC was found to be thicker and formed in a continuous layer of dentine-like tissue with well-organized dentinal tubules (Cui et al., 2017). PSC has been also used to improve the mechanical performance and bioactivity of poly (1,8-octanediol-co-citrate). The latter is a synthetic biodegradable polyester used for soft tissue engineering. However, it lacks certain properties, thus limiting its application in bone regeneration. Poly (1,8-octanediol-co-citrate) composited with PSC exhibits higher mechanical strength, bioactivity, and biocompatibility with a reduced degradation rate. It also integrated well with the surrounding tissues which would result in better bone regeneration (Ren et al., 2017). PSC/bioactive bone cement composite also showed improved injectability and maintained its shape which made it easier to manipulate during the operation (Zhu et al., 2017). A patent describing PSC-polymer bone scaffold has been recently disclosed in 2019 (Deng et al., 2019). The effect of IP6 on the characteristics of polyelectrolyte hydrogel, a tissue engineering scaffold, was studied. It was concluded that IP6 produced a hydrogel scaffold with improved mechanical properties and antimicrobial capability (Bui and Huang, 2019). Several other researchers reported enhanced characteristics of biocements with the use of IP6; however, its effect on the setting time is dependent on several factors that are beyond the scope of this review (Horiguchi et al., 2008; Konishi et al., 2012; Christel et al., 2015; Medvecky et al., 2020).

IP6 has the potential to be used in regenerative dentistry. However, further studies are needed with regard to verifying this aspect of its use (Cui et al., 2017). Collectively, the previously mentioned findings do not capture the various aspects needed when evaluating an emerging agent in the field of regeneration. Consequently, we believe that these studies serve the same fundamental objective, which is to provide guidance about future research ideas on the use of IP6 in regenerative dentistry.

CONCLUSIONS AND FUTURE DIRECTIONS

IP6 is a versatile agent that lends itself to the development of new oral care products and the improvement of currently available materials in a variety of applications in the field of dentistry (**Table 1**). Most IP6-related research is still in its infancy, and in experimental stages at best, though its uniqueness and importance for several potential dental applications had been recognized early. However, in recent years, novel and rather compelling experimental data have been produced. The evidence for use of IP6 in dentistry is growing and the results are too compelling to be ignored. However, there are several limitations within the available literature, which demand calls for further rigorous research approaches towards clinical studies to further augment this evidence. Consideration of some of the recommendations and suggested future studies described in this review paper could facilitate more efficient use of IP6 in several facets of dentistry.

AUTHOR CONTRIBUTIONS

All authors listed have made a substantial, direct, and intellectual contribution to the work and approved it for publication.

REFERENCES

Afshan, Z., Jat, S. A., Khan, J. A., Hasan, A., and Rehman Qazi, F. U. (2020). Erosive potential of 1% phytic acid on radicular dentine at different time intervals. *Eur. Endod. J.* 5, 28–34. doi:10.14744/eej.2019.02411

Al-Hashimi, I., and Levine, M. J. (1989). Characterization of *in vivo* salivary-derived enamel pellicle. *Arch. Oral Biol.* 34, 289–295. doi:10.1016/0003-9969(89)90070-8

Al-Sanabani, J. S., Madfa, A. A., and Al-Sanabani, F. A. (2013). Application of calcium phosphate materials in dentistry. *Int. J. Biomater.* 2013, 876132. doi:10.1155/2013/876132

Alghilan, M. A., Windsor, L. J., Palasuk, J., and Yassen, G. H. (2017). Attachment and proliferation of dental pulp stem cells on dentine treated with different regenerative endodontic protocols. *Int. Endod. J.* 50, 667–675. doi:10.1111/iej.12669

Amaral, K. F., Rogero, M. M., Fock, R. A., Borelli, P., and Gavini, G. (2007). Cytotoxicity analysis of EDTA and citric acid applied on murine resident

macrophages culture. *Int. Endod. J.* 40, 338–343. doi:10.1111/j.1365-2591.2007.01220.x

Amerongen, A. V. N., Oderkerk, C. H., and Veerman, E. C. (1991). Adsorption to hydroxyapatite of partially deglycosylated human salivary mucins in competition with phosvitin and phytate. *Biol. Chem. Hoppe. Seyler.* 372, 585–591. doi:10.1515/bchm3.1991.372.2.585

Amerongen, N. A. V, Oderkerk, C. H., and Veerman, E. C. (1988). Influence of phytate on the adsorption of human salivary mucins onto hydroxyapatite. *J. Biol. Buccale.* 16, 203–208.

Anderson, R. J. (1914). A contribution to the chemistry of phytin. *J. Biol. Chem.* 17, 171–190. doi:10.1016/s0021-9258(18)88416-2

Arriero, M. d. M., Ramis, J. M., Perelló, M., and Monjo, M. (2012). Inositol hexakisphosphate inhibits osteoclastogenesis on RAW 264.7 cells and human primary osteoclasts. *PLoS One.* 7, e43187. doi:10.1371/journal.pone.0043187

Atesci, A. A., Avci, C. B., Tuglu, M. I., Ozates Ay, N. P., and Eronat, A. C. (2020). Effect of different dentin conditioning agents on growth factor release, mesenchymal stem cell attachment and morphology. *J. Endod.* 46, 200–208. doi:10.1016/j.joen.2019.10.033

Attal, J. P., Asmussen, E., and Degrange, M. (1994). Effects of surface treatment on the free surface energy of dentin. *Dent. Mater.* 10, 259–264. doi:10.1016/0109-5641(94)90071-x

Aune, D., Chan, D. S., Lau, R., Vieira, R., Greenwood, D. C., Kampman, E., et al. (2011). Dietary fibre, whole grains, and risk of colorectal cancer: systematic review and dose-response meta-analysis of prospective studies. *BMJ* 343, d6617. doi:10.1136/bmj.d6617

Baron, A., DeCarlo, A., and Featherstone, J. (1999). Functional aspects of the human salivary cystatins in the oral environment. *Oral Dis.* 5, 234–240. doi:10.1111/j.1601-0825.1999.tb00307.x

Bennick, A. (1982). Salivary proline-rich proteins. *Mol. Cel. Biochem.* 45, 83–99. doi:10.1007/BF00223503

Berg, J. H. (2002). Glass ionomer cements. *Pediatr. Dent.* 24, 430–438.

Björck, I. M., and Nyman, M. E. (1987). *In vitro* effects of phytic acid and polyphenols on starch digestion and fiber degradation. *J. Food Sci.* 52, 1588–1594. doi:10.1111/j.1365-2621.1987.tb05885.x

Boelen, G.J., Boute, L., d'Hoop, J., EzEldeen, M., Lambrichts, I., and Opdenakker, G. (2019). Matrix metalloproteinases and inhibitors in dentistry. *Clin. Oral Invest.* 23, 2823–2835. doi:10.1007/s00784-019-02915-y

Bowers, K. T., Keller, J. C., Randolph, B. A., Wick, D. G., and Michaels, C. M. (1992). Optimization of surface micromorphology for enhanced osteoblast responses *in vitro*. *Int. J. Oral Maxillofac. Implants* 7, 302–310.

Breiland, A. A., Flood, B. E., Nikrad, J., Bakarich, J., Husman, M., Rhee, T., et al. (2018). Polyphosphate-accumulating bacteria: potential contributors to mineral dissolution in the oral cavity. *Appl. Environ. Microbiol.* 84, e02440–17. doi:10.1128/AEM.02440-17

Breschi, L., Gobbi, P., Mazzotti, G., Falconi, M., Ellis, T. H., and Stangel, I. (2002). High resolution SEM evaluation of dentin etched with maleic and citric acid. *Dent. Mater.* 18, 26–35. doi:10.1016/s0109-5641(01)00017-3

Bui, H. L., and Huang, C. J. (2019). Tough polyelectrolyte hydrogels with antimicrobial property via incorporation of natural multivalent phytic acid. *Polymers* 11, 1721. doi:10.3390/polym11101721

Buonocore, M. G. (1955). A simple method of increasing the adhesion of acrylic filling materials to enamel surfaces. *J. Dent. Res.* 34, 849–853. doi:10.1177/00220345550340060801

Butterworth, P. J., Warren, F. J., and Ellis, P. R. (2011). Human α-amylase and starch digestion: an interesting marriage. *Starch/Stärke* 63, 395–405. doi:10.1002/star.201000150

Buttner, W., and Muhler, J. C. (1959). The effect of oat hulls on the dental caries experience in rats. *J. Dent. Res.* 38, 823–824. doi:10.1177/00220345590380041001

Calt, S., and Serper, A. (2002). Time-dependent effects of EDTA on dentin structures. *J. Endod.* 28, 17–19. doi:10.1097/00004770-200201000-00004

Camps, J., and Pashley, D. H. (2000). Buffering action of human dentin *in vitro*. *J. Adhes. Dent.* 2, 39–50.

Carlson, D. M. (1993). Salivary proline-rich proteins: biochemistry, molecular biology, and regulation of expression. *Crit. Rev. Oral Biol. Med.* 4, 495–502. doi:10.1177/10454411930040033401

Cassidy, N., Fahey, M., Prime, S. S., and Smith, A. J. (1997). Comparative analysis of transforming growth factor-beta isoforms 1–3 in human and rabbit dentine matrices. *Arch. Oral Biol.* 42, 219–223. doi:10.1016/S0003-9969(96)00115-X

Cawley, R. W., and Mitchell, T. A. (1968). Inhibition of wheat α-amylase by bran phytic acid. *J. Sci. Food Agric.* 19, 106–108. doi:10.1002/jsfa.2740190210

Cerklewski, F. L. (1992). Phytic acid plus supplemental calcium, but not phytic acid alone, decreases fluoride bioavailability in the rat. *J. Nutr. Biochem.* 3, 87–90. doi:10.1016/0955-2863(92)90097-3

Chen, Y., Zhao, S., Liu, B., Chen, M., Mao, J., He, H., et al. (2014). Corrosion-controlling and osteo-compatible Mg ion-integrated phytic acid (Mg-PA) coating on magnesium substrate for biodegradable implants application. *ACS Appl. Mater. Inter.* 6, 19531–19543. doi:10.1021/am506741d

Chersoni, S., Suppa, P., Breschi, L., Ferrari, M., Tay, F. R., Pashley, D. H., et al. (2004). Water movement in the hybrid layer after different dentin treatments. *Dent. Mater.* 20, 796–803. doi:10.1016/j.dental.2003.11.010

Cheryan, M., and Rackis, J. J. (1980). Phytic acid interactions in food systems. *Crit. Rev. Food Sci. Nutr.* 13, 297–335. doi:10.1080/10408398009527293

Chiba, M., Itoh, K., and Wakumoto, S. (1989). Effect of dentin cleansers on the bonding efficacy of dentin adhesive. *Dent. Mater. J.* 8, 76–85. doi:10.4012/dmj.8.76

Christel, T., Christ, S., Barralet, J. E., Groll, J., and Gbureck, U. (2015). Chelate bonding mechanism in a novel magnesium phosphate bone cement. *J. Am. Ceram. Soc.* 98, 694–697. doi:10.1111/jace.13491

Cochran, D. L., Schenk, R. K., Lussi, A., Higginbottom, F. L., and Buser, D. (1998). Bone response to unloaded and loaded titanium implants with a sandblasted and acid-etched surface: a histometric study in the canine mandible. *J. Biomed. Mater. Res.* 40, 1–11. doi:10.1002/(sici)1097-4636(199804)40:1<1::aid-jbm1>3.0.co;2-q

Cohen, S., Schiff, T., McCool, J., Volpe, A., and Petrone, M. E. (1994). Anticalculus efficacy of a dentifrice containing potassium nitrate, soluble pyrophosphate, PVM/MA copolymer, and sodium fluoride in a silica base: a twelve-week clinical study. *J. Clin. Dent.* 5, 93–96.

Cole, M. F., and Bowen, W. H. (1975). Effect of sodium phytate on the chemical and microbial composition of dental plaque in the monkey (*Macaca fascicularis*). *J. Dent. Res.* 54, 449–457. doi:10.1177/00220345750540030601

Cole, M. F., Eastoe, J. E., Curtis, M. A., Korts, D. C., and Bowen, W. H. (1980). Effects of pyridoxine, phytate and invert sugar on plaque composition and caries activity in the monkey (*Macaca fascicularis*). *Caries Res.* 14, 1–15. doi:10.1159/000260428

Córdoba, A., Hierro-Oliva, M., Pacha-Olivenza, M. Á., Fernández-Calderón, M. C., Perelló, J., Isern, B., et al. (2016). Direct covalent grafting of phytate to titanium surfaces through Ti-O-P bonding shows bone stimulating surface properties and decreased bacterial adhesion. *ACS Appl. Mater. Inter.* 8, 11326–11335. doi:10.1021/acsami.6b02533

Creeth, J. E., Parkinson, C. R., Burnett, G. R., Sanyal, S., Lippert, F., Zero, D. T., et al. (2018). Effects of a sodium fluoride- and phytate-containing dentifrice on remineralisation of enamel erosive lesions-an *in situ* randomised clinical study. *Clin. Oral Investig.* 22, 2543–2552. doi:10.1007/s00784-018-2351-z

Cruz-Filho, A. M., Paula, E. A., Pécora, J. D., and Sousa-Neto, M. D. (2002). Effect of different EGTA concentrations on dentin microhardness. *Braz. Dent. J.* 13, 188–190. doi:10.1590/s0103-64402002000300009

Cui, C. Y., Wang, S. N., Ren, H. H., Li, A. L., Qiu, D., Gan, Y. H., et al. (2017). Regeneration of dental-pulp complex-like tissue using phytic acid derived bioactive glasses. *RSC Adv.* 7, 22063–22070. doi:10.1039/c7ra01480e

Cummins, D. (2016). The superior anti-caries efficacy of fluoride toothpaste containing 1.5% arginine. *J. Clin. Dent.* 27, 27–38.

Dawes, C., and Shaw, J. H. (1965). Dietary phosphate supplementation and its effects on dental caries and salivary and serum concentrations of calcium and inorganic phosphate in the rat. *Arch. Oral Biol.* 10, 567–577. doi:10.1016/0003-9969(65)90002-6

Dawood, A. E., Parashos, P., Wong, R. H. K., Reynolds, E. C., and Manton, D. J. (2017). Calcium silicate-based cements: composition, properties, and clinical applications. *J. Investig. Clin. Dent.* 8, e12195. doi:10.1111/jicd.12195

de la Macorra, J. C., and Pradíes, G. (2002). Conventional and adhesive luting cements. *Clin. Oral Investig.* 6, 198–204. doi:10.1007/s00784-002-0184-1

De Munck, J., Van Meerbeek, B., Yoshida, Y., Inoue, S., Vargas, M., Suzuki, K., et al. (2003). Four-year water degradation of total-etch adhesives bonded to dentin. *J. Dent. Res.* 82, 136–140. doi:10.1177/154405910308200212

de Souza, V. Z., Joly, J. C., Elias, C. N., Peruzzo, D. C., Napimoga, M. H., et al. (2019). Viability and collagen secretion by fibroblasts on titanium surfaces with different acid-etching protocols. *Int. J. Implant Dent.* 5, 41. doi:10.1186/s40729-019-0192-4

Delimont, N. M., Katz, B. B., Fiorentino, N. M., Kimmel, K. A., Haub, M. D., Rosenkranz, S. K., et al. (2019). Salivary cystatin SN binds to phytic acid *in vitro* and is a predictor of nonheme iron bioavailability with phytic acid supplementation in a proof of concept pilot study. *Curr. Dev. Nutr.* 3, Nzz057. doi:10.1093/cdn/nzz057

Deng, M., Qiu, D., and Zuponcic, J. L. (2019). *Bioactive glass-polymer composite bone scaffolds*. Google Patents US-2019134262-A1

Deniz Sungur, D., Aksel, H., Ozturk, S., Yılmaz, Z., and Ulubayram, K. (2019). Effect of dentine conditioning with phytic acid or etidronic acid on growth factor release, dental pulp stem cell migration and viability. *Int. Endod. J.* 52, 838–846. doi:10.1111/iej.13066

Deshpande, S. S. (2002). *Handbook of food toxicology*. Boca Raton, FL: CRC Press.

Deshpande, S. S., and Cheryan, M. (1984). Effects of phytic acid, divalent cations, and their interactions on α-Amylase activity. *J. Food Sci.* 49, 516–519. doi:10.1111/j.1365-2621.1984.tb12456.x

Deshpande, S. S., and Damodaran, S. (1989). Effect of phytate on solubility, activity and conformation of trypsin and chymotrypsin. *J. Food Sci.* 54, 695–699. doi:10.1111/j.1365-2621.1989.tb04684.x

DeVito-Moraes, A., Francci, C., Vidal, C. M., Scaffa, P. M., Nesadal, D., Yamasaki, L. C., et al. (2016). Phosphoric acid concentration affects dentinal MMPs activity. *J. Dent.* 53, 30–37. doi:10.1016/j.jdent.2016.06.002

Doğan, H., and Qalt, S. (2001). Effects of chelating agents and sodium hypochlorite on mineral content of root dentin. *J. Endod.* 27, 578–580. doi:10.1097/00004770-200109000-00006

Du, Y., Dou, S., and Wu, S. (2012). Efficacy of phytic acid as an inhibitor of enzymatic and non-enzymatic browning in apple juice. *Food Chem.* 135, 580–582. doi:10.1016/j.foodchem.2012.04.131

Duncan, H. F., Kobayashi, Y., and Shimizu, E. (2018). Growth factors and cell homing in dental tissue regeneration. *Curr. Oral Health Rep.* 5, 276–285. doi:10.1007/s40496-018-0194-y

Eick, J. D., Johnson, L. N., Fromer, J. R., Good, R. J., and Neumann, A. W. (1972). Surface topography: its influence on wetting and adhesion in a dental adhesive system. *J. Dent. Res.* 51, 780–788. doi:10.1177/00220345720510031401

El Feninat, F., Ellis, T. H., Sacher, E., and Stangel, I. (2001). A tapping mode AFM study of collapse and denaturation in dentinal collagen. *Dent. Mater.* 17, 284–288. doi:10.1016/s0109-5641(00)00083-x

Elliott, R. P., Straka, R. P., and Garibaldi, J. A. (1964). Polyphosphate inhibition of growth of pseudomonads from poultry meat. *Appl. Microbiol.* 12, 517–522. doi:10.1128/aem.12.6.517-522.1964

Englander, H. R., and Keyes, P. H. (1970). Effect of phosphate supplements on cavitation in hamsters infected with caries-conductive streptococci. *J. Dent. Res.* 49, 140–144. doi:10.1177/00220345700490010801

Eymirli, A., Nagas, E., Uyanik, M. O., and Cehreli, Z. C. (2017). Effect of laser-activated irrigation with ethylene diaminetetraacetic acid and phytic acid on the removal of calcium hydroxide and triple antibiotic paste from root dentin. *Photomed. Laser Surg.* 35, 43–48. doi:10.1089/pho.2016.4146

FAO/IZiNCG (2018). *FAO/INFOODS/IZiNCG global food composition database for phytate. Version 1.0 Phyfoodcomp 1.0*. FAO/IZiNCG: Rome, Italy.

Fernández, D., Ortega-Castro, J., and Frau, J. (2017). Theoretical study of the HAP crystal growth inhibition potency of pyrophosphate, etidronate, citrate and phytate. Deciphered the adsorbed conformation of phytate on the HAP (001) surface. *Appl. Surf. Sci.* 408, 110–116. doi:10.1016/j.apsusc.2017.03.008

Foreman, P. C., and Barnes, I. E. (1990). Review of calcium hydroxide. *Int. Endod. J.* 23, 283–297. doi:10.1111/j.1365-2591.1990.tb00108.x

Forgione, D., Nassar, M., Seseogullari-Dirihan, R., Thitthaweerat, S., and Tezvergil-Mutluay, A. (2021). The effect of phytic acid on enzymatic degradation of dentin. *Eur. J. Oral. Sci.* e12771. doi:10.1111/eos.12771

Fox, C. H., and Eberl, M. (2002). Phytic acid (IP6), novel broad spectrum anti-neoplastic agent: a systematic review. *Complement. Ther. Med.* 10, 229–234. doi:10.1016/s0965-2299(02)00092-4

Frankenberger, R., Lohbauer, U., Roggendorf, M. J., Naumann, M., and Taschner, M. (2008). Selective enamel etching reconsidered: better than etch-and-rinse and self-etch? *J. Adhes. Dent.* 10, 339–344.

França, F. L., França-Botelho, A. D. C., and Araújo, F. G. S. (2018). Phosphoric acid increases the porosity and extends the contact area of dental osseo integrated implants. *Int. J. Adv. Eng. Res. Sci.* 5, 230–236. doi:10.22161/ijaers.5.3.30

Funao, H., Nagai, S., Sasaki, A., Hoshikawa, T., Tsuji, T., Okada, Y., et al. (2016). A novel hydroxyapatite film coated with ionic silver via inositol hexaphosphate chelation prevents implant-associated infection. *Sci. Rep.* 6, 23238. doi:10.1038/srep23238

Fusayama, T., Nakamura, M., Kurosaki, N., and Iwaku, M. (1979). Non-pressure adhesion of a new adhesive restorative resin. *J. Dent. Res.* 58, 1364–1370. doi:10.1177/00220345790580041101

Galler, K. M., Buchalla, W., Hiller, K. A., Federlin, M., Eidt, A., Schiefersteiner, M., et al. (2015). Influence of root canal disinfectants on growth factor release from dentin. *J. Endod.* 41, 363–368. doi:10.1016/j.joen.2014.11.021

Galler, K. M., Widbiller, M., Buchalla, W., Eidt, A., Hiller, K. A., Hoffer, P. C., et al. (2016). EDTA conditioning of dentine promotes adhesion, migration and differentiation of dental pulp stem cells. *Int. Endod. J.* 49, 581–590. doi:10.1111/iej.12492

García-Godoy, F., Loushine, R. J., Itthagarun, A., Weller, R. N., Murray, P. E., Feilzer, A. J., et al. (2005). Application of biologically-oriented dentin bonding principles to the use of endodontic irrigants. *Am. J. Dent.* 18, 281–290.

Garlich, J. R., Masterson, T. T., and Frank, R. K. (1994). *Phytate antimicrobial compounds in oral care products*. US5300289A.

Gbureck, U., Barralet, J. E., Spatz, K., Grover, L. M., and Thull, R. (2004). Ionic modification of calcium phosphate cement viscosity. Part I: hypodermic injection and strength improvement of apatite cement. *Biomaterials* 25, 2187–2195. doi:10.1016/j.biomaterials.2003.08.066

Govindasamy, V., Abdullah, A. N., Ronald, V. S., Musa, S., Ab. Aziz, Z. A., Zain, R. B., et al. (2010). Inherent differential propensity of dental pulp stem cells derived from human deciduous and permanent teeth. *J. Endodontics* 36, 1504–1515. doi:10.1016/j.joen.2010.05.006

Graf, E., and Eaton, J. W. (1990). Antioxidant functions of phytic acid. *Free Radic. Biol. Med.* 8, 61–69. doi:10.1016/0891-5849(90)90146-a

Graf, E., Empson, K. L., and Eaton, J. W. (1987). Phytic acid. A natural antioxidant. *J. Biol. Chem.* 262, 11647–11650. doi:10.1016/s0021-9258(18)60858-0

Graf, E. (1983). Applications of phytic acid. *J. Am. Oil Chem. Soc.* 60, 1861–1867. doi:10.1007/bf02901539

Graham, L., Cooper, P. R., Cassidy, N., Nor, J. E., Sloan, A. J., and Smith, A. J. (2006). The effect of calcium hydroxide on solubilisation of bio-active dentine matrix components. *Biomaterials* 27, 2865–2873. doi:10.1016/j.biomaterials.2005.12.020

Grases, F., and Costa-Bauzá, A. (1999). Phytate (IP6) is a powerful agent for preventing calcifications in biological fluids: usefulness in renal lithiasis treatment. *Anticancer Res.* 19, 3717–3722.

Grases, F., Costa-Bauza, A., and Prieto, R. M. (2006). Renal lithiasis and nutrition. *Nutr. J.* 5, 23. doi:10.1186/1475-2891-5-23

Grases, F., Perelló, J., Sanchis, P., Isern, B., Prieto, R. M., Costa-Bauzá, A., et al. (2009). Anticalculus effect of a triclosan mouthwash containing phytate: a double-blind, randomized, three-period crossover trial. *J. Periodont Res.* 44, 616–621. doi:10.1111/j.1600-0765.2008.01168.x

Grases, F., Ramis, M., and Costa-Bauzá, A. (2000). Effects of phytate and pyrophosphate on brushite and hydroxyapatite crystallization. Comparison with the action of other polyphosphates. *Urol. Res.* 28, 136–140. doi:10.1007/s002400050152

Grases, F., Söhnel, O., Zelenková, M., and Rodriguez, A. (2015). Phytate effects on biological hydroxyapatite development. *Urolithiasis* 43, 571–572. doi:10.1007/s00240-015-0814-0

Greiner, R., Konietzny, U., and Jany, K. (2006). Phytate-an undesirable constituent of plant-based foods? *J. für Ernährungsmedizin* 8, 18–28.

Grenby, T. H. (1967a). Flour, bread and wheat grain fractions in decalcification tests. *Arch. Oral Biol.* 12, 513–521. doi:10.1016/0003-9969(67)90025-8

Grenby, T. H. (1967b). Phytates in decalcification tests *in vitro*. *Arch. Oral Biol.* 12, 531–537. doi:10.1016/0003-9969(67)90027-1

Grenby, T. H. (1973). Trials of 3 organic phosphorus-containing compounds as protective agents against dental caries in rats. *J. Dent. Res.* 52, 454–461. doi:10.1177/00220345730520031201

Grenby, T. H. (1967c). Wheat bran factors in decalcification tests. *Arch. Oral Biol.* 12, 523–529. doi:10.1016/0003-9969(67)90026-x

Grenby, T. H. (1966). White and wholemeal bread and flour in the diet of caries-susceptible rats. *Br. Dent. J.* 121, 26–29.

Grynspan, F., and Cheryan, M. (1983). Calcium phytate: effect of pH and molar ratio on *in vitro* solubility. *J. Am. Oil Chem. Soc.* 60, 1761–1764. doi:10.1007/bf02680350

Gupta, R. K., Gangoliya, S. S., and Singh, N. K. (2015). Reduction of phytic acid and enhancement of bioavailable micronutrients in food grains. *J. Food Sci. Technol.* 52, 676–684. doi:10.1007/s13197-013-0978-y

Haapasalo, M., Shen, Y., Wang, Z., and Gao, Y. (2014). Irrigation in endodontics. *Br. Dent J.* 216, 299–303. doi:10.1038/sj.bdj.2014.204

Halvorsrud, K., Lewney, J., Craig, D., and Moynihan, P. J. (2019). Effects of starch on oral health: systematic review to inform WHO guideline. *J. Dent. Res.* 98, 46–53. doi:10.1177/0022034518788283

Hanakahi, L. A., Bartlet-Jones, M., Chappell, C., Pappin, D., and West, S. C. (2000). Binding of inositol phosphate to DNA-PK and stimulation of double-strand break repair. *Cell* 102, 721–729. doi:10.1016/s0092-8674(00)00061-1

Handelman, S. L., and Kreinces, G. H. (1973). Effect of phosphate and pH on Streptococcus mutans acid production and growth. *J. Dent. Res.* 52, 651–657. doi:10.1177/00220345730520040301

He, W., Yin, X., Xie, L., Liu, Z., Li, J., Zou, S., et al. (2019). Enhancing osseointegration of titanium implants through large-grit sandblasting combined with micro-arc oxidation surface modification. *J. Mater. Sci. Mater. Med.* 30, 73. doi:10.1007/s10856-019-6276-0

Hennequin, M., Pajot, J., and Avignant, D. (1994). Effects of different pH values of citric acid solutions on the calcium and phosphorus contents of human root dentin. *J. Endod.* 20, 551–554. doi:10.1016/S0099-2399(06)80071-3

Hentenaar, D. F. M., De Waal, Y. C. M., Strooker, H., Meijer, H. J. A., Van Winkelhoff, A. J., et al. (2017). Implant decontamination with phosphoric acid during surgical peri-implantitis treatment: a RCT. *Int. J. Implant Dent.* 3, 33. doi:10.1186/s40729-017-0091-5

Hill, E. E. (2007). Dental cements for definitive luting: a review and practical clinical considerations. *Dent. Clin. North Am.* 51, 643–658vi. doi:10.1016/j.cden.2007.04.002

Hoke, I. S. H., Strand, R., Wang, X., and Zhang, Y. (2016). *Oral care compositions comprising phytic acid*. Google Patents WO2013007018A1.

Horiguchi, Y., Yoshikawa, A., Oribe, K., and Aizawa, M. (2008). Fabrication of chelate-setting hydroxyapatite cements from four kinds of commercially-available powder with various shape and crystallinity and their mechanical property. *J. Ceram. Soc. Jpn.* 116, 50–55. doi:10.2109/jcersj2.116.50

Hsieh, S. C., Teng, N. C., Lin, Y. C., Lee, P. Y., Ji, D. Y., Chen, C. C., et al. (2009). A novel accelerator for improving the handling properties of dental filling materials. *J. Endod.* 35, 1292–1295. doi:10.1016/j.joen.2009.06.007

Hu, X., Ling, J., and Gao, Y. (2010). Effects of irrigation solutions on dentin wettability and roughness. *J. Endod.* 36, 1064–1067. doi:10.1016/j.joen.2010.03.007

Hunt, J. R. (2002). Moving toward a plant-based diet: are iron and zinc at risk? *Nutr. Rev.* 60, 127–134. doi:10.1301/00296640260093788

Hurle, K., Weichhold, J., Brueckner, M., Gbureck, U., Brueckner, T., and Goetz-Neunhoeffer, F. (2018). Hydration mechanism of a calcium phosphate cement modified with phytic acid. *Acta Biomater.* 80, 378–389. doi:10.1016/j.actbio.2018.09.002

Hurrell, R. F. (2003). Influence of vegetable protein sources on trace element and mineral bioavailability. *J. Nutr.* 133, 2973S-7S. doi:10.1093/jn/133.9.2973S

Imbery, T. A., Kennedy, M., Janus, C., and Moon, P. C. (2012). Evaluating EDTA as a substitute for phosphoric acid-etching of enamel and dentin. *Gen. Dent.* 60, e55–61.

Inagawa, J., Kiyosawa, I., and Nagasawa, T. (1987). Effects of phytic acid on the digestion of casein and soybean protein with trypsin, pancreatin or pepsin. *Jjsnfs* 40, 367–373. doi:10.4327/jsnfs.40.367

Jagzap, J. B., Patil, S. S., Gade, V. J., Chandhok, D. J., Upagade, M. A., and Thakur, D. A. (2017). Effectiveness of three different irrigants—17% ethylenediaminetetraacetic acid, Q-MIX, and phytic acid in smear layer removal: a comparative scanning electron microscope study. *Contemp. Clin. Dent.* 8, 459–463. doi:10.4103/ccd.ccd_524_17

Jenkins, G. N., Forster, M. G., and Speirs, R. L. (1959a). The influence of the refinement of carbohydrates on their cariogenicity. *In vitro* studies on crude and refined sugars and animal experiments. *Br. Dent. J.* 106, 362–374.

Jenkins, G. N., Forster, M. G., Spetrs, R. L., and Kleinberg, I. (1959b). The Influence of the refinement of carbohydrates on their cariogenicity. *In vitro* experiments on white and brown flour. *Br. dent. J.* 106, 195–208.

Jenkins, G. N. (1966). The refinement of foods in relation to dental caries. *Adv. Oral Biol.* 2, 67–100. doi:10.1016/b978-1-4832-3118-1.50011-6

Johnson, L. F., and Tate, M. E. (1969). Structure of "phytic acids". *Can. J. Chem.* 47, 63–73. doi:10.1139/v69-008

Johnsson, M., Richardson, C. F., Bergey, E. J., Levine, M. J., and Nancollas, G. H. (1991). The effects of human salivary cystatins and statherin on hydroxyapatite crystallization. *Arch. Oral Biol.* 36, 631–636. doi:10.1016/0003-9969(91)90014-l

Kancheva, V. D., and Kasaikina, O. T. (2013). Bio-antioxidants—a chemical base of their antioxidant activity and beneficial effect on human health. *Curr. Med. Chem.* 20, 4784–4805. doi:10.2174/09298673113209990161

Kaufman, H. W. (1986). Interactions of inositol phosphates with mineralized tissues. in Phytic acid: chemistry and applications. Editor E. Graf. Minneapolis, USA: Pilatus Press, 303–320.

Kaufman, H. W., and Kleinberg, I. (1970). The effect of pH on the adsorption properties of the phytate molecule. *Arch. Oral Biol.* 15, 917–934. doi:10.1016/0003-9969(70)90088-9

Kim, J. S., Jang, S. W., Son, M., Kim, B. M., and Kang, M. J. (2016). Enteric-coated tablet of risedronate sodium in combination with phytic acid, a natural chelating agent, for improved oral bioavailability. *Eur. J. Pharm. Sci.* 82, 45–51. doi:10.1016/j.ejps.2015.11.011

Kim, N. H., and Rhee, M. S. (2016). Phytic acid and sodium chloride show marked synergistic bactericidal effects against nonadapted and acid-adapted *Escherichia coli* O157:H7 strains. *Appl. Environ. Microbiol.* 82, 1040–1049. doi:10.1128/AEM.03307-15

Kim, S. G., Malek, M., Sigurdsson, A., Lin, L. M., and Kahler, B. (2018). Regenerative endodontics: a comprehensive review. *Int. Endod. J.* 51, 1367–1388. doi:10.1111/iej.12954

Kleinberg, I., Acevedo, A. M., and Chatterjee, R. (1998). *Anti-caries oral compositions*. Google Patents WO1997032565A1.

Knuckles, B. E., and Betschart, A. A. (1987). Effect of phytate and other myo-inositol phosphate esters on α-amylase digestion of starch. *J. Food Sci.* 52, 719–721. doi:10.1111/j.1365-2621.1987.tb06710.x

Knuckles, B. E. (1988). Effect of phytate and other myo-inositol phosphate esters on lipase activity. *J. Food Sci.* 53, 250–252. doi:10.1111/j.1365-2621.1988.tb10221.x

Kong, K., Hiraishi, N., Nassar, M., Otsuki, M., Yiu, C. K. Y., and Tagami, J. (2017). Effect of phytic acid etchant on resin-dentin bonding: monomer penetration and stability of dentin collagen. *J. Prosthodont. Res.* 61, 251–258. doi:10.1016/j.jpor.2016.10.001

Kong, K., Islam, M. S., Nassar, M., Hiraishi, N., Otsuki, M., Yiu, C. K. Y., et al. (2015). Effect of phytic acid etchant on the structural stability of demineralized dentine and dentine bonding. *J. Mech. Behav. Biomed. Mater.* 48, 145–152. doi:10.1016/j.jmbbm.2015.03.027

König, K. G., and Grenby, T. H. (1965). The effect of wheat grain fractions and sucrose mixtures on rat caries developing in two strains of rats maintained on different regimes and evaluated by two different methods. *Arch. Oral Biol.* 10, 143–153. doi:10.1016/0003-9969(65)90066-x

Konishi, T., Mizumoto, M., Honda, M., Zhuang, Z., and Aizawa, M. (2012). Fabrication of chelate-setting cements from hydroxyapatite powders surface-modified with various sodium inositol hexaphosphate concentrations and their mechanical properties. *Proced. Eng.* 36, 137–143. doi:10.1016/j.proeng.2012.03.021

Koutsoukos, P. G., Amjad, Z., and Nancollas, G. H. (1981). The influence of phytate and phosphonate on the crystal growth of fluorapatite and hydroxyapatite. *J. Colloid Interf. Sci.* 83, 599–605. doi:10.1016/0021-9797(81)90354-4

Lee, H., Jeong, C., Ghafoor, K., Cho, S., and Park, J. (2011). Oral delivery of insulin using chitosan capsules cross-linked with phytic acid. *Biomed. Mater. Eng.* 21, 25–36. doi:10.3233/BME-2011-0654

Li, A., and Qiu, D. (2011). Phytic acid derived bioactive CaO-P2O5-SiO_2 gel-glasses. *J. Mater. Sci. Mater. Med.* 22, 2685–2691. doi:10.1007/s10856-011-4464-7

Li, J., Forberg, S., and Söremark, R. (1994). Influence of phytic acid on zinc phosphate cement. *Acta Odontol. Scand.* 52, 209–213. doi:10.3109/00016359409029048

Lilienthal, B., Bush, E., Buckmaster, M., Gregory, G., Gagolski, J., Smythe, B. M., et al. (1966). The cariostatic effect of carbohydrate phosphates in the diet. *Aust. Dent. J.* 11, 388–395. doi:10.1111/j.1834-7819.1966.tb03799.x

Limbasuta, S., Singh, B., and Johansen, E. (1961). The effect of sodium phytate and sodium acid pyrophosphate on rat caries. *J. Dent. Res.* 40, 658.

Lingström, P., van Houte, J., and Kashket, S. (2000). Food starches and dental caries. *Crit. Rev. Oral Biol. Med.* 11, 366–380. doi:10.1177/10454411000110030601

Lippert, F. (2013). An introduction to toothpaste - its purpose, history and ingredients. *Monogr. Oral Sci.* 23, 1. doi:10.1159/000350456

Liu, K., Zhang, H., Lu, M., Liu, L., Yan, Y., Chu, Z., et al. (2019). Enhanced bioactive and osteogenic activities of titanium by modification with phytic acid and calcium hydroxide. *Appl. Surf. Sci.* 478, 162–175. doi:10.1016/j.apsusc.2019.01.219

López-González, A. A., Grases, F., Roca, P., Mari, B., Vicente-Herrero, M. T., and Costa-Bauzá, A. (2008). Phytate (myo-inositol hexaphosphate) and risk factors for osteoporosis. *J. Med. Food* 11, 747–752. doi:10.1089/jmf.2008.0087

Macedo, G. V., Yamauchi, M., and Bedran-Russo, A. K. (2009). Effects of chemical cross-linkers on caries-affected dentin bonding. *J. Dent. Res.* 88, 1096–1100. doi:10.1177/0022034509351001

Machado-Silveiro, L. F., González-López, S., and González-Rodríguez, M. P. (2004). Decalcification of root canal dentine by citric acid, EDTA and sodium citrate. *Int. Endod. J.* 37, 365–369. doi:10.1111/j.1365-2591.2004.00813.x

Madsen, K. O., and Edmonds, E. J. (1962). Effect of rice hulls and other seed hulls on dental caries production in the cotton rat. *J. Dent. Res.* 41, 405–412. doi:10.1177/00220345620410021201

Magrill, D. S. (1973a). Phytate inhibition of enamel hardening by mineralizing solutions. *J. Dent. Res.* 52, 1342. doi:10.1177/00220345730520063401

Magrill, D. S. (1973b). The reduction of the solubility of hydroxyapatite in acid by adsorption of phytate from solution. *Arch. Oral Biol.* 18, 591–600. doi:10.1016/0003-9969(73)90097-6

Martin, J. Y., Schwartz, Z., Hummert, T. W., Schraub, D. M., Simpson, J., Lankford, J., Jr., et al. (1995). Effect of titanium surface roughness on proliferation, differentiation, and protein synthesis of human osteoblast-like cells (MG63). *J. Biomed. Mater. Res.* 29, 389–401. doi:10.1002/jbm.820290314

Mazzoni, A., Tjäderhane, L., Checchi, V., Di Lenarda, R., Salo, T., Tay, F. R., et al. (2015). Role of dentin MMPs in caries progression and bond stability. *J. Dent. Res.* 94, 241–251. doi:10.1177/0022034514562833

McArthur, C., Sanson, G. D., and Beal, A. M. (1995). Salivary proline-rich proteins in mammals: roles in oral homeostasis and counteracting dietary tannin. *J. Chem. Ecol.* 21, 663–691. doi:10.1007/BF02033455

McClure, F. J. (1964). Cariostatic effect of phosphates. *Science* 144, 1337–1338. doi:10.1126/science.144.3624.1337

McClure, F. J. (1960). The cariostatic effect in white rats of phosphorus and calcium supplements added to the flour of bread formulas and to bread diets. *J. Nutr.* 72, 131–136. doi:10.1093/jn/72.2.131

McClure, F. J. (1963). Further studies on the cariostatic effect of organic and inorganic phosphates. *J. Dent. Res.* 42, 693–699. doi:10.1177/00220345630420021801

Medvecky, L., Stulajterova, R., Giretova, M., Sopcak, T., Molcanova, Z., and Koval, K. (2020). Enzymatically hardened calcium phosphate biocement with phytic acid addition. *J. Mater. Sci. Mater. Med.* 31, 54. doi:10.1007/s10856-020-06387-5

Meininger, S., Blum, C., Schamel, M., Barralet, J. E., Ignatius, A., and Gbureck, U. (2017). Phytic acid as alternative setting retarder enhanced biological performance of dicalcium phosphate cement *in vitro*. *Sci. Rep.* 7, 558–610. doi:10.1038/s41598-017-00731-6

Meyer, F., Amaechi, B. T., Fabritius, H. O., and Enax, J. (2018). Overview of calcium phosphates used in biomimetic oral care. *Open Dent. J.* 12, 406. doi:10.2174/1874210601812010406

Milleman, K. R., Creeth, J. E., Burnett, G. R., and Milleman, J. L. (2018). A randomized clinical trial to evaluate the stain removal efficacy of a sodium phytate dentifrice formulation. *J. Esthet. Restor. Dent.* 30, E45–E51. doi:10.1111/jerd.12355

Millett, D. T., Glenny, A. M., Mattick, R. C., Hickman, J., and Mandall, N. A. (2016). Adhesives for fixed orthodontic bands. *Cochrane Database Syst. Rev.* 10, CD004485. doi:10.1002/14651858.CD004485

Miyamoto, S., Kuwata, G., Imai, M., Nagao, A., and Terao, J. (2000). Protective effect of phytic acid hydrolysis products on iron-induced lipid peroxidation of liposomal membranes. *Lipids* 35, 1411. doi:10.1007/s11745-000-0659-y

Mocquot, C., Attik, N., Pradelle-Plasse, N., Grosgogeat, B., and Colon, P. (2020). Bioactivity assessment of bioactive glasses for dental applications: a critical review. *Dent. Mater.* 36, 1116–1143. doi:10.1016/j.dental.2020.03.020

Morris, C., Fichtel, S. L., and Taylor, A. J. (2011). Impact of calcium on salivary α-amylase activity, starch paste apparent viscosity, and thickness perception. *Chem. Percept.* 4, 116. doi:10.1007/s12078-011-9091-7

Muana, H. L., Nassar, M., Dargham, A., Hiraishi, N., and Tagami, J. (2020). Effect of smear layer removal agents on the microhardness and roughness of radicular dentin. *Saudi Dent. J.* doi:10.1016/j.sdentj.2020.05.001

Murray, P. E., Garcia-Godoy, F., and Hargreaves, K. M. (2007). Regenerative endodontics: a review of current status and a call for action. *J. Endod.* 33, 377–390. doi:10.1016/j.joen.2006.09.013

Nakajima, M., Okuda, M., Pereira, P., Tagami, J., and Pashley, D. H. (2002). Dimensional changes and ultimate tensile strengths of wet decalcified dentin applied with one-bottle adhesives. *Dent. Mater.* 18, 603–608. doi:10.1016/s0109-5641(02)00004-0

Nakauchi, G., Eshita, Y., and Takahashi, K. (2017). *Tooth whitener*. US9757315B2.

Napper, D. H., and Smythe, B. M. (1966). The dissolution kinetics of hydroxyapatite in the presence of kink poisons. *J. Dent. Res.* 45, 1775–1783. doi:10.1177/00220345660450063201

Nassar, M., Hiraishi, N., Shimokawa, H., Tamura, Y., Otsuki, M., Kasugai, S., et al. (2014). The inhibition effect of non-protein thiols on dentinal matrix metalloproteinase activity and HEMA cytotoxicity. *J. Dent.* 42, 312–318. doi:10.1016/j.jdent.2013.11.023

Nassar, M., Hiraishi, N., Tamura, Y., Otsuki, M., Aoki, K., and Tagami, J. (2015). Phytic acid: an alternative root canal chelating agent. *J. Endod.* 41, 242–247. doi:10.1016/j.joen.2014.09.029

Nassar, M., Hiraishi, N., Islam, M. S., Aizawa, M., Tamura, Y., Otsuki, M., et al. (2013). Effect of phytic acid used as etchant on bond strength, smear layer, and pulpal cellsEffect of phytic acid used as etchant on bond strength, smear layer, and pulpal cells. *Eur. J. Oral Sci.* 121, 482–487. doi:10.1111/eos.12064

Nassar, M., Hiraishi, N., Islam, M. S., Romero, M. J. R. H., Otsuki, M., and Tagami, J. (2020). Effect of phytic acid as an endodontic chelator on resin adhesion to sodium hypochlorite-treated dentin. *Restor. Dent. Endod.* 45, e44. doi:10.5395/rde.2020.45.e44

Nassar, R. I., and Nassar, M. (2017). Antimicrobial effect of phytic acid on *Enterococcus faecalis*. *Int. Arab. J. Antimicrob. Agents* 6, 1–7. doi:10.1515/9781503603189

Nezu, T., and Winnik, F. M. (2000). Interaction of water-soluble collagen with poly (acrylic acid). *Biomaterials* 21, 415–419. doi:10.1016/s0142-9612(99)00204-5

Nikhil, V., Jaiswal, S., Bansal, P., Arora, R., Raj, S., and Malhotra, P. (2016). Effect of phytic acid, ethylenediaminetetraacetic acid, and chitosan solutions on microhardness of the human radicular dentin. *J. Conserv. Dent.* 19, 179–183. doi:10.4103/0972-0707.178705

Nissar, J., Ahad, T., Naik, H. R., and Hussain, S. Z. (2017). A review phytic acid: as antinutrient or nutraceutical. *J. Pharmacogn. Phytochem.* 6, 1554–1560.

Nordbö, H., and Rölla, G. (1972). Desorption of salivary proteins from hydroxyapatite by phytic acid and glycerophosphate and the plaque-inhibiting effect of the two compounds *in vivo*. *J. Dent. Res.* 51, 800–802. doi:10.1177/00220345720510031701

Norris, F. A., Ungewickell, E., and Majerus, P. W. (1995). Inositol hexakisphosphate binds to clathrin assembly protein 3 (AP-3/AP180) and inhibits clathrin cage assembly *in vitro*. *J. Biol. Chem.* 270, 214–217. doi:10.1074/jbc.270.1.214

Oatway, L., Vasanthan, T., and Helm, J. H. (2001). Phytic acid. *Food Rev. Int.* 17, 419–431. doi:10.1081/fri-100108531

Nygaard-Ostby, N. (1957). Chelating in root canal therapy. Ethylene-diamine tetraacetic acid for cleansing and widening of root canals. *Odontol. Tidskr.* 65, 3–11.

Pajor, K., Pajchel, L., and Kolmas, J. (2019). Hydroxyapatite and fluorapatite in conservative dentistry and oral implantology—a review. *Materials* 12, 2683. doi:10.3390/ma12172683

Pallauf, J., and Rimbach, G. (1997). Nutritional significance of phytic acid and phytase. *Arch. Tierernahr* 50, 301–319. doi:10.1080/17450399709386141

Palmquist, A., Omar, O. M., Esposito, M., Lausmaa, J., and Thomsen, P. (2010). Titanium oral implants: surface characteristics, interface biology and clinical outcome. *J. R. Soc. Interf.* 7 Suppl 5, S515–S527. doi:10.1098/rsif.2010.0118.focus

Parkinson, C. R., Burnett, G. R., Creeth, J. E., Lynch, R. J. M., Budhawant, C., Lippert, F., et al. (2018). Effect of phytate and zinc ions on fluoride toothpaste efficacy using an *in situ* caries model. *J. Dent.* 73, 24–31. doi:10.1016/j.jdent.2018.03.013

Pashley, D. H., Ciucchi, B., Sano, H., and Horner, J. A. (1993). Permeability of dentin to adhesive agents. *Quintessence Int.* 24, 618–631.

Pashley, D. H., Tay, F. R., Yiu, C., Hashimoto, M., Breschi, L., Carvalho, R., et al. (2004). Collagen degradation by host-derived enzymes during aging. *J. Dent. Res.* 83, 216–221. doi:10.1177/154405910408300306

Pashley, D. H. (1992). The effects of acid etching on the pulpodentin complex. *Oper. Dent.* 17, 229–242.

Persson, H., Türk, M., Nyman, M., and Sandberg, A. S. (1998). Binding of Cu^{2+}, Zn^{2+}, and Cd^{2+} to inositol tri-, tetra-, penta-, and hexaphosphates. *J. Agric. Food Chem.* 46, 3194–3200. doi:10.1021/jf971055w

Pető, G., Karacs, A., Pászti, Z., Guczi, L., Divinyi, T., and Joób, A. (2002). Surface treatment of screw shaped titanium dental implants by high intensity laser pulses. *Appl. Surf. Sci.* 186, 7–13.

Pfeffer, E. (1872). The inositol phosphates: chemical synthesis and biological significance. *Jahrb Wiss Bot.* 8, 429.

Porciani, P. F., Grandini, S., and Sapio, S. (2003). Anticalculus efficacy of a chewing gum with polyphosphates in a twelve-week single-blind trial. *J. Clin. Dent.* 14, 45–47.

Post, F. J., Krishnamurty, G. B., and Flanagan, M. D. (1963). Influence of sodium hexametaphosphate on selected bacteria. *Appl. Microbiol.* 11, 430–435. doi:10.1128/aem.11.5.430-435.1963

Posternak, S. (1903). Sur un nouveau principe phospho-organique d'origine végétale, la phytine. *Compt. Rend. Soc. de Biol.* 55, 1190–1192.

Prado, M., Gusman, H., Gomes, B. P., and Simão, R. A. (2011). Scanning electron microscopic investigation of the effectiveness of phosphoric acid in smear layer removal when compared with EDTA and citric acid. *J. Endod.* 37, 255–258. doi:10.1016/j.joen.2010.11.011

Prati, C., Chersoni, S., and Pashley, D. H. (1999). Effect of removal of surface collagen fibrils on resin-dentin bonding. *Dent. Mater.* 15, 323–331. doi:10.1016/s0109-5641(99)00052-4

Prosser, H. J., Brant, P. J., Scott, R. P., and Wilson, A. D. (1983). The cement-forming properties of phytic acid. *J. Dent. Res.* 62, 598–600. doi:10.1177/00220345830620052001

Pruitt, K. M., Jamieson, A. D., and Caldwell, R. C. (1970). Possible basis for the cariostatic effect of inorganic phosphates. *Nature* 225, 1249. doi:10.1038/2251249a0

Ravichandran, R., Seitz, V., Reddy Venugopal, J., Sridhar, R., Sundarrajan, S., Mukherjee, S., et al. (2013). Mimicking native extracellular matrix with phytic acid-crosslinked protein nanofibers for cardiac tissue engineering. *Macromol. Biosci.* 13, 366–375. doi:10.1002/mabi.201200391

Ravindran, V., Bryden, W. L., and Kornegay, E. T. (1995). Phytates: occurrence, bioavailability and implications in poultry nutrition. *Poult. Avian Biol. Rev.* 6, 125–143.

Reddy, N. R., Pierson, M. D., Sathe, S. K., and Salunkhe, D. K. (1989). *Phytates in cereals and legumes*. Boca Raton, FL: CRC Press.

Reddy, N. R., and Salunkhe, D. K. (1981). Interactions between phytate, protein, and minerals in whey fractions of black gram. *J. Food Sci.* 46, 564–567. doi:10.1111/j.1365-2621.1981.tb04911.x

Reddy, N. R. , Sathe, S. K., and Salunkhe, D. K. (1982). Phytates in legumes and cereals. *Adv. Food Res.* 28, 1–92. doi:10.1016/s0065-2628(08)60110-x

Ren, H., Tian, Y., Li, A., Martin, R. A., and Qiu, D. (2017). The influence of phosphorus precursor on the structure and properties of SiO2–P2O5–CaO bioactive glass. *Biomed. Phys. Eng. Express.* 3, 045017. http://dx.doi.org/10.1088/2057-1976/aa7daa.

Rickard, S. E., and Thompson, L. U. (1997). "*Interactions and biological effects of phytic acid*," in *Antinutrients and phytochemicals in food*. Editor F. Shahidi (Washington, DC: American Chemical Society), 294–312.

Rodrigues, L., Espanca, R., Costa, A. R., Antunes, C. M., Pomar, C., Capela-Silva, F., et al. (2019). Comparison of salivary proteome of children with different sensitivities for bitter and sweet tastes: association with body mass index. *Int. J. Obes.* 43, 701–712. doi:10.1038/s41366-018-0289-5

Rose, H. E., and Quarterman, J. (1984). Effects of dietary phytic acid on lead and cadmium uptake and depletion in rats. *Environ. Res.* 35, 482–489. doi:10.1016/0013-9351(84)90154-3

Sands, S. H., Biskobing, S. J., and Olson, R. M. (1986). *Commerical aspects of phytic acid: an overview. Phytic acid: chemistry and applications*. Minneapolis, MN: Pilatus Press.

Sano, H., Shono, T., Takatsu, T., and Hosoda, H. (1994). Microporous dentin zone beneath resin-impregnated layer. *Oper. Dent.* 19, 59–64.

Sasakawa, N., Sharif, M., and Hanley, M. R. (1995). Metabolism and biological activities of inositol pentakisphosphate and inositol hexakisphosphate. *Biochem. Pharmacol.* 50, 137–146. doi:10.1016/0006-2952(95)00059-9

Scannapieco, F. A., Solomon, L., and Wadenya, R. O. (1994). Emergence in human dental plaque and host distribution of amylase-binding streptococci. *J. Dent. Res.* 73, 1627–1635. doi:10.1177/00220345940730100701

Scannapieco, F. A., Torres, G., and Levine, M. J. (1993). Salivary alpha-amylase: role in dental plaque and caries formation. *Crit. Rev. Oral Biol. Med.* 4, 301–307. doi:10.1177/10454411930040030701

Schlemmer, U., Frølich, W., Prieto, R. M., and Grases, F. (2009). Phytate in foods and significance for humans: food sources, intake, processing, bioavailability, protective role and analysis. *Mol. Nutr. Food Res.* 53 Suppl 2, S330–S375. doi:10.1002/mnfr.200900099

Selle, P. H., Cowieson, A. J., Cowieson, N. P., and Ravindran, V. (2012). Protein-phytate interactions in pig and poultry nutrition: a reappraisal. *Nutr. Res. Rev.* 25, 1–17. doi:10.1017/S0954422411000151

Shafie, N. H., Esa, N. M., Ithnin, H., Saad, N., and Pandurangan, A. K. (2013). Pro-apoptotic effect of rice bran inositol hexaphosphate (IP6) on HT-29 colorectal cancer cells. *Int. J. Mol. Sci.* 14, 23545–23558. doi:10.3390/ijms141223545

Sharma, C. B., Goel, M., and Irshad, M. (1978). Myoinositol hexaphosphate as a potential inhibitor of α-amylases. *Phytochemistry* 17, 201–204. doi:10.1016/s0031-9422(00)94146-3

Shears, S. B. (2001). Assessing the omnipotence of inositol hexakisphosphate. *Cell. Signal.* 13, 151–158. doi:10.1016/s0898-6568(01)00129-2

Sheikh, Z., Zhang, Y. L., Grover, L., Merle, G. E., Tamimi, F., and Barralet, J. (2015). *In vitro* degradation and *in vivo* resorption of dicalcium phosphate cement based grafts. *Acta Biomater.* 26, 338–346. doi:10.1016/j.actbio.2015.08.031

Shibata, H., and Morioka, T. (1982). Antibacterial action of condensed phosphates on the bacterium Streptococcus mutans and experimental caries in the hamster. *Arch. Oral Biol.* 27, 809–816. doi:10.1016/0003-9969(82)90034-6

Sidhu, S. K., and Nicholson, J. W. (2016). A review of glass-ionomer cements for clinical dentistry. *J. Funct. Biomater.* 7, 16. doi:10.3390/jfb7030016

Sillanpää, M. (1997). Environmental fate of EDTA and DTPA. *Rev. Environ. Contam. Toxicol.* 152, 85–111. doi:10.1007/978-1-4612-1964-4_3

Silva, E. O., and Bracarense, A. P. (2016). Phytic acid: from antinutritional to multiple protection factor of organic systems. *J. Food Sci.* 81, R1357–R1362. doi:10.1111/1750-3841.13320

Silva, P. V., Guedes, D. F., Nakadi, F. V., Pécora, J. D., and Cruz-Filho, A. M. (2013). Chitosan: a new solution for removal of smear layer after root canal instrumentation. *Int. Endod. J.* 46, 332–338. doi:10.1111/j.1365-2591.2012.02119.x

Singh, M., and Krikorian, A. D. (1982). Inhibition of trypsin activity *in vitro* by phytate. *J. Agric. Food Chem.* 30, 799–800. doi:10.1021/jf00112a049

Sloan, A. J., and Smith, A. J. (2007). Stem cells and the dental pulp: potential roles in dentine regeneration and repair. *Oral Dis.* 13, 151–157. doi:10.1111/j.1601-0825.2006.01346.x

Smith, A. J., Duncan, H. F., Diogenes, A., Simon, S., and Cooper, P. R. (2016). Exploiting the bioactive properties of the dentin-pulp complex in regenerative endodontics. *J. Endod.* 42, 47–56. doi:10.1016/j.joen.2015.10.019

Smith, A. J. (2003). Vitality of the dentin-pulp complex in health and disease: growth factors as key mediators. *J. Dent Educ.* 67, 678–689. doi:10.1002/j.0022-0337.2003.67.6.tb03668.x

Sonoyama, W., Liu, Y., Yamaza, T., Tuan, R. S., Wang, S., Shi, S., et al. (2008). Characterization of the apical papilla and its residing stem cells from human immature permanent teeth: a pilot study. *J. Endod.* 34, 166–171. doi:10.1016/j.joen.2007.11.021

Stuart, C. H., Schwartz, S. A., Beeson, T. J., and Owatz, C. B. (2006). *Enterococcus faecalis*: its role in root canal treatment failure and current concepts in retreatment. *J. Endod.* 32, 93–98. doi:10.1016/j.joen.2005.10.049

Szwergold, B. S., Graham, R. A., and Brown, T. R. (1987). Observation of inositol pentakis- and hexakis-phosphates in mammalian tissues by 31P NMR.

Biochem. Biophys. Res. Commun. 149, 874–881. doi:10.1016/0006-291x(87)90489-x

Tabak, L. A. (1990). Structure and function of human salivary mucins. *Crit. Rev. Oral Biol. Med.* 1, 229–234. doi:10.1177/10454411900010040201

Taketa, F., and Phillips, P. H. (1957). Oat hull fractions and the development of dental caries. *J. Am. Diet. Assoc.* 33, 575–578.

Tezvergil-Mutluay, A., Mutluay, M., Seseogullari-Dirihan, R., Agee, K. A., Key, W. O., Scheffel, D. L., et al. (2013). Effect of phosphoric acid on the degradation of human dentin matrix. *J. Dent Res.* 92, 87–91. doi:10.1177/0022034512466264

Thompson, J. M., Agee, K., Sidow, S. J., McNally, K., Lindsey, K., Borke, J., et al. (2012). Inhibition of endogenous dentin matrix metalloproteinases by ethylenediaminetetraacetic acid. *J. Endod.* 38, 62–65. doi:10.1016/j.joen.2011.09.005

Thompson, L. U., and Yoon, J. H. (1984). Starch digestibility as affected by polyphenols and phytic acid. *J. Food Sci.* 49, 1228–1229. doi:10.1111/j.1365-2621.1984.tb10443.x

Toledano, M., Yamauti, M., Osorio, E., and Osorio, R. (2012). Zinc-inhibited MMP-mediated collagen degradation after different dentine demineralization procedures. *Caries. Res.* 46, 201–207. doi:10.1159/000337315

Tomson, P. L., Grover, L. M., Lumley, P. J., Sloan, A. J., Smith, A. J., and Cooper, P. R. (2007). Dissolution of bio-active dentine matrix components by mineral trioxide aggregate. *J. Dent.* 35, 636–642. doi:10.1016/j.jdent.2007.04.008

Torabinejad, M., Khademi, A. A., Babagoli, J., Cho, Y., Johnson, W. B., Bozhilov, K., et al. (2003). A new solution for the removal of the smear layer. *J. Endod.* 29, 170–175. doi:10.1097/00004770-200303000-00002

Torres, J., Domínguez, S., Cerdá, M. F., Obal, G., Mederos, A., Irvine, R. F., et al. (2005). Solution behaviour of myo-inositol hexakisphosphate in the presence of multivalent cations. Prediction of a neutral pentamagnesium species under cytosolic/nuclear conditions. *J. Inorg. Biochem.* 99, 828–840. doi:10.1016/j.jinorgbio.2004.12.011

Touger-Decker, R., and van Loveren, C. (2003). Sugars and dental caries. *Am. J. Clin. Nutr.* 78, 881S–892S. doi:10.1093/ajcn/78.4.881s

Trela, B. C. (2010). Iron stabilization with phytic acid in model wine and wine. *Am. J. Enol Vitic.* 61, 253–259.

Trevelin, L. T., Villanueva, J., Zamperini, C. A., Mathew, M. T., Matos, A. B., and Bedran-Russo, A. K. (2019). Investigation of five α-hydroxy acids for enamel and dentin etching: demineralization depth, resin adhesion and dentin enzymatic activity. *Dent. Mater.* 35, 900–908. doi:10.1016/j.dental.2019.03.005

Tu, X., Chen, X., Peng, Y., Nan, J., Wei, B., He, L., et al. (2018). Modulation of the self-assembly of collagen by phytic acid: an in vitro study. *Macromol. Res.* 26, 1233–1240. doi:10.1007/s13233-019-7016-5

Ulusoy, Ö. İ., and Görgül, G. (2013). Effects of different irrigation solutions on root dentine microhardness, smear layer removal and erosion. *Aust. Endod. J.* 39, 66–72. doi:10.1111/j.1747-4477.2010.00291.x

Uyanik, O., Nagas, E., Kucukkaya Eren, S., Cehreli, Z. C., Vallittu, P. K., and Lassila, L. V. J. (2019). Effect of phytic acid on the setting times and tensile strengths of calcium silicate-based cements. *Aust. Endod. J.* 45, 241–245. doi:10.1111/aej.12314

Van Meerbeek, B., Conn, L. J., Jr., Duke, E. S., Eick, J. D., Robinson, S. J., and Guerrero, D. (1996). Correlative transmission electron microscopy examination of nondemineralized and demineralized resin-dentin interfaces formed by two dentin adhesive systems. *J. Dent. Res.* 75, 879–888. doi:10.1177/00220345960750030401

Van Meerbeek, B., Inokoshi, S., Braem, M., Lambrechts, P., and Vanherle, G. (1992). Morphological aspects of the resin-dentin interdiffusion zone with different dentin adhesive systems. *J. Dent. Res.* 71, 1530–1540. doi:10.1177/00220345920710081301

Van Meerbeek, B., Yoshihara, K., Yoshida, Y., Mine, A., De Munck, J., and Van Landuyt, K. L. (2011). State of the art of self-etch adhesives. *Dent. Mater.* 27, 17–28. doi:10.1016/j.dental.2010.10.023

Violich, D. R., and Chandler, N. P. (2010). The smear layer in endodontics—a review. *Int. Endod. J.* 43, 2–15. doi:10.1111/j.1365-2591.2009.01627.x

Visse, R., and Nagase, H. (2003). Matrix metalloproteinases and tissue inhibitors of metalloproteinases: structure, function, and biochemistry. *Circ. Res.* 92, 827–839. doi:10.1161/01.RES.0000070112.80711.3D

Vitorino, R., de Morais Guedes, S., Ferreira, R., Lobo, M. J., Duarte, J., Ferrer-Correia, A. J., et al. (2006). Two-dimensional electrophoresis study of *in vitro* pellicle formation and dental caries susceptibility. *Eur. J. Oral Sci.* 114, 147–153. doi:10.1111/j.1600-0722.2006.00328.x

Vogel, J. J., Thompson, D. J., and Phillips, P. H. (1962). Studies on the anticariogenic activity of oat hulls. *J. Dent. Res.* 41, 707–712. doi:10.1177/00220345620410032501

Vucenik, I., and Shamsuddin, A. M. (2006). Protection against cancer by dietary IP6 and inositol. *Nutr. Cancer* 55, 109–125. doi:10.1207/s15327914nc5502_1

Wang, J. D., and Hume, W. R. (1988). Diffusion of hydrogen ion and hydroxyl ion from various sources through dentine. *Int. Endod. J.* 21, 17–26. doi:10.1111/j.1365-2591.1988.tb00949.x

Wang, X., Wen, K., Yang, X., Li, L., and Yu, X. (2017). Biocompatibility and anti-calcification of a biological artery immobilized with naturally-occurring phytic acid as the crosslinking agent. *J. Mater. Chem. B.* 5, 8115–8124. doi:10.1039/c7tb02090b

Weichhold, J., Gbureck, U., Goetz-Neunhoeffer, F., and Hurle, K. (2019). Setting mechanism of a CDHA forming α-TCP cement modified with sodium phytate for improved injectability. *Materials* 12, 2098. doi:10.3390/ma12132098

Xie, Y., Luo, H., Duan, J., Hong, C., Ma, P., Li, G., et al. (2014). Phytic acid enhances the oral absorption of isorhamnetin, quercetin, and kaempferol in total flavones of Hippophae rhamnoides L. *Fitoterapia.* 93, 216–225. doi:10.1016/j.fitote.2014.01.013

Xu, J., He, J., Shen, Y., Zhou, X., Huang, D., Gao, Y., et al. (2019). Influence of endodontic procedure on the adherence of *Enterococcus faecalis*. *J. Endod.* 45, 943–949. doi:10.1016/j.joen.2019.04.006

Xu, Q., Kanthasamy, A. G., and Reddy, M. B. (2008). Neuroprotective effect of the natural iron chelator, phytic acid in a cell culture model of Parkinson's disease. *Toxicology* 245, 101–108. doi:10.1016/j.tox.2007.12.017

Yamauchi, N., Nagaoka, H., Yamauchi, S., Teixeira, F. B., Miguez, P., and Yamauchi, M. (2011). Immunohistological characterization of newly formed tissues after regenerative procedure in immature dog teeth. *J. Endod.* 37, 1636–1641. doi:10.1016/j.joen.2011.08.025

Yao, Y., Grogan, J., Zehnder, M., Lendenmann, U., Nam, B., Wu, Z., et al. (2001). Compositional analysis of human acquired enamel pellicle by mass spectrometry. *Arch. Oral Biol.* 46, 293–303. doi:10.1016/s0003-9969(00)00134-5

Yoon, J. H., Thompson, L. U., and Jenkins, D. J. (1983). The effect of phytic acid on *in vitro* rate of starch digestibility and blood glucose response. *Am. J. Clin. Nutr.* 38, 835–842. doi:10.1093/ajcn/38.6.835

York, J. D., Odom, A. R., Murphy, R., Ives, E. B., and Wente, S. R. (1999). A phospholipase C-dependent inositol polyphosphate kinase pathway required for efficient messenger RNA export. *Science* 285, 96–100. doi:10.1126/science.285.5424.96

Zhang, J., Senger, B., Vautier, D., Picart, C., Schaaf, P., Voegel, J. C., et al. (2005). Natural polyelectrolyte films based on layer-by layer deposition of collagen and hyaluronic acid. *Biomaterials* 26, 3353–3361. doi:10.1016/j.biomaterials.2004.08.019

Zhang, X., Chen, Y., Lei, H., Zhao, S., Han, F., Xiang, X., et al. (2016). Phytic acid layer template-assisted deposition of TiO_2 film on titanium: surface electronic properties, super-hydrophilicity and bending strength. *Mater. Des.* 89, 476–484. doi:10.1016/j.matdes.2015.10.026

Zhou, Q. I., Zhao, Y. U., Dang, H., Tang, Y., and Zhang, B. (2019). Antibacterial effects of phytic acid against foodborne pathogens and investigation of its mode of action. *J. Food Prot.* 82, 826–833. doi:10.4315/0362-028X.JFP-18-418

Zhu, T., Ren, H., Li, A., Liu, B., Cui, C., Dong, Y., et al. (2017). Novel bioactive glass based injectable bone cement with improved osteoinductivity and its *in vivo* evaluation. *Sci. Rep.* 7, 3622. doi:10.1038/s41598-017-03207-9

Conflict of Interest: The authors declare that the research was conducted in the absence of any commercial or financial relationships that could be construed as a potential conflict of interest.

frontiers in Materials

ORIGINAL RESEARCH
published: 30 March 2021
doi: 10.3389/fmats.2021.640950

Analysis on Efficacy of Chitosan-Based Gel on Bone Quality and Quantity

Soher Nagi Jayash[1,2], Najihah Mohd Hashim[3], Misni Misran[4], Norliza Ibrahim[5], Nisreen Mohammed AL-Namnam[6] and N. A. Baharuddin[2]**

[1]School of Dentistry, University of Birmingham, Birmingham, United Kingdom, [2]Department of Restorative Dentistry, Faculty of Dentistry, University of Malaya, Kuala Lumpur, Malaysia, [3]Department of Pharmacy, Faculty of Medicine, University of Malaya, Kuala Lumpur, Malaysia, [4]Department of Chemistry, Faculty of Science, University of Malaya, Kuala Lumpur, Malaysia, [5]Department of Oral & Maxillofacial Clinical Sciences, Faculty of Dentistry, University of Malaya, Kuala Lumpur, Malaysia, [6]Department of Oral Surgery, Faculty of Dentistry, University of Sana'a, Sana'a, Yemen

OPEN ACCESS

Edited by:
Fabricio Mezzomo Collares, Federal University of Rio Grande do Sul, Brazil

Reviewed by:
Antonio Scarano, University of Studies G.d'Annunzio Chieti and Pescara, Italy
Vicente Leitune, Federal University of Rio Grande do Sul, Brazil

***Correspondence:**
Soher Nagi Jayash
s.jayash@bham.ac.uk,
soheernaji20@yahoo.com
N. A. Baharuddin
noradinar@um.edu.my

Specialty section:
This article was submitted to Biomaterials, a section of the journal Frontiers in Materials

Received: 12 December 2020
Accepted: 05 February 2021
Published: 30 March 2021

Citation:
Jayash SN, Hashim NM, Misran M, Ibrahim N, AL-Namnam NM and Baharuddin NA (2021) Analysis on Efficacy of Chitosan-Based Gel on Bone Quality and Quantity. Front. Mater. 8:640950. doi: 10.3389/fmats.2021.640950

Objectives: To assess and compare the quantity and the quality of the newly bone generated when using chitosan-based gel scaffold and osteoprotegerin-chitosan gel scaffold.

Methods: A total of 18 critical-sized defects on New Zealand white rabbit craniums were created. In 12 defects, either chitosan gel or osteoprotegerin-chitosan gel was implanted the last six defects were kept unfilled as a control. Bone formation was examined at 6 and 12 weeks. Bone's specimens were scanned using the High-resolution peripheral quantitative computed tomography. Histological and histomorphometric analysis were carried out to compare the volume and area of regenerated bone.

Results: The results of the HR-pQCT showed that bone volume and densities in the osteoprotegerin-chitosan gel group were significantly higher than the chitosan gel and control groups whereas, the bone volume density in the chitosan gel group was significantly higher than the control group in both intervals time ($p = 0.01$, $p = 000$). No significant difference in bone volume between the chitosan gel and control groups ($p = 0.506$, $p = 0.640$) was observed. However, similar findings were shown in the histomorphometric analysis, with the highest new bone formation was observed in the OPG-chitosan gel group followed by the chitosan group. The mean percentage of new bone was greater at 12 weeks compared to 6 weeks in all groups.

Conclusions: Chitosan-based gel demonstrated a significant bone quantity and quality compared to unfilled surgical defects. Consistently, osteoprotegerin enhanced the chitosan gel in bone regeneration.

Keywords: bone regeneration, chitosan, HR-pQCT, histomorphometry, osteoprotegerin

INTRODUCTION

Hydrogels are attractive materials because of their carrier ability of proteins, growth factors, cells, and other necessary components for tissue engineering. Successfully, injectable hydrogels systems can be used in minimally invasive surgical applications and utilized for encapsulating a variety of different biological materials such as cells, growth factors, and drugs. In addition, they can form gels capable of filling any target area of any shape following their injection (Lee, 2018; Al-Namnam and Jayash, 2019; Sharma and Sharma, 2020).

Chitosan is a natural polysaccharide copolymer which is widely used in drug delivery and bone tissue regeneration. It was reported that chitosan exhibits osteoconductive and enhanced wound healing properties, which suggested that chitosan may be useful as a bioactive coating to improve the ossification of orthopaedic and craniofacial implants (Bumgardner et al., 2003; Malviya, 2020). Combination of Chitosan with different bio-active material supports its activity in bone healing. Chitosan-γPGA polyelectrolyte complex hydrogel (C-PGA) has been developed and showed to be effective in new bone formation in the alveolar socket following tooth extraction (Chang et al., 2014). Furthermore. Combination of OPG with chitosan (OPG-chitosan matrices) in enhancing cell growth and proliferation, and in inducing the production of osteopontin and osteocalcin protein levels has been established (Jayash et al., 2016).

The technology in bone structure investigation has always been limited to a two-dimensional histological method. A microcomputed tomography (μCT) scanner allows a three-dimensional (3D) evaluation of histological specimens. Moreover, it's a rapid non-destructive process and an objective standardized approach of bone evaluation. This automated analysis method is much faster than any manual procedures (Baiker et al., 2012; Particelli et al., 2012). Good correlation between bone structural measures obtained from microcomputed tomography (μCT) datasets and from histological sections confirms that μCT may be an efficient tool for the characterization of bone structure (Particelli et al., 2012). Studies have confirmed that the High-resolution peripheral quantitative computed tomography (HR-pQCT) scanner, one type of μCT method, is a useful and reliable method for evaluating bone healing (Maréchal et al., 2005; Acar et al., 2016).

Micro-computed tomography (Micro-CT) images can be used to quantitatively represent bone geometry through a range of computed attenuation-based parameters. Xtreme CT (high-resolution peripheral quantitative computed tomography, HR-pQCT) is a new technology that uses the same principles as Micro-CT but can achieve a much higher spatial resolution and still has a very low radiation dose. It is able to define bones surfaces in a three-dimensional manner, and provides information on bone microarchitecture as well as bone density. Thus, this study aimed to investigate the osteogenic ability of chitosan-based gel in critical size defects on rabbits by evaluating the morphological feature, quantity and quality of the new bone that formed within chitosan-based gels compared to normal bone healing at several points in time using HR-pQCT and histomorphometric analysis.

MATERIALS AND METHODS

Chitosan-Based Gel and OPG Chitosan Gel Preparation

Two sets of water-soluble chitosan (25 kDa) gels were prepared by dissolving 50 mg of water-soluble chitosan in Tris buffer (5 mmol L^{-1}, pH 7.5). The mixtures were then left overnight to allow chitosan to completely dissolve. For one set of the gels, 1 mg ml^{-1} recombinant human OPG protein (Recombinant Human OPG, PeproTech, Rocky Hill, New Jersey, United States) was added. The other set was left without any addition of recombinant human OPG protein. Chitosan binder (85 kDa) was added to all the gel formulations. They were then mixed and allowed it to stand overnight under vacuum at room temperature (25°C). The gels were later sterilized by gamma radiation (4 kGy) and kept in desiccators (Jayash et al., 2017a).

Experimental Animals

The animal experiment was authorized according to the Institutional Animal Care and Use Committee. A total of 18 New Zealand white female rabbits (6 months old, 3.5–45–4 kg) were divided randomly into three groups of six; left unfilled (control) (group A), chitosan gel (group B), OPG-chitosan gel (group C). Three rabbits from each group were located randomly to be sacrificed at following time point: 6 and 12 months.

For the surgical procedures, the rabbits were anaesthetized with 30 mg/kg of ketamine 100 mg/ml and 3 mg/kg of xylazine 20 mg/ml (Troy laboratories PTY. Limited, Smithfield, Australia). Following hair shaving and disinfection of the operation site, full thickness a cranial critical size defect of 15 mm in diameter was created. After the placement of test materials or control, the defects were closed layer-by-layer. Bone formation was examined at 6 and 12 weeks time points, where three rabbits from each group were sacrificed at 6 and 12 weeks after surgery.

Animal Euthanasia

After anesthesia was induced by usual means, the rabbit was euthanized by using cardiac puncture with an overdose of barbiturates (Dolethal, Pentobarbitone sodium 200 mg ml^{-1} solution, 0.7 ml kg^{-1} IV) according to the assigned time points either 6 and 12 weeks.

HR-pQCT Evaluation

The region of interest in the bone specimens was scanned using the HR-pQCT (XtremeCT, Scanco Medical AG, Switzerland) with an isotropic voxel size of 82 μm and scanning area length of 25 mm. Each scan consists of 154 parallel CT slices. The 3D construction of surgical area, bone volume, and bone density were measured by using the XtremeCT software, Materialise Mimics Innovation Suite 17.0, Materialise 3-matic® Medical 9.0 and SkyScan "CT-analyser" software (version 1.1).

Rabbit's native parietal bone (15 × 15 mm dimension) was scanned and used as a reference. All the surgical sites were

TABLE 1 | Comparison of means bone volume and bone volume density between groups (group A (control), group B (chitosan gel), group C (OPG-chitosan gel)).

	Bone volume (mm^3)			Bone volume density%		
	6 weeks	**12 weeks**	***p* value**	**6 weeks**	**12 weeks**	***p* value[b]**
Group A	189 ± 36	267 ± 55	$p \geq 0.05$	21 ± 3.2	61 ± 6[b]	$p \leq 0.05$
Group B	256 ± 51	385 ± 30[ab]	$p \leq 0.05$	45 ± 5[a]	77 ± 7[ab]	$p \leq 0.05$
Group C	353 ± 50[a]	537 ± 55[ab]	$p \leq 0.05$	71 ± 1[a]	88 ± 2[ab]	$p \leq 0.05$
p value[a]	$p \leq 0.05$	$p \leq 0.05$		$p \leq 0.05$	$p \leq 0.05$	

[a]*indicates between groups significant difference over time based on One-Way ANOVA* ($p \leq 0.05$).
[b]*indicates between groups significant difference over time based on independent-samples* t*-test* ($p < 0.05$).

scanned at 6 and 12 weeks after surgeries. The Scanco XtremeCT device allowed the following evaluations of the healing surgical defects: 1) a 3D model color map comparison, 2) Mean bone volume and bone volume density comparison, and 3) Tissue density comparison (periphery and centre of the surgical defects). The 3D model colour map was constructed by superimposing the scanned images of the reference bone and the newly formed tissue at the surgical sites after surgery. The differences between them were shown as colour coding where green indicates no change between them, yellow indicates some change and red indicates a great difference. All measurements were analyzed using the Materialise Mimics Innovation Suite 17.0, Materialise 3-matic® Medical 9.0 and SkyScan "CT-analyser" software.

Histomorphometric Analysis

Upon completion of the experimental periods for each group, the animals were sacrificed, and the parietal bones from each rabbit were dissected and subjected to conventional decalcification, embedding, sectioning and hematoxylin and eosin staining (Jayash et al., 2017a). Histology specimens were digitized using the panoramic scan digital slide scanner (3DHISTECH, Budapest, Hungary). Subsequently, the histological images were assessed using the panoramic viewer software version 1.15.3 (3DHISTECH, Budapest, Hungary) at 200 scale bars. The Image-Pro Express software (Media Cybernetics Inc., Bethesda, MD, United States) was used for quantitative analysis. A 48-point grid of each image was overlaid to measure the amount of newly formed bone, osteoid tissue, bone marrow and fibrous tissue using the point-counting method. The amount of new bone formation, osteoid tissue, bone marrow and fibrous tissue was calculated as the percentage of new bone and graft area to the total defect area (Alyessary et al., 2017). Inter-examiner reliability for measuring methods was assessed by two blinded examiners. Reliability was evaluated using the Cronbach alpha test.

Statistical Analysis

Statistical analysis was performed using parametric One-way ANOVA test to compare the mean values of the bone volume, bone volume density and mean percentages of newly formed tissue between the groups (group A (control), group B (chitosan gel), group C (OPG-chitosan gel)). The groups were compared with Tukey's post-hoc test in case of a significant result. The significance value was set at ($p < 0.05$). Values were presented as a mean (arithmetic mean) and standard deviation.

RESULTS

Bone Volume and Bone Volume Density Results

Table 1 summarizes the means and standard deviations of bone volume (mm^3) and mean percentages of bone volume density for all groups over different time points. In intragroup comparison of the mean bone volume in the different group, it showed a highly significant mean bone volume at 12 weeks compared to 6 weeks ($p = 0.000$, $p = 0.001$) in OPG-chitosan gel group and chitosan gel group. However, no significant difference showed in control group at both interval time ($p = 0.16$). In intergroup comparison, it showed that chitosan gel group had a significantly higher mean bone volume compared to control group and chitosan gel group at both time points ($p = 0.000$). Additionally, no significant difference has been revealed in the mean bone volume between control group and chitosan gel group at week 6 after surgery ($p = 0.109$). Whereas, a significant mean difference was observed in the bone volume of control group compared to chitosan gel group at 12 weeks ($p = 0.001$) (**Figure 1**).

The intragroup comparison of bone volume densities in the different groups showed a significant difference in the mean bone volume density at 6 weeks compared to 12 weeks

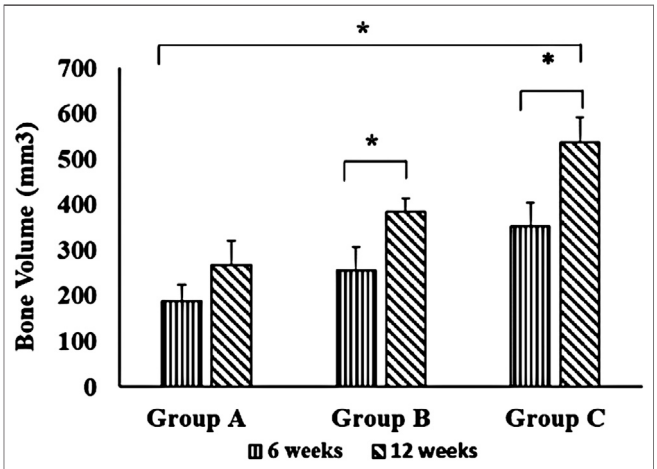

FIGURE 1 | Comparison of bone volume between groups (group A (control), group B (chitosan gel), group C (OPG-chitosan gel)). at 6 and 12 weeks. Data are expressed as mean ± SD ($n = 3$). *denotes significant difference in bone volume ($p < 0.05$) found between different groups.

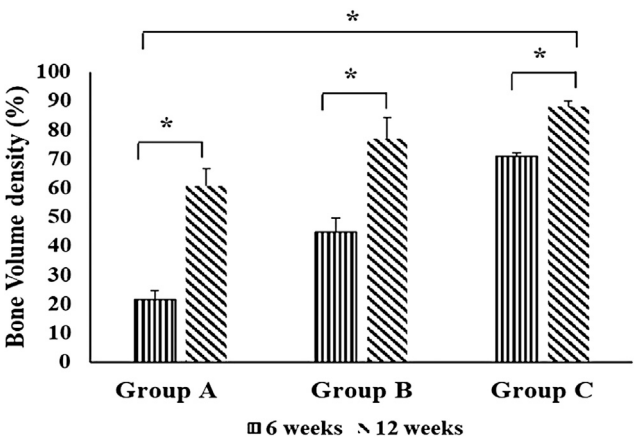

FIGURE 2 | Comparison of bone volume densities between groups (group A (control), group B (chitosan gel), group C (OPG-chitosan gel)). at 6 and 12 weeks. Data are expressed as mean ± SD ($n = 3$). *denotes significant difference in bone volume ($p < 0.05$) found between different groups.

in all groups. In the intergroup comparison, it revealed a highly significant bone volume density at 6 and 12 weeks in group C compared to control group and chitosan gel group ($p = 0.000$). Bone volume density in chitosan gel group was significantly higher than control group at 6 and 12 weeks (**Figure 2**).

Comparison of Tissue Density at the Periphery and Center of the Healing Surgical Defects

The comparison of tissue density at the periphery and center of the defect between the different groups are shown in **Figures 3**, **4**. It revealed that the density of tissue at the center and native soft tissue at the periphery of the defect was comparable in group A (unfilled defect; control group) at both interval time (6 and 12 weeks). Whereas, it exposed an increase at the center of the defect compared to the native soft tissue at the periphery in chitosan gel filled defects (group B) although this increasing was

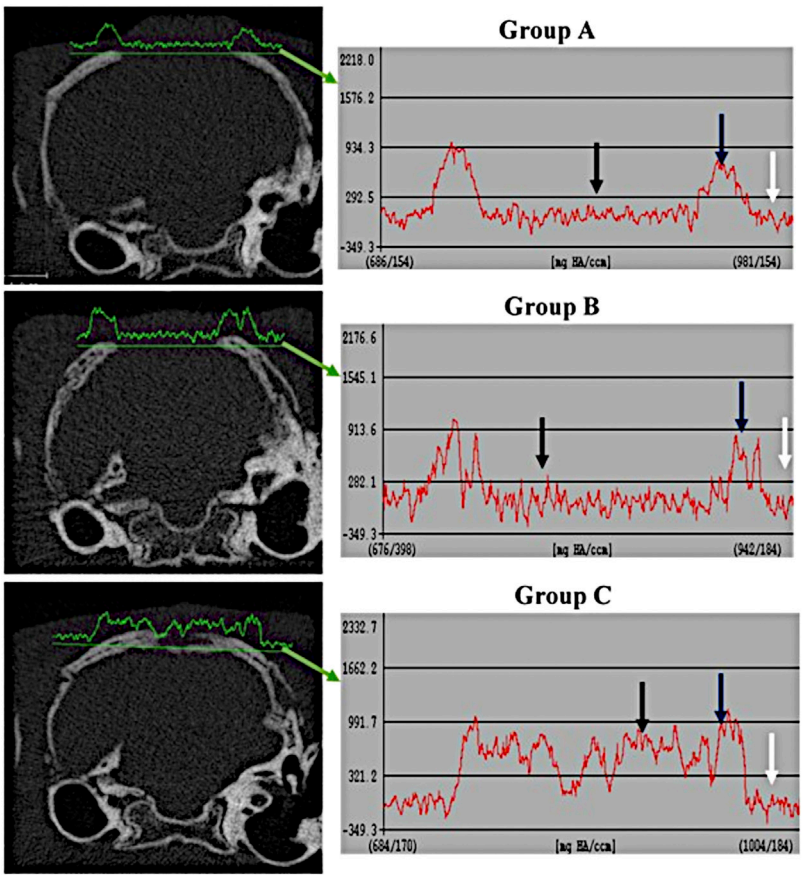

FIGURE 3 | Comparison of tissue density of the healing surgical defects between groups (group A (control), group B (chitosan gel), group C (OPG-chitosan gel)). at 6 weeks of treatment. Soft tissue at the periphery (white arrows); Normal bone (blue arrows); Center of defect (black arrows).

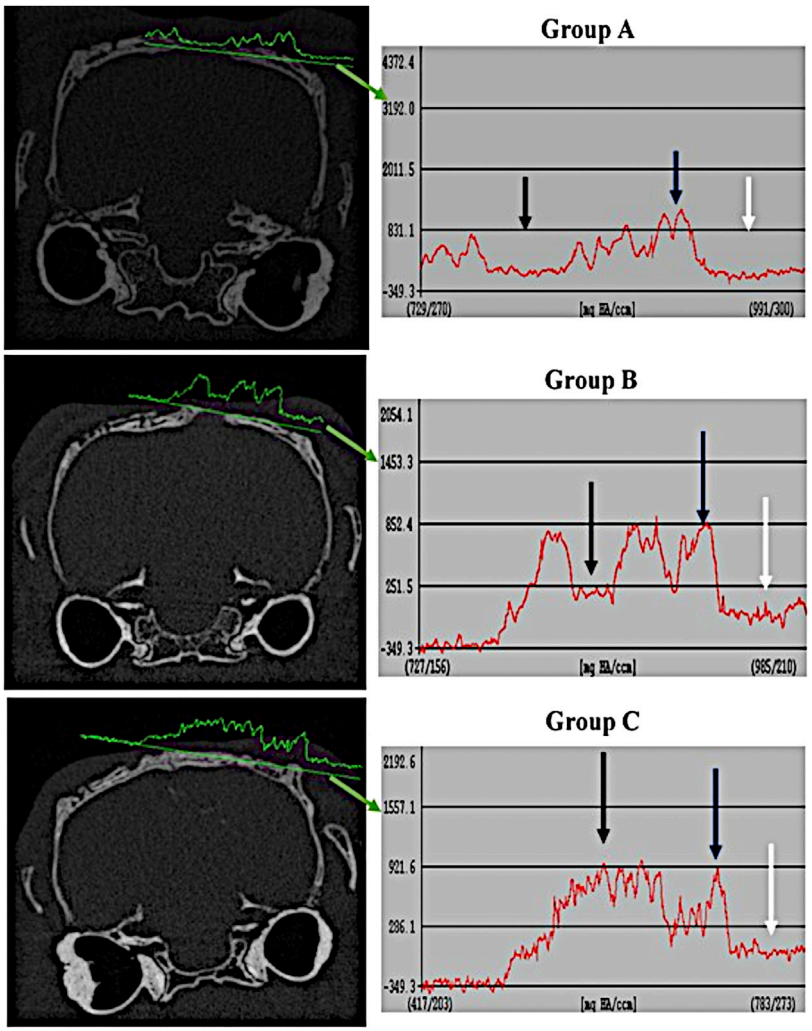

FIGURE 4 | Comparison of tissue density of the healing surgical defects between the groups (group A (control), group B (chitosan gel), group C (OPG-chitosan gel)) at 12 weeks. Soft tissue at the periphery (white arrows); Normal bone (blue arrows); Center of defect (black arrows).

lower than the density of the reference bone at both interval time. In OPG-chitosan gel filled defects (group C), the density of tissue in the center was markedly higher than the density of native soft tissue at the periphery at both interval time which revealed nearly comparable to the density of the reference bone at 12 weeks.

3D Models of Treated Groups

The construction of a 3D model of the surgical area of the different groups at 6 and 12 weeks post-surgery is shown in **Figure 5**. It exhibited the bone formation commenced along the margin of the defect progressing centrally where all the groups showed evidence of varying increasing in bone defect closure from 6 to 12 weeks post-surgery.

In the control and chitosan gel groups, the defects were not completely filled by the bone. It showed a discontinuous bone tissue layers centrally although it was continuous at the margin at both time interval time which covered the superficial portions of the defects partially. Even though, chitosan gel group displayed more bone tissue than control group group at both interval time. While the defects closure was more prominent in OPG-chitosan gel group compared to the others groups at 6 and 12 where it showed complete surgical bone defect closure at 12 weeks.

Part Comparison Color Map Results

Figure 6 shows the construction of a 3D model of the surgical areas of different groups at 6 and 12 weeks post-surgery. It was observed that the bone formation began along the margin of the defect toward the centre. The groups showed variation in the defect closure at 6 and 12 weeks post-surgery.

At 6 weeks post-surgery, the newly formed bone was more prominent in OPG-chitosan gel group where it covered most of the surgical defect compare to chitosan gel and control groups. At 12 weeks, control and chitosan gel groups showed partial defect closure, with more defects closing in chitosan gel group than control group, while OPG-chitosan gel group exhibited complete surgical bone defect closure.

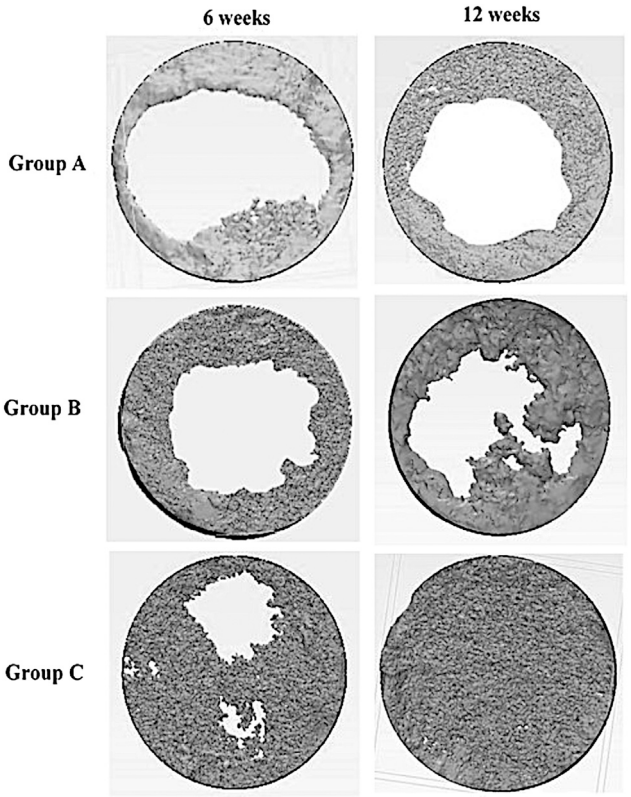

FIGURE 5 | Construction of a 3D model of defects in rabbits in different groups (group A (control), group B (chitosan gel), group C (OPG-chitosan gel)) after treatment at 6 and 12 weeks.

In comparison to the reference bone, control group showed the most major differences in the bone tissues (green colour) covering the surgical defects at 6 and 12 weeks. However, it showed more bone formation at the periphery of defects at 12 weeks compared to that observed at 6 weeks. More bone formation and less soft tissue (red colour) was observed in chitosan gel group than that in control group in comparison to the reference bone at both time points. Remarkably, OPG-chitosan gel group showed comparable bone formation to the reference bone at both interval times, where green colour was noticed covering all the surface area of the defect.

Histomorphometric Analysis

In terms of intragroup comparison, histomorphometric analysis of histological sections showed an increase in mean percentages of newly osteoid and bone marrow from 6 to 12 weeks. Conversely, it showed a decrease in mean percentage of connective tissue from 6 to 12 weeks in all the groups.

For intergroup comparison, OPG-chitosan gel group showed the highest mean percentages value in new bone formation (41.02 ± 1.00), osteoid (27.02 ± 0.97) and bone marrow (10.28 ± 1.62) at 6 weeks followed by chitosan gel group. At 12 weeks, group C exhibited the highest mean percentages in new bone formation (55.27 ± 11.10) and bone marrow (15.00 ± 7.00), whereas chitosan gel group showed the highest mean percentages of osteoid (34.13 ± 1.03). There were no significant results in bone marrow between chitosan gel and OPG-chitosan gel groups (p = 1.000) at 12 weeks. Controversially, control group showed significantly (p = 0.000) the highest mean percentages of fibrous tissue (98.33 ± 0.58) at both time points (**Table 2**).

DISCUSSION

The current study aimed to study the characteristics of newly formed bone (microstructure, volume, and density) in the implanted chitosan-based gel scaffolds using HR-pQCT and histomorphometric analysis.

In the present study, rabbit was selected as an experimental model because it is available, simple to house, easy to handle, economical, adequate for the preparation of bone cavities, and suitable model for bone ingrowth and biomaterial studies. Rabbit animal model is considered one of the most used animals for medical research and covers approximately 35% of musculoskeletal research studies (Neyt et al., 1998). Moreover, it is one of the International Standards established regarding the species suitable for testing implantation of materials in bone for reconstruction, fracture or osteotomy, bone in-growth and bone defect repair, and for evaluating the potential application of the material such as the process of material degradation and replacement by host tissue.

The critical size defect (CSD) has been defined as the smallest intraosseous wound in an animal that will not heal spontaneously when left untreated for a certain time period or which shows less than 10% bone regeneration during the lifetime of the animal. It has been shown that the animal calvaria is an accurate and reproducible model for testing bone graft materials as it has many similarities to the maxillofacial region as acceptor site (Isaksson, 1991). Furthermore, the cranial defect does not require fixation as it is supported by dura and the overlying skin as reported by An and Freidman (1998). Rentsch et al., in 2014 created a circular skull defect of 15 mm diameter placed centrally within the parietal bone (Rentsch et al., 2014). Since the clinical outcome of grafting procedure depends on the local and systemic conditions and in agreement with the previous mentioned studies, the authors of this study found that the most suitable area to create a well-defined critical size defect without affect the major anatomic structure in the rabbit cranium was the central part which couldn't be created without involving the sagittal suture. Furthermore, the central part of the cranium has a good size for easier surgical procedure, simple specimen handling, well established reproducibility and less morbidity. Additionally, it is a plate which permits creations of a uniform circular defect that allows appropriate radiographic and histological analysis. Sohn et al. (2010) reported that the other part of cranium could not get more than 11 mm in diameter. Concerning sample size determination, three rabbit in each group were suitable for this study according to sample size formula for animal studies published in 2013 (Charan and Biswas, 2013).

The HR-pQCT is an automated method that could be used to evaluate the trabecular and cortical bone microstructure and has several advantages over manual analysis. This is an agreement

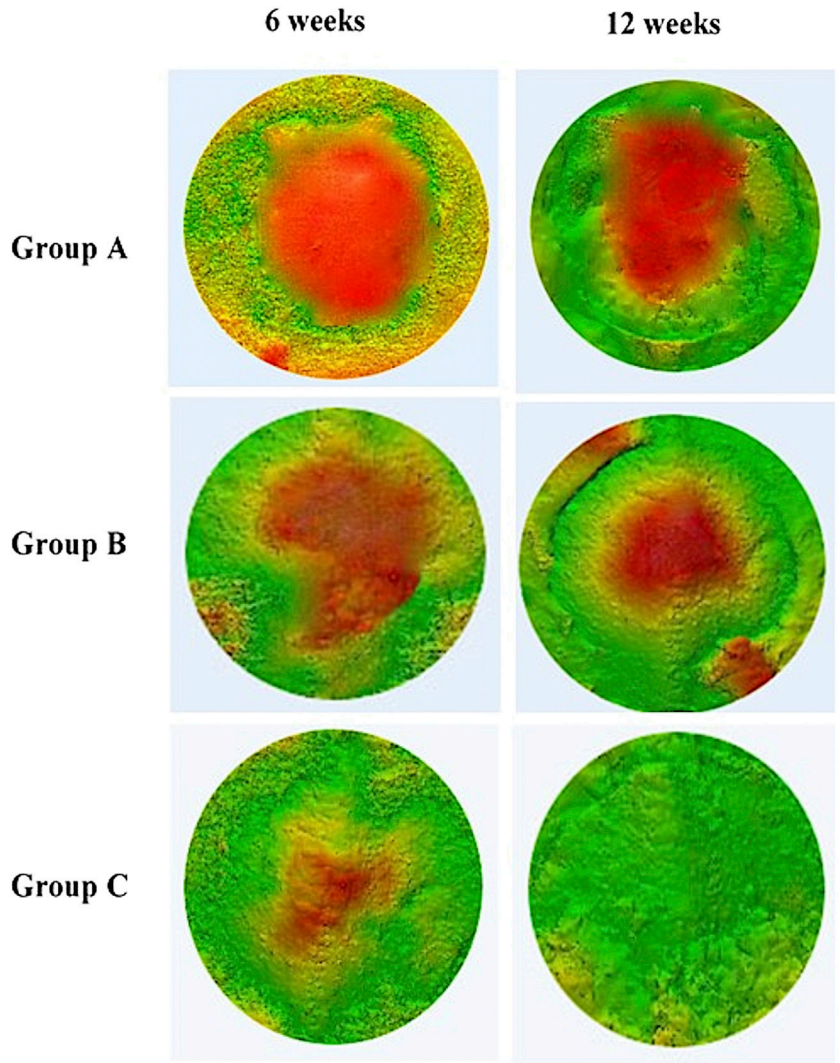

FIGURE 6 | Comparison of 3D color map of different groups (group A (control), group B (chitosan gel), group C (OPG-chitosan gel)) at 6 and 12 weeks after treatments.

with Baiker study, mentioning the automated method of analysis can be purely objective, handle every dataset in the same manner and much faster than any manual procedures (Baiker et al., 2012). In addition, HR-pQCT has been considered a useful and reliable method for evaluating bone healing as shown in previous term studies (Maréchal et al., 2005; Acar et al., 2016). Baek et al. used μCT to evaluate chitosan-based membrane in a rat model and concluded that the membrane had a significant effect on the new bone formation (Baek et al., 2016). It was suggested that the membrane has the potential for guided bone regeneration application. The same finding was observed by Him et al. (He et al., 2015) who evaluated nano-hydroxyapatite-chitosan in a rat model. In the present study, the amount of newly formed bone volume, bone volume densities, and microstructure that were measured using the histomorphometric analysis and HR-pQCT analysis was highly correlated in the newly formed bone in chitosan gel and OPG-chitosan gel implantation sites on rabbit calvarial defects. This result was similar to Park et al. study who reported that histomorphometric analysis and micro-CT analysis were valid methods for measurement of the new bone (Park et al., 2011).

Chitosan has favorable properties including biocompatibility, biodegradability, antibacterial, and biological activity, as well as its renewable character. Some studies reported that creating a chitosan in hydrogel form would provide a good environment for encapsulation and localized delivery of cells and cell proliferation (Shariatinia and Jalali, 2018; Ahsan et al., 2020). Additionally, the hydrogel would make chitosan respond to various stimuli for example, temperature, heat, light, pH, ionic strength, humidity, and redox potential that are playing an important role for biomedical applications such as drug delivery and tissue engineering (Hu et al., 2017). Aycan and Alemdar in 2018 reported that bone ash-reinforced, pH-sensitive, chitosan-

TABLE 2 | Histomorphometri results demonstrating the mean percentages of new bone formation, osteoid, bone marrow and fibrous tissue in groups (group A (control), group B (chitosan gel), group C (OPG-chitosan gel)) at 6 and 12 weeks.

Bone regeneration	Group A	Group B	Group C
6 weeks			
New bone %	0.67 ± 0.05	11.39 ± 0.79	41.02 ± 1.00
Osteoid %	1.00 ± 0.14	19.10 ± 1.02	27.02 ± 0.97
Bone marrow %	0.00	3.00 ± 0.23	10.28 ± 1.62
Fibrous tissue %	98.33 ± 0.58	64.31 ± 1.34	19.00 ± 1.00
12 weeks			
New bone %	15.01 ± 1.00	25.53 ± 1.50	55.27 ± 11.10
Osteoid %	9.40 ± 1.51	34.13 ± 1.03	29.79 ± 8.58
Bone marrow %	2.33 ± 1.50	9.00 ± 1.00	15.00 ± 7.00
Fibrous tissue %	68.28 ± 8.11	30.03 ± 4.78	5.00 ± 2.04

Significant difference over time based on One-Way ANOVA ($p \leq 0.05$). Significant difference over time based on independent-samples t-test ($p < 0.05$).

based hydrogel could be used as a drug carrier for the controlled release of amoxicillin in the treatment of gastric ulcer. They verified that it would be a good alternative to present biomaterials for the future applications in tissue engineering and regenerative drug systems (Aycan and Alemdar, 2018). In corresponding with previous mentioned studies, all the present investigation was consistent and revealed that the chitosan gel and OPG-chitosan gel demonstrating a significant bone quantity and quality on rabbit calvarial defects compared to unfilled surgical defect. It showed that the density of tissue in the center of the chitosan filled defects was much higher than the density of soft tissue in the unfilled defects in both time points (6 and 12 weeks). This indicated earlier woven and lamellar bone formation subsequently in chitosan filled defects, which could establish and maintain defect healing in a dynamic process in chitosan's' groups, than those occurred in unfiled defects. In terms of bone quantity, the histomorphometric result showed that the chitosan gel group showed higher bone mean percentage than the control group by 10.52% but less than in OPG-chitosan group by 29.74% at 12 weeks. The author suggests that the superiority of chitosan's groups on bone quantity and quality to control group is related to the cationic nature of chitosan which allow electrostatic interactions with anionic glycosaminoglycans that modulate the action of several cytokines and growth factors. This property is of crucial importance in bone regeneration as reported by Di Martino et al. (2005). While the superiority of OPG-chitosan gel group in bone volume and density compared to other groups at both time points referred to the enhancement of chitosan gel with the OPG protein, which could regulate bone remodeling and osteoclastogenesis (Jayash et al., 2020). This is an agreement with the previous studies that showed an increase in bone mineral density by using recombinant OPG protein in rodents (Capparelli et al., 2003; Graber et al., 2016).

Chitosan has been described as a potent wound-healing accelerator (Di Martino et al., 2005). In the present study, 3D models of surgical sites showed major differences between reference bone and the newly formed bone tissues after 6 and 12 weeks in the control group, whereas it was comparable to chitosan's' groups. This could verify that all parts of the defects in chitosan's' groups were filled with thicker trabecular new bone than that in unfilled defects. Moreover, the chitosan gel enables the defect to heal more rapidly than an empty, unfilled defect, which was filled with just osteoid tissue at 6 weeks. The authors suggested that the earlier and more bone formed in chitosan gel and OPG-chitosan gel filled defects were resulted from the action of the hydrophilic surface of chitosan gel that promotes cell adhesion and supports the attachment and proliferation of bone-forming osteoblast cells as well as formation of a mineralized bone matrix. Additionally, as a result of the advantage of hydrogels in chitosan that can easily adopt the geometry of the defect that they occupy which has a role in stability that supports the cell differentiation and proliferation as reported by Levengood and Zhang (2014).

In a bony defect, the most intense cellular reaction occurs during the first 6 weeks. In another word, the defect is first bridged by a trabecular framework consisting of primitive woven bone. Following, there is a reduction in the numbers of cells in these areas, as well as an increase in calcium deposition as reported by Gehrke (2013). The quantity of osteoblasts is significantly changed, and the bone remodeling occur between 30 and 45 days (Piattelli et al., 1995). Moreover, the defect closure and the new bone area ratio gradually increased with the healing time, but these parameters did not differ significantly between weeks 2 and 4 or between weeks 8 and 12 (Sohn et al., 2010). An observation period of at least 12 weeks was recommended by Bodde et al. (2008). Furthermore, Seo and Kim (2020) stated that the volume analysis of rabbit calvarial defects and bone grafts using CT can be done after 2 and 8 weeks. In point of fact, the HR-pQCT results were corresponding to the histological results of our published literature in 2007 (Jayash et al., 2017a; Jayash et al., 2017b). Likewise, in the current study, the part-comparison map and histomorphometrical analyses results confirmed the changes in microstructure between the reference bone and the newly formed bone after surgery at 6 and 12 weeks. They showed that the rate of the bone healing was higher in the OPG-chitosan gel and chitosan gel than in the unfilled defect. Furthermore, the defects healed completely at 12 weeks in the OPG-chitosan gel implanted defects and partially, more prominent at chitosan gel than the control defects. Although both control and chitosan gel groups both exhibited partially defects closure at 12 weeks, chitosan gel group showed higher mean percentages of osteoid with no significant results in bone marrow with OPG-chitosan gel group at 12 weeks which indicated more newly formed bone quantity in chitosan gel than the control group. This is an evidence of the ability of chitosan gel to play a supportive role in the early repair process and provides a favorable surface for osteoprogenitor cell attachment.

To sum up, the chitosan gel was capable of regenerating new bone which is beneficial in tissue engineering applications, and the HR-pQCT analysis was an efficient method to evaluate the newly formed bone and it was as effective as the histomorphometry bone analysis. Potentially, these findings could be translated into clinical use and would be of great interest to the vision scientists, researchers, clinicians, and trainees.

CONCLUSION

The chitosan-based gel promoted the cell migration, proliferation, and differentiation in support of tissue regeneration by demonstrating a significant bone quantity and quality in a cranial critical size defect in a rabbit model compared to unfilled surgical defect. Correspondingly, the OPG enhanced the chitosan gel in bone regeneration. This study has revealed that chitosan-based gel is potential candidates for bone tissue engineering.

DATA AVAILABILITY STATEMENT

The original contributions presented in the study are included in the article/Supplementary Material, further inquiries can be directed to the corresponding authors.

ETHICS STATEMENT

The animal study was reviewed and approved by Institutional Animal Care and Use Committee (FOM IACUC).

AUTHOR CONTRIBUTIONS

SJ conceived and designed the experiments, performed the experiments, analyzed the data, wrote the paper, prepared figures and/or tables, reviewed drafts of the paper. NH, MM, and NB conceived and designed the experiments, contributed in reagents/materials/analysis tools, reviewed drafts of the paper. NA-N and NI reviewed drafts of the paper and contributed in analysis tools.

FUNDING

This study was also supported by a grant from a research grant (PG0882013A) from University of Malaya and UM.C/625/1/HIR/MOHE/SC/09.

ACKNOWLEDGMENTS

We thank the University of Birmingham and Cara for their support.

REFERENCES

Acar, A. H., Yolcu, Ü., Altındiş, S., Gül, M., Alan, H., and Malkoç, S. (2016). Bone regeneration by low-level laser therapy and low-intensity pulsed ultrasound therapy in the rabbit calvarium. *Arch. Oral Biol.* 61, 60–65. doi:10.1016/j.archoralbio.2015.10.011

Ahsan, A., Farooq, M. A., and Parveen, A. (2020). Thermosensitive chitosan-based injectable hydrogel as an efficient anticancer drug carrier. *ACS omega* 5, 20450–20460. doi:10.1021/acsomega.0c02548

Al-Namnam, N., and Jayash, S. N. (2019). Recent advances in bone graft substitute for oral and maxillofacial applications:A review. *Int. J. Biosci.* 15, 70–94. doi:10.12692/ijb/15.4.70-94

Alyessary, A. S., Yap, A. U. J., Othman, S. A., Rahman, M. T., and Radzi, Z. (2017). Effect of piezoelectric sutural ostectomies on accelerated bone-borne sutural expansion. *J. Oral Maxillofac. Surg.* 76, 616–630. doi:10.1016/j.joms.2017.08.018

An, Y. H., and Freidman, R. J. (1998). *Animal models in orthopaedic research*. Boca Rato, FL; CRC Press .

Aycan, D., and Alemdar, N. (2018). Development of pH-responsive chitosan-based hydrogel modified with bone ash for controlled release of amoxicillin. *Carbohydr. Polym.* 184, 401–407. doi:10.1016/j.carbpol.2017.12.023

Baek, Y. J., Kim, J. H., Song, J. M., Yoon, S. Y., Kim, H. S., and Shin, S. H. (2016). Chitin-fibroin-hydroxyapatite membrane for guided bone regeneration: micro-computed tomography evaluation in a rat model. *Maxillofac. Plast. Reconstr. Surg.* 38, 14. doi:10.1186/s40902-016-0060-6

Baiker, M., Snoeks, T. J., Kaijzel, E. L., Que, I., Dijkstra, J., Lelieveldt, B. P., et al. (2012). Automated bone volume and thickness measurements in small animal whole-body microCT data. *Mol. Imaging Biol.* 14, 420–430. doi:10.1007/s11307-011-0522-2

Bodde, E. W., Spauwen, P. H., Mikos, A. G., and Jansen, J. A. (2008). Closing capacity of segmental radius defects in rabbits. *J. Biomed. Mater. Res. A.*, 85, 206–217. doi:10.1002/jbm.a.31549

Bumgardner, J., Wiser, R., Elder, S., Jouett, R., Yang, Y., and Ong, J. (2003). Contact angle, protein adsorption and osteoblast precursor cell attachment to chitosan coatings bonded to titanium. *J. Biomater. Sci. Polym. Ed.* 14, 1401–1409. doi:10.1163/156856203322599734

Capparelli, C., Morony, S., Warmington, K., Adamu, S., Lacey, D., Dunstan, C. R., et al. (2003). Sustained antiresorptive effects after a single treatment with human recombinant osteoprotegerin (OPG): a pharmacodynamic and pharmacokinetic analysis in rats. *J. Bone Miner Res.* 18, 852. doi:10.1359/jbmr.2003.18.5.852

Chang, H. H., Wang, Y. L., Chiang, Y. C., Chen, Y. L., Chuang, Y. H., Tsai, S. J., et al. (2014). A novel chitosan-γPGA polyelectrolyte complex hydrogel promotes early new bone formation in the alveolar socket following tooth extraction. *PLoS one* 9, e92362. doi:10.1371/journal.pone.0092362

Charan, J., and Biswas, T. (2013). How to calculate sample size for different study designs in medical research? *Indian J. Psychol. Med.* 35 (2), 121. doi:10.4103/0253-7176.116232

Di Martino, A., Sittinger, M., and Risbud, M. V. (2005). Chitosan: a versatile biopolymer for orthopaedic tissue-engineering. *Biomaterials* 26, 5983–5990. doi:10.1016/j.biomaterials.2005.03.016

Gehrke, S. A. (2013). Analysis of bone tissue healing around titanium implant surface treated with tio sandblasted after three and six weeks used different histological methods-a study in rabbits. *Sci. J. Med. Clin. Trials* 2013, 1–7. doi:10.7237/sjmct/150

Graber, L. W., Vanarsdall, R. L., Jr, Vig, K. W., and Huang, G. J. (2016). *Orthodontics: Current principles and techniques*. New York, NY: Elsevier Health Sciences.

He, Y., Dong, Y., Cui, F., Chen, X., and Lin, R. (2015). Ectopic osteogenesis and scaffold biodegradation of nano-hydroxyapatite-chitosan in a rat model. *PLoS one* 10, e0135366. doi:10.1371/journal.pone.0135366

Hu, J., Chen, Y., Li, Y., Zhou, Z., and Cheng, Y. (2017). A thermo-degradable hydrogel with light-tunable degradation and drug release. *Biomaterials* 112, 133–140. doi:10.1016/j.biomaterials.2016.10.015

Isaksson, S. (1991). Aspects of bone healing and bone substitute incorporation. An experimental study in rabbit skull bone defects. *Swed Dent J. Suppl.* 84, 1–46.

Jayash, S. N., Hashim, N. M., Misran, M., and Baharuddin, N. (2017a). Formulation and *in vitro* and *in vivo* evaluation of a new osteoprotegerin-chitosan gel for bone tissue regeneration. *J. Biomed. Mater. Res. A.* 105, 398–407. doi:10.1002/jbm.a.35919

Jayash, S. N., Hashim, N. M., Misran, M., and Baharuddin, N. (2016). *In vitro* evaluation of osteoprotegerin in chitosan for potential bone defect applications. *PeerJ.* 4, e2229. doi:10.7717/peerj.2229

Jayash, S. N., Hashim, N. M., Misran, M., and Baharuddin, N. (2017b). Local application of osteoprotegerin-chitosan gel in critical-sized defects in a rabbit model. *PeerJ.* 5, e3513. doi:10.7717/peerj.3513

Jayash, S. N., Al-Namnam, N. M., and Shaghayegh, G. (2020). Osteoprotegerin (OPG) pathways in bone diseases and its application in therapeutic

perspectives. *Biointerface Res. Appl. Chem.* 10, 5913–5200. doi:10.33263/BRIAC102.193200

Lee, J. H. (2018). Injectable hydrogels delivering therapeutic agents for disease treatment and tissue engineering. *Biomater. Res.* 22, 1–14. doi:10.1186/s40824-018-0138-6

Levengood, S. L., and Zhang, M. (2014). Chitosan-based scaffolds for bone tissue engineering. *J. Mater. Chem. B Mater. Biol. Med.* 2, 3161–3184. doi:10.1039/C4TB00027G

Malviya, R. (2020). Exploration of neem gum-chitosan and kheri gum-chitosan polyelectrolyte complex-based film for transdermal delivery of protein/peptideBiointerface. *Biointerface Res. Appl. Chem.* 10, 5860–5868. doi:10.2174/2210315509666190515112704

Maréchal, M., Luyten, F., Nijs, J., Postnov, A., Schepers, E., and van Steenberghe, D. (2005). Histomorphometry and micro-computed tomography of bone augmentation under a titanium membrane. *Clin. Oral Implants Res.* 16, 708–714. doi:10.1111/j.1600-0501.2005.01205.x

Neyt, J., Buckwalter, J. A., and Carroll, N. (1998). Use of animal models in musculoskeletal research. *Iowa Orthop. J.* 118, 118–123.

Park, S. Y., Kim, K. H., Koo, K. T., Lee, K. W., Lee, Y. M., Chung, C. P., et al. (2011). The evaluation of the correlation between histomorphometric analysis and micro-computed tomography analysis in AdBMP-2 induced bone regeneration in rat calvarial defects. *J. Periodontal Implant Sci.* 41, 218–226. doi:10.5051/jpis.2011.41.5.218

Particelli, F., Mecozzi, L., Beraudi, A., Montesi, M., Baruffaldi, F., and Viceconti, M. (2012). A comparison between micro-CT and histology for the evaluation of cortical bone: Effect of polymethylmethacrylate embedding on structural parameters. *J. Microsc.* 245, 302–310. doi:10.1111/j.1365-2818.2011.03573.x

Piattelli, A., Scarano, A., and Piattelli, M. (1995). Detection of alkaline and acid phosphatases around titanium implants: a light microscopical and histochemical study in rabbits. *Biomaterials* 16, 1333–1338. doi:10.1016/0142-9612(95)91049-5

Rentsch, C., Rentsch, B., Heinemann, S., Bernhardt, R., Bischoff, B., Förster, Y., et al. (2014). ECM inspired coating of embroidered 3D scaffolds enhances calvaria bone regeneration. *Biomed. Res. Int.* 2014, 217078. doi:10.1155/2014/217078

Seo, S. J., and Kim, Y. G. (2020). Improved bone regeneration using collagen-coated biphasic calcium phosphate with high porosity in a rabbit calvarial model. *Biomed. Mater.* 16, 015012. doi:10.1088/1748-605x/abb1fc

Shariatinia, Z., and Jalali, A. M. (2018). Chitosan-based hydrogels: Preparation, properties and applications. *Int. J. Biol. Macromol.* 115, 194–220. doi:10.1016/j.ijbiomac.2018.04.034

Sharma, A., and Sharma, P. K. (2020). Stimuli-responsive supramolecules for bone tissue engineering. *Biointerface Res. Appl. Chem.* 10, 5122–5127. doi:10.33263/BRIAC102.122127

Sohn, J. Y., Park, J. C., Um, Y. J., Jung, U. W., Kim, C. S., Cho, K. S., et al. (2010). Spontaneous healing capacity of rabbit cranial defects of various sizes. *J. Periodontal Implant Sci.* 40, 180–187. doi:10.5051/jpis.2010.40.4.180

Conflict of Interest: The authors declare that the research was conducted in the absence of any commercial or financial relationships that could be construed as a potential conflict of interest.

frontiers in Materials

MINI REVIEW
published: 22 April 2021
doi: 10.3389/fmats.2021.666202

Plant-Derived Nanobiomaterials as a Potential Next Generation Dental Implant Surface Modifier

*Jaison Jeevanandam[1], Michael K. Danquah[2] and Sharadwata Pan[3]**

[1] Centro de Química da Madeira (CQM), MMRG, Universidade da Madeira, Funchal, Portugal, [2] Department of Chemical Engineering, University of Tennessee, Chattanooga, TN, United States, [3] TUM School of Life Sciences, Technical University of Munich, Freising, Germany

Dental implants resemble synthetic materials, mainly designed as teeth-mimics to replace the damaged or irregular teeth. Specifically, they are demarcated as a surgical fixture of artificial implant materials, which are placed into the jawbone, and are allowed to be fused with the bone, similar to natural teeth. Dental implants may be categorized into endosteal, subperiosteal, and zygomatic classes, based on the placement of the implant "in the bone" or on top of the jawbone, under the gum tissue. In general, titanium and its alloys have found everyday applications as common, successful dental implant materials. However, these materials may also undergo corrosion and wear, which can lead to degradation into their ionic states, deposition in the surrounding tissues, as well as inflammation. Consequently, nanomaterials are recently introduced as a potential alternative to replace the conventional titanium-based dental implants. However, nanomaterials synthesized *via* physical and chemical approaches are either costly, non/less biocompatible, or toxic to the bone cells. Hence, biosynthesized nanomaterials, or bionanomaterials, are proposed in recent studies as potential non-toxic dental implant candidates. Further, nanobiomaterials with plant origins, such as nanocelluloses, nanometals, nanopolymers, and nanocarbon materials, are identified to possess enhanced biocompatibility, bioavailability and no/less cytotoxicity with antimicrobial efficacy at low costs and ease of fabrication. In this minireview, we present an outline of recent nanobiomaterials that are extensively investigated for dental implant applications. Additionally, we discuss their action mechanisms, applicability, and significance as dental implants, shortcomings, and future perspectives.

Keywords: dental implants, nanobiomaterials, biocompatibility, endosteal, titanium alloys, zygomatic implants

OPEN ACCESS

Edited by:
Mary Anne Sampaio Melo, University of Maryland, Baltimore, United States

Reviewed by:
Isadora Martini Garcia, Federal University of Rio Grande do Sul, Brazil
Ingrid Fernandes Mathias-Santamaria, University of Maryland, Baltimore, United States

***Correspondence:**
Sharadwata Pan
sharadwata.pan@tum.de

Specialty section:
This article was submitted to Biomaterials, a section of the journal Frontiers in Materials

Received: *09 February 2021*
Accepted: *06 April 2021*
Published: *22 April 2021*

Citation:
Jeevanandam J, Danquah MK and Pan S (2021) Plant-Derived Nanobiomaterials as a Potential Next Generation Dental Implant Surface Modifier. Front. Mater. 8:666202. doi: 10.3389/fmats.2021.666202

INTRODUCTION

In general, implants are synthetic components that are placed in a living organism as a replacement for a damaged part and eventually supports the normal activity of the organism (Prakasam et al., 2017). In humans, dental implants are the most common types of implants, which are widely utilized to replace damaged or malfunctioning dental parts throughout the world (Rupp et al., 2018). The dental implants are generally necessary for humans, when there is a dental damage due to accident, lifestyle changes including excessive smoking and alcohol consumption, and several

complications that lead to gum damage. Further, the usage of dental implants has been increased recently due to their safe clinical results and low cost (Sanguida et al., 2019). Conventionally, these dental implants are artificial materials, which are designed as teeth to replace the damaged or irregular teeth (Neldam and Pinholt, 2012). It can be noted that the history of dental implants to replace damaged dental parts in humans dated back to 600 AD, where the Mayan civilization has been found to utilize small sea shell parts resembling insertions with the purpose mandibular teeth substitution (Abraham, 2014). Due to the recent advantages in biomedical science and surgical techniques, dental implants are also defined as a surgical fixture of artificial implant material, which are placed into the jawbone and are allowed to be fused with the bone, similar to a natural teeth (Huang et al., 2017). Further, screws to fix the teeth and braces to align the teeth arrangement for facial symmetry were also considered as dental implants (Travess et al., 2004). Endosteal, subperiosteal and zygomatic are the classes of dental implants, which were classified based on the placement of implant "in the bone" or on top of the jawbone under the gum tissue. Zygomatic implants are distinct from conventional implants, where they are anchored in the zygomatic region of the bone rather than maxilla (Henri Diederich and Abou-Rabii, 2019). Generally, titanium and its alloys, such as nitinol were used as a common and successful materials for dental implant applications (Shah et al., 2019). However, these materials are identified to undergo corrosion and wear, which can lead to degradation into their ionic state, deposition in the surrounding tissues and inflammation (Park et al., 2020).

Nanomaterials are gaining essential significance due to their exclusive properties in various biomedical applications, ranging from drug delivery to biosensors (Jeevanandam et al., 2020a); Tan et al., 2019; Pan et al., 2021; Tan et al., 2020). Chemical and physical approaches are the commonly used synthesis methods to yield smaller sized novel nanomaterials (Jeevanandam et al., 2016). However, the toxicity toward bone cells (chemically synthesized nanomaterials are mostly toxic toward pre-osteoclast (RAW264.7) and pre-osteoblast (MC3T3-E1), depending on their dose and concentration), less biocompatibility depending on their size, surface, and composition, and high cost of these nanoparticles are the limitations of these nanomaterials, which has led to the introduction of biological approaches or biosynthesis, i.e., utilization of biomolecular extracts of microbes and plants (Ha et al., 2018; Rasouli et al., 2018). Among biosynthesis approaches, microbial-mediated synthesis of nanomaterial called nanobiomaterials has been identified to yield non-toxic nanomaterials, however, the process is tedious, requires high reaction time and difficult to fabricate nanomaterials with discrete architectures (Andra et al., 2019). Thus, currently, plant isolates are comprehensively employed to synthesize non-toxic nanomaterials with distinct morphologies and surface properties (Shanmuganathan et al., 2019). These plant-derived nanobiomaterials are recently under extensive research to be included as novel materials to manufacture the next generation dental implants as a potential alternative for conventional implant materials (Augustine and Hasan, 2020). This review is an overview of recent nanobiomaterials, which are under extensive research for dental implant applications. Further, significance of these nanomaterials as dental implants, mechanism of action, drawbacks and future perspective will also be discussed.

CONVENTIONAL DENTAL IMPLANTS AND THEIR LIMITATIONS

Conventional dental implants are broadly made up of metals, ceramics, polymer or combination of all these materials as composites. In the category of metals, titanium, titanium alloys such as nitinol (nickel and titanium), stainless steel, gold alloys, tantalum, and cobalt chromium alloy are commonly used to fabricate dental implants. Further, alumina, beta-tricalcium phosphate, carbon materials, carbon-silicon, zirconia, bioglass, and zirconia-toughened alumina are the ceramics and polysulfone, polytetrafluoroethylene, polyurethane, polymethymethacrylate, polyethylene, and polyether ether ketone are the polymers, which are used to fabricate conventional dental implants (Osman and Swain, 2015). These dental implants are usually beneficial for the replacement of single tooth without high costs, compared to the traditional fixation of dental prostheses (Vogel et al., 2013). Apart from cost-based advantages, conventional dental implants behave similar to natural teeth, last for a long time, prevent bone loss, provide stability to adjacent teeth, reduce gum disease complications and prevent facial sagging and premature aging-related issues (Li J. et al., 2020). Further, the mechanical strength of these materials, evaluated *via* both *in vitro* and *in vivo* studies, is on par with natural bone and dental tissues, which makes them the most common implant materials (Li J. et al., 2020). However, these materials undergo degradation during interaction with the biological fluids, leading to corrosion and wear, which can be deposited in the surrounding cells or tissues and cause inflammation (Apaza-Bedoya et al., 2017; Park et al., 2020). Furthermore, osteoporosis, immunocompromised patients of diabetes [3.89% of failure rate (Chrcanovic et al., 2014)], Acquired Immunodeficiency Syndrome (AIDS) condition [10% of failure rate (May et al., 2016)], smoking and radiotherapy in head and neck cancers are the factors that can lead to dental implant failures (Bazli et al., 2020). Additionally, conventional dental implants involve high initial costs for mandibular edentulism patients, compared to mucosa-borne dentures (Vogel et al., 2013). Thus, nanomaterials are currently under extensive research and are used in certain cases as a surface modifier of conventional dental implants or to fabricate novel nanomaterial-based implants for eliminating the limitations of conventional dental implants.

NANOMATERIALS IN DENTAL IMPLANT APPLICATIONS

Nanomaterials are recently incorporated in several aspects of dental applications, such as preventive dentistry, dental implants, restoration of implants, periodontics, endodontics, dental tissue engineering, and

scaffolds (Zafar et al., 2019). Among these applications, carbon, metal, polymer, and metal oxide nanoparticles and certain nanocomposites were used for dental implant applications.

Metal Nanomaterials

Metal nanomaterials, such as gold, silver, platinum, copper, and selenium possess enhanced antimicrobial properties. Hence, these nanomaterials find applications in the form of an antimicrobial, surface coating substance of the conventional dental implants, to prevent them from microbial attack-mediated degradation (Parnia et al., 2017). Likewise, these nanoparticles are incorporated with conventional dental implant materials, such as titanium and hydroxyapatite also possess osteointegration property for 12 weeks (Woźniak and Markuszewski, 2019). Recently, silver nanoparticles are deposited on the surface of commercially pure titanium *via* exposed air "laser ablation" to enhance the dental graft antibacterial property (Boutinguiza et al., 2018). Further, it has been identified that the chitosan-gold nanoparticles possess enhanced ability to deliver c-myb gene at the target site, which is a transcription factor belongs to myoblastosis family, that can control survival, differentiation, cell proliferation, and death. The c-myb delivery by the gold nanocomposite has facilitated dental implant osseointegration in ovariectomized rat model (Takanche et al., 2018). Furthermore, nanocrystalline titanium-copper alloy has demonstrated a strong biocompatibility, antibacterial, osseointegration, and mechanical properties to be a highly beneficial orthopedic material, especially for dental implant application (Moniri Javadhesari et al., 2020). Moreover, silver nanoparticle decorated graphene nanocomposites were identified to possess osteointegration property with enhanced antibacterial activity against an oral pathogen named *Aggregatibacter actinomycetemcomitans* along with *Streptococcus mutans*, *Candida albicans*, and *Lactobacillus acidophilus* (Peng et al., 2017).

Metal Oxide Nanomaterials

Nanosized metal oxides are highly stable, compared to metal nanoparticles, which brands them highly beneficial as antimicrobial agents with high osseointegration and mechanical property to be coated on the surface of the insert (Ghiciuc et al., 2017). Recently, silver and zinc nanoparticles embedded in the layers of titanium oxide nanotube has shown enhanced antimicrobial actions toward oral microbes, for instance *S. mutans*, *C. albicans*, and *Candida parapsilosis*, and are proposed to be beneficial toward the management of dental contagions (Roguska et al., 2018). Likewise, porous tantalum oxide nanoparticles along with calcium phosphate and osteoconductive elements were fabricated into a core-shell structure and are proposed as a next generation dental implant material (Fialho et al., 2021). Similarly, nanocomposites of titania-zinc oxide fabricated as thin films on the substrates of silicon exhibited enhanced biocompatibility and antibacterial activity, which can be a potential coating films for the dental implant applications (Goel et al., 2019).

Carbon and Polymer Nanomaterials

Carbon-based nanoparticles, for instance carbon nanotubes, graphene, diamond nanoparticles, and quantum dots were also utilized as a coating or dental implant material. However, these carbon nanomaterials are incorporated with metallic or polymer nanomaterials as nanocomposites to retain their mechanical properties and enhance their biological properties. In a recent study, graphene incorporated with zinc oxide as nanocomposite film has been found possess ability to protect the surfaces of dental implants from cariogenic *S. mutans* bacteria (Kulshrestha et al., 2014). Likewise, carbon-based nanodots, nanotubes, nanofibers, fullerenes, graphene derivatives, and nanocrystalline diamonds were reported to be beneficial a surface functionalization material to improve the surface property of the dental implant (Kang et al., 2021). Besides, nanosized polymers or polymer matrix composites, such as natural or biopolymers namely poly (lactic acid) and chitosan, synthetic polymers including polyetheretherketone (PEEK) and glycidyl methacrylate/triethylene glycol dimethacrylate (BisGMA/TEGDMA) are widely fabricated as nanoparticles or incorporated with nanoparticles to exhibit enhanced efficiency in dental implant applications (Kadambi et al., 2021).

LIMITATIONS OF NANOMATERIALS AS DENTAL IMPLANTS

It may be noted that all the nanomaterials mentioned in the previous section are fabricated *via* either chemical or physical approaches. These nanomaterials possess significant properties, such as chemical compositions similar to teeth and its components, wettability, surface energy, and surface roughness, which makes them highly beneficial for the dental applications (Rasouli et al., 2018). However, the chemicals used for the fabrication of these nanomaterials are toxic toward human cells and high energies are involved in the nanomaterial formation, which has been identified as potential limitations to recommend them for large-scale commercial dental implant applications (Jeevanandam et al., 2020b). The toxicity of these chemical or physical synthesized nanomaterials depends on the type of reducing and stabilizing agent used for nanomaterial fabrication, size, morphology, and surface functional groups as well as their surface charge of nanomaterials (Ganguly et al., 2018; Qu et al., 2018). Further, it can be noted that the traces of reducing and stabilizing agents in the nanomaterials, will also affect their biocompatibility, bioavailability, bioreactivity, and eventually cause acute or chronic side effects (Zhang et al., 2017). Furthermore, the costs involved in the chemical and physical synthesis are higher to be recommended for large-scale commercial nanomaterial synthesis (Jamkhande et al., 2019). Thus, biosynthesis approaches *via* microbes and their extracts has been introduced as an effective green synthesis approach for the formation of nanomaterials with less toxicity and high biocompatibility, compared to conventional chemical and physical synthesis approaches (Khan and Lee, 2020). Fungi, bacteria and algae are the most common microbes, which find applications

toward the microbial production of nanomaterials (Yadav et al., 2020). Microbial nanomaterial fabrication outside the cellular space, especially using the biomolecules extracted from the microbes are extensively used to form nanoparticles, compared to the intracellular approach, where the extraction and purification of nanomaterials is tedious (Li et al., 2017). Even though, microbial synthesis is beneficial in yielding non-toxic, smaller sized nanobiomaterials, there are certain limitations that constrains their exploitation in large-scale biomedical applications (Kulkarni et al., 2021). Bacteria-mediated nanomaterial synthesis possess limitations, such as high time consumption and reduced control over the size, crystallinity, and morphology. Likewise, difficulties in down-streaming process and 24–120 h for nanomaterial formation are the limitations of fungal and algal-mediated nanobiomaterial synthesis (Jeevanandam et al., 2016). Hence, extracts of plants known as phytochemicals are introduced as an alternative and potential reducing and stabilizing agent for the formation of nanobiomaterials to be beneficial in biomedical applications, especially for dental implant applications as summarized in **Table 1**.

PLANT-DERIVED NANOBIOMATERIALS AS DENTAL IMPLANTS

In recent times, several nanobiomaterials have been fabricated using plant extracts to be employed in the dental implant applications, as an alternative to conventional dental implants as shown in **Figure 1**. Recently, it has been reported that the 71.5 nm sized spherical gold nanobiomaterial, that are synthesized *via* the aqueous bark extract of *Salacia chinensis*, can be utilized for dental implant application. The *in vitro* studies revealed that the synthesized nanobiomaterial possess superior stability in blood components, such as 2% of human serum albumin 0.2 M of histidine and 0.2 M cysteine of 2% bovine serum albumin. Further, the study showed that the phytosynthesized nanomaterial are cyto-compatible and compatible toward blood, such as periodontal fibroblasts and erythrocytes. Besides, the gold nanobiomaterial increased the cell viability of human MG-63 bone osteosarcoma cell lines, which indicates that the nanomaterial possess enhanced osteoinductive potential, which can be useful for dental graft treatment as a "bone inductive agent" (Jadhav et al., 2018). Similarly, another study showed

TABLE 1 | Advantages and limitations of conventional and nanomaterial-based dental implants.

Dental implant materials	Advantages	Limitations	References
Metals, ceramics, polymers, alloys, and composites	Low cost, compared to prostheses and behave similar to natural tooth	Degradation in biological fluids, corrosion and wear, and leading to inflammation	Vogel et al., 2013; Apaza-Bedoya et al., 2017; Li J. et al., 2020; Park et al., 2020
Physical and chemical synthesized nanomaterials	Chemical compositions similar to teeth and its components, wettability, surface energy, and surface roughness	Toxicity toward human cells, low biocompatibility, bioavailability, and high cost for synthesis	Zhang et al., 2017; Rasouli et al., 2018; Jeevanandam et al., 2020b
Microbial synthesized nanobiomaterials	Less toxicity, high biocompatibility, and biological property	Longer synthesis time, reduced control in stability, and tedious down-streaming process	Jeevanandam et al., 2016; Khan and Lee, 2020
Plant-derived nanobiomaterials	Less toxicity, control in stability, ease in down streaming process, biocompatibility, and bone induction ability	Difficult to modify shape, lack of in-depth dental studies	Sundeep et al., 2017; Jadhav et al., 2018

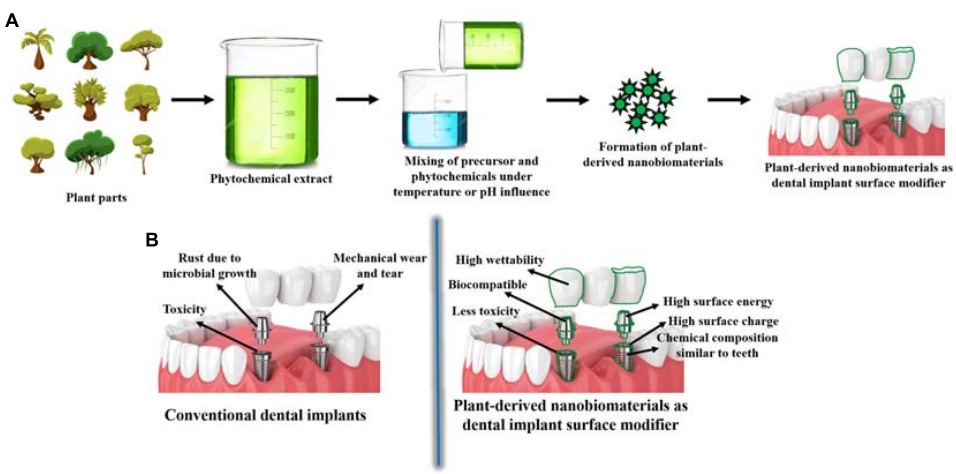

FIGURE 1 | (A) Schematics of nanobiomaterials synthesized from plants for dental implant applications; **(B)** Schematics showing the limitations of conventional dental implants and advantages of plant-derived nanobiomaterials as surface modifiers of dental implants.

that the 32.4 nm sized flake-like shaped silver nanoparticles synthesized *via* aqueous leaf extract of *Mangifera indica*, which can be beneficial for the dental restoration applications. "Glass ionomer cement" (GIC) was employed to strengthen the synthesized silver nanobiomaterials, which improved the low wear of conventional GIC, enhanced their mechanical strength with exclusive protective features against *Staphylococcus aureus* and *Escherichia coli*. Therefore, these nanobiomaterial reinforced GIC can be useful to improve the mechanical strength of the conventional dental implant materials by blending with them as a composite or as a surface coating to improve their antibacterial activities (Sundeep et al., 2017).

Likewise, the polyphenols extracted from the *Anogeissus latifolia* plant leaves has been utilized for the fabrication of gold nanobiomaterials for the management of pain in dental tissue implantation applications. The nanobiomaterial exhibited enhanced stability in human serum albumin, cysteine, histidine, and bovine serum albumin, and improved biocompatibility as well as cytocompatibility toward periodontal fibroblasts and erythrocytes *in vitro*. Further, the study revealed that the gold nanobiomaterial improved the cell viability of MG-63 cell lines with strong antinociperceptive activity, which is beneficial for dental pain management applications during tissue implantation (Wang and Wang, 2020). Moreover, plant synthesized zinc oxide nanoparticles has also been proposed to be a potential nanobiomaterial with *in vitro* osteogenic activity and antibacterial property for dental implant applications (Li Y. et al., 2020). Moreover, silver nanoparticles synthesized *via* white pepper oleoresin (Paul et al., 2020), *Oleo europaea* extract (Umai et al., 2020), clove and cinnamon extracts synthesized with zinc oxide nanoparticles (Mohapatra et al., 2020), exhibited enhanced antimicrobial activities against oral pathogens. These can be beneficial as a surface modifier of conventional dental implants, to prevent microbial attacks or infections. All these studies demonstrated that the plant-mediated synthesis of nanobiomaterials are highly significant for dental implant applications. It is conceivable that advancements in modern synthesis techniques, will lead to greater success in producing novel phytonanobiomaterials as dental implants.

FUTURE PERSPECTIVES AND CONCLUSION

It is noteworthy that noteworthy *in vitro* research findings and breakthroughs are increasingly being reported in the context of plant-synthesized nanobiomaterials for dental implant applications, especially as a surface modifier of implants. Nevertheless, numerous challenges and critical shortcomings could also be noticed with regards to plant-mediated nanobiomaterial fabrication. Even though, plant-mediated synthesis can yield smaller sized bionanomaterials in short time, their stability is not comparable with conventional approaches. Also, the shape of the resultant nanobiomaterials are spherical and polydispersed in most cases and pH variations are required to transform their morphologies and dispersity. However, addition of chemicals to alter pH may also lead to increase in toxicity of these phytosynthesized nanobiomaterials. Thus, it is necessary to incorporate novel techniques in plant-mediated nanomaterial to eliminate limitations and improve their efficiency. Moreover, there are no reports, which shows that the plant-mediated nanomaterials are toxic or less efficient in dental implant applications. Also, it can be noted that the nanobiomaterials that are synthesized *via* plant extracts for dental applications in recent times are standalone nanobiomaterials. Hence, nanobiocomposites can be synthesized *via* plant extracts in the future, to render them beneficial toward large-scale commercial surface-modified dental implant applications with exclusive biomedical properties.

AUTHOR CONTRIBUTIONS

JJ and SP conceived and designed the structure of the minireview. JJ contributed to literature exploration and analysis, illustration, and writing the manuscript, which was reviewed, amended, and finalized by SP and MD. All authors ratified the submitted and revised versions.

FUNDING

SP acknowledges the Open Access funding provided by the Technical University of Munich, Germany. JJ acknowledges the support of FCT-Fundação para a Ciência e a Tecnologia (Base Fund UIDB/00674/2020 and Programmatic Fund UIDP/00674/2020, Portuguese Government Funds), ARDITI-Agência Regional para o Desenvolvimento da Investigação Tecnologia e Inovação through the project M1420-01-0145-FEDER-000005-CQM^{+} (Madeira 14-20 Program).

ACKNOWLEDGMENTS

The authors thank the reviewers for their valuable feedback and suggestions, which greatly improved the quality of the manuscript.

REFERENCES

Abraham, C. M. (2014). A brief historical perspective on dental implants, their surface coatings and treatments. *Open Dent. J.* 8, 50–55. doi: 10.2174/1874210601408010050

Andra, S., Balu, S. K., Jeevanandham, J., Muthalagu, M., Vidyavathy, M., San Chan, Y., et al. (2019). Phytosynthesized metal oxide nanoparticles for pharmaceutical applications. *Naunyn Schmiedebergs Arch. Pharmacol.* 392, 755–771. doi: 10.1007/s00210-019-01666-7

Apaza-Bedoya, K., Tarce, M., Benfatti, C.a.M, Henriques, B., Mathew, M. T., Teughels, W., et al. (2017). Synergistic interactions between corrosion and wear at titanium-based dental implant connections: a scoping review. *J. Periodontal Res.* 52, 946–954. doi: 10.1111/jre.12469

Augustine, R., and Hasan, A. (2020). Emerging applications of biocompatible phytosynthesized metal/metal oxide nanoparticles in healthcare. *J. Drug Deliv. Sci. Technol.* 56:101516. doi: 10.1016/j.jddst.2020.101516

Bazli, L., Nargesi Khoramabadi, H., Modarresi Chahardehi, A., Arsad, H., Malekpouri, B., Asgari Jazi, M., et al. (2020). Factors influencing the failure of dental implants: a systematic review. *J. Compos. Compd.* 2, 18–25. doi: 10.29252/jcc.2.1.3

Boutinguiza, M., Fernández-Arias, M., Del Val, J., Buxadera-Palomero, J., Rodríguez, D., Lusquiños, F., et al. (2018). Synthesis and deposition of silver nanoparticles on cp Ti by laser ablation in open air for antibacterial effect in dental implants. *Mater. Lett.* 231, 126–129. doi: 10.1016/j.matlet.2018.07.134

Chrcanovic, B. R., Albrektsson, T., and Wennerberg, A. (2014). Diabetes and oral implant failure: a systematic review. *J. Dent. Res.* 93, 859–867. doi: 10.1177/0022034514538820

Fialho, L., Grenho, L., Fernandes, M. H., and Carvalho, S. (2021). Porous tantalum oxide with osteoconductive elements and antibacterial core-shell nanoparticles: a new generation of materials for dental implants. *Mater. Sci. Eng. C* 120, 111761. doi: 10.1016/j.msec.2020.111761

Ganguly, P., Breen, A., and Pillai, S. C. (2018). Toxicity of nanomaterials: exposure, pathways, assessment, and recent advances. *ACS Biomater. Sci. Eng.* 4, 2237–2275. doi: 10.1021/acsbiomaterials.8b00068

Ghiciuc, C.M., Ghiciuc, O.N., Ochiuz, L., and Lupuşoru, C.E. (2017). "Antibacterial effects of metal oxides-containing nanomaterials in dentistry". In *Proceedings of the 2017 E-Health and Bioengineering Conference (EHB)*. Sinaia: IEEE, 365-368.

Goel, S., Dubey, P., Ray, S., Jayaganthan, R., Pant, A. B., and Chandra, R. (2019). Co-sputtered antibacterial and biocompatible nanocomposite titania-zinc oxide thin films on si substrates for dental implant applications. *Mater. Technol.* 34, 32–42. doi: 10.1080/10667857.2018.1488924

Ha, S.-W., Viggeswarapu, M., Habib, M. M., and Beck, G. R. (2018). Bioactive effects of silica nanoparticles on bone cells are size, surface, and composition dependent. *Acta Biomater.* 82, 184–196. doi: 10.1016/j.actbio.2018.10.018

Henri Diederich, D. M. D., and Abou-Rabii, I. (2019). The cortically fixed at once approach: a treatment option in an atrophied maxilla. *Oral Health Dent. Sci* 3, 1–4.

Huang, Y. S., Mcgowan, T., Lee, R., and Ivanovski, S. (2017). "7.23 Dental Implants: biomaterial properties influencing osseointegration," in *Comprehensive Biomaterials II*, ed. P. Ducheyne (Oxford: Elsevier), 444–466. doi: 10.1016/b978-0-12-803581-8.09306-1

Jadhav, K., Hr, R., Deshpande, S., Jagwani, S., Dhamecha, D., Jalalpure, S., et al. (2018). Phytosynthesis of gold nanoparticles: characterization, biocompatibility, and evaluation of its osteoinductive potential for application in implant dentistry. *Mater. Sci. Eng. C* 93, 664–670. doi: 10.1016/j.msec.2018.08.028

Jamkhande, P. G., Ghule, N. W., Bamer, A. H., and Kalaskar, M. G. (2019). Metal nanoparticles synthesis: an overview on methods of preparation, advantages and disadvantages, and applications. *J. Drug Deliv. Sci. Technol.* 53:101174. doi: 10.1016/j.jddst.2019.101174

Jeevanandam, J., Chan, Y. S., and Danquah, M. K. (2016). Biosynthesis of metal and metal oxide nanoparticles. *ChemBioEng. Rev.* 3, 55–67. doi: 10.1002/cben.201500018

Jeevanandam, J., Kulabhusan, P. K., Sabbih, G., Akram, M., and Danquah, M. K. (2020a). Phytosynthesized nanoparticles as a potential cancer therapeutic agent. *3 Biotech* 10:535.

Jeevanandam, J., Sundaramurthy, A., Sharma, V., Murugan, C., Pal, K., Kodous, M. H. A., et al. (2020b). "Sustainability of one-dimensional nanostructures: fabrication and industrial applications," in *Sustainable Nanoscale Engineering*, eds G. Szekely and A. Livingston (Amsterdam: Elsevier), 83–113.

Kadambi, P., Luniya, P., and Dhatrak, P. (2021). Current advancements in polymer/polymer matrix composites for dental implants: a systematic review. *Mater. Today Proc.* doi: 10.1016/j.matpr.2020.12.396

Kang, M. S., Lee, J. H., Hong, S. W., Lee, J. H., and Han, D.-W. (2021). Nanocomposites for enhanced osseointegration of dental and orthopedic implants revisited: surface functionalization by carbon nanomaterial coatings. *J. Compos. Sci.* 5:23doi:

Khan, S. A., and Lee, C.-S. (2020). "Green biological synthesis of nanoparticles and their biomedical applications," in *Applications of Nanotechnology for Green Synthesis*, eds Inamuddin and A. Asiri (Cham: Springer), 247–280. doi: 10.1007/978-3-030-44176-0_10

Kulkarni, A. G., De Britto, S., and Jogaiah, S. (2021). "Economic considerations and limitations of green synthesis vs chemical synthesis of nanomaterials," in *Advances in Nano-Fertilizers and Nano-Pesticides in Agriculture*, eds S. Jogaiah, H. Bahadur Singh, and R. de Lima (Amsterdam: Elsevier), 459–468. doi: 10.1016/b978-0-12-820092-6.00018-5

Kulshrestha, S., Khan, S., Meena, R., Singh, B. R., and Khan, A. U. (2014). A graphene/zinc oxide nanocomposite film protects dental implant surfaces against cariogenic *Streptococcus mutans*. *Biofouling* 30, 1281–1294. doi: 10.1080/08927014.2014.983093

Li, J., Jansen, J. A., Walboomers, X. F., and Van Den Beucken, J. J. J. P. (2020). Mechanical aspects of dental implants and osseointegration: a narrative review. *J. Mech. Behav. Biomed. Mater.* 103:103574. doi: 10.1016/j.jmbbm.2019.103574

Li, S., Duan, Y., Li, R., and Wang, X. (2017). Intracellular and extracellular biosynthesis of antibacterial silver nanoparticles by using *Pseudomonas aeruginosa*. *J. Nanosci. Nanotechnol.* 17, 9186–9191. doi: 10.1166/jnn.2017.13920

Li, Y., Yang, Y., Qing, Y. A., Li, R., Tang, X., Guo, D., et al. (2020). Enhancing ZnO-NP antibacterial and osteogenesis properties in orthopedic applications: a review. *Int. J. Nanomed.* 15, 6247–6262. doi: 10.2147/ijn.s262876

May, M. C., Andrews, P. N., Daher, S., and Reebye, U. N. (2016). Prospective cohort study of dental implant success rate in patients with AIDS. *Int. J. Implant Dent.* 2:20.

Mohapatra, S., Leelavathi, L., Meignana, A. I., Pradeep, K. R., and Rajeshkumar, S. (2020). Assessment of antimicrobial efficacy of zinc oxide nanoparticles synthesized using clove and cinnamon formulation against oral pathogens–an in vitro study. *J. Evol. Med. Dent. Sci.* 9, 2034–2040. doi: 10.14260/jemds/2020/443

Moniri Javadhesari, S., Alipour, S., and Akbarpour, M. R. (2020). Biocompatibility, osseointegration, antibacterial and mechanical properties of nanocrystalline Ti-Cu alloy as a new orthopedic material. *Colloids Surf. B Biointerfaces* 189:110889. doi: 10.1016/j.colsurfb.2020.110889

Neldam, C. A., and Pinholt, E. M. (2012). State of the art of short dental implants: a systematic review of the literature. *Clin. Implant Dent. Relat. Res.* 14, 622–632. doi: 10.1111/j.1708-8208.2010.00303.x

Osman, R. B., and Swain, M. V. (2015). A critical review of dental implant materials with an emphasis on titanium versus zirconia. *Materials* 8, 932–958. doi: 10.3390/ma8030932

Pan, S., Jeevanandam, J., Acquah, C., Tan, K. X., Udenigwe, C. C., and Danquah, M. K. (2021). "Drug delivery systems for cardiovascular ailments," in *Drug Delievry Devices and Therapeutic Systems*, ed. E. Chappel (Amsterdam: Elsevier), 567–599. doi: 10.1016/b978-0-12-819838-4.00019-5

Park, J.-H., Odkhuu, M., Cho, S., Li, J., Park, B.-Y., and Kim, J.-W. (2020). 3D-printed titanium implant with pre-mounted dental implants for mandible reconstruction: a case report. *Maxillofac. Plast. Reconstr. Surg.* 42:28.

Parnia, F., Yazdani, J., Javaherzadeh, V., and Dizaj, S. M. (2017). Overview of nanoparticle coating of dental implants for enhanced osseointegration and antimicrobial purposes. *J. Pharm. Pharm. Sci.* 20, 148–160. doi: 10.18433/j3gp6g

Paul, R. P., Roy, A., and Shanmugam, R. (2020). Antibacterial activity of white pepper oleoresin mediated silver nanoparticles against oral pathogens. *J. Evol. Medi. Dent. Sci.* 9, 2352–2356. doi: 10.14260/jemds/2020/510

Peng, J.-M., Lin, J.-C., Chen, Z.-Y., Wei, M.-C., Fu, Y.-X., Lu, S.-S., et al. (2017). Enhanced antimicrobial activities of silver-nanoparticle-decorated reduced graphene nanocomposites against oral pathogens. *Mater. Sci. Eng. C* 71, 10–16. doi: 10.1016/j.msec.2016.09.070

Prakasam, M., Locs, J., Salma-Ancane, K., Loca, D., Largeteau, A., and Berzina-Cimdina, L. (2017). Biodegradable materials and metallic implants—a review. *J. Funct. Biomater.* 8:44. doi: 10.3390/jfb8040044

Qu, Y., He, F., Yu, C., Liang, X., Liang, D., Ma, L., et al. (2018). Advances on graphene-based nanomaterials for biomedical applications. *Mater. Sci. Eng. C* 90, 764–780.

Rasouli, R., Barhoum, A., and Uludag, H. (2018). A review of nanostructured surfaces and materials for dental implants: surface coating, patterning and functionalization for improved performance. *Biomater. Sci.* 6, 1312–1338. doi: 10.1039/c8bm00021b

Roguska, A., Belcarz, A., Zalewska, J., Hołdyński, M., Andrzejczuk, M., Pisarek, M., et al. (2018). Metal TiO2 nanotube layers for the treatment of dental implant

infections. *ACS Appl. Mater. Interfaces* 10, 17089–17099. doi: 10.1021/acsami.8b04045

Rupp, F., Liang, L., Geis-Gerstorfer, J., Scheideler, L., and Hüttig, F. (2018). Surface characteristics of dental implants: a review. *Dent. Mater.* 34, 40–57. doi: 10.1016/j.dental.2017.09.007

Sanguida, A., Vinothini, V., Prathima, G. S., Santhadevy, A., Premlal, K., and Kavitha, M. (2019). Age and reasons for first dental visit and knowledge and attitude of parents toward dental procedures for Puducherry children aged 0–9 years. *J. Pharm. Bioallied Sci.* 11:S413.

Shah, K. C., Chao, D., Wu, B. M., and Jensen, O. T. (2019). Shape-memory retained complete arch guided implant treatment using nitinol (Smileloc) abutments. *Oral and Maxillofac. Surg. Clin.* 31, 427–435. doi: 10.1016/j.coms.2019.03.005

Shanmuganathan, R., Karuppusamy, I., Saravanan, M., Muthukumar, H., Ponnuchamy, K., Ramkumar, V. S., et al. (2019). Synthesis of Silver nanoparticles and their biomedical applications-A comprehensive review. *Curr. Pharm. Des.* 25, 2650–2660. doi: 10.2174/1381612825666190708185506

Sundeep, D., Vijaya Kumar, T., Rao, P. S. S., Ravikumar, R. V. S. S. N., and Gopala Krishna, A. (2017). Green synthesis and characterization of Ag nanoparticles from *Mangifera indica* leaves for dental restoration and antibacterial applications. *Prog. Biomater.* 6, 57–66. doi: 10.1007/s40204-017-0067-9

Takanche, J. S., Kim, J.-E., Kim, J.-S., Lee, M.-H., Jeon, J.-G., Park, I.-S., et al. (2018). Chitosan-gold nanoparticles mediated gene delivery of c-myb facilitates osseointegration of dental implants in ovariectomized rat. *Artif. Cells Nanomed. Biotechnol.* 46, S807–S817.

Tan, K. X., Jeevanandam, J., Pan, S., Yon, L. S., and Danquah, M. K. (2020). Aptamer-navigated copolymeric drug carrier system for in vitro delivery of MgO nanoparticles as insulin resistance reversal drug candidate in Type 2 diabetes. *J. Drug Deliv. Sci. Technol.* 57:101764. doi: 10.1016/j.jddst.2020.101764

Tan, K. X., Pan, S., Jeevanandam, J., and Danquah, M. K. (2019). Cardiovascular therapies utilizing targeted delivery of nanomedicines and aptamers. *Int. J. Pharam.* 558, 413–425. doi: 10.1016/j.ijpharm.2019.01.023

Travess, H. C., Williams, P. H., and Sandy, J. R. (2004). The use of osseointegrated implants in orthodontic patients: 2. absolute anchorage. *Dent. Update* 31, 355–362. doi: 10.12968/denu.2004.31.6.355

Umai, D., Vikranth, A., and Meenambiga, S. S. (2020). A study on the green synthesis of silver nanoparticles from Olea europaea and its activity against oral pathogens. *Mater. Today Proc.* 6:e04493

Vogel, R., Smith-Palmer, J., and Valentine, W. (2013). Evaluating the health economic implications and cost-effectiveness of dental implants: a literature review. *Int. J. Oral Maxillofac. Implants* 28, 343–356. doi: 10.11607/jomi.2921

Wang, M., and Wang, L. (2020). Plant polyphenols mediated synthesis of gold nanoparticles for pain management in nursing care for dental tissue implantation applications. *J. Drug Deliv. Sci. Technol* 58:101753. doi: 10.1016/j.jddst.2020.101753

Woźniak, W., and Markuszewski, J. (2019). Osseointegration of hydroxyapatite coatings doped with silver nanoparticles: scanning electron microscopy studies on a rabbit model. *Folia morphol.* 78, 107–113. doi: 10.1111/j.1365-2818.1993.tb03364.x

Yadav, V. K., Khan, S. H., Malik, P., Thappa, A., Suriyaprabha, R., Ravi, R. K., et al. (2020). "Microbial synthesis of nanoparticles and their applications for wastewater treatment," in *Microbial Biotechnology: Basic Research and Applications*, eds J. Singh, A. Vyas, S. Wang, and R. Prasad (Singapore: Springer), 147–187. doi: 10.1007/978-981-15-2817-0_7

Zafar, M. S., Alnazzawi, A. A., Alrahabi, M., Fareed, M. A., Najeeb, S., and Khurshid, Z. (2019). "18 - Nanotechnology and nanomaterials in dentistry," in *Advanced Dental Biomaterials*, eds Z. Khurshid, S. Najeeb, M. S. Zafar, and F. Sefat (Cambridge: Woodhead Publishing), 477–505. doi: 10.1016/b978-0-08-102476-8.00018-9

Zhang, J., Tang, H., Liu, Z., and Chen, B. (2017). Effects of major parameters of nanoparticles on their physical and chemical properties and recent application of nanodrug delivery system in targeted chemotherapy. *Int. J. Nanomed.* 12:8483. doi: 10.2147/ijn.s148359

Conflict of Interest: The authors declare that the research was conducted in the absence of any commercial or financial relationships that could be construed as a potential conflict of interest.

frontiers in Materials

ORIGINAL RESEARCH
published: 22 April 2021
doi: 10.3389/fmats.2021.655156

Preparation and Characterization of Sodium Aluminum Silicate-Polymer Composites and Effects of Surface Roughness and Scratch Directions on Their Flexural Strengths

Bencang Cui[1], Fengbo Sun[1], Qian Ding[2], Huining Wang[3], Yuanhua Lin[1], Yang Shen[1], Ming Li[1], Xuliang Deng[4,5], Lei Zhang[2] and Cewen Nan[1]*

[1] State Key Laboratory of New Ceramics and Fine Processing, School of Materials Science and Engineering, Tsinghua University, Beijing, China, [2] Department of Prosthodontics, School and Hospital of Stomatology, Peking University, Beijing, China, [3] Department of Periodontics, School and Hospital of Stomatology, Institute of Stomatology, Wenzhou Medical University, Wenzhou, China, [4] Department of Geriatric Dentistry, Peking University School and Hospital of Stomatology, Beijing, China, [5] Department of Prosthodontics, Peking University School and Hospital of Stomatology, Beijing, China

OPEN ACCESS

Edited by:
Mary Anne Sampaio Melo, University of Maryland, Baltimore, United States

Reviewed by:
Samira Camargo, University of Florida, United States
Lamia Sami Mokeem, University of Maryland, Baltimore, United States
Jingwei He, South China University of Technology, China

***Correspondence:**
Yuanhua Lin
linyh@mail.tsinghua.edu.cn

Specialty section:
This article was submitted to Biomaterials, a section of the journal Frontiers in Materials

Received: *20 January 2021*
Accepted: *09 March 2021*
Published: *22 April 2021*

Citation:
Cui B, Sun F, Ding Q, Wang H, Lin Y, Shen Y, Li M, Deng X, Zhang L and Nan C (2021) Preparation and Characterization of Sodium Aluminum Silicate-Polymer Composites and Effects of Surface Roughness and Scratch Directions on Their Flexural Strengths. Front. Mater. 8:655156. doi: 10.3389/fmats.2021.655156

Although efforts have been put into the research in polymer-infiltrated ceramic network composites (PICNs), data are needed to understand the relationship between surface roughness and flexural strength. In this work, a novel dental restorative composite was fabricated *via* infiltrating mixtures of Bis-GMA/TEGDMA and UDMA/TEGDMA into partially sintered porous sodium aluminum silicate blocks and curing. Bars with different surface conditions were produced by sanding with abrasive and polishing. Flexural strength was measured using three-point-bending. Scanning electron microscopy (SEM) was employed to observe the microstructure of surface areas. One-way analysis of variance was applied for statistical calculations, with $p < 0.05$ being considered significant. Weibull plots were used to evaluate the reliability of flexural strength. The results demonstrated that the flexural strength of the resultant composites was affected by the scratch direction and the value of roughness. The flexural strength increased with decrease of surface roughness. A higher strength value was found for parallel types than for vertical types with nearly the same surface roughness. A large roughness value and a scratch direction perpendicular to tensile stress produced a low Weibull modulus. Of particular importance with this work is that these factors should be taken into consideration when using PICNs as dental restorative composites.

Keywords: polymer infiltrated ceramic network composites, mechanical properties, dental composites, CAD/CAM blocks, crack bridging

INTRODUCTION

Increased demand for dental restorative materials with high mechanical properties and esthetic performances leads to the extensive use of ceramics (Denry and Kelly, 2008; Miyazaki et al., 2013; Li et al., 2014) and composites (Moszner and Salz, 2001; Mitra et al., 2003; Klapdohr and Moszner, 2005; Ferracane, 2011; Acar et al., 2016; Alharbi et al., 2017). Ceramics possess excellent esthetic

performance and high flexural strength, hardness, and elastic modulus in comparison with resin composites. However, the hardness and elastic modulus are so much higher than that of natural enamel and dentin, which lead to the wear of the natural tooth, such that these kinds of materials were even not suggested to be used in areas of crowns (Moszner and Salz, 2001; Mitra et al., 2003; Klapdohr and Moszner, 2005; Ferracane, 2011; Lawson et al., 2014; Acar et al., 2016; Alharbi et al., 2017). Furthermore, it is difficult to machine thoroughly sintered ceramics because of the ultra-high hardness.

Composites are classified into filled composites and polymer-infiltrated ceramic network composites (PICNs) according to processing characteristics. Filled composites are fabricated by adding inorganic particles to polymerizable monomers and curing. For filled composites, the polymer is continuous phase, while inorganic particles are dispersed into that phase (Klapdohr and Moszner, 2005). Early dental restorative composites were all filled composites. Because of low flexural strength, hardness, and modulus of filled composites, they are mainly used as adhesives and direct restorative materials. PICNs are prepared *via* infiltrating polymerizable monomers into porous ceramic networks (He and Swain, 2011; Swain et al., 2016). The corresponding porous ceramics are mainly partially sintered under a lower temperature and with a shorter holding time in case of the formation of dense ceramics. Differently from filled composites, PICNs are composed of two inter-penetrating phases, i.e., polymer and porous ceramic networks. The effects of the characteristics of inorganic particles and inorganic/organic ratios on mechanical properties have been thoroughly examined. The conclusion was that the hardness and elastic modulus of the resultant composites increased with the increase of inorganic particle loading.

Polymerization shrinkage and low degrees of conversion (DC) are two factors that limit the performance of direct restorative composite. As monomers are converted into polymers, covalent bonds are created from Van der Waals band causing a volume reduction. Reduction of DC and polymerization rate may be beneficial to decreasing polymerization shrinkage, but both have drawbacks. A low DC may cause a substantial compromise of mechanical properties (Ferracane and Greener, 1986). An effective approach is soft-start curing, hypothesized to decrease polymerization rate without compromising other properties (Rueggeberg, 2011). However, several studies showed that soft-start curing often resulted in the reduction of mechanical properties (Feng and Suh, 2006; Silva Prezotto et al., 2018). Furthermore, the DC of light-cured direct restorative composites is low and decreases with increase of depth and addition of inorganic fillers (Aljabo et al., 2015).

With the developments of material process technology, high particle loading filled composites and PICNs were fabricated and launched by manufacturers. These composites are used as CAD/CAM blocks, the same as ceramics. Lava Ultimate (filled composites) and VITA ENAMIC (PICNs) were launched by 3M ESPE in 2012 and VITA in 2013, respectively (Thornton, 2014). The mechanical properties of PICNs are more similar to that of the natural tooth. Of particular significance will be to develop novel PICNs and their unique mechanical behaviors.

Dental materials are used in complex oral environments, so it is necessary to pay attention to the specific service state (real service state) and explore their properties accordingly. Though PICNs possess high flexural strength, the restoration could fail at an early age because of the developing roughness. The increasing roughness may be caused by insufficient polishing during restoration and by the wear in oral environment. However, little information is available about the effects of roughness and defect dimensions on the flexural strength of dental restorative composites. Therefore, knowledge about how surface roughness and scratch directions affect flexural strength is necessary to improve the usage of composites. Clinicians should take into consideration that PICNs may be susceptible to surface roughness and scratch directions perpendicular to tensile stress.

The null hypothesis was that surface roughness and defect direction have equally decreasing effects on the flexural strength of composites.

MATERIALS AND METHODS

Materials

The raw materials used in this study were sodium aluminum silicate (SIPERNAT 820A, Degussa AG, Germany), Bis-GMA, UDMA, TEGDMA (Aladdin Reagents Company, Shanghai, China), and BPO (J&K Scientific, Ltd.).

Specimen Preparation

Sodium aluminum silicate powder was compressed into blocks using a steel mold 30 mm in diameter with a pressure of 3 MPa and a holding time of 3 min. Then, the blocks were subjected to isostatic cool pressing with a pressure of 220 MPa and a stay time of 2 min. Finally, the blocks were sintered at 700°C with a heating rate of 5°C/min and a preservation time of 2 h. Partially sintered porous blocks were infiltrated with Bis-GMA/TEGDMA (with a mass ratio of 50/50) and UDMA/TEGDMA (with a mass ratio of 80/20), respectively, and cured at 70°C for 8 h. Dibenzoylperoxide, BPO (J&K Scientific, Ltd.), was used as the thermoinitiator. Two PICNs were obtained, i.e., Bis-GMA/TEGDMA-infiltrated PICNs (PICN BTC) and UDMA/TEGDMA-infiltrated PICNs (PICN UTC).

A precision cutting machine loaded with a diamond saw was used to cut the bending bars (2.2 mm × 2.2 mm × 20 mm, n = 15) from corresponding composite blocks. Three groups of bars (2 mm × 2 mm × 20 mm, with different roughness) for each material were fabricated by sanding the bars with 400# and 1500# abrasive papers and polishing with a 0.5-μm diamond suspension. Two scratch directions were exerted on each group, i.e., perpendicular and parallel to the bending span.

Mid-infrared Spectroscopy Tests

Fourier transform infrared spectroscopy were often used to characterize the conversion degree of dental composites. The Bis-GMA/TEGDMA and UDMA/TEGDMA monomers cured at 70°C for 8 h were tested with uncured monomers as control using mid-infrared spectroscopy. As for the Bis-GMA/TEGDMA group, there are peaks of around 1,608 cm^{-1} (aromatic

C–C) and 1,637 cm^{-1} (aliphatic C=C) for both mid-infrared spectroscopies. As for the UDMA/TEGDMA group, there are peaks of around 1,537 cm^{-1} (N–H) and 1,637 cm^{-1} (aliphatic C=C). The 1,608 and 1,537 cm^{-1} peaks remain constant before and after polymerization, serving as internal standards. The percentage of unconverted C=C bonds was calculated by comparing the intensity of the aliphatic C=C peak at 1,637 cm^{-1} and the reference peak of polymer and monomer. DC were calculated from the results of both mid-infrared spectroscopies according to the following formula:

$$\%conversion = 1 - \frac{\left[aliphatic\,(C=C)\,/reference\right]_{polymer}}{\left[aliphatic\,(C=C)\,/reference\right]_{monomer}} \quad (1)$$

Surface Roughness Testing

Roughness tests of sanded and polished specimens were performed using a profilometer (DektakXT, Bruker, Germany). The measurement was assessed with a scan length of 300 μm and a scan time of 7 s. The test direction was perpendicular to the scratch. Arithmetic mean deviation (Pa) and root mean square deviation (Pq) were calculated automatically by the system.

Flexural Strength Testing

The testing of flexural strength was carried out with a universal test machine (Shimadzu, EZ-100, Japan) in a three-point bending format. The maximum stress at fracture was calculated by the equation:

$$\sigma_f = \frac{3Fl}{2bd^2} \quad (2)$$

Where F is the maximum load at the point of fracture, l is the distance of the roller span (here l = 10 mm), b is the width (here 2 mm), and h is the height (here 2 mm) of the specimen. The loading speed was 0.75 mm/min.

Vickers hardness and elastic modulus were calculated from 10 nano-indentations for each PICN. The nano-indentations were carried out with a fixed depth of 1,000 nm using a nano-indentation tester (MTS, Keysight, G200, America).

Observations of Surface and Inner Micro-structure

Five Vickers indentations with a maximum load of 5 kg were exerted to highly polished surfaces of two PICNs and the dense ceramic counterparts using a hardness tester (Wilson Hardness, America). The samples were observed using SEM (ΣIGMA HD Zeiss, Germany). Sodium aluminum silicate particles were observed using a transmission electron microscope (TEM). The characteristics of the cracks were compared, and the reinforcing mechanism of PICNs was evaluated.

Statistics

Flexural strength results were evaluated using single-factor ANOVA by SPSS with respect to 95% confidence interval. The flexural strength values were also analyzed using Weibull statistics according to the equation:

$$\ln\ln\left(1/\left(1-P_i\right)\right) = m\ln\sigma - m\ln\sigma_0 \quad (3)$$

Where σ is flexural strength, σ_0 is the scale parameter or characteristic strength, and m is the Weibull modulus. P_i is the probability of failure, calculated according to the equation:

$$P_i = (i-0.5)/N \quad (4)$$

where i is the ith sample, and N is the whole number of the samples in each group.

RESULTS

Degree of Conversion

Figure 1 shows the FTIR spectra of the Bis-GMA/TEGDMA and UDMA/TEGDMA monomers before and after polymerization.

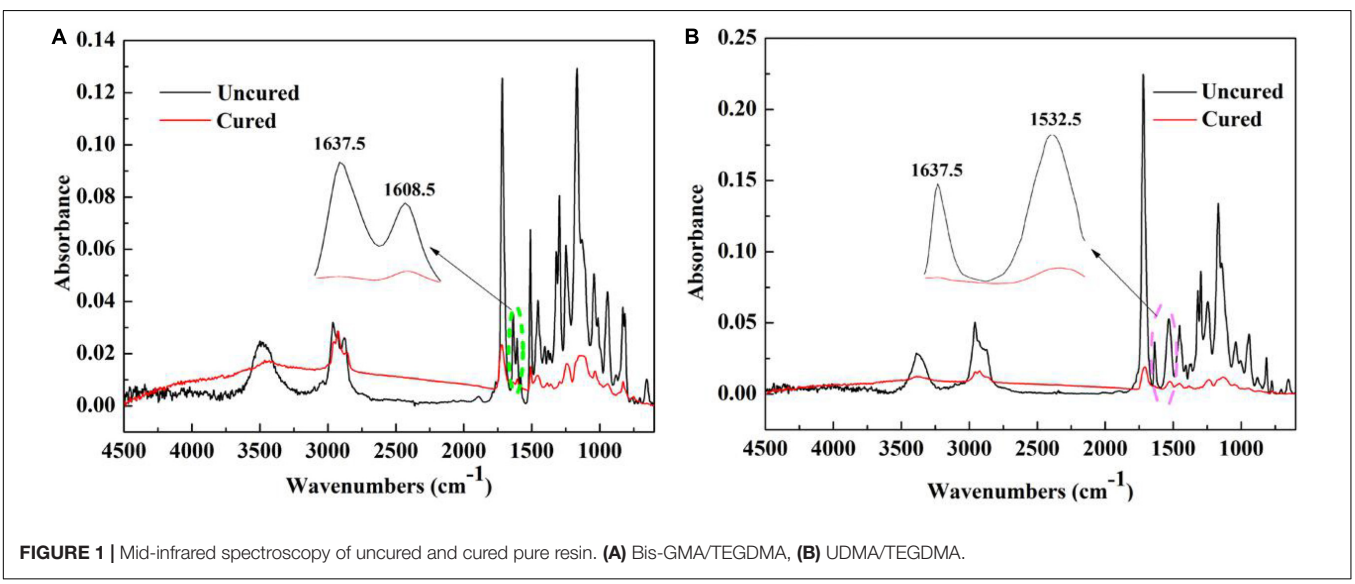

FIGURE 1 | Mid-infrared spectroscopy of uncured and cured pure resin. **(A)** Bis-GMA/TEGDMA, **(B)** UDMA/TEGDMA.

After polymerization, decreases of the C=C peak (around 1,640 cm^{-1}) were notably observed in both FTIR spectroscopy.

The calculated DC values from the FITR results of Bis-GMA/TEGDMA and UDMA/TEGDMA are listed in **Table 1**. Both indicated a high polymerization degree.

Transmission Electron Microscope Observations of Inorganic Particles

The TEM observations (**Figure 2**) show the nano-cluster characteristic of the inorganic component. Each individual particle appeared to be spherical, with an average diameter of less than 100 nm.

Macroscopic and Microscopic Photographs of Two PICNs

Figure 3 shows the photographs and SEM images of two PICNs, i.e., PICN BTC and PICN UTC. PICN UTC exhibited a higher transparency than PICN BTC. For PICN UTC, the background could be seen clearly through the composite. PICN BTC showed a translucent characteristic with a low light transmittance and an opalescent appearance.

The Mechanical Properties of Two PICNs

The mechanical properties of two PICNs are listed in **Table 2**. There were no significant differences between each other.

The SEM Micrographs of Composites' Surface

The SEM micrographs (**Figures 4a–f**) of the composites' surfaces reveal evident unidirectional scratches (**Figures 4a,b,d,e**) after grinding with abrasive papers and smooth surfaces (**Figures 4c,f**) after polishing.

TABLE 1 | Degrees of conversion (DC) of Bis-GMA/TEGDMA and UDMA/TEGDMA specimens.

Monomer mixture	Bis-GMA/TEGDMA	UDMA/TEGDMA
Calculated DC (%)	81.9	81.7

Surface Roughness Values

The average roughness values of sanded and polished samples are presented in **Table 3**. The arithmetic mean deviation (Pa) and root mean square deviation (Pq) of PICN BTC varied from 11.5 ± 7.9 to 828.8 ± 127.6 nm and from 14.2 ± 9.4 to 1,016.8 ± 149.5 nm, respectively. Those two values of PICN UTC varied from 18.7 ± 17.1 to 984.1 ± 238.2 nm and from 23.7 ± 20.9 to 1,195.8 ± 276.9 nm, respectively. Slightly higher surface roughness values were produced for PICN UTC even for the same sanding or polishing procedure.

Comparison of Flexural Strength

The results of the flexural strength are shown in **Figures 5A,B**.

The flexural strengths of PICN BTC varied from 83.37 ± 9.45 to 140.24 ± 7.65 MPa, while that of PICN UTC varied from 108.71 ± 9.25 to 156.26 ± 9.52 MPa.

Weibull Plots of Flexural Strength

Weibull plots of flexural strength are shown in **Figures 6A,B**. The Weibull modulus showed an increasing trend with decrease of surface roughness for both PICN BTC and PICN UTC. A high Weibull modulus indicated a centralized degree of flexural strength values.

Crack Propagation Observation of Ceramics and Two PICNs

The indentation areas of ceramics and two PICNs at an indentation load of 50 N are shown in **Figure 7**. For ceramics, crack propagation from indentation diagonals was observed clearly (**Figures 7a,b**). For two PICNs, no cracks emanating from the diagonals were observed. Cracks could only be found under diamond indenter (**Figures 7c,e**). For the cracks under diamond indenter induced in the high-gloss-polished surfaces of two PICNs, crack bridging phenomenon was observed.

DISCUSSION

Dental composites have been developed rapidly in recent years. Ferracane (2011) gave a thorough classification about

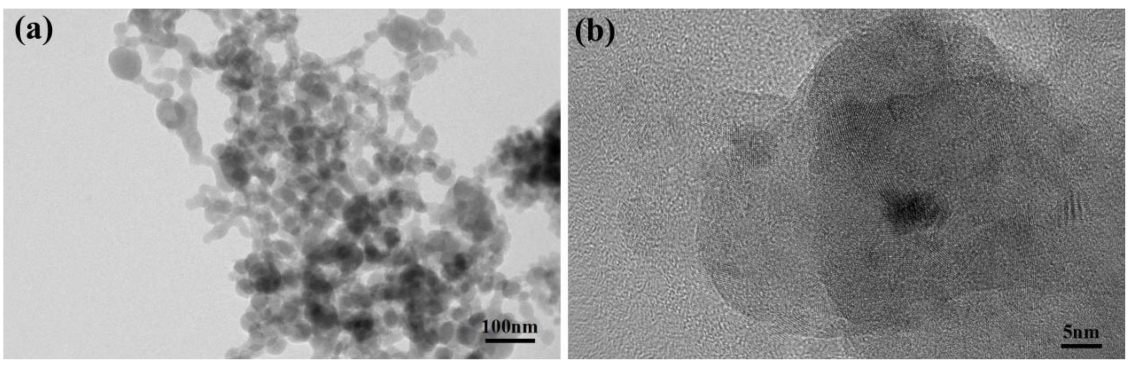

FIGURE 2 | Microstructures of sodium aluminum silicate nano-clusters. **(a)** TEM observations of the inorganic component. **(b)** Zoomed-in view of A.

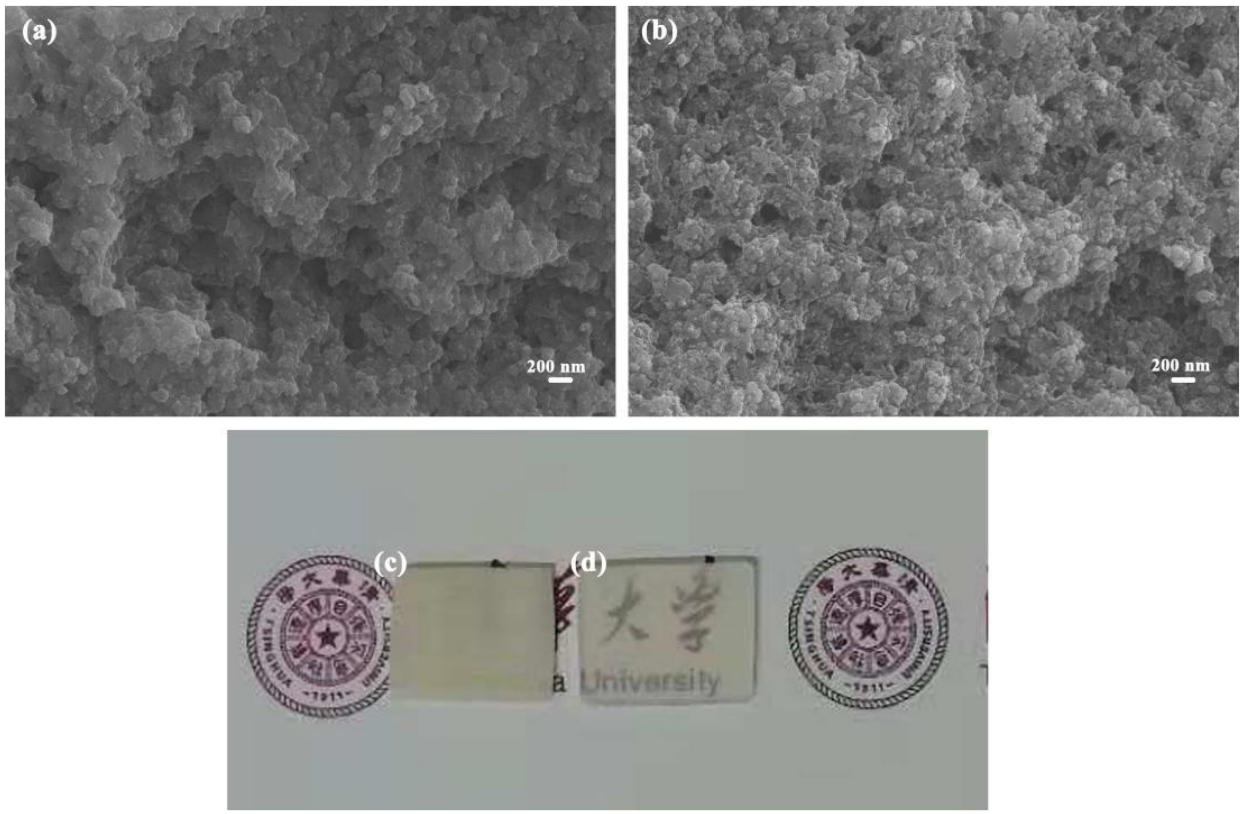

FIGURE 3 | Micro-structures and sample photographs of two PICNs. **(a,c)** PICN BTC, **(b,d)** PICN UTC.

TABLE 2 | Mechanical properties of two polymer-infiltrated ceramic network composites (PICNs).

	Flexural strength (MPa)	Elastic modulus (GPa)	Vickers hardness (GPa)
PICN BTC	140.24 ± 7.65	18.69 ± 2.02	1.198 ± 0.090
PICN UTC	156.26 ± 9.52	18.93 ± 2.07	1.209 ± 0.097

conventional dental composites based on the characteristics of inorganic fillers. In the present study, a novel dental composite was fabricated, with its properties being evaluated. This novel composite was of a special structure. The TEM micrographs (**Figures 2a,b**) indicate sodium aluminum silicate with a nano-cluster structure. Bis-GMA-based and UDMA-based composites are two main contemporary restorative options in either direct composite restorations or CAD/CAM composite blocks, and Bis-GMA/TEGDMA and UDMA/TEGDMA resin systems were used in this study. As for this novel restorative composite, the DC value can reach a very high level *via* thermal polymerization (Aljabo et al., 2015).

The ceramic components used in this work were different from the irregular micron ones used in VITA Enamic. As could be observed in **Figure 2**, the inorganic components are nanoclusters. Silica/zirconia nano-clusters have already been used as fillers in Lava Ultimate, with a high flexural strength obtained. Due to the characteristics of the particles, there is a complete infiltration of the monomer mixture into the partially sintered blocks. SEM observations of PICNs' microstructure indicate the thorough infiltration of polymer (**Figures 3a,b**). Increasing demands for esthetic restoration led the manufacturers to provide restorative composites with an appearance similar to that of natural tooth. Color match and transparency are two important criteria in esthetic dentistry. PICN BTC (**Figure 3c**) and PICN UTC (**Figure 3d**) exhibit an opalescent appearance and a high translucent characteristic, respectively. These performances are desirable, as they provide the ability to formulate a large range of colors to mimic the natural tooth. A highly translucent characteristic makes it resemble the appearance of natural enamel. The higher light transmission of PICN UTC than PICN BTC may be attributed to the close match of the refractive indices between silica and UDMA. Shade matching is a frustrating clinical process for direct light-cured restorative composites, as there exists color changes as a result of polymerization (Lee et al., 2003). Because of *in vitro* polymerization of PICNs, the color of dental composites is fixed and stabilized before restoration, and it does not pose the problems of color changes caused by polymerization.

As reported (Sakaguchi and Powers, 2012), the flexural strength, elastic modulus, and hardness of natural enamel were 60–90 MPa, 60–120 GPa, and 3–6 GPa, respectively;

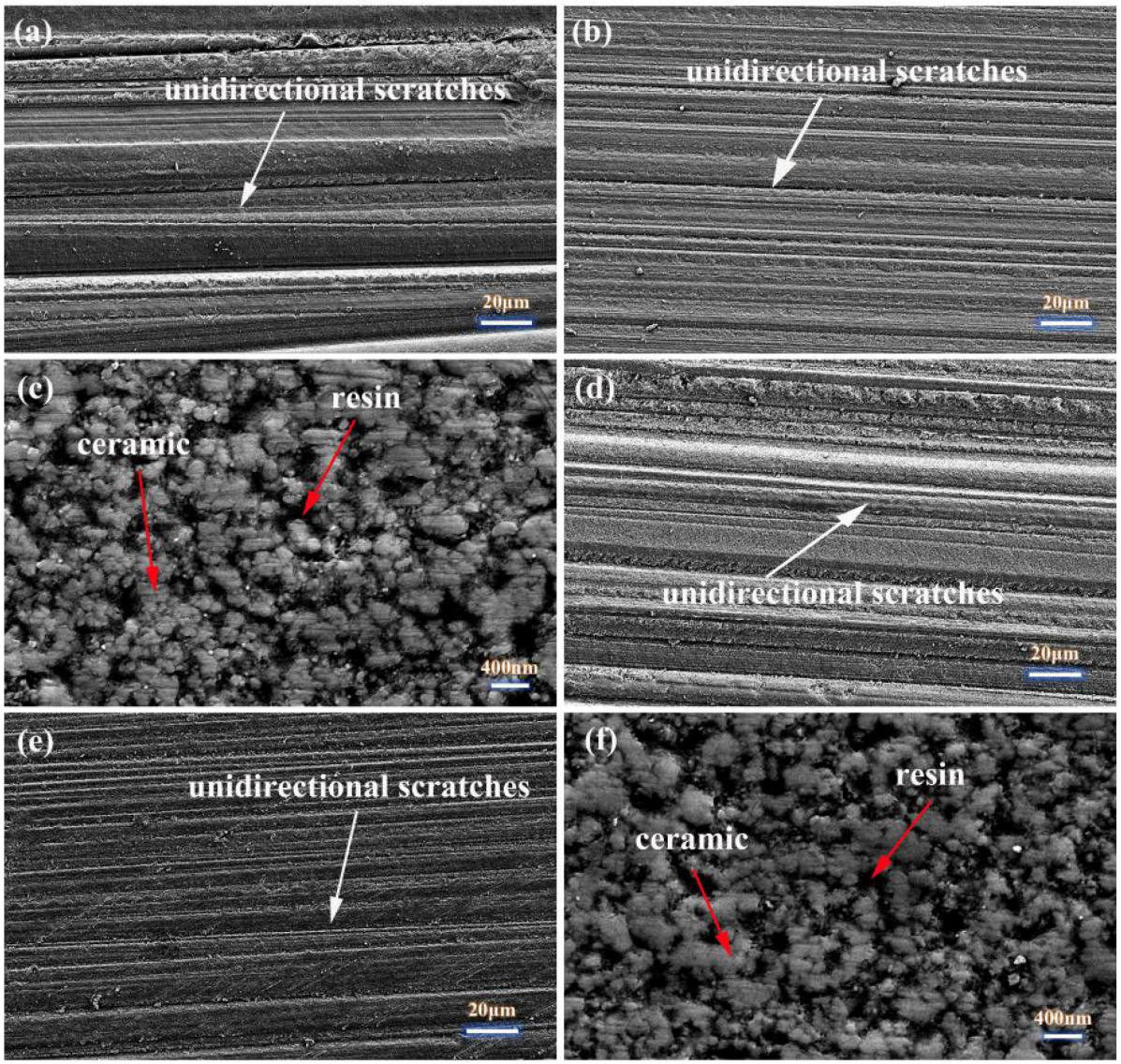

FIGURE 4 | Microstructures of sanded and polished surfaces of composites. **(a)** 400# sanded PICN BTC. **(b)** 1500# sanded PICN BTC. **(c)** Polished PICN BTC. **(d)** 400# sanded PICN UTC. **(e)** 1500# sanded PICN UTC. **(f)** Polished PICN UTC.

TABLE 3 | Surface roughness values of sanded and polished samples.

Material	400# sanded		1500# sanded		Polished	
	Pa (nm)	Pq (nm)	Pa (nm)	Pq (nm)	Pa (nm)	Pq (nm)
PICN BTC	828.8 ± 127.6	1,016.8 ± 149.5	138.6 ± 64.6	172.2 ± 87.6	11.5 ± 7.9	14.2 ± 9.4
PICN UTC	984.1 ± 238.2	1,195.8 ± 276.9	325.5 ± 143.2	395.5 ± 162.1	18.7 ± 17.1	23.7 ± 20.9

those values of natural dentin were 245–280 MPa, 18–24 GPa, and 0.13–0.92 GPa (Mahoney et al., 2000). The mechanical properties of two PICNs are listed in **Table 2**. The flexural strength values (140.24 and 156.26 MPa) of two PICNs were between that of natural enamel and natural dentin. The high flexural strength of PICNs may be attributed to the unique structure of this kind of material. The tested Vickers hardness values were 1.198 and 1.209 GPa, respectively, very close to that of natural dentin (0.13–0.92 GPa). The elastic modulus (18.69 and 18.93 GPa) of these two PICNs resembles that of natural dentin (18–24 GPa). It is the goal of dental material research to achieve a similarity of the mechanical properties of

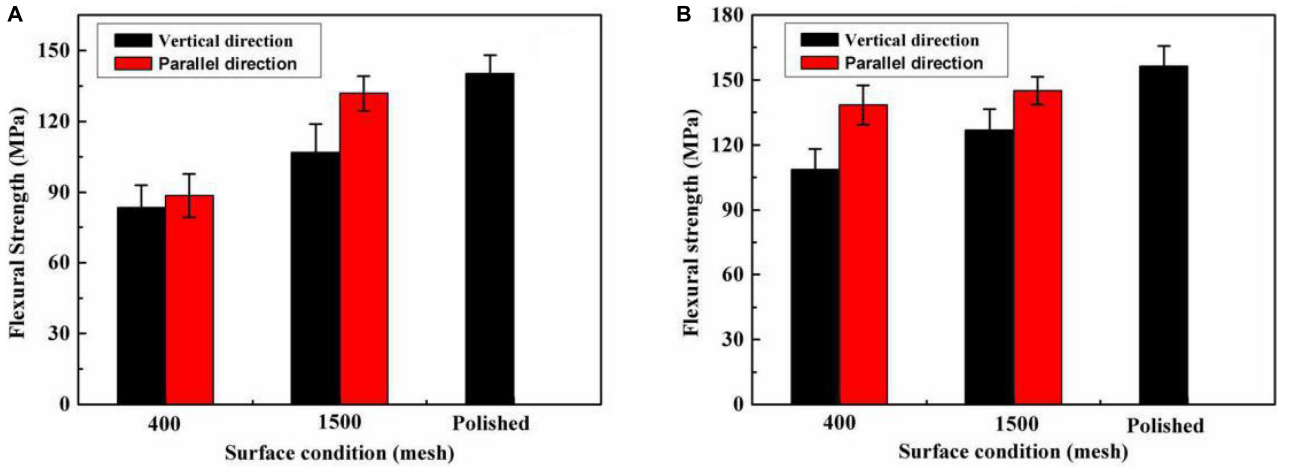

FIGURE 5 | Results of flexural strength of polymer-infiltrated ceramic networks (PICNs) with respect to surface condition. **(A)** PICN BTC which were sanded and polished with 400# and 1500# abrasive paper. **(B)** PICN UTC which were sanded and polished with 400# and 1500# abrasive paper.

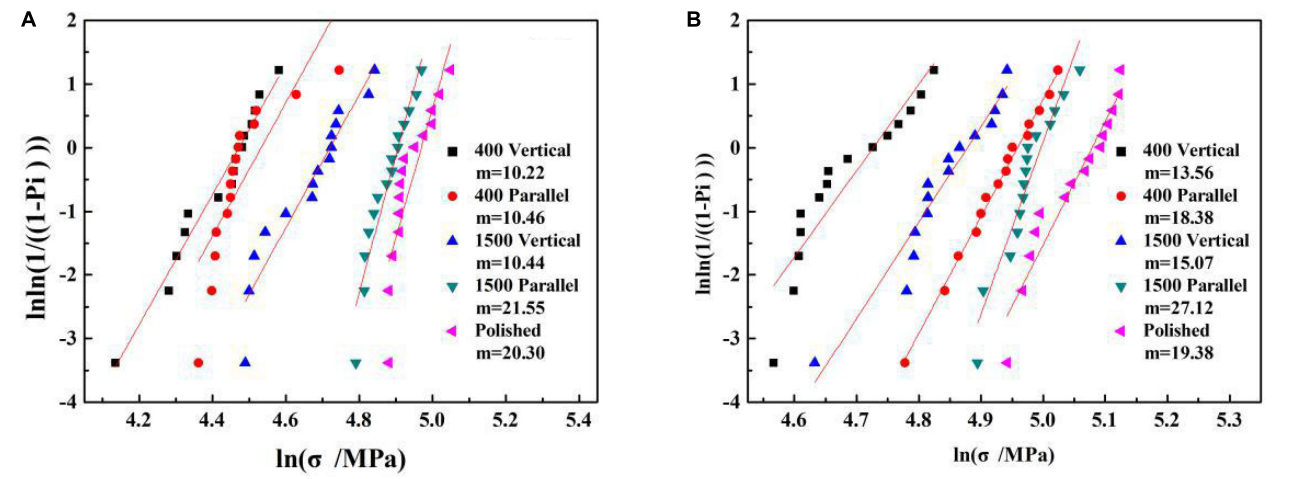

FIGURE 6 | Weibull plots of flexural strength of PICN BTC in panel **(A)** and PICN UTC in panel **(B)**.

restorative materials to that of natural enamel and dentin. The characteristics of moderate hardness and elastic modulus may be of considerable advantage, as the wear of the antagonist could be avoided.

Dental restoration involves many processes. The processing procedures during clinical adjustment, i.e., cutting, machining, grinding, polishing, sandblasting, etc., could have potential effects on the loss of strength (Al-Haj Husain et al., 2016; Curran et al., 2017; Hatanaka et al., 2017; Mohammadi-Bassir et al., 2017). Dental restorative materials are adjusted in the complicated oral environment. The surface roughness of dental materials could be affected by physical and chemical factors such as wear, food, tooth brushing, and temperature change (Da Costa et al., 2010; Heintze et al., 2010; Roselino et al., 2013, 2015; Kamonkhantikul et al., 2016). Previous studies showed that many factors could induce the increase of surface roughness which could decrease the flexural strength of restorative composites (Da Costa et al., 2010; Coldea et al., 2013; Belli et al., 2014; Al-Harbi et al., 2017). The composites used for CAD/CAM must be shaped to a final size *via* material removal before being adjusted to the areas to be restored. Sanding with abrasive paper may be an available method to produce unidirectional scratches, as shown in **Figures 1C,D,F,G**. Sanding the samples with different abrasive paper and polishing could produce a significantly different surface roughness at $p < 0.05$ (**Table 1**). For either vertical types or parallel types, the flexural strength increased with the decrease of surface roughness. The source of failure may be located at the extrinsic defects (flaws or surface cracks) in the unidirectional scratches.

The flexural strength values were compared among groups of different roughness values and defect directions. The null hypothesis was rejected as significant differences were observed for the same surface roughness values with different defect directions.

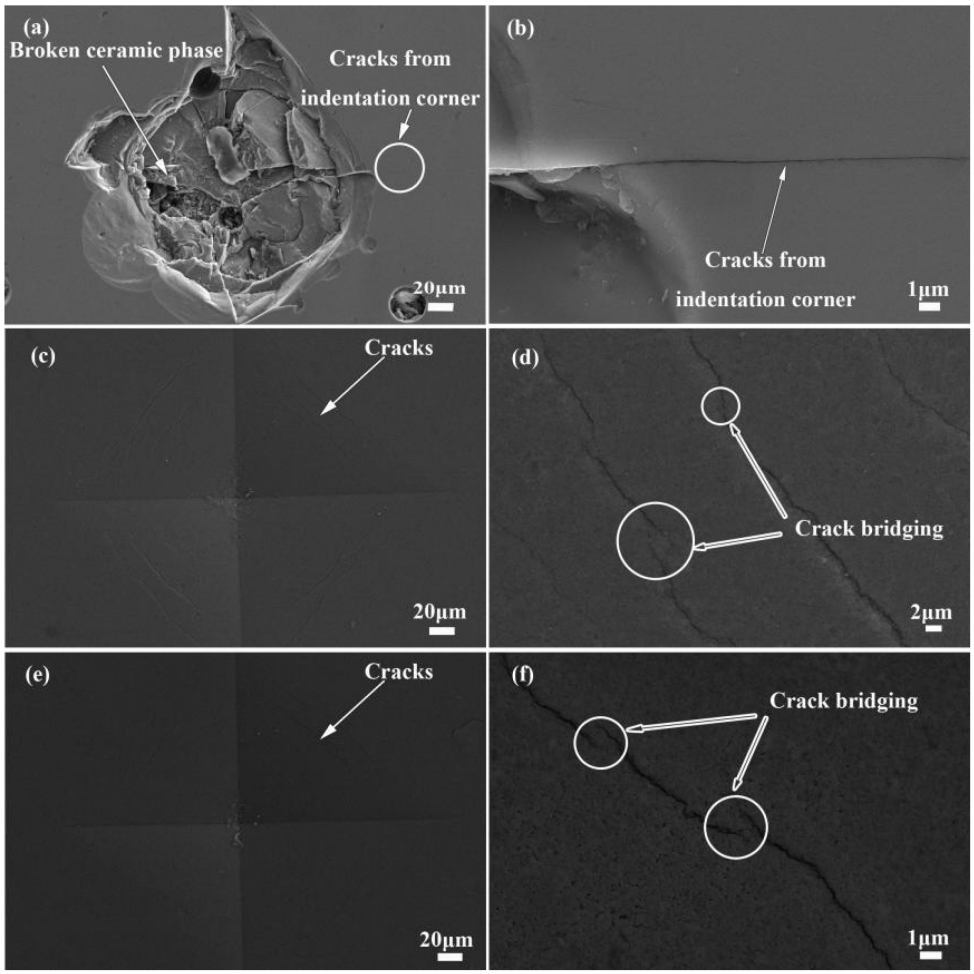

FIGURE 7 | Scanning electron microscope of indentation areas of ceramics and PICNs at an indentation load of 50 N. **(a,b)** Ceramic, **(c,d)** PICN BTC, and **(e,f)** PICN UTC.

As for PICN BTC, the effects of roughness and scratch directions on flexural strength could be observed. When the samples were sanded with 400# abrasive paper, there were no significant differences (p = 1) between vertical types and parallel types. When the samples were sanded with 1500# abrasive paper, the flexural strength of parallel types (131.77 ± 7.28 MPa) was significantly higher than that of vertical types (106.95 ± 11.93 MPa) at $p < 0.05$. There were even no significant differences between that of samples sanded with 1500# abrasive paper (parallel type) and that of thoroughly polished samples, although the roughness of the former (Pa = 311.86 nm and Pq = 366.89 nm) is obviously larger than that of the latter (Pa = 11.76 nm and Pq = 17.71 nm). As for PICN UTC, similar effects could also be observed. The scratch directions of sample surfaces could affect the flexural strength significantly for both 400# and 1500# abrasive paper-sanded samples at $p < 0.05$. The differences between the flexural strength of samples sanded with 1500# abrasive paper (parallel type) and that of polished samples could also be seen as significant at $p = 0.009$.

There was an increasing trend of Weibull modulus with the decrease of surface roughness (**Figure 3**). A low Weibull modulus indicates that there exists a big variation in surface appearance and an inhomogeneous microcrack density as suggested in some research in zirconia (Luthardt et al., 2002; Wang et al., 2008; Hatanaka et al., 2017). Sanding with higher-mesh abrasive papers or polishing could contribute to less and homogeneous microcrack dentistry, leading to higher values of Weibull modulus or a lower scatter of flexural strength values. According to the Weibull plots of flexural strength (**Figure 6**), the reliability of dental composites could be increased *via* thorough polishing.

No previous investigations were found in literature about the effects of scratch direction on flexural strength. The observations from this study suggest that this factor plays an important role in the flexural strength of dental composites. The flexural strength of parallel types was significantly higher than that of vertical types, with nearly the same surface roughness for most of the data. There existed more micro-cracks perpendicular to tensile stress, leading to the fracture of materials at a relatively low stress for vertical types. The Weibull modulus values were higher

for parallel types than for vertical types even with nearly the same surface roughness. These results indicate that the failure of restorative composites occurs with a high probability in the direction perpendicular to the force for the same roughness value.

The mechanical properties are all attributed to the unique structure. The reinforcing mechanisms of PICNs were observed by comparing the crack propagation to that of dense ceramic after indention (**Figure 7**). The crack bridging observed in PICNs indicates an enhanced resistance to crack propagation. This performance was also interpreted as R-curve (resistance curve) behavior (Swain et al., 2016). In PICNs, the constituent ceramic phase and polymer phase are mutually interconnected with each other in a three-dimensional topological structure. This unique structure enables the reinforcement phase to distribute stresses introduced to PICNs. Polymer, which plays the part of the reinforcing phase, offers effective resistance to crack propagation *via* crack bridging. This structural feature endows PICNs with an insensitive property to microcracks.

CONCLUSION

This paper has focused on the fabrication of a novel restorative composite and its characterization. The effects of surface roughness on the flexural strength of experimental PICNs were evaluated. The surface with different roughness values were produced by sanding with abrasive paper and polishing. The results indicated that both the surface roughness value and scratch directions affected the flexural strength. A large roughness value and a scratch direction perpendicular to tensile stress are detrimental to PICNs. It is suggested that these factors should be taken into consideration during clinical process. The reinforcing mechanism was analyzed. The fabricated PICNs with a unique structure may be a promising candidate for dental restoration.

DATA AVAILABILITY STATEMENT

The original contributions presented in the study are included in the article/supplementary material, further inquiries can be directed to the corresponding author.

AUTHOR CONTRIBUTIONS

YL: conceptualization, project administration, resources, and supervision. LZ: formal analysis. YL and HW: funding acquisition. BC, YS, ML, XD, and CN: methodology. QD and LZ: software. BC: writing – original draft. BC and FS: writing – review and editing. All authors discussed the results.

FUNDING

This work was financially supported by Beijing Municipal Science and Technology Commission (No. Z171100002017009), National Natural Science Foundation of China (No. 51972240) and National Science Foundation (51532003, 51221291, 51328203, and 81671026).

REFERENCES

Acar, O., Yilmaz, B., Altintas, S. H., Chandrasekaran, I., and Johnston, W. M. (2016). Color stainability of CAD/CAM and nanocomposite resin materials. *J. Prosthet. Dent.* 115, 71–75. doi: 10.1016/j.prosdent.2015.06.014

Al-Haj Husain, N., Camilleri, J., and Özcan, M. (2016). Effect of polishing instruments and polishing regimens on surface topography and phase transformation of monolithic zirconia: An evaluation with XPS and XRD analysis. *J. Mech. Behav. Biomed.* 64, 104–112. doi: 10.1016/j.jmbbm.2016.07.025

Alharbi, A., Ardu, S., Bortolotto, T., and Krejci, I. (2017). Stain susceptibility of composite and ceramic CAD/CAM blocks versus direct resin composites with different resinous matrices. *Odontology*. 105, 162–169. doi: 10.1007/s10266-016-0258-1

Al-Harbi, F. A., Ayad, N. M., ArRejaie, A. S., Bahgat, H. A., and Baba, N. Z. (2017). Effect of Aging Regimens on Resin Nanoceramic Chairside CAD/CAM Material. *J. Prosthodont.* 26, 432–439. doi: 10.1111/jopr.12408

Aljabo, A., Xia, W., Liaqat, S., Khan, M. A., Knowles, J. C., Ashley, P., et al. (2015). Conversion, shrinkage, water sorption, flexural strength and modulus of re-mineralizing dental composites. *Dent. Mater.* 31, 1279–1289. doi: 10.1016/j.dental.2015.08.149

Belli, R., Geinzer, E., Muschweck, A., Petschelt, A., and Lohbauer, U. (2014). Mechanical fatigue degradation of ceramics versus resin composites for dental restorations. *Dent. Mater.* 30, 424–432. doi: 10.1016/j.dental.2014.01.003

Coldea, A., Swain, M. V., and Thiel, N. (2013). In-vitro strength degradation of dental ceramics and novel PICN material by sharp indentation. *J. Mech. Behav. Biomed.* 26, 34–42. doi: 10.1016/j.jmbbm.2013.05.004

Curran, P., Cattani-Lorente, M., Anselm Wiskott, H. W., Durual, S., and Scherrer, S. S. (2017). Grinding damage assessment for CAD-CAM restorative materials. *Dent. Mater.* 33, 294–308. doi: 10.1016/j.dental.2016.12.004

Da Costa, J., Adams-Belusko, A., Riley, K., and Ferracane, J. L. (2010). The effect of various dentifrices on surface roughness and gloss of resin composites. *J. Dent.* 38, e123–e128. doi: 10.1016/j.jdent.2010.02.005

Denry, I., and Kelly, J. R. (2008). State of the art of zirconia for dental applications. *Dent. Mater.* 24, 299–307. doi: 10.1016/j.dental.2007.05.007

Feng, L., and Suh, B. I. (2006). The effect of curing modes on polymerization contraction stress of a dual cured composite. *J. Biomed. Mater. Res. B: Appl. Biomater.* 76, 196–202.

Ferracane, J. L. (2011). Resin composite—State of the art. *Dent. Mater.* 27, 29–38. doi: 10.1016/j.dental.2010.10.020

Ferracane, J. L., and Greener, E. H. (1986). The effect of resin formulation on the degree of conversion and mechanical properties of dental restorative resins. *J. Biomed. Mater. Res.* 20, 121–131. doi: 10.1002/jbm.820200111

Hatanaka, G. R., Polli, G. S., Fais, L. M. G., Reis, J. M. D. S., and Pinelli, L. A. P. (2017). Zirconia changes after grinding and regeneration firing. *J. Prosthet. Dent*. 118, 61–68. doi: 10.1016/j.prosdent.2016.09.026

He, L., and Swain, M. (2011). A novel polymer infiltrated ceramic dental material. *Dent. Mater.* 27, 527–534. doi: 10.1016/j.dental.2011.02.002

Heintze, S. D., Forjanic, M., Ohmiti, K., and Rousson, V. (2010). Surface deterioration of dental materials after simulated toothbrushing in relation to brushing time and load. *Dent. Mater.* 26, 306–319. doi: 10.1016/j.dental.2009.11.152

Kamonkhantikul, K., Arksornnukit, M., Lauvahutanon, S., and Takahashi, H. (2016). Toothbrushing alters the surface roughness and gloss of composite resin CAD/CAM blocks. *Dent. Mater. J.* 35, 225–232. doi: 10.4012/dmj.2015-228

Klapdohr, S., and Moszner, N. (2005). New inorganic components for dental filling composites. *Monatsh. Chem*. 136, 21–45. doi: 10.1007/s00706-004-0254-y

Lawson, N. C., Janyavula, S., Syklawer, S., McLaren, E. A., and Burgess, J. O. (2014). Wear of enamel opposing zirconia and lithium disilicate after adjustment, polishing and glazing. *J. Dent.* 42, 1586–1591. doi: 10.1016/j.jdent.2014.09.008

Lee, Y., Lim, B., and Kim, C. (2003). Difference in polymerization color changes of dental resin composites by the measuring aperture size. *J. Biomed. Mater. Res. B: Appl. Biomater*. 66B, 373–378. doi: 10.1002/jbm.b.10034

Li, R. W. K., Chow, T. W., and Matinlinna, J. P. (2014). Ceramic dental biomaterials and CAD/CAM technology: State of the art. *J. Prosthodont. Res*. 58, 208–216.

Luthardt, R. G., Holzhüter, M., Sandkuhl, O., Herold, V., Schnapp, J. D., Kuhlisch, E., et al. (2002). Reliability and properties of ground Y-TZP-Zirconia ceramics. *J. Dent. Res*. 81, 487–491. doi: 10.1177/154405910208100711

Mahoney, E., Holt, A., Swain, M., and Kilpatrick, N. (2000). The hardness and modulus of elasticity of primary molar teeth:an ultra-micro-indentation study. *J. Dent.* 28, 589–594. doi: 10.1016/S0300-5712(00)00043-9

Mitra, S. B., Wu, D., and Holmes, B. N. (2003). An application of nanotechnology in advanced dental materials. *J. Am. Dent. Assoc.* 134, 1382–1390. doi: 10.14219/jada.archive.2003.0054

Miyazaki, T., Nakamura, T., Matsumura, H., Ban, S., and Kobayashi, T. (2013). Current status of zirconia restoration. *J. Prosthodont. Res.* 57, 236–261. doi: 10.1016/j.jpor.2013.09.001

Mohammadi-Bassir, M., Babasafari, M., Rezvani, M. B., and Jamshidian, M. (2017). Effect of coarse grinding, overglazing, and 2 polishing systems on the flexural strength, surface roughness, and phase transformation of yttrium-stabilized tetragonal zirconia. *J. Prosthet. Dent*. 118, 658–665. doi: 10.1016/j.prosdent.2016.12.019

Moszner, N., and Salz, U. (2001). New developments of polymeric dental composites. *Prog. Polym. Sci.* 26, 535–576. doi: 10.1016/S0079-6700(01)00005-3

Roselino, L. D. M. R., Chinelatti, M. A., Alandia-Román, C. C., and Pires-de-Souza, F. D. C. P. (2015). Effect of brushing time and dentifrice abrasiveness on color change and surface roughness of resin composites. *Braz. Dent. J.* 26, 507–513.

Roselino, L. D. M. R., Cruvinel, D. R., Chinelatti, M. A., and Pires-de-Souza, F. D. C. P. (2013). Effect of brushing and accelerated ageing on color stability and surface roughness of composites. *J. Dent.* 41, e54–e61. doi: 10.1016/j.jdent.2013.07.005

Rueggeberg, F. A. (2011). State-of-the-art: Dental photocuring—a review. *Dent. Mater.* 27, 39–52. doi: 10.1016/j.dental.2010.10.021

Sakaguchi, R. L., and Powers, J. M. (2012). "The Oral Environment," in *Craig's Restorative Dental Materials*, 13th Edn, (Saint Louis, MO: Mosby). **Q.

Silva Prezotto, A. F., Silva, D. B., Vitti, R. P., Sinhoreti, M. A. C., and Brandt, W. C. (2018). Light curing and ratio of glass/fumed silica fillers on degree of conversion and mechanical properties of experimental composite resins. *J. Appl. Polym. Sci.* 136, 47008. doi: 10.1002/app.47008

Swain, M. V., Coldea, A., Bilkhair, A., and Guess, P. C. (2016). Interpenetrating network ceramic-resin composite dental restorative materials. *Dent. Mater.* 32, 34–42. doi: 10.1016/j.dental.2015.09.009

Thornton, I. (2014). *Mechanical properties of dental resin composite CAD/CAM blocks. Master of science*. Vancouver, BC: The University of British Columbia.

Wang, H., Aboushelib, M. N., and Feilzer, A. J. (2008). Strength influencing variables on CAD/CAM zirconia frameworks. *Dent. Mater.* 24, 633–638. doi: 10.1016/j.dental.2007.06.030

Conflict of Interest: The authors declare that the research was conducted in the absence of any commercial or financial relationships that could be construed as a potential conflict of interest.

frontiers in Materials

REVIEW
published: 23 April 2021
doi: 10.3389/fmats.2021.655495

Bioactive Synthetic Peptides for Oral Tissues Regeneration

Mercedes Bermúdez[1†], Lía Hoz[2†], Gonzalo Montoya[2†], Mikado Nidome[2], Adriana Pérez-Soria[2†], Enrique Romo[2†], Uriel Soto-Barreras[3†], Julio Garnica-Palazuelos[4], Maribel Aguilar-Medina[1], Rosalío Ramos-Payán[1] and Carlos Villegas-Mercado[4*†]*

[1]Facultad de Ciencias Químico Biológicas, Universidad Autónoma de Sinaloa, Culiacán, Mexico, [2]Facultad de Odontología, Universidad Nacional Autónoma de México, CDMX, Mexico, [3]Facultad de Odontología, Universidad Autónoma de Chihuahua, Chihuahua, Mexico, [4]Facultad de Odontología, Universidad Autónoma de Sinaloa, Culiacán, Mexico

Regenerative therapy in oral tissues has gained relevance since tissue loss due to congenital or acquired diseases as well as trauma is a major health problem worldwide. Regeneration depends on the natural capacity of the body and the use of biomaterials and bioactive molecules that can module the processes to replace lost or damaged tissues and restore function. The combined use of scaffolds, cells, and bioactive molecules such as peptides is considered the best approach to achieve tissue regeneration. These peptides can induce diverse cellular processes as they can influence cell behavior and also can modify scaffold properties, giving as a result the enhancement of cell adhesion, proliferation, migration, differentiation, and biomineralization that are required given the complex nature of oral tissues. Specifically, synthetic peptides (SP) have a positive influence on scaffold biocompatibility since in many cases they can mimic the function of a natural peptide or a full-length protein. Besides, they are bioactive molecules easy to produce, process, and modify, and they can be prepared under well-defined and controlled conditions. This review aims to compile the most relevant information regarding advances in SP for dental and periodontal tissue regeneration, their biological effects, and their clinical implications. Even though most of the SP are still under investigation, some of them have been studied *in vitro* and *in vivo* with promising results that may lead to preclinical studies. Besides there are SP that have shown their efficacy in clinical trials such as P11-4 for enamel regeneration or caries prevention and ABM/P-15 for cementum, periodontal ligament (PDL), and alveolar bone on a previously calculus- and biofilm-contaminated zone. Also, some SP are commercially available such as PTH1-34 and PepGen P-15 which are used for bone defects treatment.

Keywords: synthetic peptide, oral tissue, periodontal regeneration, dental materials, bioactive peptides, dental regeneration

OPEN ACCESS

Edited by:
Fabricio Mezzomo Collares, Federal University of Rio Grande do Sul, Brazil

Reviewed by:
Vivian Petersen Wagner, The University of Sheffield, United Kingdom
Fernanda Visioli, Federal University of Rio Grande do Sul, Brazil

***Correspondence:**
Mercedes Bermúdez
bermudezcm@uas.edu.mx
Carlos Villegas-Mercado
carlosvillegas@uas.edu.mx

[†]These authors have contributed equally to this work

Specialty section:
This article was submitted to Biomaterials, a section of the journal Frontiers in Materials

Received: *19 January 2021*
Accepted: *17 February 2021*
Published: *23 April 2021*

Citation:
Bermúdez M, Hoz L, Montoya G, Nidome M, Pérez-Soria A, Romo E, Soto-Barreras U, Garnica-Palazuelos J, Aguilar-Medina M, Ramos-Payán R and Villegas-Mercado C (2021) Bioactive Synthetic Peptides for Oral Tissues Regeneration. Front. Mater. 8:655495. doi: 10.3389/fmats.2021.655495

INTRODUCTION

A peptide can be defined as a short polymer of amino acids. Depending on the definition of different authors, sizes can vary from <20, <50, to <100 (Lien and Lowman, 2003; Sato et al., 2006; Vlieghe et al., 2010; Hamley, 2017). In the last decades, more than 7,000 native peptides (NP) with important human physiological functions have been studied (Fosgerau and Hoffmann, 2015) since they have

roles as cell adhesion motifs, structural peptides, cell-penetrating, and tumor-homing peptides, antimicrobial peptides, peptide hormones, growth factors, and matrix metalloprotease substrates, amyloid peptides, neuropeptides, peptide tags, and other miscellaneous NP (Hamley, 2017). However, NP are often not directly suitable for therapeutic use because they have intrinsic weaknesses, like poor chemical and physical stability, short circulating plasma half-life, low oral bioavailability, and rapid removal from the circulation by the liver and kidneys (Vlieghe et al., 2010; Fosgerau and Hoffmann, 2015; Erak et al., 2018; Lau and Dunn, 2018).

The use of peptides for human therapeutic began with peptides such as insulin and adrenocorticotrophic hormone (ACTH) isolated from natural sources in the first half of the 20th century (Banting et al., 1922). Further, with sequence elucidation and chemical synthesis of peptides in the 1950s, synthetic oxytocin and vasopressin entered to clinical use (Stürmer, 1989).

In recent years the pharmaceutical industry has increased attention to new therapeutic peptides, constantly reaching clinical application (Vlieghe et al., 2010; Dang and Süssmuth, 2017). By 2018 more than 60 peptides were approved by the FDA and more than 600 were in clinical and preclinical trials (Vlieghe et al., 2010; Erak et al., 2018). The production of therapeutic synthetic peptides (SP) has become possible with recent developments of solid-phase peptide synthesis (Vlieghe et al., 2010) and novel synthetic strategies allow the modulation of pharmacokinetic properties and target specificity through amino acid, backbone modification, incorporation of non-natural amino acids, and peptide conjugates (Conjugation to polyethylene glycol (PEG), lipids, and proteins such as Fc fragments) extending the half-life or improving solubility (Sato et al., 2006; Fosgerau and Hoffmann, 2015; Lau and Dunn, 2018).

Based on their chemistry, SP are categorized concerning their relationship to NP molecules: native, analog, and heterologous. A native has the same sequence as an NP product, analogs are defined as modified or substituted versions of NP with improved drug properties, and heterologous peptides were discovered independently of the natural peptide through synthetic library screening, phage display, or other methods (Sato et al., 2006; Vlieghe et al., 2010; Hamley, 2017; Lau and Dunn, 2018).

As potential therapeutics SP offer several advantages over other molecules: increased specificity, small size (increasing their potential to penetrate further into tissues) (Sato et al., 2006), excellent safety, tolerability, and efficacy profiles in humans (Fosgerau and Hoffmann, 2015). SP also have lower cost and production complexity compared with protein-based biopharmaceuticals (Fosgerau and Hoffmann, 2015). They are generally less immunogenic than recombinant proteins and antibodies, show higher activity per unit mass, and have greater stability (can be stored at room temperature for a long time). Additionally, degradation products of peptides are amino acids, and given their short half-life, few peptides accumulate in tissues, minimizing the risks of complications caused by their metabolites and the risks of systemic toxicity (Vlieghe et al., 2010).

Oral tissue regeneration is crucial since their congenital or acquired loss by trauma or diseases is a major health problem (Abou Neel et al., 2014). In this regard, the healing capacity of the body and the use of bioactive molecules able to module the processes to replace lost tissue and restore function are key. The best approach to achieve tissue regeneration is the combined use of scaffolds, cells, and bioactive molecules such as SP which can induce diverse cellular processes as they can influence cell behavior and also can modify scaffold properties. SP enhance cell adhesion, proliferation, migration, differentiation, and biomineralization that are required given the complex nature of oral tissues. Therefore, the purpose of this review is to discuss recently developed advances regarding SP for dental and periodontal tissue regeneration. Our goal is to highlight the current approaches in their applications to demonstrate their potential and at the same time to draw attention to the advances and the issues which need to be addressed for progressing in oral tissues enginnering.

DENTAL TISSUE REGENERATION

Dental caries remains the most common disease worldwide, and it is defined as pathophysiological processes in the dental biofilm that cause an imbalance in the demineralization-remineralization equilibrium, leading to a net loss of tooth minerals progressing to a cavity. This process begins by dissolution of the subsurface mineral tooth structure knowing like white spot, followed by progression to irreversible cavitation of the mineralized surface layer (Han et al., 2017; Jablonski-Momeni et al., 2019; Pandya and Diekwisch, 2019).

When a tooth is damaged by caries, the enamel and dentin are degraded by enzymes and acids from microorganisms. In this situation, the odontoblast layer in the pulp chamber releases bioactive molecules with reparative potential for dentinogenesis. However, the exact mechanism that regulates this process is unclear and dentin regeneration remains a great challenge in the clinic (Smith et al., 1995; Bleicher, 2014; Wang et al., 2014).

Additionally, after caries occur, the clinical intervention is focused on removing the infection, preserving as much natural tooth structure as possible to use adhesive restorative materials to replace the lost enamel and dentin. In the case of the pulp chamber exposition, the direct capping with calcium hydroxide ($CaOH_2$) and/or mineral trioxide aggregate (MTA) is the only clinical treatment option focused on the preservation of pulp vitality by the formation of reactionary dentin (tertiary dentin) (Huang, 2011; Hilton et al., 2013). Although these treatments have, in some cases, success rates (60–80%), nowadays, there is not an effective treatment in the clinical area to induce cellular repair of the enamel, dentin, and pulp. SP (**Figure 1**) have emerged as an alternative for the regeneration of dental organ tissues (**Table 1**).

Enamel

Dental enamel is a calcified tissue that forms the outer protective covering of the anatomical crown of a tooth and is produced by ameloblasts. However, these enamel-forming cells, as well as the enamel organ stem cells are lost at the time of tooth eruption.

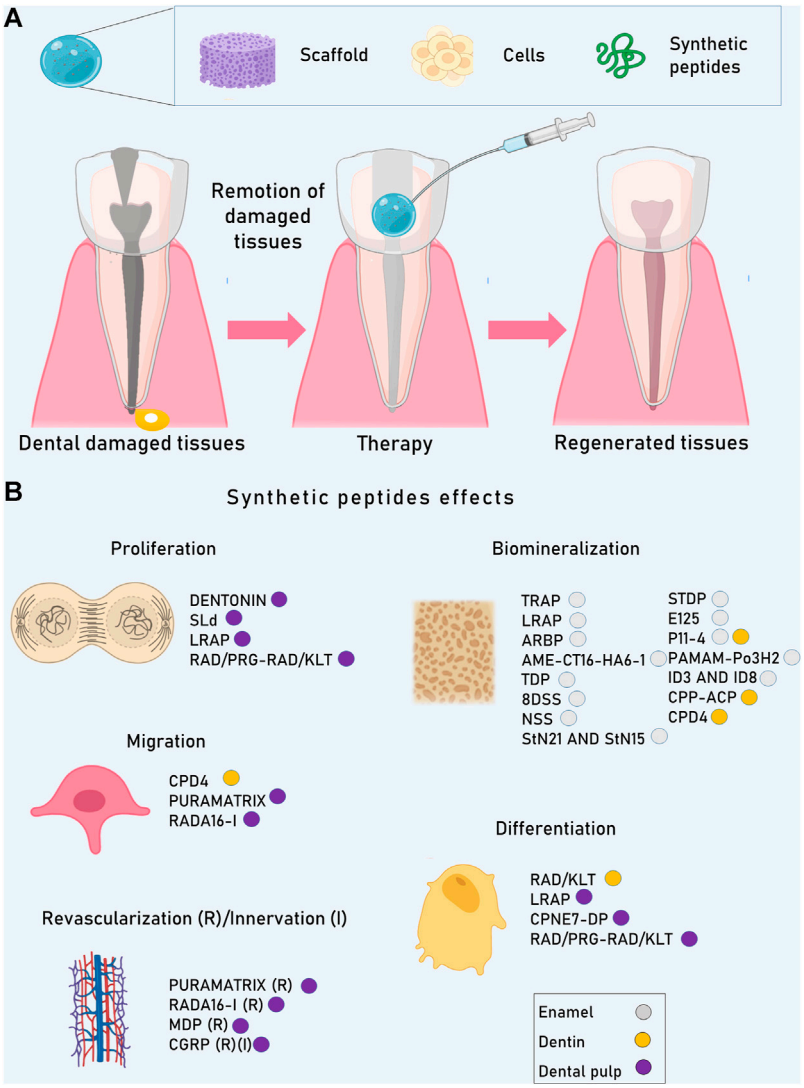

FIGURE 1 | The combined use of scaffolds, cells, and bioactive molecules such as SP is considered the best approach to achieve tissue regeneration. **(A)** Dental organs can be damaged principally by caries. Depending on the damage level, enamel, dentin or even pulp can be injured. Advances in the field of SP could be beneficial to treat and regenerate lost tissues. **(B)** SP can induce diverse cellular processes in dental tissues as they can influence cell behavior and also can modify scaffold properties, giving as a result the enhancement of cell proliferation, migration, revascularizatión, innervation, differentiation, and biomineralization.

Mature enamel is mainly composed of inorganic material (96%) formed by crystals of hydroxyapatite (HA) and a small proportion of water (3%) and proteins (1%) that bind the mineralized fibers together (Hara and Zero, 2010; Pandya and Diekwisch, 2019). Also, more than 40 trace elements have been identified in enamel, which can be incorporated in various ways: ion exchange in the hydration shell, which is the layer of water adjacent to the crystal; direct absorption on the surface of the crystal; and substitution with components of the crystal of similar size and charge. The acid solubility of a tooth and thus its caries resistance can be affected by the crystal size and shape, and the proximity of the crystals (Hara and Zero, 2010; Kind et al., 2017; González-Cabezas and Fernández, 2018; Dissanayake et al., 2020; Farooq and Bugshan, 2020).

Peptides Derived from the Amino Acid Sequence of Enamel and Dentin Proteins

Peptides derived from enamel and dentin proteins have been developed to prevent demineralization and/or promote the remineralization process (Chung and Huang, 2013; Yang et al., 2016; Buzalaf et al., 2017). For instance, amelogenin is an important protein involved in the growth and maturation of enamel crystals in the newly formed enamel matrix and is absent in mature enamel (Buzalaf et al., 2017; Farooq and Bugshan, 2020). This protein has been used to form chitosan-amelogenin hydrogel (CS-AMEL) to promotes enamel remineralization. As a result of proteolysis of amelogenin by matrix metalloproteinase 20 (MMP-20) during the biomimetic enamel regrowth, the newly

TABLE 1 | Synthetic peptides used for dental tissue regeneration.

ENAMEL			
Peptide	**Methodology**	**Effect**	**References**
Amelogenin peptide (TRAP)/(LRAP)	*In vitro* study with samples from bovine enamel and human molars Artificial lesion: 30% phosphoric acid for 10 s. Remineralization: Artificial saliva for either 5 or 10 days at 37°C	Promotes enamel crystal nucleation and growth. Improves remineralization of enamel surface lesions	Han et al. (2017); Dissanayake et al. (2020); Farooq and Bugshan (2020); Wang et al. (2020)
Amelogenin repeat-based peptide consisting of 22-residues in five tandem amelogenin polyproline repeat (GLn-Pro-X) and a seven residues hydrophilic tail	*In vitro* study in bovine permanent incisors. Artificial lesions: 50 mM acetic acid (pH 4.5), 2.2 mM $Ca(NO_3)_2$, 2.2 mM KH_2PO_4, 5.0 mM NaN_3, and 0.5 ppm NaF; at 37°C for 3 days Remineralization: 12 days at 37°C pH cycling model. Remineralization solution: 20 mM HEPES (pH 7.0), 0.9 mM KH_2PO_4, 1.5 mM $CaCl_2$, 130 mM KCl, 1.0 mM NaN_3 for 22 h *In vivo* study in rat caries model using the sprague-dawley rat model of early enamel lesions induced by *S. mutans*	Promotes the remineralization of enamel caries. Bind on the enamel surface, can stabilize amorphous calcium phosphate (ACP), it can control the crystallization of hydroxyapatite (HA)	Lv et al. (2015); Han et al. (2017); Kind et al. (2017); Mukherjee et al. (2019); Ding et al. (2020)
Ame-CT16-HA6-1 (16 carboxyl-terminal residues of amelogenin join to a sequence of SVSVG-MKSPRR denominated HA6-1)	*In vitro* study in human un-erupted third molars Artificial lesions: 37% phosphoric acid for 30 s Remineralization: Simulated saliva (1.5 mM Ca^{2+}, 0.9 mM HPO_4, and HEPES) for 7 days	In combination with carboxymethyl chitosan and ACP, form enamel-like apatite crystals and bind to demineralized enamel specifically	Chung and Huang (2013); Chung and Li (2013); Kind et al. (2017); Xiao et al. (2017); Ding et al. (2020)
Tufteline derived peptide (TDP)	*In vitro* study in human third molars Artificial lesions: 50 mM acetic acid (pH 4.5), 2.2 mM $Ca(NO_3)_2$, 2.2 mM KH_2PO_4, 5.0 mM NaN_3, and 0.5 ppm NaF at 37°C for 3 days Remineralization: 12 days pH cycling model remineralization solution: 20 mM HEPES (pH 7.0), 0.9 mM KH_2PO_4, 1.5 mM $CaCl_2$, 130 mM KCl, and 1.0 mM NaN_3 for 22 h	Nucleation of HA crystals and promotion of remineralization of initial carious lesions	Chung and Huang (2013); Chung and Li (2013); Kind et al. (2017); Xiao et al. (2017); Ding et al. (2020)
DPP-derived peptide: (8DSS)	*In vitro* study in bovine permanent incisors. Artificial lesions: 50 mM acetic acid (pH 4.5), 2.2 mM $Ca(NO_3)_2$, 2.2 mM KH_2PO_4, 5.0 mM NaN_3 and 0.5 ppm NaF at 37°C for 3 days and low-speed magnetic stirring (100 rpm). Remineralization: 12 days of pH cycling model remineralization solution: 20 mM HEPES (pH 7.0), 1.5 mM $CaCl_2$, 0.9 mM KH_2PO_4, 130 mM KCl, 1.0 mM NaN_3 for 23 h *In vivo* study in rat caries model using the sprague-dawley rat model of early enamel lesions induced by *S. mutans*	Promotes the uniform deposition of nanocrystalline calcium phosphate over demineralized enamel. Nucleates the formation of HA and inhibit demineralization	Hsu et al. (2011); Chung and Huang (2013); Chung and Li (2013); Yang et al. (2014); Yang et al. (2016); Alkilzy et al. (2018a); Ding et al. (2020)
NSS peptide (an aspartate is replaced for asparagine from DSS sequence of DPP)	*In vitro* study in human third molars Artificial lesions: 1M citric acid (pH 2) for 2 min. Remineralization: Artificial saliva (6.84 mM NaCl, 5.37 mM KCl, 5.44 mM $CaCl_2$-$2H_2O$, 4.42 mM NaH_2PO_4-$2H_2O$, 0.21 mM Na_2S-$9H_2O$ and 16.65 mM urea) at 37°C for 14 days	Promotes HA crystals formation onto the enamel surface	Chung and Huang (2013); Chung and Li (2013); Kind et al. (2017); Xiao et al. (2017); Ding et al. (2020)
StN21 and StN15	*In vitro* study in porous HA blocks Artificial lesions: 0.1 M acetic acid at pH 4 for 120 h. Modified buffer (100 mM NaCl, 40 mM KCl, 4.3 mM Na_2HPO_4, and 1.4 mM KH_2PO_4) pH 7.39 for 120 h	Bind to HA and have a protective effect on HA against acid attack	Buzalaf et al. (2017); Valente et al. (2018); Arifa et al. (2019)
Statherin-derived peptide (DpSpSEEKC)	*In vitro* study in human premolars Artificial lesions: 37% phosphoric acid for 45 s. Remineralization: Artificial saliva (1.5 mM $CaCl_2$, 0.9 mM KH_2PO_4, 130 mM KCl, 1 mM NaN_3, and 20 mM HEPES) at 37°C for 12 h	Acts as a nucleation template	Yang et al. (2017)

(Continued on following page)

TABLE 1 | (*Continued*) Synthetic peptides used for dental tissue regeneration.

ENAMEL			
Peptide	**Methodology**	**Effect**	**References**
Elastin-like polypeptide (E125)	*In vitro* study in bovine enamel Artificial lesions: 37% phosphoric acid for 1 min. Remineralization: Simulated oral fluid (137.35 mM NaCl,4.17 mM NaHCO3, 3.01mM KCl, 7.17 mM K2HPO4•3H2O, 1.53 mM MgCl2•6H2O, 20 mM HCl, 0.90 mM CaCl2, 0.51 mM Na2SO4 and tris) at 37°C for 12 h, pH 7.3	Stabilizes ACP and induces the oriented crystal growth along the original enamel apatite nanocrystals, inducing the regeneration of enamel apatite crystal structure	Lv et al. (2015); Han et al. (2017); Zhou et al. (2018)
P11-4 (N-terminally acetylated, C-terminal amidated 11 amino acid residue peptide)	*In vitro* study in human third molars. Artificial lesions: 2.2 mM $CaCl_2$, 2.2 mM NaH_2PO_4, 50 mM acetic acid; pH 4.4 for 3 days at 37°C. Remineralization: Buffer 2 mM $Ca(NO_3)_2$, 1.2 mM $KHPO_4$, and 60 mM Tris/HCl (pH 7.4) for 14 days *In vivo* study, clinical application first an uncontrolled safety trial. Then randomized controlled trial (RCT) single-blinded study. 35% phosphoric acid and application of the peptide P11-4 and waiting for 3–5 min	Induces the precipitation of HA to attract Ca2+ ions, regenerate early carious lesions (white spot lesions)	Alkilzy et al. (2018a); González-Cabezas and Fernández (2018); Arifa et al. (2019); Jablonski-Momeni et al. (2019); Üstün and Aktören (2019); Kamal et al. (2020); Li et al. (2020)
The fourth-generation polyamidoamine dendrimer (PAMAM-Po3H2)	*In vitro* study in human third molars Artificial lesions: 37% phosphoric acid. Remineralization: Artificial saliva (1.5 mmol $CaCl_2$, 0.9 mmol K_2HPO_4, 130 mmol KCl, 1 mmol NaN_3 and 20 mmol HEPES) pH 7	Induces crystal remineralization with the same structure, orientation, and mineral phase of the intact enamel in a relatively short time	Brunton et al. (2013); Kind et al. (2017); Alkilzy et al. (2018b); Arifa et al. (2019); Pandya and Diekwisch (2019); Üstün and Aktören (2019); Bröseler et al. (2020); Dissanayake et al. (2020); Farooq and Bugshan (2020); Wang et al. (2020)
ID4 and ID8 peptides self-assembly	*In vitro* study in bovine permanent incisors Artificial lesions: 50 mM acetic acid (pH 4.5), 2.2 mM $Ca(NO_3)_2$, 2.2 mM KH_2PO_4, 5.0 mM NaN_3 and 0.5 ppm NaF at 37°C for 3 days and low-speed magnetic stirring (100 rpm). Remineralization: Artificial saliva (1.5 mmol $CaCl_2$, 0.9 mmol K_2HPO_4, 130 mmol KCl, 1 mmol NaN_3 and 20 mmol HEPES) pH 7	In combination with hydrogels could serve as the template to induce HA nucleation and promote biomimetic remineralization	Brunton et al. (2013); Kind et al. (2017); Alkilzy et al. (2018b); Arifa et al. (2019); Pandya and Diekwisch (2019); Üstün and Aktören (2019); Bröseler et al. (2020); Dissanayake et al. (2020); Farooq and Bugshan (2020); Wang et al. (2020)
DENTIN			
Peptide	**Methodology**	**Effect**	**References**
CPP-ACP Random from casein digestion	*In vivo*/*In vitro* studies in extracted intact human third molar teeth. After demineralization, the samples were cover with CPP-ACP and incubated in artificial saliva	Prevention of demineralization and enhancement of remineralization of enamel and dentin lesions. The enhancement of the bond strength at the resin/dentin interface during the restorative intervention	Rahiotis and Vougiouklakis (2007); Cao et al. (2013); Sattabanasuk et al. (2014)
P11-4 $CH_3COQQRFEWEFEQQNH_2$	*In vitro* study, extracted non-carious human third molars were used to create an artificial carious lesion and treated with the P11-4 peptide	To form hydroxyapatite crystals from supersaturated solutions/remineralization of caries lesions	Koch et al. (2018); de Sousa et al. (2019)
RAD/KLT peptide KLTWQELYQLKYKGI	*In vitro* studies to evaluate cell adhesion, viability, proliferation, morphology on hydrogel scaffolds, and odontogenic differentiation of hDPSCs. Also the proliferation, migration, and tube formation of human umbilical vein endothelial cells (HUVECs) cultured with hDPSCs/SAP-conditioned medium *In vivo* study in a rat partially pulpotomized molar model to evaluate the inductive role of the RAD/KLT peptides over rDPSC to induce tissue regeneration after 28 days	Induce odontoblastic differentiation from dental pulp stem cells, and achieve dentin regeneration *in vivo*	D'Andrea et al. (2005); Xia et al. (2020)

(Continued on following page)

TABLE 1 | (*Continued*) Synthetic peptides used for dental tissue regeneration.

DENTIN			
Peptide	**Methodology**	**Effect**	**References**
CPD4 VNPKYKQKRR	*In vitro* studies with dental pulp stem cells (DPSCs) from human deciduous teeth. After osteogenic differentiation under peptides and proteins treatment, a Western blot (RUNX2, Smad1/5/8, and pSmad1/5/8, Col1, OCN, OPN, ALP, TAZ, and GAPDH) immunofluorescence (OCN, DAPI) and histological staining (ALP) were performed *In vivo*, mouse calvarial defect model with defect size of 5 mm, they used 25 animals in five groups as follows: 1) defect, 2) non-treated (NT)/collagen, 3) CDP4/collagen, 4) CPNE7/collagen, and 5) BMP-2/collagen	Cell penetration activity and regenerate mineralized tissues like bone and dentin	Creutz et al. (1998); Choung et al. (2016); Seo et al. (2017); Lee et al. (2019)
Dentonin TDLQERGDNDISPFSGDGQPFKD	*In vivo* study where agarose beads, either soaked with dentonin or unloaded, were implanted into the pulps of half-moon-shaped class V cavities on the mesial aspect of the first maxillary rat molars and examined 8, 15, and 30 days after treatment	Enhances dental pulp stem cell proliferation and promotes the regeneration of damaged dentin	Liu et al. (2004); Nagel et al. (2004); Six et al. (2007)
PULP			
Peptide	**Methodology**	**Effect**	**References**
SLd (TDLQERGDNDISPFSGDGQPFKD)	*In vitro* cytocompatibility and proliferation assays with mouse 3T3 fibroblasts, and a test for proliferation and efficacy with DSPCs and alizarin red staining were performed *In vivo* test for biodegradation: Subcutaneous dorsal implantation in female wistar rats and histological staining	Enhances dental pulp stem cell proliferation	Nguyen et al. (2018)
Leucine-Rich Amelogenin Peptide (LRAP)	*In vitro* analyses included the effects of the addition of the recombinant proteins or peptides on cell proliferation, differentiation, and adhesion of postnatal human dental pulp cells (DPCs) *In vivo* analyses were completed following the insertion of agarose beads containing LRAP or LRAP 8, 9 into exposed cavity preparations of rat molars. After 8, 15, or 30 days' exposure, the pulp tissues were analyzed for changes in histomorphometry and cell proliferation by PCNA staining	Proliferation and differentiation of dental pulp cells	Huang et al. (2012)
Copine 7 derived peptide (Cpne7-DP) (KYKQKRRSYK)	Human dental pulp cells (HDPCs) and a mouse pre-odontoblast cell line, MDPC-23, were chosen for *in vitro* studies to characterize lineage-specific cell responses after Cpne7-DP treatment *In vivo* Cpne7-DP was tested using a beagle dog model by generating dentinal defects of various degrees. Overall mineralization capacity of Cpne7-DP was tested *ex vivo*	Promotes dentin regeneration, differentiation cellular	Lee et al. (2020)
PuraMatrix™ (RAD Ac-(RADA)4-NH2)	The peptide hydrogel PuraMatrix™ was used as a scaffold system to investigate the role of dental pulp stem cells (DPSCs) in triggering angiogenesis and the potential for regenerating vascularized pulp *in vivo*. Human umbilical vein endothelial cells (HUVECs), DPSCs, or co-cultures of both cell types were encapsulated in three-dimensional PuraMatrix™ in a SCID mouse model for subcutaneous transplantation of human tooth root fragments loaded with cell/PuraMatrix™ constructs	Enables cell survival, cell migration, and capillary network formation in the absence of exogenous growth factors. Besides, DPSCs increases early vascular network formation and increases VEGF expression	Dissanayaka et al. (2015)

(Continued on following page)

TABLE 1 | (*Continued*) Synthetic peptides used for dental tissue regeneration.

PULP			
Peptide	**Methodology**	**Effect**	**References**
Peptide hydrogel RADA16-I ($COCH_3$-RADARADARADARADA-$CONH_2$)	The β-sheet and grid structure were observed by circular dichroism, SEM, and AFM. Living cell staining, proliferation, cytoskeleton in DPSCs. Migration assay in DPSCs and HUEVECs. Western blot	Self-assembly, microenvironment-simulating extracellular matrix, therapeutic delivery	Fermini et al. (2018); Mu et al. (2020)
RAD/PRG – RAD/KLT (RAD Ac-(RADA)4-NH2) (PRG Ac (RADA) 4GPRGDSGYRGDS-NH2) (KLT Ac-(RADA) 4G4KLTWQELYQLKYKGI- NH2)	*In vitro* studies; hDPSCs were isolated from extracted premolars and third molars without caries or periodontal diseases. Human umbilical vein endothelial cells (HUVECs) were obtained from the Chinese academy of sciences (category number: EAhy926). Rat DPSCs (rDPSCs) were isolated from the lower incisors of 3-weeks- old male sprague-dawley rats. Cell adhesion, viability, proliferation, morphology, and odontogenic differentiation assay were performed. Angiogenesis-inducing Activity of hDPSCs/SAP-Conditioned Medium in Matrigel matrix. *In vivo*; thirty-five 8-week-old male sprague-dawley rats divided into 7 groups (n = 5 animals per group). In groups, 1 through 6, the dental pulp under the occlusal surface of the left upper first molar was exposed and partially pulpotomized the residual pulp was implanted with one or a mixed SP with rDPSCs for 28 days	Shows an enhanced regenerative and reparative effect on a pulpotomized molar rat model, achieving pulp recovery and dentin regeneration	Xia et al. (2020)
Multidomain peptide (MDP)	An *ex vivo* mandible organ culture model was used. MDP hydrogel scaffolds were injected either at the interface of the odontoblasts and the dentin or into the pulp core of mandible slices and subsequently cultured for up to 10 days. Histological (alizarin red staining) and immunohistochemical analysis (dentin sialophosphoprotein, (collagen III, MMP2) were performed	Scaffolds design and self-assembly, release/ delivery, and bioactivity	Moore et al. (2015); Seyhan, 2019, (172)
Calcitonin gene-related peptide (CGRP)	Commercially available DPSCs were treated with varying doses of CGRP, and metabolic activity, viability, proliferation, and cell death were evaluated using 3-(4,5-dimethylthiazol-2yL)-2,5-diphenyl tetrazolium bromide assays, trypan blue staining, 5-bromo2′-deoxyuridine cell proliferation assay, and caspase-3 staining, respectively. DPSC differentiation was assessed with alizarin red staining and by quantifying messenger RNA expression of odontoblast makers	Mediating neurogenic inflammation, vascular and innervation in the pulp, and healing of periapical lesions is extensively	Caviedesbucheli et al. (2008); Michot et al. (2020)

grown enamel-like layer exhibits well-regulated crystal growth and improved composition, structure, and mechanical properties of artificial enamel (Yarbrough et al., 2010; Buzalaf et al., 2017; Prajapati et al., 2018; Bröseler et al., 2020; Farooq and Bugshan, 2020).

The tyrosine-rich peptides (TRAP) domain derived from amelogenin N-terminus has been associated with matrix self-assembly meanwhile, the amelogenin central polyproline repeat region could control crystal spacing, and the hydrophilic C-terminus facilitates amelogenin protein solubility and its adhesion to the crystal surface (Han et al., 2017; Dissanayake et al., 2020; Farooq and Bugshan, 2020; Wang et al., 2020). On the other hand, leucine-rich peptides (LRAP) can promote both, enamel crystal nucleation and growth in mouse models (Ding et al., 2020). LRAP improves the remineralization of enamel surface lesions on extracted teeth *in vitro* more effectively than full-length amelogenin (Han et al., 2017; Dissanayake et al., 2020; Farooq and Bugshan, 2020; Wang et al., 2020) and has been modified with phosphorylation using a calcium and phosphate-rich solution forming spherical nanoparticles in a linear chain-like pattern. These self-assembled peptides formed spherical amorphous calcium phosphate (ACP) particles and triggered ACP to hydroxyapatite phase transformation (Ieong et al., 2011; Bagheri et al., 2015; González-Cabezas and Fernández, 2018; Arifa et al., 2019; Mukherjee et al., 2019; Pandya and Diekwisch, 2019; Dissanayake et al., 2020; Farooq and Bugshan, 2020).

There is also an amelogenin repeat-based peptide that consists of 22-residues in five tandem polyproline repeat (GLn-Pro-X) and a seven residues hydrophilic tail. This peptide has shown the ability to promote the remineralization of enamel caries in an *in vitro* pH-cycling system. Besides, it could bind on the enamel

surface, and can stabilize ACP, meanwhile is able to control the crystallization of HA, and promotes the remineralization of caries lesion (Lv et al., 2015; Han et al., 2017; Kind et al., 2017; Mukherjee et al., 2019; Ding et al., 2020). Finally, the chimeric peptide Ame-CT16-HA6-1 is formed by 16 carboxyl-terminal residues of amelogenin attached to a sequence of SVSVGMKSPRR denominated HA6-1. This peptide in combination with carboxymethyl chitosan and ACP forms enamel-like apatite crystals and binds to demineralized enamel specifically to achieve rapid remineralization (Chung and Huang, 2013; Chung and Li, 2013; Kind et al., 2017; Xiao et al., 2017; Ding et al., 2020).

An important non-amelogenin protein synthesized by ameloblast is tufteline, which induces and regulates the initial mineralization of enamel owing to its acidic nature. Tufteline contains a self-assembly domain near the C-terminus and an anionic domain near the N-terminus that could be involved in the initial crystallization of enamel. The tufteline derived peptide (TDP) has a significant effect on the nucleation of HA and remineralization of initial carious lesions *in vitro*, suggesting that this peptide has the potential to regenerate the structure and mechanical properties of enamel (Chung and Huang, 2013; Chung and Li, 2013; Kind et al., 2017; Xiao et al., 2017; Ding et al., 2020).

On the other hand, a dentin phosphoprotein (DPP)-derived peptide constituted of octuplet repeats of aspartate-serine-serine (8DSS), has been applied to the enamel surface to prevent leaching of ions from the enamel surface and to promote the uniform deposition of nanocrystalline calcium phosphate over demineralized enamel surface given that this peptide possesses the ability to bind calcium and phosphate ions from the saliva (Yarbrough et al., 2010; Hsu et al., 2011; Buzalaf et al., 2017; Bröseler et al., 2020; Farooq and Bugshan, 2020). When 8DSS is combined with fluoride shows a more effective synergistic interaction to inhibit demineralization, reducing the concentration of fluoride used to prevent caries. (Hsu et al., 2011; Chung and Huang, 2013; Chung and Li, 2013; Yang et al., 2014; Yang et al., 2016; Alkilzy et al., 2018a; Ding et al., 2020). Finally, an NSS peptide is obtained when an aspartate is replaced for asparagine from the DSS sequence of DPP. NSS enhances the formation of HA crystals onto the enamel surface when compared whit non-peptide treatment (Chung and Huang, 2013; Chung and Li, 2013; Kind et al., 2017; Xiao et al., 2017; Ding et al., 2020).

Peptides Non-Derived from the Amino Acid Sequence of Enamel and Dentin Proteins

Several studies have shown that specific salivary proteins such as histatin, statherin, mucins, and cystatins play an important role to protect against dental caries (Buzalaf et al., 2017; Valente et al., 2018; Arifa et al., 2019; Wang et al., 2020). For instance, statherin derived peptides containing at least 15 N-terminal residues (StN21 and StN15) bind to HA and enhance remineralization (Buzalaf et al., 2017; Valente et al., 2018; Arifa et al., 2019). Also, the statherin-derived peptide (DpSpSEEKC) can act as a nucleation template and can gather calcium ions to a high concentration given its secondary structure or its negatively charged groups when is incubated in artificial saliva (Yang et al., 2017).

Another studied peptide is the elastin-like polypeptide (E125) which is rich in acidic amino acids and can stabilize ACP, and induces the orientation of crystal growth along the original enamel apatite nano-crystals, resulting in regeneration of the enamel apatite crystal structure including both the prismatic and inter-prismatic structures in oral simulated environment (Lv et al., 2015; Han et al., 2017; Zhou et al., 2018).

Self-Assembled Peptides

Regarding self-assembled peptides, these can form a three-dimensional scaffold and can promote early caries/white lesion remineralization (Pandya and Diekwisch, 2019; Bröseler et al., 2020; Dissanayake et al., 2020; Farooq and Bugshan, 2020; Li et al., 2020). For instance, P11-4 is an N-terminally acetylated, C-terminal amidated, 11 amino acid residue peptide. This β-sheet forming self-assembling peptide possesses anionic groups in the side chains that attract Ca^{2+} ions, diffuses well into the body of the caries lesions due to its low viscosity, and triggers self-assembly within the lesion inducing the precipitation of HA *in situ*. A single application of P11-4 improves the appearance of white spot lesions after 180 days in a small-scale clinical study (Alkilzy et al., 2018a; González-Cabezas and Fernández, 2018; Arifa et al., 2019; Jablonski-Momeni et al., 2019; Üstün and Aktören, 2019; Kamal et al., 2020; Li et al., 2020). However, more evidence is still needed before this peptide can be used in caries prevention and regular therapy (Alkilzy et al., 2018a; González-Cabezas and Fernández, 2018; Arifa et al., 2019; Jablonski-Momeni et al., 2019; Üstün and Aktören, 2019; Kamal et al., 2020; Li et al., 2020).

In the case of the fourth-generation polyamidoamine dendrimer (PAMAM-Po3H2) which mimic the self-assembly behavior of amelogenins, it is used as an organic template to induce crystal remineralization with the same structure, orientation, and mineral phase of the intact enamel in a relatively short time (Brunton et al., 2013; Kind et al., 2017; Alkilzy et al., 2018b; Arifa et al., 2019; Pandya and Diekwisch, 2019; Üstün and Aktören, 2019; Bröseler et al., 2020; Dissanayake et al., 2020; Farooq and Bugshan, 2020; Wang et al., 2020). Another strategy is to form films by amyloid-like lysozyme to obtain β-sheet stacked, which are combined with synthetic peptide based on the functional domains of C-terminal of amelogenin to promotes the oriented growth of HA crystals, which have a hardness and interfacial bonding stability higher than those of enamel repaired by fluoride. (Brunton et al., 2013; Kind et al., 2017; Alkilzy et al., 2018b; Arifa et al., 2019; Pandya and Diekwisch, 2019; Üstün and Aktören, 2019; Bröseler et al., 2020; Dissanayake et al., 2020; Farooq and Bugshan, 2020; Wang et al., 2020).

ID4 and ID8 are peptides with shorter and optimized sequence patterns that are programmed to self-assembly into predefined conformations and nanostructures and in combination with hydrogels could serve as the template to induce HA nucleation and promote biomimetic remineralization of initial caries lesions. (Brunton et al., 2013; Kind et al., 2017; Alkilzy et al., 2018b; Arifa et al.,

2019; Pandya and Diekwisch, 2019; Üstün and Aktören, 2019; Bröseler et al., 2020; Dissanayake et al., 2020; Farooq and Bugshan, 2020; Wang et al., 2020).

Dentin

Dentin comprises the major mineralized part of the tooth and it is cover and protected by enamel in the tooth crown and surrounded by cementum in the radicular portion. The responsible cells in the dentin formation are the odontoblast, these cells are long-living post-mitotic cells (comparable to cardiomyocytes and neurons in the fact that they are stable and are not replaced throughout the whole life of a tooth) (Sasaki and Garant, 1996; Goldberg et al., 2011; Kawashima and Okiji, 2016). Its inorganic matrix is composed of HA crystals while its organic matrix is mainly composed of a collagenous structural component, formed of collagen type I (about 90%), collagen type III and V, and a small quantity of organic matrix molecules (proteoglycans of chondroitin sulfate (biglycan and decorin), heparan sulfate (perlecan and entactin), keratan and dermatan sulfate. It has also non-collagen proteins that participate in the mineralization process. These proteins are members of the SIBLING family (small integrin-binding ligand N-linked glycoprotein) and include the sialophosphoprotein (DSPP), dentin matrix protein 1 (DMP-1), osteopontin (OPN), matrix extracellular phosphoglycoprotein (MEPE), and integrin-binding sialoprotein (IBSP) (Huang et al., 2008; Zhang et al., 2010) Due to odontoblast specifically expresses DSPP and DMP-1, these proteins are considered specific markers for these cells (Staines et al., 2012).

The dentin-pulp complex regeneration has two major limitations: 1) When the reactionary dentin has been formed, is permeable and fragmentable, resulting in microorganisms recontamination. This problem is caused by the poor attachment of the biomaterials to the dentin and lack of dental pulp stem cells (DPSCs) induction. 2) The second limitation is the pulp necrosis which avoids the blood supply to the exposed wall. The approach to overcome these problems is to create strategies to improve the adhesion of the biomaterials to dentin, promoting the HA nucleation, and the development of scaffolds with molecules that provide signals for dentinogenesis (Piva et al., 2014; Fawzy El-Sayed et al., 2019; Moussa and Aparicio, 2019). In this regard, the development of peptide therapies and biomaterials functionalized with peptides to promote dentinogenesis in the dentin-pulp complex are increasing and are presented below.

Casein Phosphopeptide with Amorphous Calcium Phosphate (CPP-ACP)

This agent is based on a nano-complex of the milk protein casein-phosphopeptide (CPP) combined with ACP and it has been used for the prevention of demineralization and enhancement of remineralization of enamel and dentin lesions (Rahiotis and Vougiouklakis, 2007). Its mechanism of action involves the fixing of calcium phosphate under neutral or alkaline pH solutions and promoting their assembling in HA on the dentin surface. Its biological mechanism allows the replacement of the minerals in the intra and interfibrillar collagen spaces after demineralization is covered with CPP-ACP and incubated with artificial saliva. The experimental result of this therapy over dentin samples of extracted intact human third molar is the enhancement of the bond strength at the resin/dentin interface during the restorative intervention (Cao et al., 2013; Sattabanasuk et al., 2014). Nevertheless, the results do not reflect what occurs at the bonding interface in a clinical situation since some conditions cannot be replicated *in vitro* such as the volume of cement or cement thickness, the surface area of adhesion, and the cavity configuration.

Self-Assembling Peptide P11-4

P11-4 is a rational designed biomimetic peptide that has self-assembling behavior into beta-sheet fibrillar hydrogel at pH <7 (Koch et al., 2018). This peptide attracts calcium ions and form HA crystals from supersaturated solutions such as saliva and binds to collagen I in dentin tissue acting as a protector against proteolytic activity of collagenases in artificial dentin caries. These characteristics show that this peptide could be as a pretreatment of caries-affected dentin enhancing significantly the performance of the bond interface over time (de Sousa et al., 2019).

RAD/KLT Peptide

KLT peptide is formed by the amino acids 17–25 of the vascular endothelial growth factor (VEGF) and activates VEGF receptors inducing angiogenesis (D'Andrea et al., 2005). When this peptide is coupled to the beta-sheet self-assembling peptide RAD (Ac-RADARADARADA) to create the RAD/KLT peptide (Ac-$(RADA)_4G_4$KLTWQELYQLKYKGI- NH_2) forms, a gel of nanofibers of 16 nm that induces the odontoblastic differentiation from DPSCs. When this peptide is mixed with the self-assembling PRG peptide (Ac-$(RADA)_4$GPRGDSGYRGDS-NH_2), provides binding motifs for integrins by directly coupling a 2-unit RGD binding sequence to RAD (Xia et al., 2020). DPSCs grown on RAD/PRG/KLT shows improved survival and can be differentiated to angiogenic and odontogenic phenotypes *in vitro*. Histological and functional evaluations of a partially pulpotomized rat model showed its capability to stimulate pulp and dentin regeneration *in vivo* over the course of 28 days (Xia et al., 2020).

Derived Peptides from Calcium Phospholipid-Binding Protein, Copine 7 Protein (CPNE7)

The CPNE7 is a member of the family CPNE proteins which are Ca^{2+} dependent and phospholipid-binding proteins (Creutz et al., 1998), it induces reparative dentin and odontoblast differentiation from mesenchymal stem cells (Choung et al., 2016; Seo et al., 2017). Given its short half-life, some bioactive peptides derived from the sequence 321–360 (STTFEEMQKA FEEGQAQWDC VNPKYKQKRR SYKNSGVVL) region of CPNE7 have been developed. CPD4: VNPKYKQKRR, have shown an enhanced cell-penetrating activity as well as osteogenic efficiency in DPSCs. It also induces the expression of biomineralization markers *in vitro* and when is mixed with collagen gel, forms mineralized tissue in the calvaria rat defects model. These results suggest that CPD4 peptide has the potential to be used as a biotechnological material to

regenerate mineralized tissues like bone and dentin (Lee et al., 2019).

Dentonin

Dentonin or AC-100 is an SP derived from the central region of MEPE protein (residues 242–264: TDLQERGDNDISPFSGDGQPFKD). This peptide includes an integrin-binding sequence (RGD), a glycosaminoglycan-attachment sequence (SGDG), and a calcium-binding motif (Six et al., 2007). Dentonin peptide stimulates human bone marrow stromal cell proliferation and differentiation into osteoblast precursors and enhances dental pulp stem cell proliferation *in vitro* (Liu et al., 2004; Nagel et al., 2004). Also, it has been shown that agarose beads soaked with a solution of 5 mg dentonin/0.5 ml PBS and implanted into rat molars pulps promote pulp cell proliferation and reparative dentin formation at day 8, suggesting that dentonin promotes the regeneration of damaged dentin (Six et al., 2007).

Dental Pulp

The dental pulp is a soft ecto-mesenchymal tissue surrounded by dentin and it is highly vascularized and highly innerved. It consists of 75% water and 25% organic material. It contains a heterogeneous population of cells such as fibroblastic cells, stem cells, capillary blood vessels, peripheral nerves, lymphatic elements, as well as cells from the immune system, extracellular matrix represented by fibers, and fundamental substance. Collagen fibers are concentrated to form supporting elements for blood vessels and nerve trunks that course from the root apex to the coronal pulp chamber (Garant, 2003; Yoshida et al., 2020).

The pulp tissue is unique given its volume and its confinement within the dentin. It has little blood supply, except in the apical foramen, and lacks collateral blood supply, hindering infection eradication by the immune system (Yoshida et al., 2020). Dental pulp is an important component of teeth and plays important roles in 1) forming the dentin: this is the essential function of the pulp and it is maintained as long as the pulp is vital. The cells in charge of producing it are the odontoblasts. Depending on the moment in which it is produced, different types arise: primary, secondary and tertiary, 2) nutrition: the pulp is responsible for nourishing the dentine through the odontoblastic extensions and metabolites coming from the pulp vascular system, 3) sensitive: in the face of stimuli, aggression or pain, the pulp is capable of responding; in the sensitivity of the pulp, no matter the nature of the stimulus, there will always be a painful response, and 4) defense/repairing: it includes the ability to form dentin in the face of aggression (Zero et al., 2011; Mu et al., 2020).

Dental pulp is considered one of the most difficult tissues to regenerate given the loss of fibrous connective tissue and its anatomical distribution. The process of pulp regeneration begins with the revascularization as it plays a fundamental role in the reparative processes of dentin tissues and the homeostasis of the dentin-pulp complex itself (Saghiri et al., 2015; Kim, 2017; Jung et al., 2019). In the field of regenerative endodontics, the most important point is to provide a favorable environment to achieve the regeneration of the lost tissues. Thus, crucial factors such as cells, scaffolds, and signaling molecules are required.

Peptides for Dentin-Pulp Complex Regeneration

SLd peptide is a minimally invasive injectable peptide scaffold that was developed from Dentonin sequence and demonstrated to be a self-assembled platform to support DPSCs and stromal cells in a biomimetic hydrogel environment. This peptide supports the proliferation of DPSCs and increases calcium phosphate deposition being cytocompatible to other critical stromal cells found in the dental pulp (Nguyen et al., 2018).

In the case of LRAP plus amelogenin exons 8 and 9 peptide (LRAP 8, 9), it was used to determine their effects on odontoblasts and dental pulp cells (DPCs). *In vitro* LRAP 8, 9 demonstrated to promote DPCs proliferation and differentiation to a greater extent than LRAP. These data suggest that amelogenin exons 8 and 9 may be useful in amelogenin-mediated pulp repair cell proliferation (Huang et al., 2012).

Another peptide is Cpne7-DP, which can be placed on 0.5% fibrin gel and then transplanted subcutaneously into immunocompromised mice. Twelve weeks after the transplantation, the Cpne7-DP treatment group showed the formation of dentin-pulp-like tissue with cells inserting long cellular processes into the tubule-like structure formed within newly mineralized tissue (Lee et al., 2020).

Peptide Scaffolds

The self-assembling peptide hydrogel PuraMatrix™ is a repeating polymer of the amino acid sequence RADA and is formulated as an injectable scaffold that assembles into nanofibers when is exposed to physiologic concentrations of salts. The SP has been used to investigate the role of DPSCs in triggering angiogenesis and the potential to regenerate vascularized pulp *in vivo*. The nanofiber microenvironment provided by this SP enables cell survival, cell migration, and capillary network formation in the absence of exogenous growth factors. Besides, an *in vivo* study shows that DPSCs increases early vascular network formation and increases VEGF expression in a mice model (Dissanayaka et al., 2015).

The RADA16-I sequence is a self-assembled peptide hydrogel that has amino acids positively (arginine) and negatively (aspartic acid) charged, and hydrophobic residues (alanine). It promotes the formation of hydrophobic and hydrophilic faces for B-sheets; it also promotes the migration of cells like DPSCs and the angiogenesis of human umbilical vein endothelial cells (Mu et al., 2020). Another SP is the functionalized scaffold RAD/PRG/KLT which shows an enhanced regenerative and reparative effect on a pulpotomized molar rat model, achieving pulp recovery and dentin regeneration *in vivo* (Xia et al., 2020).

The multidomain peptide (MDP) scaffolds can be used as injectables, bioactive, and biodegradable hydrogel scaffolds for tissue regeneration. It is a short sequence of amino acids that self-assemble to form fibers in an aqueous solution. The sequence $K(SL)_3RG\ (SL)_3KGRGDS$ is compatible with the dental pulp and promotes differential responses depending on the cell type

(Moore et al., 2015). It has been shown that subcutaneous transplantation of the hydrogel within dentin cylinders into immunocompromized mice led to the formation of a vascularized soft connective tissue similar to dental pulp, supporting the use of this biomaterial as a candidate for regenerative endodontics (Galler et al., 2012).

Synthetic Neuropeptides

Neuropeptides are defined as peptide neurotransmitters or neuromodulators. Multiple studies have demonstrated that trigeminal afferent neurons express Calcitonin gene-related peptide (CGRP), which innervates the dental pulp and also increases the expression of proteins associated with dentine formation in human pulp cells. CGRP and substance P mediate neurogenic inflammation and contribute to reparative dentin production and pulp tissue regeneration (Caviedesbucheli et al., 2008; Michot et al., 2020).

PERIODONTAL REGENERATION

The concept of periodontium includes a set of tissues that comprise the root cementum, alveolar bone, gingiva, and a functionally oriented PDL. Periodontal tissue damage affects dental organ support; hence, gingivitis and periodontitis are commonly caused by trauma or bacterial infection (Elango et al., 2020). These diseases attempt against periodontium homeostasis, causing tooth-loss (Polimeni et al., 2000).

As for every dental tissue replacement, it is necessary to mimic the physical and mechanical properties of naturally formed tissues (Yen and Yelick, 2011). Another challenge for restoring damaged periodontium is the fact that the inductive microenvironment given during the formation of periodontal tissues, is not the same after total development of the tooth (Liang et al., 2020). Although structure and function could be partially restored (Liang et al., 2020) through enamel matrix, grafting materials, guided tissue regeneration technique (GTRT), the use of growth factors, and stem cells, all of them present difficulties to be successful. Since natural microenvironmental characteristics are almost impossible to imitate, research focuses on biomimetic systems that combine natural or synthetic molecules like peptides (**Table 2**), amino acids and even cells with diverse biomaterials to build cell-3D scaffolds that enhance cell-material interactions (Elango et al., 2020). SP could be used as scaffolds or signals to achieve periodontal regeneration (**Figure 2**).

Periodontal Ligament

The PDL is a specialized connective tissue located around dental roots and serves as an anchor to the alveolar bone, controls tooth homeostasis, allowing its reparation and nutrition (Tomokiyo et al., 2019). The PDL consists of well-organized collagen fibers that anchor the root cement with alveolar bone, thus, is critical for periodontal regeneration (Liang et al., 2020). The extracellular matrix of these tissues is composed of members of the collagen family, proteoglycans, and a heterogeneous set of glycoproteins.

The PDL also acts as a sensory organ necessary for the proper positioning of the jaws during mastication with very high adaptability to rapid changes in applied forces and the capacity to maintain its width (McCulloch and Melcher, 1983). PDL fibroblasts are the dominant heterogeneous cell population in the PDL, being capable to differentiate into cementoblasts and osteoblasts (Roberts et al., 1982; McCulloch and Melcher, 1983). There is a low level of periodontal ligament stem cells (PDLSCs), which possess the capacity to differentiate into periodontal ligament fibroblasts, cementoblasts, and osteoblasts. In this regard, is important the distinction between PDLSCs and PDL fibroblast populations since PDLSCs are normally quiescent and can be only activated during tissue damage. Other cell types include the epithelial cell rests of Malassez, monocytes, macrophages, cementoblasts, osteoblasts, fibroblasts, myofibroblasts, nerve cells, epithelial cells, and endothelial cells (Barczyk et al., 2000; Bartold et al., 2000). Thus, PDL is a complex tissue and its regeneration is hampered since it is mandatory the control of infection and inflammation to then promote cell adhesion, proliferation, and differentiation for new tissue formation (Liang et al., 2020).

One of the first attempts for restoring PDL was the use of Enamel matrix derivative (EMD) obtained from animal tissue. Then, a synthetic oligopeptide derived from EMD was developed, showing enhancement of proliferation of PDLSCs (Kato et al., 2013). However, its functional mechanisms are still not entirely clear.

Another extensively studied peptide is the tri-amino acid sequence, arginine-glycine-aspartate (RGD) which has been demonstrated to improve the attachment of several cell types to different materials (Hautanen et al., 1989; Aota et al., 1994). Besides, RGD mixed with extracellular matrix (EMC) proteins, reduces the risk of immune reactivity or pathogen transfer (Bellis, 2011), and *in vitro* studies has shown that synthetic RDG conjugated with poly-L-lysine backbone and oligo-DL-alanine or with L-serine-oligo-DL-alanine increases cell adhesion and migration of PDL-derived cells, which is promising for periodontal regeneration (Khorolsuren et al., 2020). Also, the integrin-binding cyclic and linear synthetic RGD-EPRGDNYR has shown enhancement of attachment, cell proliferation, and spreading of PDLC, being the cyclic forms of EPRGDNYR-BSA the most effective (Grzesik et al., 1998). A fibronectin peptide containing their RGD and PHSRN sequences coupled with six glycines (G3PHSRNG6RGDG) is able to enhance attachment and spreading of human PDLC by increasing ERK1/2 activity. This SP could be used to improve the environment for PDLC and achieve periodontal regeneration (Kim et al., 2004).

The ameloblastin-derived peptide (VPAFPRQPGTPGVASL) was first related to an increase in cell attachment and proliferation of PDL cells (PDLC), acting as a growth factor during periodontal regeneration (Zeichner-David et al., 2006). Recent studies do not show effects over proliferation of PDLC, but a stimulating effect on the mineralization capacity of PDLC (Kitagawa et al., 2011).

A peptide matrix named dendritic lysine-appended polydiacetylene (Lys-PDA) has shown the promotion of cell

TABLE 2 | Synthetic peptides used in periodontal tissues regeneration.

PERIODONTAL LIGAMENT			
Peptide	**Methodology**	**Effect**	**References**
Oligopeptide derived from EMD (OP-EMD) (WYQNMIR)	*In vitro* study with human mesenchymal stem cells. Solid-phase peptide synthesis + "tea-bag" methodology, cell proliferation assay, alkaline phosphatase activity, measurement of procollagen type 1 C-Peptide, osteocalcin production, mineralization assay, extracellular signal-related kinases (ERK) were performed	Enhanced proliferation of PDL cells, as well as ALP activity, expression of osteonectin, osteocalcin production, the formation of calcified nodules, and mineralization	Kato et al. (2013)
Integrin-binding cyclic and linear synthetic RGD-EPRGDNYR. (EPRGDNYR) linear and cyclic	*In vitro* study with human PDLSCs. PDL cells adhesion, proliferation, and the *novo* protein synthesis *in vitro*	For attachment, cell proliferation, and spreading, the cyclic forms of EPRGDNYR-BSA conjugate were most potent than linear conjugate. The effects of all collagen/conjugate mixtures were equivalent to that of type I collagen	Grzesik et al. (1998)
Fibronectin peptide containing their RGD and PHSRN sequences coupled with six glycines (FP-RGD-PHSRN) (G3PHSRNG6RGDG)	*In vitro* study with human PDL cells. The cells were applied to peptide-coated wells at a density of 1×10^4/well. After 1 h incubation at 37°C, adhered cells were fixed, stained, and examined by phase contrasts microscopy for cell spreading assay. The attached PDL cells were solubilized with 2% sodium dodecyl sulfate (SDS) for the cell attachment assay by measuring absorbance at 595 nm in a microplate reader. Western blot analysis was performed to determine extracellular signal-regulated kinase (ERK1/2) activity	Enhances attachment and spreading of human PDLC by increasing ERK1/2 activity	Kim et al. (2004)
Ameloblastin peptide, based on the 16 amino acid sequence of the N-terminal porcine ameloblastin. (AMB-DP) (VPAFPRQPGTPGVASL)	*In vitro* study with PDLC. Ameloblastin peptide synthesized by a pink technology method, cell proliferation assay, and alkaline phosphatase activity, inhibition assay with anti-ameloblastin antibody, mineralization assay, and RT-PCR were performed	Increase in cell attachment and proliferation of PDL cells. Stimulates ALP activity in a dose-dependent manner, promotes mineralized nodule formation by PDL cells, and upregulates ALP and bone sialoprotein (BSP)	Zeichner-David et al. (2006); Kitagawa et al. (2011)
Dendritic lysine-appended polydiacetylene (Lys-PDA)	*In vitro* study with human PDLSCs. hPDL cell viability, adhesion, and spreading on Lys-PDA, FDA/PI live/dead assay, MTT assay, actin cytoskeleton staining, osteogenic differentiation, and alizarin red staining were performed	Supports periodontal cell adhesion and differentiation. The functionalized electrospun PCL mat also promoted cell viability, adhesion, and spreading	Das et al. (2019)
HydroMatrix (HydM)	*In vitro* study with human PDLSCs. Measurement of adhesion and proliferation using real-time impedance analysis, cell viability assay, cell morphology studies, osteogenic differentiation, and real-time RT-PCR.	PDL cells can adhere, migrate, survive, proliferate, and differentiate into the osteogenic direction on the HydM gel	Nagy et al. (2018)
ALVEOLAR BONE			
Peptide	**Methodology**	**Effect**	**References**
Osteogenic growth peptide (OGP ())	In vitro studies include; cell isolation and primary osteogenic cell cultures, cell morphology, cell proliferation and viability, evaluation of total protein content, ALP activity, and mineralized matrix formation In vivo studies include a surgical protocol where 60 male adult rats divided into three experimental groups with five animals each: Group I (GI): BC and BC OGP (10–14), group II (GII): BC-COL and BC-COL OGP (10–14) and group III (CG): Negative control group (no treatment) for periods at 1, 2, 4 and 16 weeks with a noncritical size bone defect (2 mm) in the femur. Histological, radiographic, and histomorphometric analyses were performed	Promotes proliferation, differentiation, and biomineralization of osteoblastic linage cells	Saska et al. (2018)
BMP-2 peptide (BMP-2P) (KIPKASSVPTELSAISTLYLGGK)	In vitro cytotoxicity assessment with the MTT assay using L929 mouse areolar fibroblasts In vivo critical-sized alveolar defect model with sprague dawley rats. A standardized tooth extraction rodent model was used, and post extraction the defects were either filled with graft materials for the experimental groups or left unfilled for the control group. Radiographic and histopathological analyses were performed	Osteogenic differentiation and biomineralization	Boda et al. (2019)

(Continued on following page)

TABLE 2 | (*Continued*) Synthetic peptides used in periodontal tissues regeneration.

ALVEOLAR BONE			
Peptide	**Methodology**	**Effect**	**References**
Peptide derived from parathyroid hormone residues 1–34. (PTH1-34)	In vitro, the expression of TNF-α, IL-1β, and IL-6 was assessed by immunohistochemistry and western blot In vivo diabetic rats were treated subcutaneously with low-dose (40 μg/kg, once daily for 5 days per week), middle-dose (80 μg/kg) or high-dose (160 μg/kg) PTHrP1-34 peptide. Treatment continued for 12 weeks. Changes in periodontal tissues were confirmed by micro-computerized tomography assay and H&E analysis	Bone mineralization and an inhibitory effect on alveolar bone resorption	Zhang et al. (2017)
AMB/P-15	In vivo 7 mm diameter fenestrations were made with a trephine in the mid-root of both maxillary canines in each dog. Bone, periodontal ligament, and cementum were removed. Block sections were retrieved at 3 and 8 weeks for histologic processing	Enhance fibroblast attachment with greater regeneration of fenestration defects	Vastardis et al. (2005)
CGRP	In vitro Quantitative real-time RT-PCR was performed for embryonic CGRP, VEGF-A, CD31, Col I, Col II, OPN, MMP-2, LYVE-1, and GAPDH. Also In situ hybridization of murine CGRP and VEGF-A In vivo, they used mandible and tibia mouse at various times (E12.5, E14.5, E17.5, E18.5, P0, P1, and P5), then isolated total RNA and performed a RT-PCR	Biomineralization and vascularization	Maeda et al. (2017)
RGD	In vitro PDL cell cytotoxicity was tested with 3-[4, 5- dimethylthiazol-2yl]-2, 5-diphenyl-2H-tetrazolium bromide assay. Cell migration toward the chitosan-based materials was analyzed with a trans-well migration assay In vivo Horizontal periodontal defect model was created in four maxillary and mandibular lateral incisors of Macaca nemestrina. Following periodontal therapy, the sites were transplanted with various regenerative materials: 1) chitosan, 2) RGD-modified chitosan, 3) PDL cell sheet with chitosan, 4) PDL cell sheet with RGD-modified chitosan. The periodontal tissue regeneration was evaluated clinically and radiographically. Gingival crevicular fluids were collected each week to evaluate cementum protein-1 (CEMP-1) expression with enzyme-linked immunosorbent assay, while the biopsies were retrieved after 4 weeks for histological and microcomputed	Higher alveolar bone density, as well as higher CEMP-1 protein expression. Adhesion and proliferation of osteoblasts	Amir et al. (2020)
HydroMatrix	In vitro study with human PDLSCs. Measurement of adhesion and proliferation using real-time impedance analysis, cell viability assay, cell morphology studies, osteogenic differentiation, and real-time RT-PCR.	Osteogenic differentiation of PDLSCs	Nagy et al. (2018)
RADICULAR CEMENTUM			
Peptide	**Methodology**	**Effect**	**References**
CEMP-1-p1	*In vitro* nucleation assay is a slow and controlled chemical reaction between the calcium and phosphate ions (without organic matrix) in a semisolid medium made of sodium metasilicate solution polymer at physiological pH and room temperature	This peptide has been related to the formation of spherical mineral structures on a nanometric scale and with a well-defined growth center of octacalcium phosphate, a precursor of HA.	Correa et al. (2019)
Amelogenin-derived peptide 5 (ADP5)	*In vitro* studies where an alkaline phosphatase based mineralization model was used to investigate the mineralization behaviors of the peptides. Cell adhesion and proliferation experiments were accomplished using cultured human periodontal ligament (hPDL) fibroblasts *Ex vivo* studies where the cementum-root stock blocks were prepared from single-rooted, extracted adult teeth. Cylindrical blocks of 4 mm diameter were cut from the acellular cementum, close to the cementoenamel junction the specimens were coated with the peptide and incubated. The mechanical properties of the cementomimetic layer were assessed by nanoindentation and qualitative mechanical abrasion tests	Facilitate cell-free formation of a cementum-like hydroxyapatite mineral layer on demineralized human root dentin that supported attachment of periodontal ligament cells	Gungormus et al. (2012)

(Continued on following page)

TABLE 2 | (*Continued*) Synthetic peptides used in periodontal tissues regeneration.

RADICULAR CEMENTUM			
Peptide	**Methodology**	**Effect**	**References**
BMP-6p	*In vivo* studies in a rat model where surgery to create a bony window on the buccal aspects of mandibular molar roots were performed. 24 male sprague dawley rats were divided into four groups according to BMP application (0, 1, 3, and 10 microg, respectively). Animals were killed after 28 days and the mandible was taken for histological examination. Histometric measurements were performed on sections selected from three levels (coronal, middle, and apical levels; with 240 μm apart from the central) of the defect. New bone and cementum formation (including area and thickness) were analyzed and compared	Induces the formation of cellular cementum-like tissue, with Sharpey´s fiber attachment after 28 days in a rat model	Huang et al. (2005)
ABM/P-15	*Case report* a maxillary lateral incisor with advanced adult periodontitis that was treatment planned for extraction was treated with sulcular incisions, full-thickness flap reflection, debridement of granulomatous tissue from the defect, placement of a notch in the root at the apical extent of calculus, mechanical root planing, brief cleansing with citric acid, grafting with abm/p-15, wound closure with sutures, and placement of a periodontal dressing. Biweekly to monthly recalls were made until removal of a small block section biopsy at about 6 months	In a human case shown favorable histologic healing, including cementum, PDL, and alveolar bone on a previously calculus and biofilm contaminated zone	Yukna et al. (2002)
Synthetic anabolic peptide (AP)	*In vivo* study where periodontal defects were created bilaterally adjacent to four mandibular teeth in five baboons. The plaque was allowed to accumulate around wire ligatures placed into the defects. After 2 months, the wire ligatures were removed, and a notch was placed at the base of the defect. The four teeth were randomly treated with one of the following treatments: 1) saline + ACS serving as the control, 2) AP + ACS, 3) saline + beta-TCP serving as another control, or 4) AP + beta-TCP. The baboons were sacrificed 5 months post-treatment, and histomorphometric analyses were performed under masked conditions	Induces new cementum formation by the stimulation of cell activity on the root surface	Yamashita et al. (2010)
GINGIVA AND OTHER SOFT TISSUES			
Peptide	**Methodology**	**Effect**	**References**
P2 (PLVPSQPLVPSQPLVP SQPQPP LPP)	*In vivo* study has a split-mouth, randomized, placebo-controlled design. Test and control wounds were created on the palatal mucosa of 54 sprague-dawley rats. Wounds were histologically processed, and re-epithelialization, leukocyte infiltration, and angiogenesis were assessed at days 1, 3, and 7 post-surgery	Promotes epithelial migration, induces reduction of inflammation, increased angiogenesis, and accelerated wound closure in the oral mucosa	Villa et al. (2015)
KSL-W (KKVVFWVKFK)	*In vitro* normal human gingival fibroblasts were cultured. t Of primary human gingival fibroblasts were incubated with different concentrations (0, 10,50, or 100 μg/ml) of peptide KSL-W and used to evaluate the effect of KSL-W on the attachment (phase-contrast microscopy, stained F-actin filaments) cell cycle analysis, a trypan blue exclusion assay to determine viable cell numbers was performed. MMP-1, MMP-2, TIMP-1, and TIMP-2 protein levels were analyzed by ELISA. Type I collagen assay system was used to evaluate the effect of peptide KSL-W on collagen gel contraction by gingival fibroblasts	Promotes gingival fibroblast adhesion, cell growth and enhances the secretion of MMP1, MMP2, and α-smooth muscle actin	Park et al. (2017)
SV (SVVYGLR)	*In vitro* normal human-derived gingival fibroblasts (NHGF) and human oral mucosa keratinocytes (HOMK) were used for *in vitro* experiments. WST-1 assay. Either NHGF (3.0 × 104 cells) or HOMK (4.0 × 104 cells) were added into each well of 96-well plates and cultured in a medium containing SV peptide (20 ng/ml), rSV peptide (20 ng/ml), or phosphate-buffered saline (PBS). Fibronectin (10 μg/ml)-precoated 96-well microplates were used for the adhesion assay. The boyden chamber principle was applied for the cell migration assay. A standard scratch wound healing assay was adopted to evaluate the motility of NHGF or HOMK. *In vivo* study, a rat model was used. Male sprague–Dawley rats. An oral punch wound was prepared at the left buccal mucosa approximately 7–8 mm behind the angle of mouth. A 5-mm dermal biopsy punch was used for this purpose, and a full-thickness mucosal wound was created in each animal. After the preparation of the wound, SV peptide (20 ng/ml, n = 5), rSV peptide (20 ng/ml, n = 5), or PBS (n = 5) was dividedly injected into four sites of wound periphery as a total amount of 1 ml solution for each site. Immunohistochemical and photographic analyses were performed	Is implicated in angiogenesis, and fibroblast differentiation into myofibroblasts in oral mucosa regeneration	Tanaka et al. (2020)

adhesion and proliferation of isolated PDLC *in vitro*. However, by its structure, the main issue is to build a thick scaffold, and efforts are focused on finding a carrier material alternative to Lys-PDA (Das et al., 2019).

HydroMatrix (HydM; Sigma-Aldrich, St. Louis, MO, United States) is a nanofiber scaffold for tissue engineering which can self-assemble and shows ideal conditions for PDLSCs proliferation without morphological changes (Nagy et al., 2018).

Alveolar Bone

The alveolar bone is the portion of the maxilla and mandible that surrounds the teeth and represents the primary support structure for the teeth. Two of the main causes of alveolar bone loss are periodontitis and trauma (Fu and Yap, 2007). The procedures for the regeneration of the alveolar bone are mainly based on the use of natural or synthetic scaffolds and bioactive agents (Kao et al., 2015). However, there are some inherent limitations associated with biomaterials and traditional techniques (Soldatos et al., 2017). An interesting alternative is the design of biomaterials modified with bioactive peptides that can interact with the surrounding tissues through biomolecular recognition. As a treatment strategy, peptides offer many of the advantages of protein therapeutics while addressing some of their limitations (Jabbari, 2013).

Osteogenic Growth Peptide

Osteogenic growth peptide (OGP) is a naturally occurring molecule with a primary structure similar to the C-terminal end of histone H4, whose sequence contains a highly conserved 14 amino acid motif (Pigossi et al., 2016). Furthermore, OGP and OGP-(10–14) are potent regulators of marrow stromal cells, and as a soluble peptide, their main activity includes promoting proliferation, differentiation, alkaline phosphatase activity, and matrix mineralization of osteoblastic lineage cells (Chen et al., 2007; Fei et al., 2010; An et al., 2014). OGP has been incorporated into regenerative membranes used in the GTRT. For instance, it has been shown that membranes based on biopolymers combined with OGP-(10–14) stimulate the proliferation and activity of osteoblasts *in vitro*, as well as the repair of bone tissue *in vivo* (Saska et al., 2018). Both, *in vitro* and *in vivo* experiments showed that the material is beneficial for cell adhesion, has good biocompatibility, enhances the expressions of osteogenic-related genes, and accelerates bone regeneration. Moreover, a novel osteogenic polypeptide hydrogel-based in photo-cross-linked gelatin methacryloyl with photo-cross-linkable OGP has been proposed as a promising alternative for bone repair and regeneration (Qiao et al., 2020).

Peptides Derived From Bone Morphogenic Proteins

The bone morphogenetic proteins (BMPs) have great biomedical potential as osteogenic factors (McKay and Sandhu, 2002; Kelly et al., 2016). An attractive approach to reduce the BMPs side effects in bone regeneration such as bone overgrowth or immune response (Carragee et al., 2011), is to use peptides derived from the bioactive domains of rhBMP-2 or other osteoinductive proteins (Jabbari, 2013). Peptides derived mainly from BMP-2, BMP-7 and BMP-9 have been studied for their ability to promote osteogenic differentiation *in vitro* and bone formation *in vivo* (Wang et al., 2017). It has been shown that human mesenchymal stem cells cultured on functionalized nanopatterned substrates with immobilized BMP-2 peptide (KIPKASSVPTELSAISTLYLGGK) exhibited greater potential for osteogenic differentiation (Kim et al., 2013). A previous study revealed that the application of mineralized nanofiber segments loaded with the E7-conjugated BMP-2 peptide in rat maxillae defects enabled a sustained peptide release over 4 weeks. Also, the X-ray microtomography analysis of peptide-loaded nanofiber graft filled defects revealed approximately three times greater new bone volume and density in comparison to unfilled control defects (Boda et al., 2019).

Parathyroid Hormone-Related Peptides

Parathyroid hormone (PTH) is considered as one of the major systemic regulators of calcium metabolism and bone remodeling (Goltzman, 2018). The peptide derived from PTH residues 1–34 (PTH1-34) is one of the earliest artificially synthesized amino acid fragments that was approved for the prevention and treatment of osteoporosis (Tashjian and Gagel, 2006). In a previous placebo-controlled clinical trial, PTH1-34 was associated with improved clinical outcomes, greater resolution of alveolar bone defects, and accelerated osseous wound healing in the oral cavity (Bashutski et al., 2010). It has been revealed that an RGD modified polyethylene glycol hydrogel containing PTH1-34 exhibited a clear beneficial effect on bone regeneration in circumferential bone defects around dental implants in a dog model (Jung et al., 2007). Besides, a recent study, showed that adding PTH1-34 to a xenograft increased the hardness of regenerated bone and accelerated bone mineralization in reconstructing mandible defects of pigs (Emam et al., 2020). Also, PTH1-34 may prevent alveolar bone resorption in type 1 diabetic rats, and that its intermittent administration could play an anabolic role in alveolar bone (Zhang et al., 2017).

Other Peptides

Peptide P-15 is a highly conserved peptide analog of the cellular binding domain of type I collagen (Bhatnagar et al., 1999). A previous research reported that the application of an organic bone mineral graft coated with a biomimetic collagen peptide (ABM/P-15) resulted in greater regeneration of fenestration defects in dogs at 8 weeks compared to controls (Vastardis et al., 2005). Additionally, it has been shown that ABM/P-15 associated with acellular dermal matrix, efficiently promotes the maintenance of the buccal-palatal dimension after tooth extraction in humans (Fernandes et al., 2011).

Another peptide that can be synthesized is the calcitonin gene-related peptide (CGRP) which is widely distributed in bone tissue and is known to be closely associated with osteogenesis (Maeda et al., 2017). Also, the RGD SP constitutes a system of cell surface signaling that enhances cell attachment and spreading of osteoblasts onto scaffolds and graft material (Durrieu et al., 2004). A recent study revealed enhanced regeneration of the horizontal periodontal defect in RGD-modified chitosan

macaque model, showing higher alveolar bone density than controls (Amir et al., 2020). Finally, HydM has even shown osteogenic differentiation on PDLSCs *in vitro*. Even though the study has shown the potential of the HydM scaffold, more studies *in vitro* and *in vivo* are needed (Nagy et al., 2018).

Dental Cementum

Dental cementum is a hard and avascular connective tissue located on the dental root, whose main function is to connect the fibers of the PDL that emerge from the alveolar bone to the dental organ. Two types of cementum can be distinguished according to the presence (cellular cementum) or absence of internal cells (acellular cementum). Their composition is distributed by approximately 50% of mineral matter, mainly HA (Ca_{10} $(PO_4)_6$ $(HO)_2$) and 50% of organic matrix, being type I collagen 90% of the organic composition. Another cement-related collagen protein includes type III collagen, involved in the development, repair, and regeneration of periodontal support structures (Nanci and Bosshardt, 2000).

The participation of dental cementum in processes such as maintaining stability and chewing charge distribution is crucial. Thus, when cementum is affected by periodontal disease or trauma, periodontal therapy must provide a root surface free of etiological factors to promote the reinsertion of collagen fibers and avoid the formation of pathological spaces that promote bacterial proliferation. Therefore, the success of periodontal regenerative therapy relies on the dental cementum, its health, and its well-regenerative capacities (Grzesik and Narayanan, 2002).

There are two typical cementum-specific proteins. The 3-Hydroxyacyl coenzyme A dehydratase 1/Cementum Attachment Protein (HACD1/CAP), induces the nucleation, regulation, and direction of hydroxyapatite crystal growth and enhances regeneration of critical bone defects in rat calvaria. Cementum protein 1 (CEMP-1) (Arzate et al., 1992; Bermúdez et al., 2015; Villegas-Mercado et al., 2018) regulates the activity of cementoblasts by inducing differentiation and intervenes in the process of mineralization, migration, and proliferation of gingival fibroblasts. CEMP1 also promotes the nucleation of OCP crystals (Alvarez-Perez et al., 2006).

Peptides Derived from the Amino Acid Sequence of Cementum Proteins

Some SP derived from dental cementum proteins such as CEMP-1 (CEMP-1-p1) and HACD1/CAP (CAP-pi) have biological activity associated with the *in vitro* biomineralization (Correa et al., 2019; Montoya et al., 2019; Montoya et al., 2020). CEMP-1-p1 induces the formation of spherical mineral structures on a nanometric scale and with a well-defined growth center of OCP (Correa et al., 2019). CAP-pi shows inhibitory activity of mineral crystal nucleation and growth (Montoya et al., 2020). The behavior of CEMP1- derived peptides is related to their capacity to activate Wnt/β-catenin signaling pathways, which is associated with the enhancement of the biomineralization process (Arroyo et al., 2020).

Peptides Non-Derived from the Amino Acid Sequence of Cementum Proteins

The amelogenin-derived peptide 5 (ADP5) enhances cell-free formation of a cementum-like HA mineral layer on demineralized human root dentin that supports attachment of periodontal ligament cells *in vitro*. Additionally, ADP5 has shown a kinetic control over calcium phosphate nucleation governed by interactions with precursor ions attracting Ca^{2+} and PO_4^{3-} and creating an increased local supersaturation of those ions. Cell adhesion and cell proliferation assays on the surface of ADP5-mediated cementum-like tooth material showed that the mineral layer favors adhesion and proliferation of periodontal cells. Thus, the cementomimetic layer formed by ADP5 could have the potential clinical application to repair diseased root surfaces and promote the regeneration of periodontal tissues (Gungormus et al., 2012).

The synthetic BMP-6 polypeptide, induces a thicker formation of cellular cementum-like tissue, with the incorporation of Sharpey's fiber attachment when is applied to periodontal fenestration defect in rats, after 28 days of healing (Huang et al., 2005).

The ABM/P-15 SP has been used in a human histologic case demonstrating favorable histologic healing of cementum, PDL, and alveolar bone on a previously calculus- and biofilm-contaminated zone, demonstrating its regenerative potential (Yukna et al., 2002).

A 23-amino acid peptide that corresponds to the central region (242 through 264) of human MEPE, the synthetic anabolic peptide (AP) (Nagel et al., 2004) has effects on normal osteoblast precursor cells. When is combined with a-tricalcium phosphate and an absorbable collagen sponge as the carrier induces the formation of new periodontal tissue on the root surfaces, showing that the sites with AP have more cementum formation than control sites. These results suggest that AP may affect cementogenesis by stimulating cell activity on the root surface (Yamashita et al., 2010).

Gingiva and Other Soft Tissues

The gingiva is the oral mucosa that covers the alveolar bone and cervical part of the tooth. The gingiva is composed of a layer of epithelial tissue (divided into three functional compartments; gingival, sulcular, and junctional epithelium) and the connective tissue into superficial and deep compartments (Nanci and Bosshardt, 2000). The gingiva forms a physical barrier against oral bacterial and provides mechanical protection to the underlying tissues (Hassell, 2000). Given its protective nature, the gingiva is key for wound healing since is constantly exposed to trauma or bacterial products that lead to inflammatory and infectious events. (Häkkinen et al., 2000). Some authors claim that wound healing represents a conserved process while the cellular processes of oral soft tissue resemble the healing of skin wounds (Polimeni et al., 2000; Wikesjö and Selvig, 2000). Nevertheless, important differences occur since it is commonly stated that oral wounds heal better and with less scar formation than dermal wounds (Häkkinen et al., 2000; Sculean et al., 2014).

The normal response to injury involves three overlapping stages: 1) inflammation, 2) new tissue formation, and 3)

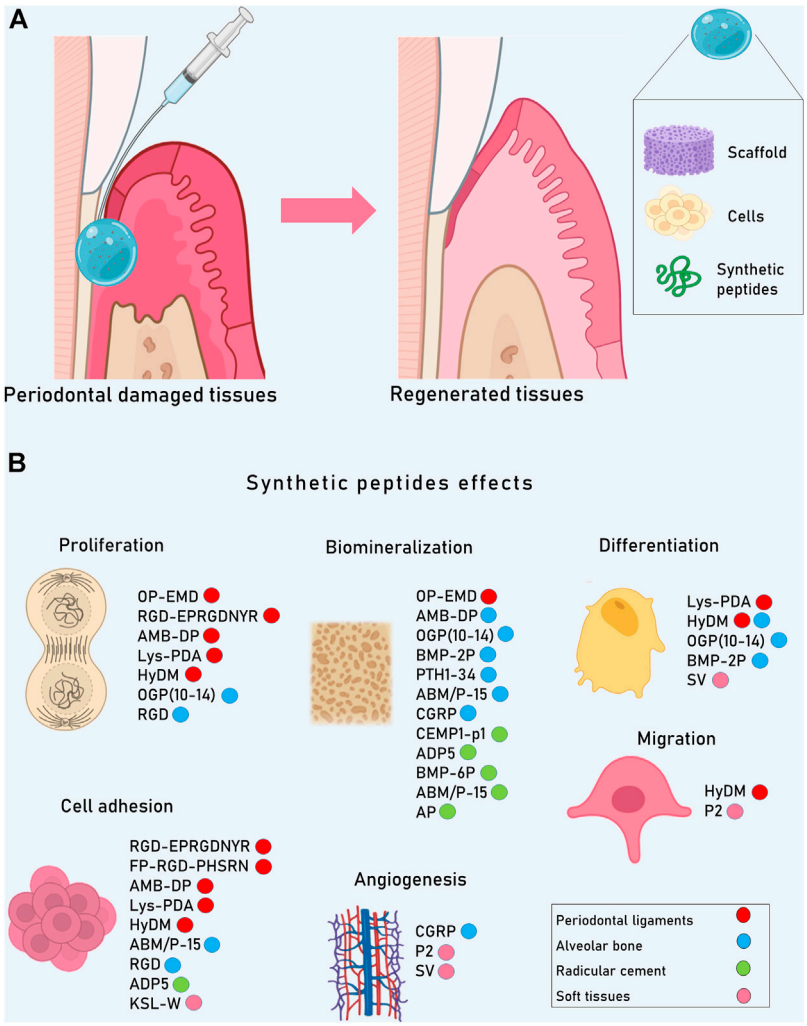

FIGURE 2 | Although the periodontium could be partially restored through tissue regeneration techniques, its complete regeneration is not possible yet since natural microenvironmental characteristics are almost impossible to imitate. **(A)** Research focuses on biomimetic systems that combine natural or synthetic molecules like peptides with scaffolds and cells to restore structure and function of the periodontal complex. **(B)** SP in periodontal cells are able to induce proliferation, migration, adhesion, angiogenesis, differentiation and biomineralization, enabling the formation of new tissue.

remodeling (Smith et al., 2015). After tissue injury, distinct biological pathways immediately become activated and are synchronized to prevent infection and restore the damaged tissues (Smith et al., 2015). The cells recruited during wound healing include components of the immune system, endothelial cells, keratinocytes, and fibroblast (Gurtner et al., 2008). In the last years, SP have arisen like a novel approach to enhance this process.

Synthetic Proline-Rich Peptide (P2)

The peptide P2 (PLVPSQPLVPSQPLVPSQPQPP LPP) was evaluated in a rat oral mucosal incisional wound healing model (Villa et al., 2015). P2 SP was previously shown to promote mesenchymal stem cell differentiation, induces bone formation, and mineralization *in vitro* (Ramis et al., 2012; Petzold et al., 2013). P2 enhances epithelial migration over the wound, reduces inflammation, increases angiogenesis, and accelerates the wound closure. P2 peptide contains proline-rich sequences, which are related to the immune response, wound repair (Zanetti, 2004), and angiogenesis (Li et al., 2000).

Antimicrobial Peptide KSL-W

The synthetic decapeptide KSL-W (KKVVFWVKFK) has an antimicrobial effect, promotes gingival fibroblast adhesion by increasing F-actin production, enhances cell growth by increasing the S, and induces G2/M cell cycle phases. Besides, increases the secretion of MMP-1, MMP-2, and the expression of α-smooth muscle actin, inducing wound healing (in the wound scratch assay) at 50 and 100 μg/ml. Also, KSL-W induces activation/differentiation of gingival fibroblast to myofibroblasts at the wound site contributing to tissue repair (Park et al., 2017).

Synthetic Peptide SV

An osteopontin-derived 7-amino-acid (SVVYGLR) SV is implicated in angiogenesis and fibroblasts differentiation to myofibroblasts. SV peptide induces cell migration of oral fibroblast and keratinocytes by activation of TGF-β/Smad signaling pathway *in vitro*. *In vivo*, the SV peptide accelerates the healing process of oral mucosal wounds by facilitating angiogenesis and increasing the production of fibroblasts and myofibroblasts in a rat-oral wound model (Tanaka et al., 2020).

CLINICAL IMPLICATIONS AND SIDE EFFECTS

Until now, it is well-known that human dental tissues once formed cannot be biologically repaired or replaced. And their complex configurations demand different strategies for regeneration. In this regard, enamel and dentin require the use of cells in 3-D scaffolds for their eventual mineralization meanwhile pulp tissue requires processes such as revascularization and innervation. Thus, regenerative approaches and their potential clinical implementation remain a challenging task to achieve.

From a clinical perspective, SP combined with conventional treatments or alone can enhance remineralization or increase thickness and mechanical properties of the regenerated enamel and dentin. Furthermore, short peptides are not targeted for hydrolytic enzymes in the oral cavity, and some of them have minimal or null toxicity since their sequences are derived from natural proteins. Nevertheless, most of them remain under experimental investigation on *in vitro* cell models and preclinical models and have to be validated to determine their effectiveness, and the dose to be used.

To bridge the gap between *in vitro* and *in vivo,* one approach is mathematical modeling which is used to support clinical predictions, providing richer data sets for model calibration, facilitating a model-based translation of *in vitro* cell assays to *in vivo* response (Lee et al., 2013; Checkley et al., 2015). Another strategy is the use of clinical trials in a dish (CTiD) which bridges preclinical testing and clinical trials allowing to test potential therapies for safety or efficacy on cells collected from a representative sample of human patients (Fermini et al., 2018; Seyhan, 2019).

Nowadays, for dental tissues, only P11–4 has been used in a clinical trial on children aged >5 years with visible active early caries on erupting permanent molars, showing enamel tissue regeneration and prevention of lesion progression (Alkilzy et al., 2018b). These results could change the clinical approach, avoiding additional loss of healthy tissue.

Regarding periodontal tissues, due to their complex composition, regenerative biomaterials should be capable to interact with hard and soft tissues at the same time (Elango et al., 2020). Many options have been studied *in vitro* with promising results that may lead to preclinical studies (Nagy et al., 2018). In this regard, it has to be considered that the success of the translation research from bench to bedside depends on the adoption of multidisciplinary strategies to overcome each of the many problems during the development process of SP therapy.

In normal conditions, PDL is under the influence of occlusal mechanical forces. However, these conditions cannot be completely achieved during *in vitro* or *ex vivo* tests. The *in vivo* model is the unique option that can imitate the occlusal state to support the functional regeneration design. Another challenge is the Sharpey's fiber regeneration and their insertion. The fibers absence nullify this important connection, defeating the tooth support and occlusal force (Liang et al., 2020).

Given this intricate relationship, few clinical studies using SP have shown regeneration. For instance, ABM/P-15, shows a favorable histologic healing, finding cementum, PDL, and alveolar bone on a previously calculus- and biofilm-contaminated zone, demonstrating its regenerative potential (Yukna et al., 2002).

In the case of SP used to promote bone healing and regeneration, most of them have only been evaluated *in vitro* or in preclinical animal studies. Among the SP reported for alveolar regeneration, PTH1-34 and P-15 have more extensive clinical use and are commercially available. PTH1-34 has therapeutic potential for oral bone lesions in periodontitis (Magda, 2010) and PepGen P-15 has been tested in human periodontal bone defects with favorable results (Pountos et al., 2016).

Regarding soft tissue, its healing and stability are essential to obtain predictive results from other regenerative procedures. Wound healing can be promoted by the application of SP to induce an accelerated wound healing, which should also benefit the clinical outcome of oral surgical procedures by assuring that the wound is more rapidly sealed off from the contaminated oral environment. This will lead to a more rapid connective tissue reorganization and contribute to a faster gain in wound strength, reducing the potential for scarring and scar tissue contraction (Villa et al., 2015).

Oral tissues work as an integrated unit and during their development, some proteins can participate in more than one tissue. This fact has led researchers to test the function of some SP designed for one tissue in another closely related one. In this regard, some promising SP could induce biomineralization in enamel, dentin, cementum, and alveolar bone, and other SP could function for regeneration of dentin-pulp and periodontal tissue complexes.

CONCLUDING REMARKS

SP used for oral tissue regeneration offer several advantages including increased specificity, small size, excellent safety, less immunogenicity, great stability, low risk of systemic toxicity, and low cost. Additionally, SP can be combined with scaffolds and cells, to induce cellular processes such as adhesion, proliferation, migration, differentiation, angiogenesis, and biomineralization that are required given the complex nature of oral tissues.

Even though most of the SP are still under investigation, some of them have been studied *in vitro* and *in vivo* with promising results that may lead to preclinical studies. There are SP that have

shown their efficacy in clinical trials such as P11-4 for enamel regeneration or caries prevention and ABM/P-15 for cementum, PDL, and alveolar bone on a previously calculus- and biofilm-contaminated zone. Also, some SP are commercially available such as PTH1-34 and PepGen P-15 which are used for bone defects treatment.

Finally, the use of SP could become a more accessible therapy for the treatment of damaged oral tissues, thus replacing the use of inert materials or therapies with recombinant proteins and growth factors that are currently highly used in practice dental. Nevertheless, well-designed clinical studies need to prove their value before they can be broadly used.

AUTHOR CONTRIBUTIONS

MB, LH, GM, AP-S, ER, US-B, and CV-M conceived and designed the content of this review; MB, LH, GM, MN, AP-S, ER, US-B, JG-P, MA-M, RR-P, and CV-M wrote de paper; all authors contributed to the final version of the paper and approved the submitted version.

FUNDING

Partially supported by UNAM PAPIIT IN206420 and IN204120.

REFERENCES

Abou Neel, E. A., Chrzanowski, W., Salih, V. M., Kim, H. W., and Knowles, J. C. (2014). Tissue engineering in dentistry. *J. Dent.* 42 (8), 915–928. doi:10.1016/j.jdent.2014.05.008

Alkilzy, M., Santamaria, R. M., Schmoeckel, J., and Splieth, C. H. (2018a). Treatment of carious lesions using self-assembling peptides. *Adv. Dent Res.* 29 (1), 42–47. doi:10.1177/0022034517737025

Alkilzy, M., Tarabaih, A., Santamaria, R. M., and Splieth, C. H. (2018b). Self-assembling peptide P11-4 and fluoride for regenerating enamel. *J. Dent Res.* 97 (2), 148–154. doi:10.1177/0022034517730531

Alvarez-Perez, M. A., Narayanan, S., Zeichner-David, M., Rodriguez Carmona, B., and Arzate, H. (2006). Molecular cloning, expression and immunolocalization of a novel human cementum-derived protein (CP-23). *Bone.* 38 (3), 409–19. doi:10.1016/j.bone.2005.09.009

Amir, L. R., Soeroso, Y., Fatma, D., Sunarto, H., Sulijaya, B., Idrus, E., et al. (2020). Periodontal ligament cell sheets and RGD-modified chitosan improved regeneration in the horizontal periodontal defect model. *Eur. J. Dent.* 14 (2), 306–314. doi:10.1055/s-0040-1709955

An, G., Xue, Z., Zhang, B., Deng, Q. K., Wang, Y. S., and Lv, S. C. (2014). Expressing osteogenic growth peptide in the rabbit bone mesenchymal stem cells increased alkaline phosphatase activity and enhanced the collagen accumulation. *Eur. Rev. Med. Pharmacol. Sci.* 18 (11), 1618–1624.

Aota, S., Nomizu, M., and Yamada, K. M. (1994). The short amino acid sequence Pro-His-Ser-Arg-Asn in human fibronectin enhances cell-adhesive function. *J. Biol. Chem.* 269 (40), 24756–24761. doi:10.1016/s0021-9258(17)31456-4

Arifa, M. K., Ephraim, R., and Rajamani, T. (2019). Recent advances in dental hard tissue remineralization: a review of literature. *Int. J. Clin. Pediatr. Dent* 12 (2), 139–144. doi:10.5005/jp-journals-10005-1603

Arroyo, R., López, S., Romo, E., Montoya, G., Hoz, L., Pedraza, C., et al. (2020). Carboxy-terminal cementum protein 1-derived peptide 4 (cemp1-p4) promotes mineralization through wnt/β-catenin signaling in human oral mucosa stem cells. *Int. J. Mol. Sci.* 21 (4), 1307. doi:10.3390/ijms21041307

Arzate, H., Olson, S. W., Page, R. C., Gown, A. M., and Narayanan, A. S. (1992). Production of a monoclonal antibody to an attachment protein derived from human cementum. *Faseb j.* 6 (11), 2990–2995. doi:10.1096/fasebj.6.11.1644261

Bagheri, G. H., Sadr, A., Espigares, J., Hariri, I., Nakashima, S., Hamba, H., et al. (2015). Study on the influence of leucine-rich amelogenin peptide (LRAP) on the remineralization of enamel defects via micro-focus x-ray computed tomography and nanoindentation. *Biomed. Mater.* 10 (3), 035007. doi:10.1088/1748-6041/10/3/035007

Banting, F. G., Best, C. H., Collip, J. B., Campbell, W. R., and Fletcher, A. A. (1922). Pancreatic extracts in the treatment of diabetes mellitus. *Can. Med. Assoc. J.* 12 (3), 141–146.

Barczyk, M., Bolstad, A. I., and Gullberg, D. (2000). Role Integrins Periodontal Ligament: Organizers Facilitators. *Periodontol 2000*. 63 (1), 29–47. doi:10.1111/prd.12027

Bartold, P. M., Shi, S., and Gronthos, S. (2000). Stem cells and periodontal regeneration. *Periodontol. 2000*. 40 (40), 164–172. doi:10.1111/j.1600-0757.2005.00139.x

Bashutski, J. D., Eber, R. M., Kinney, J. S., Benavides, E., Maitra, S., Braun, T. M., et al. (2010). Teriparatide and osseous regeneration in the oral cavity. *N. Engl. J. Med.* 363 (25), 2396–2405. doi:10.1056/NEJMoa1005361

Bellis, S. L. (2011). Advantages of RGD peptides for directing cell association with biomaterials. *Biomaterials* 32 (18), 4205–4210. doi:10.1016/j.biomaterials.2011.02.029

Bermúdez, M., Imaz-Rosshandler, I., Rangel-Escareño, C., Zeichner-David, M., Arzate, H., and Mercado-Celis, G. E. (2015). CEMP1 induces transformation in human gingival fibroblasts. *PLoS One*. 10 (5), e0127286. doi:10.1371/journal.pone.0127286

Bhatnagar, R. S., Qian, J. J., Wedrychowska, A., Sadeghi, M., Wu, Y. M., and Smith, N. (1999). Design of biomimetic habitats for tissue engineering with P-15, a synthetic peptide analogue of collagen. *Tissue Eng.* 5 (1), 53–65. doi:10.1089/ten.1999.5.53

Bleicher, F. (2014). Odontoblast physiology. *Exp. Cel Res.* 325 (2), 65–71. doi:10.1016/j.yexcr.2013.12.012

Boda, S. K., Almoshari, Y., Wang, H., Wang, X., Reinhardt, R. A., Duan, B., et al. (2019). Mineralized nanofiber segments coupled with calcium-binding BMP-2 peptides for alveolar bone regeneration. *Acta Biomater.* 85, 282–293. doi:10.1016/j.actbio.2018.12.051

Bröseler, F., Tietmann, C., Bommer, C., Drechsel, T., Heinzel-Gutenbrunner, M., and Jepsen, S. (2020). Randomised clinical trial investigating self-assembling peptide P11-4 in the treatment of early caries. *Clin. Oral Investig.* 24 (1), 123–132. doi:10.1007/s00784-019-02901-4

Brunton, P. A., Davies, R. P., Burke, J. L., Smith, A., Aggeli, A., Brookes, S. J., et al. (2013). Treatment of early caries lesions using biomimetic self-assembling peptides--a clinical safety trial. *Br. Dent J.* 215 (4), E6. doi:10.1038/sj.bdj.2013.741

Buzalaf, M. A. R., and Jp Pessan, I. (2017). New preventive approaches Part I: functional peptides and other therapies to prevent tooth demineralization. *Monogr. Oral Sci.* 26, 88–96. doi:10.1159/000479350

Cao, Y., Mei, M. L., Xu, J., Lo, E. C., Li, Q., and Chu, C. H. (2013). Biomimetic mineralisation of phosphorylated dentine by CPP-ACP. *J. Dent.* 41 (9), 818–825. doi:10.1016/j.jdent.2013.06.008

Carragee, E. J., Hurwitz, E. L., and Weiner, B. K. (2011). A critical review of recombinant human bone morphogenetic protein-2 trials in spinal surgery: emerging safety concerns and lessons learned. *Spine J.* 11 (6), 471–491. doi:10.1016/j.spinee.2011.04.023

Caviedesbucheli, J., Munoz, H., Azueroholguin, M., and Ulate, E. (2008). Neuropeptides in dental pulp: the silent protagonists. *J. Endodontics*. 34 (7), 773–788. doi:10.1016/j.joen.2008.03.010

Checkley, S., MacCallum, L., Yates, J., Jasper, P., Luo, H., Tolsma, J., et al. (2015). Bridging the gap between *in vitro* and *in vivo*: dose and schedule predictions for the ATR inhibitor AZD6738. *Sci. Rep.* 5 (1), 13545. doi:10.1038/srep13545

Chen, Z. X., Chang, M., Peng, Y. L., Zhao, L., Zhan, Y. R., Wang, L. J., et al. (2007). Osteogenic growth peptide C-terminal pentapeptide [OGP(10-14)] acts on rat bone marrow mesenchymal stem cells to promote differentiation to osteoblasts and to inhibit differentiation to adipocytes. *Regul. Pept.* 142 (1-2), 16–23. doi:10.1016/j.regpep.2007.01.003

Choung, H. W., Lee, D. S., Lee, J. H., Shon, W. J., Lee, J. H., Ku, Y., et al. (2016). Tertiary dentin formation after indirect pulp capping using protein CPNE7. *J. Dent Res.* 95 (8), 906–912. doi:10.1177/0022034516639919

Chung, H. Y., and Huang, K. C. (2013). Effects of peptide concentration on remineralization of eroded enamel. *J. Mech. Behav. Biomed. Mater.* 28, 213–221. doi:10.1016/j.jmbbm.2013.08.004

Chung, H. Y., and Li, C. C. (2013). Microstructure and nanomechanical properties of enamel remineralized with asparagine-serine-serine peptide. *Mater. Sci. Eng. C Mater. Biol. Appl.* 33 (2), 969–973. doi:10.1016/j.msec.2012.11.031

Correa, R., Arenas, J., Montoya, G., Hoz, L., López, S., Salgado, F., et al. (2019). Synthetic cementum protein 1-derived peptide regulates mineralization *in vitro* and promotes bone regeneration *in vivo*. *FASEB J.* 33 (1), 1167–1178. doi:10.1096/fj.201800434RR

Creutz, C. E., Tomsig, J. L., Snyder, S. L., Gautier, M. C., Skouri, F., Beisson, J., et al. (1998). The copines, a novel class of C2 domain-containing, calcium-dependent, phospholipid-binding proteins conserved from Paramecium to humans. *J. Biol. Chem.* 273 (3), 1393–1402. doi:10.1074/jbc.273.3.1393

D'Andrea, L. D., Iaccarino, G., Fattorusso, R., Sorriento, D., Carannante, C., Capasso, D., et al. (2005). Targeting angiogenesis: structural characterization and biological properties of a de novo engineered VEGF mimicking peptide. *Proc. Natl. Acad. Sci. USA*. 102 (40), 14215–14220. doi:10.1073/pnas.0505047102

Dang, T., and Süssmuth, R. D. (2017). Bioactive peptide natural products as lead structures for medicinal use. *Acc. Chem. Res.* 50 (7), 1566–1576. doi:10.1021/acs.accounts.7b00159

Das, E. C., Dhawan, S., Babu, J., Anil Kumar, P. R., Kumary, T. V., Haridas, V., et al. (2019). Self-assembling polymeric dendritic peptide as functional osteogenic matrix for periodontal regeneration scaffolds-an *in vitro* study. *J. Periodontal Res.* 54 (5), 468–480. doi:10.1111/jre.12647

de Sousa, J. P., Carvalho, R. G., Barbosa-Martins, L. F., Torquato, R. J. S., Mugnol, K. C. U., Nascimento, F. D., et al. (2019). The self-assembling peptide P11-4 prevents collagen proteolysis in dentin. *J. Dent Res.* 98 (3), 347–354. doi:10.1177/0022034518817351

Ding, L., Han, S., Wang, K., Zheng, S., Zheng, W., Peng, X., et al. (2020). Remineralization of enamel caries by an amelogenin-derived peptide and fluoride *in vitro*. *Regen. Biomater.* 7 (3), 283–292. doi:10.1093/rb/rbaa003

Dissanayaka, W. L., Hargreaves Km Fau - jin, L., Jin L Fau - samaranayake, LP., Samaranayake Lp Fau - Zhang, C., and Zhang, C. (2015). The interplay of dental pulp stem cells and endothelial cells in an injectable peptide hydrogel on angiogenesis and pulp regeneration *in vivo*. *Tissue Eng Part A*. 21 (3-4), 550-63. doi:10.1089/ten.TEA.2014.0154

Dissanayake, S. S. M., Ekambaram, M., Li, K. C., Harris, P. W. R., and Brimble, M. A. (2020). Identification of key functional motifs of native amelogenin protein for dental enamel remineralisation. *Molecules* 25 (18), 4214. doi:10.3390/molecules25184214

Durrieu, M. C., Pallu, S., Guillemot, F., Bareille, R., Amédée, J., Baquey, C. H., et al. (2004). Grafting RGD containing peptides onto hydroxyapatite to promote osteoblastic cells adhesion. *J. Mater. Sci. Mater. Med.* 15 (7), 779–786. doi:10.1023/b:jmsm.0000032818.09569.d9

Elango, J., Selvaganapathy, P. R., Lazzari, G., Bao, B., and Wenhui, W. (2020). Biomimetic collagen-sodium alginate-titanium oxide (TiO2) 3D matrix supports differentiated periodontal ligament fibroblasts growth for periodontal tissue regeneration. *Int. J. Biol. Macromol.* 163, 9–18. doi:10.1016/j.ijbiomac.2020.06.173

Emam, H., Leach, D., Sun, Z., Tee, B. C., Karatas, B., Kim, D. G., et al. (2020). The effect of parathyroid hormone analogues when added to mineralized bone xenografts. *J. Oral Implantol.* 46 (4), 372–379. doi:10.1563/aaid-joi-D-19-00016

Erak, M., Bellmann-Sickert, K., Els-Heindl, S., and Beck-Sickinger, A. G. (2018). Peptide chemistry toolbox - transforming natural peptides into peptide therapeutics. *Bioorg. Med. Chem.* 26 (10), 2759–2765. doi:10.1016/j.bmc.2018.01.012

Farooq, I., and Bugshan, A. (2020). The role of salivary contents and modern technologies in the remineralization of dental enamel: a narrative review. *F1000Res.* 9, 171. doi:10.12688/f1000research.22499.2

Fawzy El-Sayed, K. M., Ahmed, G. M., Abouauf, E. A., and Schwendicke, F. (2019). Stem/progenitor cell-mediated pulpal tissue regeneration: a systematic review and meta-analysis. *Int. Endod. J.* 52 (11), 1573–1585. doi:10.1111/iej.13177

Fei, Q., Guo, C., Xu, X., Gao, J., Zhang, J., Chen, T., et al. (2010). Osteogenic growth peptide enhances the proliferation of bone marrow mesenchymal stem cells from osteoprotegerin-deficient mice by CDK2/cyclin A. *Acta Biochim. Biophys. Sin (Shanghai)*. 42 (11), 801–806. doi:10.1093/abbs/gmq086

Fermini, B., Coyne, S. T., and Coyne, K. P. (2018). Clinical trials in a dish: a perspective on the coming revolution in drug development. *SLAS Discov.* 23 (8), 765–776. doi:10.1177/2472555218775028

Fernandes, P. G., Novaes, A. B., Jr., de Queiroz, A. C., de Souza, S. L., Taba, M., Jr., Palioto, D. B., et al. (2011). Ridge preservation with acellular dermal matrix and anorganic bone matrix cell-binding peptide P-15 after tooth extraction in humans. *J. Periodontol.* 82 (1), 72–79. doi:10.1902/jop.2010.100241

Fosgerau, K., and Hoffmann, T. (2015). Peptide therapeutics: current status and future directions. *Drug Discov. Today*. 20 (1), 122–128. doi:10.1016/j.drudis.2014.10.003

Fu, J. H., and Yap, A. U. (2007). Occlusion and periodontal disease--where is the link?. *Singapore Dent J.* 29 (1), 22–33.

Galler, K. M., Hartgerink, J. D., Cavender, A. C., Schmalz, G., and D'Souza, R. N. (2012). A customized self-assembling peptide hydrogel for dental pulp tissue engineering. *Tissue Eng. Part. A*. 18 (1-2), 176–184. doi:10.1089/ten.TEA.2011.0222

Garant, P. R. (2003). *Oral cells and tissues*. Chicago: Quintessence Pub. Co

Goldberg, M., Kulkarni, A. B., Young, M., and Boskey, A. (2011). Dentin: structure, composition and mineralization. *Front Biosci (Elite Ed)*. 3, 711–735. doi:10.2741/e281

Goltzman, D. (2018). Physiology of parathyroid hormone. *Endocrinol. Metab. Clin. North. Am.* 47 (4), 743–758. doi:10.1016/j.ecl.2018.07.003

González-Cabezas, C., and Fernández, C. E. (2018). Recent advances in remineralization therapies for caries lesions. *Adv. Dent Res.* 29 (1), 55–59. doi:10.1177/0022034517740124

Grzesik, W. J., Ivanov, B., Robey, F. A., Southerland, J., and Yamauchi, M. (1998). Synthetic integrin-binding peptides promote adhesion and proliferation of human periodontal ligament cells *in vitro*. *J. Dent Res.* 77 (8), 1606–1612. doi:10.1177/00220345980770080801

Grzesik, W. J., and Narayanan, A. S. (2002). Cementum and periodontal wound healing and regeneration. *Crit. Rev. Oral Biol. Med.* 13 (6), 474–484. doi:10.1177/154411130201300605

Gungormus, M., Horst, J. A., Fong, H., Hnilova, M., Somerman, M. J., Snead, M. L., et al. (2012). Cementomimetics-constructing a cementum-like biomineralized microlayer via amelogenin-derived peptides. *Int J Oral Sci.* 4 (2), 69–77. doi:10.1038/ijos.2012.40

Gurtner, G. C., Werner, S., Barrandon, Y., and Longaker, M. T. (2008). Wound repair and regeneration. *Nature*. 453 (7193), 314–321. doi:10.1038/nature07039

Häkkinen, L., Uitto, V. J., and Larjava, H. (2000). Cell biology of gingival wound healing. *Periodontol. 2000*. 24 (24), 127–152. doi:10.1034/j.1600-0757.2000.2240107.x

Hamley, I. W. (2017). Small bioactive peptides for biomaterials design and therapeutics. *Chem. Rev.* 117 (24), 14015–14041. doi:10.1021/acs.chemrev.7b00522

Han, S., Fan, Y., Zhou, Z., Tu, H., Li, D., Lv, X., et al. (2017). Promotion of enamel caries remineralization by an amelogenin-derived peptide in a rat model. *Arch. Oral Biol.* 73, 66–71. doi:10.1016/j.archoralbio.2016.09.009

Hara, A. T., and Zero, D. T. (2010). The caries environment: saliva, pellicle, diet, and hard tissue ultrastructure. *Dent Clin. North. Am.* 54 (3), 455–467. doi:10.1016/j.cden.2010.03.008

Hassell, T. M. (2000). Tissues and cells of the periodontium. *Periodontol. 2000*. 3 (3), 9–38. doi:10.1111/j.1600-0757.1993.tb00230.x

Hautanen, A., Gailit, J., Mann, D. M., and Ruoslahti, E. (1989). Effects of modifications of the RGD sequence and its context on recognition by the fibronectin receptor. *J. Biol. Chem.* 264 (3), 1437–1442. doi:10.1016/s0021-9258(18)94206-7

Hilton, T. J., Ferracane, J. L., and Mancl, L. (2013). Comparison of CaOH with MTA for direct pulp capping: a PBRN randomized clinical trial. *J. Dent Res.* 92 (7 Suppl. l), 16s–22s. doi:10.1177/0022034513484336

Hsu, C. C., Chung, H. Y., Yang, J. M., Shi, W., and Wu, B. (2011). Influence of 8DSS peptide on nano-mechanical behavior of human enamel. *J. Dent Res.* 90 (1), 88–92. doi:10.1177/0022034510381904

Huang, B., Sun, Y., Maciejewska, I., Qin, D., Peng, T., McIntyre, B., et al. (2008). Distribution of SIBLING proteins in the organic and inorganic phases of rat dentin and bone. *Eur. J. Oral Sci.* 116 (2), 104–112. doi:10.1111/j.1600-0722.2008.00522.x

Huang, G. T. (2011). Dental pulp and dentin tissue engineering and regeneration: advancement and challenge. *Front Biosci (Elite Ed)*. 3, 788–800. doi:10.2741/e286

Huang, K. K., Shen, C., Chiang, C. Y., Hsieh, Y. D., and Fu, E. (2005). Effects of bone morphogenetic protein-6 on periodontal wound healing in a fenestration defect of rats. *J. Periodont Res.* 40 (1), 1–10. doi:10.1111/j.1600-0765.2004.00752.x

Huang, Y., Goldberg, M., Le, T., Qiang, R., Warner, D., Witkowska, H. E., et al. (2012). Amelogenin exons 8 and 9 encoded peptide enhances leucine rich amelogenin peptide mediated dental pulp repair. *Cells Tissues Organs (Print)* 196 (2), 151–160. doi:10.1159/000331248

Ieong, C. C., Zhou, X. D., Li, J. Y., Li, W., and Zhang, L. L. (2011). Possibilities and potential roles of the functional peptides based on enamel matrix proteins in promoting the remineralization of initial enamel caries. *Med. Hypotheses* 76 (3), 391–394. doi:10.1016/j.mehy.2010.10.050

Jabbari, E. (2013). Osteogenic peptides in bone regeneration. *Curr. Pharm. Des.* 19 (19), 3391–3402. doi:10.2174/1381612811319190006

Jablonski-Momeni, A., Korbmacher-Steiner, H., Heinzel-Gutenbrunner, M., Jablonski, B., Jaquet, W., and Bottenberg, P. (2019). Randomised *in situ* clinical trial investigating self-assembling peptide matrix P11-4 in the prevention of artificial caries lesions. *Sci. Rep.* 9 (1), 269. doi:10.1038/s41598-018-36536-4

Jung, C., Kim, S., Sun, T., Cho, Y. B., and Song, M. (2019). Pulp-dentin regeneration: current approaches and challenges. *J. Tissue Eng.* 10, 2041731418819263. doi:10.1177/2041731418819263

Jung, R. E., Cochran, D. L., Domken, O., Seibl, R., Jones, A. A., Buser, D., et al. (2007). The effect of matrix bound parathyroid hormone on bone regeneration. *Clin. Oral Implants Res.* 18 (3), 319–325. doi:10.1111/j.1600-0501.2007.01342.x

Kamal, D., Hassanein, H., Elkassas, D., and Hamza, H. (2020). Complementary remineralizing effect of self-assembling peptide (P11-4) with CPP-ACPF or fluoride: an *in vitro* study. *J. Clin. Exp. Dent* 12 (2), e161–e168. doi:10.4317/jced.56295

Kao, R. T., Nares, S., and Reynolds, M. A. (2015). Periodontal regeneration - intrabony defects: a systematic review from the AAP Regeneration Workshop. *J. Periodontol.* 86 (2 Suppl. l), S77–S104. doi:10.1902/jop.2015.130685

Kato, H., Taguchi, Y., Tominaga, K., Umeda, M., and Tanaka, A. (2013). A synthetic oligopeptide derived from enamel matrix derivative promotes the differentiation of human periodontal ligament stem cells into osteoblast-like cells with increased mineralization. *J Periodontol.* 84 (10), 1476-83. doi:10.1902/jop.2012.120469

Kawashima, N., and Okiji, T. (2016). Odontoblasts: specialized hard-tissue-forming cells in the dentin-pulp complex. *Congenit. Anom. (Kyoto)* 56 (4), 144–153. doi:10.1111/cga.12169

Kelly, M. P., Vaughn, O. L., and Anderson, P. A. (2016). Systematic review and meta-analysis of recombinant human bone morphogenetic protein-2 in localized alveolar ridge and maxillary sinus augmentation. *J. Oral Maxillofac. Surg.* 74 (5), 928–939. doi:10.1016/j.joms.2015.11.027

Khorolsuren, Z., Lang, O., Pallinger, E., Foldes, A., Szabolcs, G. G., Varga, G., et al. (2020). Functional and cell surface characteristics of periodontal ligament cells (PDLCs) on RGD-synthetic polypeptide conjugate coatings. *J Periodontal Res.* 55 (5), 713–723. doi:10.1111/jre.12760

Kim, M. J., Lee, B., Yang, K., Park, J., Jeon, S., Um, S. H., et al. (2013). BMP-2 peptide-functionalized nanopatterned substrates for enhanced osteogenic differentiation of human mesenchymal stem cells. *Biomaterials* 34 (30), 7236–7246. doi:10.1016/j.biomaterials.2013.06.019

Kim, S. G. (2017). Biological molecules for the regeneration of the pulp-dentin complex. *Dent Clin. North. Amissue*. 611, 127–141. doi:10.1016/j.cden.2016.08.005

Kim, T. I., Jang, J. H., Lee, Y. M., Rhyu, I. C., Chung, C. P., Han, S. B., et al. (2004). Biomimetic approach on human periodontal ligament cells using synthetic oligopeptides. *J. Periodontol.* 75 (7), 925–932. doi:10.1902/jop.2004.75.7.925

Kind, L., Stevanovic, S., Wuttig, S., Wimberger, S., Hofer, J., Müller, B., et al. (2017). Biomimetic remineralization of carious lesions by self-assembling peptide. *J. Dent Res.* 96 (7), 790–797. doi:10.1177/0022034517698419

Kitagawa, M., Kitagawa, S., Nagasaki, A., Miyauchi, M., Uchida, T., and Takata, T. (2011). Synthetic ameloblastin peptide stimulates differentiation of human periodontal ligament cells. *Arch. Oral Biol.* 56 (4), 374–379. doi:10.1016/j.archoralbio.2010.10.012

Koch, F., Müller, M., König, F., Meyer, N., Gattlen, J., Pieles, U., et al. (2018). Mechanical characteristics of beta sheet-forming peptide hydrogels are dependent on peptide sequence, concentration and buffer composition. *R Soc Open Sci.* 5 (3), 171562. doi:10.1098/rsos.171562

Lau, J. L., and Dunn, M. K. (2018). Therapeutic peptides: historical perspectives, current development trends, and future directions. *Bioorg. Med. Chem.* 26 (10), 2700–2707. doi:10.1016/j.bmc.2017.06.052

Lee, D., Park, K. S., Yoon, G. J., Lee, H. J., Lee, J. Y., Park, Y. S., et al. (2019). Identification of cell-penetrating osteogenic peptide from copine-7 protein and its delivery system for enhanced bone formation. *J. Biomed. Mater. Res. A.* 107 (11), 2392–2402. doi:10.1002/jbm.a.36746

Lee, J. H., Mand, M. R., Deshpande, R. A., Kinoshita, E., Yang, S. H., Wyman, C., et al. (2013). Ataxia telangiectasia-mutated (ATM) kinase activity is regulated by ATP-driven conformational changes in the Mre11/Rad50/Nbs1 (MRN) complex. *J. Biol. Chem.* 288 (18), 12840–12851. doi:10.1074/jbc.M113.460378

Lee, Y. S., Park, Y. H., Lee, D. S., Seo, Y. M., Lee, J. H., Park, J. H., et al. (2020). Tubular dentin regeneration using a CPNE7-derived functional peptide. *Materials (Basel)*. 13 (20),4618. doi:10.3390/ma13204618

Li, J., Volk, R., Gao, Y., Li, M., Metais, C., Sato, K., et al. (2000). PR39, a peptide regulator of angiogenesis. *Nat. Med.* 6 (1), 49–55. doi:10.1038/71527

Li, Z. C., Qin, X., Ren, Q., Hu, D., Tian, T., He, T., et al. (2020). Rational design of β-sheet peptides with self-assembly into nanofibres on remineralisation of initial caries lesions. *Chin. J. Dent Res.* 23 (2), 131–141. doi:10.3290/j.cjdr.a44749

Liang, Y., Luan, X., and Liu, X. (2020). Recent advances in periodontal regeneration: a biomaterial perspective. *Bioact Mater.* 5 (2), 297–308. doi:10.1016/j.bioactmat.2020.02.012

Lien, S., and Lowman, H. B. (2003). Therapeutic peptides. *Trends Biotechnol.* 21 (12), 556–562. doi:10.1016/j.tibtech.2003.10.005

Liu, H., Li, W., Gao, C., Kumagai, Y., Blacher, R. W., and DenBesten, P. K. (2004). Dentonin, a fragment of MEPE, enhanced dental pulp stem cell proliferation. *J. Dent Res.* 83 (6), 496–499. doi:10.1177/154405910408300612

Lv, X., Yang, Y., Han, S., Li, D., Tu, H., Li, W., et al. (2015). Potential of an amelogenin based peptide in promoting reminerlization of initial enamel caries. *Arch. Oral Biol.* 60 (10), 1482–1487. doi:10.1016/j.archoralbio.2015.07.010

Maeda, Y., Miwa, Y., and Sato, I. (2017). Expression of CGRP, vasculogenesis and osteogenesis associated mRNAs in the developing mouse mandible and tibia. *Eur. J. Histochem.* 61 (1), 2750. doi:10.4081/ejh.2017.2750

Magda, S. (2010). Teriparatide and bone regeneration in the jaw. *Maedica (Buchar)* 5 (4), 303

McCulloch, C. A., and Melcher, A. H. (1983). Cell density and cell generation in the periodontal ligament of mice. *Am. J. Anat.* 167 (1), 43–58. doi:10.1002/aja.1001670105

McKay, B., and Sandhu, H. S. (2002). Use of recombinant human bone morphogenetic protein-2 in spinal fusion applications. *Spine (Phila Pa 1976).* 27, S66–S85. doi:10.1097/00007632-200208151-00014

Michot, B., Casey, S. M., and Gibbs, J. L. (2020). Effects of calcitonin gene-related peptide on dental pulp stem cell viability, proliferation, and differentiation. *J. Endod.* 46 (7), 950–956. doi:10.1016/j.joen.2020.03.010

Montoya, G., Correa, R., Arenas, J., Hoz, L., Romo, E., Arroyo, R., et al. (2019). Cementum protein 1-derived peptide (CEMP 1-p1) modulates hydroxyapatite crystal formation *in vitro*. *J. Pept. Sci.* 25 (10), e3211. doi:10.1002/psc.3211

Montoya, G., Lopez, K., Arenas, J., Zamora, C., Hoz, L., Romo, E., et al. (2020). Nucleation and growth inhibition of biological minerals by cementum attachment protein-derived peptide (CAP-pi). *J. Pept. Sci.* 26 (12), e3282. doi:10.1002/psc.3282

Moore, A. N., Perez, S. C., Hartgerink, J. D., D'Souza, R. N., and Colombo, J. S. (2015). *Ex Vivo* modeling of multidomain peptide hydrogels with intact dental pulp. *J. Dent Res.* 94 (12), 1773–1781. doi:10.1177/0022034515600380

Moussa, D. G., and Aparicio, C. (2019). Present and future of tissue engineering scaffolds for dentin-pulp complex regeneration. *J. Tissue Eng. Regen. Med.* 13 (1), 58–75. doi:10.1002/term.2769

Mu, X., Shi, L., Pan, S., He, L., Niu, Y., and Wang, X. (2020). A customized self-assembling peptide hydrogel-wrapped stem cell factor targeting pulp

regeneration rich in vascular-like structures. *ACS Omega*. 5 (27), 16568–16574. doi:10.1021/acsomega.0c01266

Mukherjee, K., Ruan, Q., and Moradian-Oldak, J. (2019). Peptide-mediated biomimetic regrowth of human enamel in situ. *Methods Mol. Biol.* 1922, 129–138. doi:10.1007/978-1-4939-9012-2_13

Nagel, D. E., Khosla, S., Sanyal, A., Rosen, D. M., Kumagai, Y., and Riggs, B. L. (2004). A fragment of the hypophosphatemic factor, MEPE, requires inducible cyclooxygenase-2 to exert potent anabolic effects on normal human marrow osteoblast precursors. *J. Cel Biochem* 93 (6), 1107–1114. doi:10.1002/jcb.20249

Nagy, K., Láng, O., Láng, J., Perczel-Kovách, K., Gyulai-Gaál, S., Kádár, K., et al. (2018). A novel hydrogel scaffold for periodontal ligament stem cells. *Interv. Med. Appl. Sci.* 10 (3), 162–170. doi:10.1556/1646.10.2018.21

Nanci, A., and Bosshardt, D. D. (2000). Structure of periodontal tissues in health and disease. *Periodontol. 2000* 40 (40), 11–28. doi:10.1111/j.1600-0757.2005.00141.x

Nguyen, P. K., Gao, W., Patel, S. D., Siddiqui, Z., Weiner, S., Shimizu, E., et al. (2018). Self-assembly of a dentinogenic peptide hydrogel. *ACS Omega*. 3 (6), 5980–5987. doi:10.1021/acsomega.8b00347

Pandya, M., and Diekwisch, T. G. H. (2019). Enamel biomimetics-fiction or future of dentistry. *Int. J. Oral Sci.* 11 (1), 8. doi:10.1038/s41368-018-0038-6

Park, H. J., Salem, M., Semlali, A., Leung, K. P., and Rouabhia, M. (2017). Antimicrobial peptide KSL-W promotes gingival fibroblast healing properties *in vitro*. *Peptides*. 93, 33-43. doi:10.1016/j.peptides.2017.05.003

Petzold, C., Monjo, M., Rubert, M., Reinholt, F. P., Gomez-Florit, M., Ramis, J. M., et al. (2013). Effect of proline-rich synthetic peptide-coated titanium implants on bone healing in a rabbit model. *Int. J. Oral Maxillofac. Implants* 28 (6), e547–55. doi:10.11607/jomi.te35

Pigossi, S. C., Medeiros, M. C., Saska, S., Cirelli, J. A., and Scarel-Caminaga, R. M. (2016). Role of osteogenic growth peptide (OGP) and OGP(10-14) in bone regeneration: a review. *Int. J. Mol. Sci.* 17 (11), 1885. doi:10.3390/ijms17111885

Piva, E., Silva, A. F., and Nör, J. E. (2014). Functionalized scaffolds to control dental pulp stem cell fate. *J. Endod.* 40 (4, Suppl. ment), S33–S40. doi:10.1016/j.joen.2014.01.013

Polimeni, G., Xiropaidis, A. V., and Wikesjö, U. M. (2000). Biology and principles of periodontal wound healing/regeneration. *Periodontol. 20002006*. 41 (1), 30–47. doi:10.1111/j.1600-0757.2006.00157.x

Pountos, I., Panteli, M., Lampropoulos, A., Jones, E., Calori, G. M., and Giannoudis, P. V. (2016). The role of peptides in bone healing and regeneration: a systematic review. *BMC Med.* 14, 103. doi:10.1186/s12916-016-0646-y

Prajapati, S., Ruan, Q., Mukherjee, K., Nutt, S., and Moradian-Oldak, J. (2018). The presence of MMP-20 reinforces biomimetic enamel regrowth. *J. Dent Res.* 97 (1), 84–90. doi:10.1177/0022034517728504

Qiao, Y., Liu, X., Zhou, X., Zhang, H., Zhang, W., Xiao, W., et al. (2020). Gelatin templated polypeptide Co-Cross-Linked hydrogel for bone regeneration. *Adv. Healthc. Mater.* 9 (1), e1901239. doi:10.1002/adhm.201901239

Rahiotis, C., and Vougiouklakis, G. (2007). Effect of a CPP-ACP agent on the demineralization and remineralization of dentine *in vitro*. *J. Dent.* 35 (8), 695–698. doi:10.1016/j.jdent.2007.05.008

Ramis, J. M., Rubert, M., Vondrasek, J., Gayà, A., Lyngstadaas, S. P., and Monjo, M. (2012). Effect of enamel matrix derivative and of proline-rich synthetic peptides on the differentiation of human mesenchymal stem cells toward the osteogenic lineage. *Tissue Eng. Part. A.* 18 (11-12), 1253–1263. doi:10.1089/ten.tea.2011.0404

Roberts, W. E., Mozsary, P. G., and Klingler, E. (1982). Nuclear size as a cell-kinetic marker for osteoblast differentiation. *Am. J. Anat.* 165 (4), 373–384. doi:10.1002/aja.1001650403

Saghiri, M. A., Asatourian, A., Sorenson, C. M., and Sheibani, N. (2015). Role of angiogenesis in endodontics: contributions of stem cells and proangiogenic and antiangiogenic factors to dental pulp regeneration. *J. Endod.* 41 (6), 797–803. doi:10.1016/j.joen.2014.12.019

Sasaki, T., and Garant, P. R. (1996). Structure and organization of odontoblasts. *Anat. Rec.* 245 (2), 235–249. doi:10.1002/(SICI)1097-0185(199606)245:2<235::AID-AR10>3.0.CO;2-Q

Saska, S., Pigossi, S. C., Oliveira, G. J. P. L., Teixeira, L. N., Capela, M. V., Gonçalves, A., et al. (2018). Biopolymer-based membranes associated with osteogenic growth peptide for guided bone regeneration. *Biomed. Mater.* 13 (3), 035009. doi:10.1088/1748-605X/aaaa2d

Sato, A. K., Viswanathan, M., Kent, R. B., and Wood, C. R. (2006). Therapeutic peptides: technological advances driving peptides into development. *Curr. Opin. Biotechnol.* 17 (6), 638–642. doi:10.1016/j.copbio.2006.10.002

Sattabanasuk, V., Burrow, M. F., Shimada, Y., and Tagami, J. (2014). Bonding of resin luting cements to dentine after casein phosphopeptide-amorphous calcium phosphate (CPP-ACP) treatment. *Int. J. Adhes. Adhesives* 54, 93–99. doi:10.1016/j.ijadhadh.2014.05.008

Sculean, A., Gruber, R., and Bosshardt, D. D. (2014). Soft tissue wound healing around teeth and dental implants. *J. Clin. Periodontol.* 41 (Suppl 15), S6–S22. doi:10.1111/jcpe.12206

Seo, Y. M., Park, S. J., Lee, H. K., and Park, J. C. (2017). Copine-7 binds to the cell surface receptor, nucleolin, and regulates ciliogenesis and Dspp expression during odontoblast differentiation. *Sci. Rep.* 7 (1), 11283. doi:10.1038/s41598-017-11641-y

Seyhan, A. A. (2019). Lost in translation: the valley of death across preclinical and clinical divide – identification of problems and overcoming obstacles. *Translational Med. Commun.* 4 (1), 18. doi:10.1186/s41231-019-0050-7

Six, N., Septier, D., Chaussain-Miller, C., Blacher, R., DenBesten, P., and Goldberg, M. (2007). Dentonin, a MEPE fragment, initiates pulp-healing response to injury. *J. Dent Res.* 86 (8), 780–785. doi:10.1177/154405910708600818

Smith, A. J., Cassidy, N., Perry, H., Bègue-Kirn, C., Ruch, J. V., and Lesot, H. (1995). Reactionary dentinogenesis. *Int. J. Dev. Biol.* 39 (1), 273–280.

Smith, P. C., Cáceres, M., Martínez, C., Oyarzún, A., and Martínez, J. (2015). Gingival wound healing: an essential response disturbed by aging?. *J. Dent Res.* 94 (3), 395–402. doi:10.1177/0022034514563750

Soldatos, N. K., Stylianou, P., Koidou, V. P., Angelov, N., Yukna, R., and Romanos, G. E. (2017). Limitations and options using resorbable versus nonresorbable membranes for successful guided bone regeneration. *Quintessence Int.* 48 (2), 131–147. doi:10.3290/j.qi.a37133

Staines, K. A., MacRae, V. E., and Farquharson, C. (2012). The importance of the SIBLING family of proteins on skeletal mineralisation and bone remodelling. *J. Endocrinol.* 214 (3), 241–255. doi:10.1530/JOE-12-0143

Stürmer, E. (1989). Vasopressin, oxytocin and synthetic analogues: the use of bioassays. *J. Pharm. Biomed. Anal.* 7 (2), 199–210. doi:10.1016/0731-7085(89)80084-6

Tanaka, S., Yasuda, T., Hamada, Y., Kawaguchi, N., Fujishita, Y., Mori, S., et al. (2020). Synthetic peptide SVVYGLR upregulates cell motility and facilitates oral mucosal wound healing. *Peptides*. 134, 170405. doi:10.1016/j.peptides.2020.170405

Tashjian, A. H., Jr., and Gagel, R. F. (2006). Teriparatide [human PTH(1-34)]: 2.5 years of experience on the use and safety of the drug for the treatment of osteoporosis. *J. Bone Miner Res.* 21 (3), 354–365. doi:10.1359/JBMR.051023

Tomokiyo, A., Wada, N., and Maeda, H. (2019). Periodontal ligament stem cells: regenerative potency in periodontium.*Stem Cells Dev.* 28 (15), 974-985. doi:10.1089/scd.2019.0031

Üstün, N., and Aktören, O. (2019). Analysis of efficacy of the self-assembling peptide-based remineralization agent on artificial enamel lesions. *Microsc. Res. Tech.* 82 (7), 1065–1072. doi:10.1002/jemt.23254

Valente, M. T., Moffa, E. B., Crosara, K. T. B., Xiao, Y., de Oliveira, T. M., Machado, M. A. A. M., et al. (2018). Acquired enamel pellicle engineered peptides: effects on hydroxyapatite crystal growth. *Sci. Rep.* 8 (1), 3766. doi:10.1038/s41598-018-21854-4

Vastardis, S., Yukna, R. A., Mayer, E. T., and Atkinson, B. L. (2005). Periodontal regeneration with peptide-enhanced anorganic bone matrix in particulate and putty form in dogs. *J. Periodontol.* 76 (10), 1690–1696. doi:10.1902/jop.2005.76.10.1690

Villa, O., Wohlfahrt, J. C., Mdla, I., Petzold, C., Reseland, J. E., Snead, M. L., et al. (2015). Proline-rich peptide mimics effects of enamel matrix derivative on rat oral mucosa incisional wound healing. *J Periodontol.* 86 (12), 1386-95. doi:10.1902/jop.2015.150207

Villegas-Mercado, C. E., Agredano-Moreno, L. T., Bermúdez, M., Segura-Valdez, M. L., Arzate, H., Del Toro-Rangel, E. F., et al. (2018). Cementum protein 1 transfection does not lead to ultrastructural changes in nucleolar organization of human gingival fibroblasts. *J. Periodontal Res.* 53 (4), 636–642. doi:10.1111/jre.12553

Vlieghe, P., Lisowski, V., Martinez, J., and Khrestchatisky, M. (2010). Synthetic therapeutic peptides: science and market. *Drug Discov. Today* 15 (1-2), 40–56. doi:10.1016/j.drudis.2009.10.009

Wang, C., Liu, Y., Fan, Y., and Li, X. (2017). The use of bioactive peptides to modify materials for bone tissue repair. *Regen. Biomater.* 4 (3), 191–206. doi:10.1093/rb/rbx011

Wang, D., Deng, J., Deng, X., Fang, C., Zhang, X., and Yang, P. (2020). Controlling enamel remineralization by amyloid-like amelogenin mimics. *Adv. Mater.* 32 (31), e2002080. doi:10.1002/adma.202002080

Wang, X., He, H., Wu, X., Hu, J., and Tan, Y. (2014). Promotion of dentin regeneration via CCN3 modulation on Notch and BMP signaling pathways. *Biomaterials* 35 (9), 2720–2729. doi:10.1016/j.biomaterials.2013.12.029

Wikesjö, U. M., and Selvig, K. A. (2000). Periodontal wound healing and regeneration. *Periodontol. 2000* 19 (19), 21–39.

Xia, K., Chen, Z., Chen, J., Xu, H., Xu, Y., Yang, T., et al. (2020). RGD- and VEGF-mimetic peptide epitope-functionalized self-assembling peptide hydrogels promote dentin-pulp complex regeneration. *Int. J. Nanomedicine* 15, 6631–6647. doi:10.2147/IJN.S253576

Xiao, Z., Que, K., Wang, H., An, R., Chen, Z., Qiu, Z., et al. (2017). Rapid biomimetic remineralization of the demineralized enamel surface using nano-particles of amorphous calcium phosphate guided by chimaeric peptides. *Dent Mater.* 33 (11), 1217–1228. doi:10.1016/j.dental.2017.07.015

Yamashita, M., Lazarov, M., Jones, A. A., Mealey, B. L., Mellonig, J. T., and Cochran, D. L. (2010). Periodontal regeneration using an anabolic peptide with two carriers in baboons. *J. Periodontol.* 81 (5), 727–736. doi:10.1902/jop.2010.090224

Yang, Y., Lv, X., Shi, W., Zhou, X., Li, J., and Zhang, L. (2016). Synergistic inhibition of enamel demineralization by peptide 8DSS and fluoride. *Caries Res.* 50 (1), 32–39. doi:10.1159/000442896

Yang, Y., Lv, X. P., Shi, W., Li, J. Y., Li, D. X., Zhou, X. D., et al. (2014). 8DSS-promoted remineralization of initial enamel caries *in vitro*. *J. Dent Res.* 93 (5), 520–524. doi:10.1177/0022034514522815

Yang, Y., Yang, B., Li, M., Wang, Y., Yang, X., and Li, J. (2017). Salivary acquired pellicle-inspired DpSpSEEKC peptide for the restoration of demineralized tooth enamel. *Biomed. Mater.* 12 (2), 025007. doi:10.1088/1748-605X/aa5daf

Yarbrough, D. K., Hagerman, E., Eckert, R., He, J., Choi, H., Cao, N., et al. (2010). Specific binding and mineralization of calcified surfaces by small peptides. *Calcif Tissue Int.* 86 (1), 58–66. doi:10.1007/s00223-009-9312-0

Yen, A. H., and Yelick, P. C. (2011). Dental tissue regeneration - a mini-review. *Gerontology*. 57, 85–94. doi:10.1159/000314530

Yoshida, S., Tomokiyo, A., Hasegawa, D., Hamano, S., Sugii, H., and Maeda, H. (2020). Insight into the role of dental pulp stem cells in regenerative therapy. *Biology (Basel)*. 9 (7), 160. doi:10.3390/biology9070160

Yukna, R., Salinas, T. J., and Carr, R. F. (2002). Periodontal regeneration following use of ABM/P-1 5: a case report. *Int. J. Periodontics Restorative Dent.* 22 (2), 146–155.

Zanetti, M. (2004). Cathelicidins, multifunctional peptides of the innate immunity. *J. Leukoc. Biol.* 75 (1), 39–48. doi:10.1189/jlb.0403147

Zeichner-David, M., Chen, L. S., Hsu, Z., Reyna, J., Caton, J., and Bringas, P. (2006). Amelogenin and ameloblastin show growth-factor like activity in periodontal ligament cells. *Eur. J. Oral Scidiscussion* 114 (Suppl 1), 244–253. doi:10.1111/j.1600-0722.2006.00322.x

Zero, D. T., Zandona, A. F., Vail, M. M., and Spolnik, K. J. (2011). Dental caries and pulpal disease. *Dent Clin. North. Am.* 55 (1), 29–46. doi:10.1016/j.cden.2010.08.010

Zhang, B., Sun, Y., Chen, L., Guan, C., Guo, L., and Qin, C. (2010). Expression and distribution of SIBLING proteins in the predentin/dentin and mandible of hyp mice. *Oral Dis.* 16 (5), 453–464. doi:10.1111/j.1601-0825.2010.01656.x

Zhang, W., Wu, S. Z., Zhou, J., Chen, H. M., Gong, Y. L., Peng, F. F., et al. (2017). Parathyroid hormone-related peptide (1-34) reduces alveolar bone loss in type 1 diabetic rats. *Arch. Oral Biol.* 83, 13–19. doi:10.1016/j.archoralbio.2017.06.013

Zhou, Y., Zhou, Y., Gao, L., Wu, C., and Chang, J. (2018). Synthesis of artificial dental enamel by an elastin-like polypeptide assisted biomimetic approach. *J. Mater. Chem. B.* 6 (5), 844–853. doi:10.1039/c7tb02576a

Conflict of Interest: The authors declare that the research was conducted in the absence of any commercial or financial relationships that could be construed as a potential conflict of interest.

frontiers in Materials

ORIGINAL RESEARCH
published: 10 May 2021
doi: 10.3389/fmats.2021.681415

Chemometrics-Assisted Raman Spectroscopy Characterization of Tunable Polymer-Peptide Hybrids for Dental Tissue Repair

Paulette Spencer[1,2,3], Qiang Ye[1]*, Nilan J. B. Kamathewatta[1,3], Sarah K. Woolfolk[1,3], Brenda S. Bohaty[4], Anil Misra[1,5] and Candan Tamerler[1,2,3]*

[1] Institute for Bioengineering Research, University of Kansas, Lawrence, KS, United States, [2] Department of Mechanical Engineering, University of Kansas, Lawrence, KS, United States, [3] Bioengineering Program, University of Kansas, Lawrence, KS, United States, [4] Department of Pediatric Dentistry, School of Dentistry, University of Missouri-Kansas City, Kansas City, MO, United States, [5] Department of Civil Engineering, University of Kansas, Lawrence, KS, United States

OPEN ACCESS

Edited by:
Mary Anne Sampaio Melo, University of Maryland, Baltimore, United States

Reviewed by:
Roberto Braga, University of São Paulo, Brazil
Ingrid Fernandes Mathias-Santamaria, University of Maryland, Baltimore, United States
May Lei Mei, University of Otago, New Zealand
Lamia Sami Mokeem, University of Maryland, Baltimore, United States
Isadora Garcia, Federal University of Rio Grande do Sul, Brazil

***Correspondence:**
Paulette Spencer
pspencer@ku.edu
Qiang Ye
yeq@ku.edu

Specialty section:
This article was submitted to Biomaterials, a section of the journal Frontiers in Materials

Received: 16 March 2021
Accepted: 15 April 2021
Published: 10 May 2021

Citation:
Spencer P, Ye Q, Kamathewatta NJB, Woolfolk SK, Bohaty BS, Misra A and Tamerler C (2021) Chemometrics-Assisted Raman Spectroscopy Characterization of Tunable Polymer-Peptide Hybrids for Dental Tissue Repair. Front. Mater. 8:681415. doi: 10.3389/fmats.2021.681415

The interfaces that biological tissues form with biomaterials are invariably defective and frequently the location where failure initiates. Characterizing the phenomena that lead to failure is confounded by several factors including heterogeneous material/tissue interfaces. To seamlessly analyze across these diverse structures presents a wealth of analytical challenges. This study aims to develop a molecular-level understanding of a peptide-functionalized adhesive/collagen hybrid biomaterial using Raman spectroscopy combined with chemometrics approach. An engineered hydroxyapatite-binding peptide (HABP) was copolymerized in dentin adhesive and dentin was demineralized to provide collagen matrices that were partially infiltrated with the peptide-functionalized adhesive. Partial infiltration led to pockets of exposed collagen—a condition that simulates defects in adhesive/dentin interfaces. The spectroscopic results indicate that co-polymerizable HABP tethered to the adhesive promoted remineralization of the defects. The spatial distribution of collagen, adhesive, and mineral as well as crystallinity of the mineral across this heterogeneous material/tissue interface was determined using micro-Raman spectroscopy combined with chemometrics approach. The success of this combined approach in the characterization of material/tissue interfaces stems from its ability to extract quality parameters that are related to the essential and relevant portions of the spectral data, after filtering out noise and non-relevant information. This ability is critical when it is not possible to separate components for analysis such as investigations focused on, *in situ* chemical characterization of interfaces. Extracting essential information from complex bio/material interfaces using data driven approaches will improve our understanding of heterogeneous material/tissue interfaces. This understanding will allow us to identify key parameters within the interfacial micro-environment that should be harnessed to develop durable biomaterials.

Keywords: raman chemical imaging, chemometrics, divisive clustering analysis, peptide-mediated remineralization, peptide-tethered adhesive, collagen, hybrid

Abbreviations: AdhI, Adhesive Infiltration; DCA, divisive clustering analysis; DD, Demineralized Dentin; FWHM, Full-width half-maximum; GMC, Gradient in Mineral Content; HABP, hydroxyapatite-binding peptide; ID, Intact Dentin; MMES, mono(2-methacryloyloxy)ethyl succinate; MMR, Mineral-matrix Ratio; P-AIDD, (Peptide-functionalized-adhesive)-Adhesive-Infiltrated Demineralized Dentin; P-PIDD, (Peptide-functionalized adhesive)-Partially-Infiltrated Demineralized Dentin.

INTRODUCTION

Clinical Need

Untreated dental caries of permanent teeth impact 2.3 billion people across the globe and more than 530 million children suffer from untreated dental caries of primary teeth (WHO, 2020). Tooth decay is the most common chronic childhood disease (Garvin, 2021).

The most popular material for the repair of lost or damaged tooth structure is dental composite (Ferracane, 2017; Eltahlah et al., 2018), but composite fails at a rate 2–3.5 times the rate of dental amalgam (Ferracane, 2013; Schwendicke et al., 2016; Afrashtehfar et al., 2017; Makvandi et al., 2018). The cycle of repeated composite-restoration replacements is a pernicious problem—each replacement risks pulpal injury, increased tooth weakness, and eventually, tooth loss (Opdam et al., 2016). Patients at high risk for caries, such as the 4 million United States children (Palmer, 2013) and more than 100 million adults (National Center for Health Statistics (US), 2007) who do not receive regular dental care, are particularly vulnerable to composite-restoration failure and the downward spiral associated with frequent replacements (Kopperud et al., 2015; Schwendicke et al., 2016).

Composite Restoration Failure

The leading cause of composite-restoration failure is recurrent marginal decay (**Figure 1**; Stewart and Finer, 2019). Unlike amalgam, composite lacks the inherent capability to seal gaps at the interface between the restorative material and tooth structure. The low-viscosity adhesive that bonds the composite to the tooth is intended to seal this interface, but the adhesive seal to dentin is fragile—it is readily damaged by acids, enzymes, and oral fluids. The fragility of the adhesive/dentin seal is traced to the hybrid layer.

The ideal hybrid layer is described as a 3D polymer/collagen construct that provides a continuous and stable link between the bulk adhesive and mineralized dentin, but this ideal is not achieved—the hybrid layer retains pockets of resin-sparse collagen that are at inherent risk of degradation (Spencer and Swafford, 1999; Spencer and Wang, 2002; Wang and Spencer, 2005; Spencer et al., 2006; Kermanshahi et al., 2010; Liu et al., 2011; Pashley et al., 2011; Tjaderhane et al., 2013). The pockets of resin-sparse collagen are readily infiltrated by bacterial enzymes and acids—hydrolysis provoked by these agents leads to a breach of the interfacial seal. Once the seal is breached, acids and enzymes permeate defects in the adhesive bond to the inter-, intra-, and peritubular dentin (**Figure 2**). Bacteria and bacterial by-products traverse these imperfections, destroying tooth structure and eroding adhesive in its path.

Bioactive Strategies to Increase Stability of the Hybrid Layer

A variety of strategies have been explored to increase the stability and durability of the hybrid layer. One particularly promising strategy is remineralization—voids are filled with mineral to reduce the permeability of the hybrid layer.

Several groups have proposed biomimetic remineralization as a novel approach to increase the durability of the hybrid layer (Lin et al., 2016; Nurrohman et al., 2016; Panseri et al., 2016; Moussa and Aparicio, 2019; Ye et al., 2021). As an example, a calcium phosphate polymer-induced liquid precursor (Ca/P-PILP) was used to promote the repair of artificially induced, carious dentin (Bacino et al., 2019; Chen et al., 2020). The PILP promoted the recovery of both the structure and mechanical properties of the damaged dentin (Saeki et al., 2017; Saxena et al., 2019).

Our group used peptides to promote the remineralization of defective dentin matrices (Ye et al., 2017). With this peptide-mediated approach, we demonstrated that calcium phosphate minerals were formed at the deficient adhesive/dentin interface. While these results were promising, self- assembled peptide binding at this interface could lead to peptide diffusion and limited active conformations due to the challenges associated at the hybrid layer. To address this limitation, we prepared a peptide-functionalized adhesive to provide *in situ* presentation of the bioactive cues at the adhesive/dentin interface. The hydroxyapatite binding peptides (HABP) were synthesized using oligomeric spacers to tether them to a methacrylic acid (MA) as co-polymerizable peptide in the dental adhesive. Demineralized dentin collagen was partially infiltrated with the peptide-functionalized adhesive—the adhesive/collagen hybrids mimic adhesive/dentin interfaces that contain defects such as pockets of resin-sparse collagen (Spencer and Swafford, 1999; Spencer et al., 2000; Wang et al., 2007).

In situ Characterization

The adhesive/collagen hybrids contain vastly different structures and heterogeneous composition. To seamlessly analyze across these complex, heterogeneous interfaces presents numerous analytical challenges. Regardless of the challenges, *in situ* characterization is central to identifying factors key to designing a peptide-functionalized adhesive that promotes remineralization of defective dentin matrices.

Raman microspectroscopy has steadily evolved to become a versatile method for *in situ* structural characterization of the adhesive/dentin interface (Suzuki et al., 1991; Van Meerbeek et al., 1993; Lemor, 1997; Wang and Spencer, 2002b; Spencer and Wang, 2007; Wang et al., 2007). The Raman spectrum probes the chemical structure and provides a distinct "fingerprint" of the molecules present in a sample and can be used for both qualitative identification and quantitative determination. This vibrational spectroscopy technique has many advantages—it is non-destructive, non-invasive, and multi-dimensional results are obtained in minutes. This technique provides suitable sensitivity for analyzing mineral polymorphism and crystallinity (Wang et al., 1994, 2006; Ohsaki et al., 1995; Tsuda et al., 1996; Kontoyannis et al., 1997).

Usually, hyperspectral Raman imaging consists of thousands of spectra gathered in a data-cube, i.e., a three-dimensional matrix with two spatial dimensions (x, y) and one spectral dimension (λ). It can be challenging to extract useful information from these large, complex datasets (Paudel et al., 2015; Rebiere et al., 2018). If an individual component can be uniquely identified by a spectral band, analysis of its band intensity is

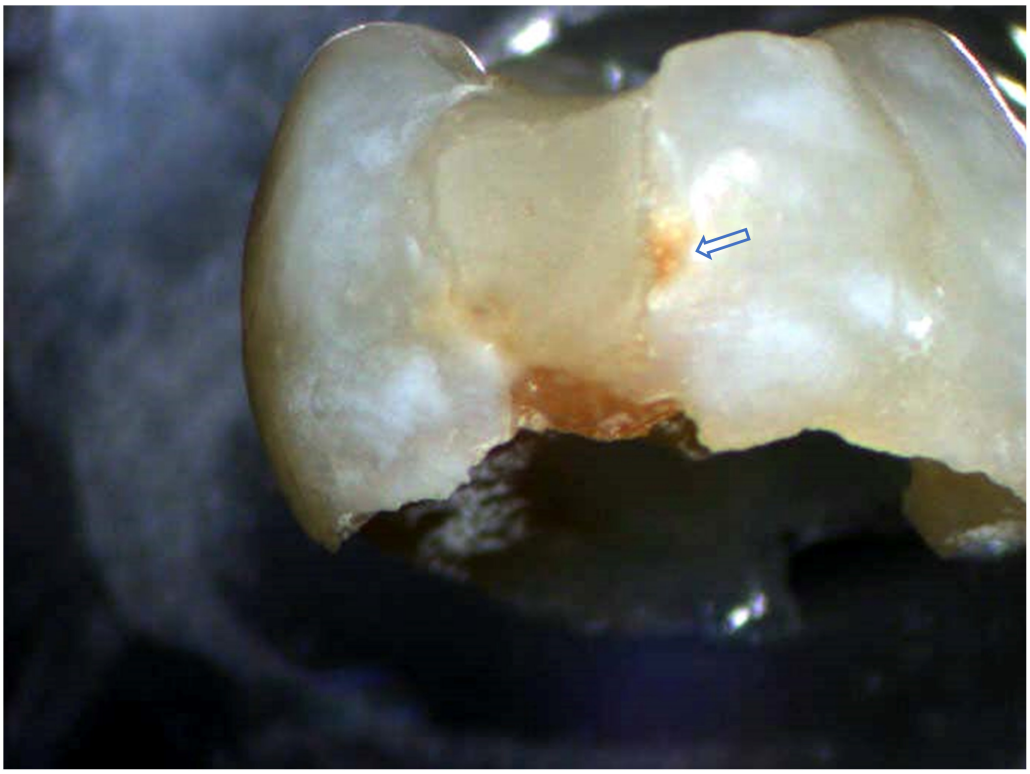

FIGURE 1 | Exfoliated primary molar with Class II composite restoration. Brown stain along the interface between the composite material and tooth structure indicates recurrent decay at the material/tooth interface.

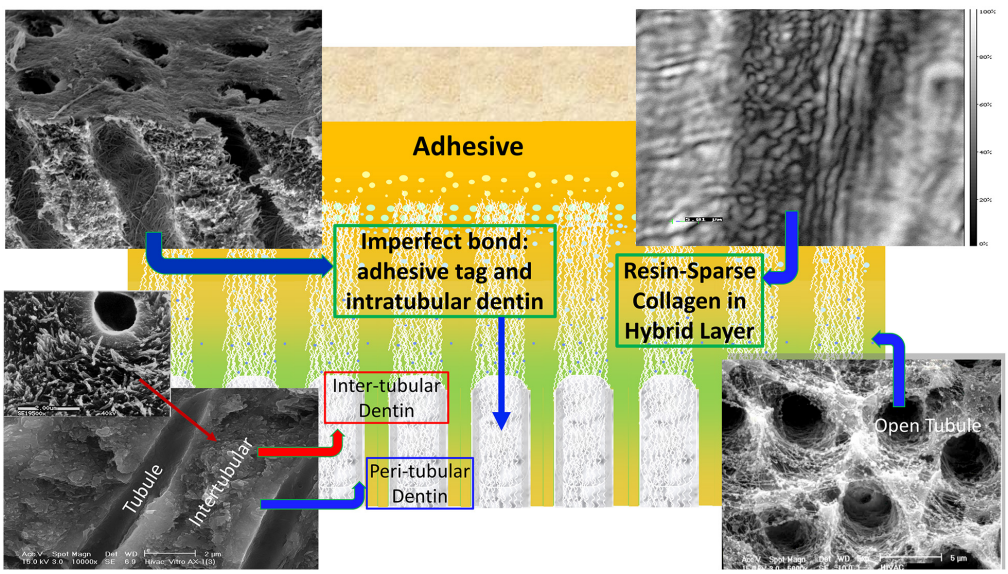

FIGURE 2 | A schematic depicting cross-section of adhesive infiltrating dentin. Areas of resin-sparse collagen within the hybrid layer are illustrated as well as imperfect adhesive bonds to intra-, inter-, and peritubular dentin.

relatively straightforward and such analysis is used to identify its location in the sample. This univariate analysis is considered the simplest and most frequently used method and, in many cases, can provide sufficient information and reliable predictability (Wieliczka et al., 1997; Salzer et al., 2000; Wang and Spencer, 2002a,b; Wang et al., 2006; Sinjab et al., 2017).

Univariate analysis is generally not sufficient when spectral bands partially overlap due to interference from other components in the specimen. Under these circumstances, the analysis of spectra datasets requires additional procedures to extract useful information (Calvo et al., 2018). Multi-variate analysis, i.e., chemometrics can be used to address these challenges and to identify important details hidden in the structure. Common multivariate methods include principal component analysis, partial least square regression (PLS), classical least square (CLS), multivariate curve resolution (MCR), partial least square discriminant analysis (PLS-DA), and so forth (Paudel et al., 2015; Dina et al., 2018; Pisapia et al., 2018; Rebiere et al., 2018; Fang et al., 2020).

In this study, divisive cluster analysis was used in combination with micro-Raman spectroscopy to analyze details hidden in the structure of the peptide-functionalized adhesive/collagen hybrid before and after peptide-mediated remineralization. The spatial distribution and relative concentration of the components as well as crystallinity of the mineral produced as a result of peptide-mediated remineralization were determined. To analyze the earliest stage of peptide-mediate mineralization at the collagen interface, type I collagen model and co-polymerizable hydroxyapatite-binding peptide were studied using atomic force microscopy as a complementary technique to micro-Raman spectroscopy. Our results demonstrate that the structural details revealed by Raman spectroscopy combined with chemometrics enhance our understanding of the composition and mineralization capability at the challenging biohybrid interfaces.

MATERIALS AND METHODS

Materials

The following components were obtained from Sigma-Aldrich (St. Louis, MO): 2-hydroxyethyl methacrylate (HEMA), triethylene glycol dimethacrylate (TEGDMA), methacrylic acid (MA), camphoroquinone (CQ), ethyl-4-(dimethylamino) benzoate (EDMAB), diphenyliodonium hexafluorophosphate (DPIHP), mono(2-methacryloyloxy)ethyl succinate (MMES), dodecyltrichlorosilane, chlorhexidine digluconate (CHX), N, N-Dimethylformamide (DMF), dichloromethane (DCM), and N-methyl morpholine (NMM). γ-methacryloxypropyl trimethoxysilane (MPS) was used as received from MP Biomedicals (Solon, OH). Rink amide resin, Fmoc-amino acid building blocks and 2-(1H-benzotriazole-1-yl)-1,1,3,3-tetramethyluranium hexafluorophosphate (HBTU) were purchased from AAPPTec LLC (Louisville, KY). All chemicals were used as received without further purification.

Co-polymerizable Hydroxyapatite-Binding Peptide

We demonstrated that hydroxyapatite-binding peptide (HABP) having CMLPHHGAC sequence can selectively self-assemble on hydroxyapatite minerals, control mineralization nucleation and growth kinetics, and guide the nano- to micro-structure organization of the mineral in the absence of cells (Gungormus et al., 2008; Ye et al., 2017). We developed spacer design to conjugate peptides to the methacrylate-based monomers by providing reactive groups for monomer conjugation as well as sufficient length and flexibility to preserve the peptide's properties once the polymer has cured (Xie et al., 2020). The co-polymerizable hydroxyapatite-binding peptide, MMES-KGGG_HABP or MA-KGGG-HABP was synthesized in our lab (with KGGG as the spacer), via an amidation reaction between the free amine group (peptide) and carboxylic acid group of the monomers (Xie et al., 2020). Briefly, Fmoc-resin-bound peptide with a spacer was first synthesized through Fmoc-chemistry using a solid-phase peptide synthesizer (AAPPTEC Focus XC). Upon peptide-chain completion (including spacer sequence), MA or MMES, NMM, and HBTU were added to react with the Fmoc-resin-bound peptide in DMF at 23 ± 2°C overnight under constant gentle rotation. After the conjugation reaction, the Fmoc-resin-bound product was washed sequentially with DMF, DCM, acetone, and ethanol. The crude co-polymerizable HABP was then cleaved from the Fmoc resin and purified on a HPLC system (Waters Corp., Milford, MA, United States) equipped with a Luna® column packed with 10 μm C18 silica (250 × 4.6 mm, Phenomenex Inc., Torrance, CA, United States). The co-polymerizable peptide was lyophilized, and stored at −20°C. Crude peptides were also cleaved from the resin and then purified. The purified peptide fractions were combined and lyophilized (Xie et al., 2020).

Preparation of Peptide-Functionalized Adhesive Formulation

The model hydrophilic adhesive consisted of 2-hydroxyethylmethacrylate (HEMA), triethylene glycol dimethacrylate (TEGDMA) and (trimethoxysilyl) propyl methacrylate (MPS) with a mass ratio of 8/1/1 (HEMA/TEGDMA/MPS). This model hydrophilic adhesive system has been developed and optimized for peptide engineering in our previous investigations (Ye et al., 2011; Abedin et al., 2014; Xie et al., 2020). The following photoinitiators (all from Aldrich, Milwaukee, WI, United States) were used: camphoroquinone (CQ), ethyl-4-(dimethylamino) benzoate (EDMAB) and diphenyliodonium hexafluorophosphate (DPIHP). The amounts of photosensitizer, coinitiator amine and iodonium salt were fixed at 0.5 mass% with respect to the total amount of monomer (Guo et al., 2008; Ye et al., 2009; Song et al., 2014). The resin mixtures were prepared in a brown glass vial under amber light. Continuous shaking and sonication for 48 h were required to yield well-mixed homogenous resin solutions (Song et al., 2016). The hydrophilic adhesive formulation was mixed with 10 mass per-cent co-polymerizable hydroxyapatite-binding peptide, e.g., MMES- KGGG_HABP, and diluted with ethanol in a weight ratio of 80/20.

Dentin Demineralization

Extracted unerupted human third molars (n = 8) were collected and stored at 4°C in 0.9% w/v NaCl containing 0.002% sodium azide (these teeth would otherwise be discarded, no patient identifiers are associated with the teeth and thus, this is not

considered human subjects research). The occlusal 1/3 of the crown was sectioned perpendicular to the long axis of a human molar using a water-cooled low-speed diamond saw (**Scheme 1**). The retrieved disc-shaped specimens are ∼1-mm thick. The dentin surface was polished on 600-, 1, 200-, and 2000-grit silicon carbide papers, respectively, under running water, followed by sonication for 10 min between each grit to remove cutting debris. The dentin discs with surrounding enamel were etched for 6 h with 10% phosphoric acid. This etching protocol is different from the commonly employed clinical treatment, i.e., 20 s etching with 34% phosphoric acid. Our objective was to provide a substantial and uniform zone of completely demineralize dentin—the resultant collagen network was used to monitor the remineralization effect. To evaluate the extent of demineralization, randomly selected specimens were fractured in liquid nitrogen and the exposed fracture surface was characterized using micro-Raman spectroscopy. The depth of demineralization was usually 100–200 microns for the 1 mm thick dentin disc, and the etched zone was uniform and presented as a completely demineralized collagen network. There was no detectable mineral loss in the region identified as intact dentin (ID).

Preparation of Test Group and Control Samples

Test Group Samples

Following demineralization, randomly selected dentin disc specimens were immersed in the liquid resin, i.e., the peptide-functionalized adhesive, and stored for 48 h in the dark. Dark storage for 48 h allowed time for full infiltration of the liquid resin throughout the demineralized dentin zone, that means the infiltration depth reached 100–200 microns for the 1-mm thick disc specimens. At 48 h, the sample was removed from the liquid resin and a stream of air was blown across the surface to remove excess resin. The sample was polymerized using a halogen light curing unit of irradiance 550 mW/cm^2 for 60 s. The specimen was stored in the dark at room temperature for 24 h to provide time for post-cure polymerization. The test group samples are noted as (Peptide-functionalized-adhesive)-Adhesive-Infiltrated Demineralized Dentin (P-AIDD).

Control Specimens

Randomly selected demineralized dentin discs were used as the control group. The control specimens are noted as demineralized dentin (DD).

Remineralization

The mineralization solution (2X) was prepared using 48 mM $CaCl_2$ and 28.8 mM β-Glycerophosphate (β-GP) in 50 mM Tris-HCl buffer, pH 7.4 (Ye et al., 2017). The test group and control samples were fractured in the middle, and then incubated with mineralization solution for 72 h at 37°C with a daily change of fresh biomineralization solution. The remineralization reaction was initiated by adding alkaline phosphatase (AP, Thermo Scientific) at a final concentration of 1.4×10^{-6} g/mL. In this reaction, the enzyme alkaline phosphatase hydrolyses the organic phosphate compound to PO_4^{-3}. Shaking at 100 rpm continued throughout the exposure of the samples to the mineralization solution.

Raman Spectroscopy

The demineralized dentin specimens (as control) and P-AIDD specimens (as test group samples) before and after remineralization were imaged using a LabRAM ARAMIS Raman microscope (HORIBA Jobin Yvon, Edison, NJ, United States). This Raman spectrometer was equipped with a HeNe laser (λ = 633 nm, a laser power of 17 mW) as an excitation source. The samples were mounted in a computer-controlled, high-precision x-y stage. Raman spectra were acquired under these instrument conditions: 200 μm confocal hole, 150 μm wide entrance slit, 600 g/mm grating, 15 s spectra acquisition time, four acquisitions per cycle, and 50X long working distance objective Olympus lens. With the assistance of HORIBA's EasyNav^{TM} package, Raman spectra were acquired over a range of 300–1,800 cm^{-1} and data processing was performed using LabSPEC 6 software (HORIBA Jobin Yvon, Edison, NJ, United States). In this work, two-dimensional micro-Raman mapping/imaging was used to determine the spatial relationships and distribution of the functional or chemical groups. The spectra were collected from the defined area at regular intervals of 15 μm in both X and Y planes. At least four rectangular areas from test group or control group samples were imaged and submitted to spectral analysis.

Chemometrics Analysis

A number of multivariate chemometric methods powered by Eigenvector Research Inc. are fully integrated in LabSPEC 6's Multivariate Analysis (MVA) module (HORIBA Jobin Yvon, Edison, NJ). Divisive Clustering Analysis (DCA) was selected for this study to classify and group related spectra. Using DCA the specimen was divided into chemically different regions with successively increasing detail. A rectangular area of the surface was imaged and submitted to DCA, which includes a statistical pattern to derive the independent clusters. Principal Components Analysis decomposed the data set into a bilinear model of linear independent variables, the so-called principal components (PCs). DCA initially assumes that all spectra belong to a class. Through an iterative process, spectra are divided into the specified number of groups, so that spectra belonging to the same group are similar to each other. The results are class memberships for each spectrum. Once analysis is completed the average spectrum of each class will be displayed together with the analysis statistics. The class membership images reveal which class each pixel spectrum has been assigned. For each test group or control group, at least four rectangular areas are imaged and submitted to DCA, and a representative image was presented.

Further Spectral Analysis

The average spectra were calculated for each cluster, which can be used to provide information on peak parameters (e.g., position, width, amplitude, area) and component distribution in Raman images. At this point, the components were analyzed as follows.

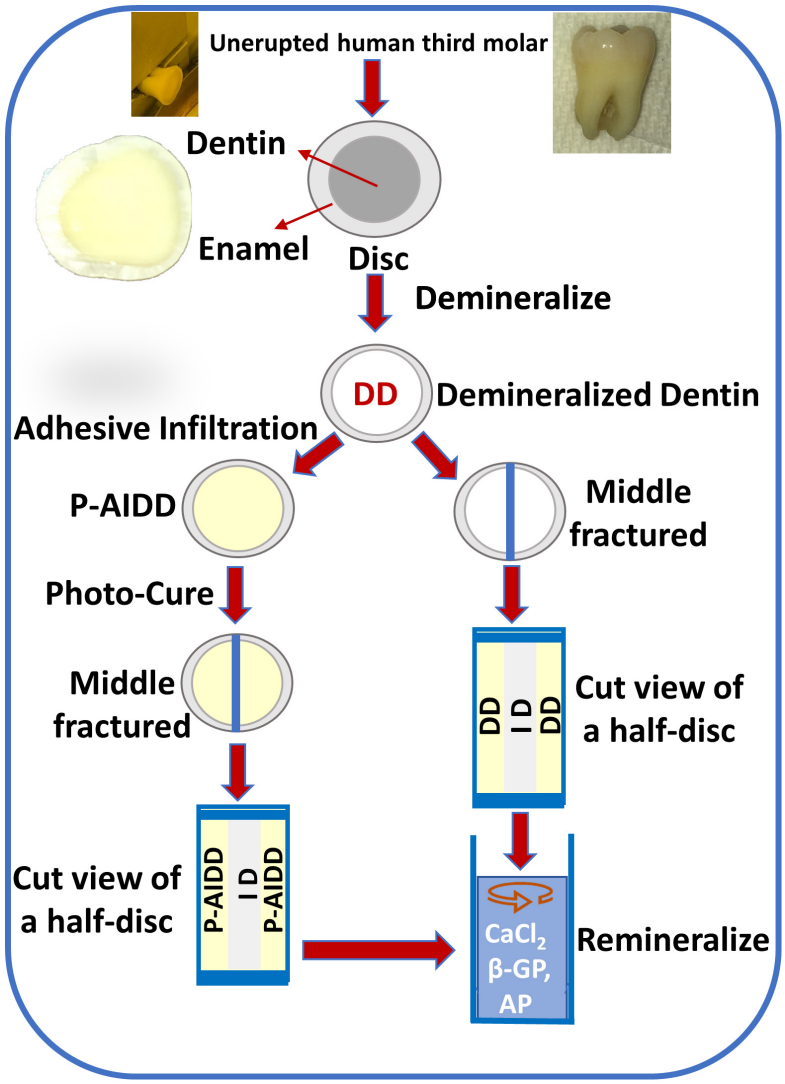

SCHEME 1 | Flow chart of the steps involved in obtaining demineralized dentin (DD) samples and peptide-functionalized adhesive-infiltrated demineralized dentin (P-AIDD) samples and their remineralization protocol.

Relative Mineral Concentration

Mineral-to-matrix ratio (MMR) was inferred from the ratio of the intensities of the peaks at 960 cm^{-1} (phosphate) and 1,460 cm^{-1} (CH_2 wagging, amide II). The index was representative of the maximum relative degree of mineralization.

Crystallinity

Crystallinity was evaluated based on the full width at half maximum (FWHM) of the $\nu 1$ phosphate band at 960 cm^{-1}. This index expressed the crystallographic or relative atomic order, since narrower peaks suggest less structural variation in bond distances and angles. In general, the narrower the spectral peak width, the higher the degree of mineral crystallinity.

Gradient in mineral content (GMC), or carbonate content of mineral crystallites: GMC was based on the ratio of the relative peak heights of 1,070 cm^{-1} (carbonate) to 960 cm^{-1} (phosphate). This ratio provided an assessment of carbonate substitution for phosphate.

Adhesive Infiltration (AdhI)

The ratio of the relative peak heights of 1,450/1,667 was used to assess the extent of adhesive infiltrated into the collagen matrix. The peak at 1,450 cm^{-1} is assigned to the CH_2 group of methacrylate-based adhesive, and the peak at 1,667 cm^{-1} is assigned to amide I associated with collagen.

Statistical analysis was used to identify significant differences in the means. The results (FWHM, GMC, Relative mineral concentration, and adhesive infiltration) were analyzed using one-way analysis of variance (ANOVA) together with Tukey's test at $\alpha = 0.05$ (Microcal Origin Version 8.0, Microcal Software Inc., Northampton, MA, United States).

Analyses of Earliest Stage Mineralization

To assess the earliest stages of peptide-mediated mineralization at the interface between collagen and co-polymerizable hydroxyapatite-binding peptide (MAHABP), type I collagen model specimens prepared by spin-coating were analyzed using atomic force microscopy. Aqueous collagen solution (type I) from rat tail (Sigma C3867) mixed with 4mg/ml HABP or MAHABP was coated on round glass coverslip (12 mm diameter, 26023, Ted Pella Inc.) with a WS-400E-6NPP-LITE spin coater (Laurell Technologies, North Wales, PA) at speed of 1000 RPM. The resultant thin film was incubated with mineralization solution for 20 or 40 min, and then analyzed using AFM and Raman. The AFM images were obtained with a Multimode 8 HR scanning probe microscope (Bruker Corporation, Camarillo, CA) operated in tapping mode under ambient conditions ($24 \pm 2°C$, $40\% \pm 5\%$ RH). Tapping mode etched silicon probes (Prod No.: RTESPA-300, Bruker) were used, having a resonant frequency of about 285 KHz. The length and thickness of the probes were 115–135 μm and 38–42 μm, respectively. Images of each sample were recorded with Nanoscope 8.15 software and analyzed with the Nanoscope Analysis 2.0 software. Related, but separate samples of type I collagen model specimens mixed with MAHABP were analyzed using Raman.

RESULTS

Two-dimensional XY Raman imaging is acquired from the scan area of the demineralized dentin specimen shown in the light micrograph (**Figure 3A**). Spectra are acquired at points across the DD (left, **Figure 3A**) and ID (right, **Figure 3A**). The most straightforward method of spectral analysis is to create functional group maps based on band intensities, band areas, or band ratios (univariate analysis). The micro-Raman mineral map (**Figure 3B**) is a "false-color composite" image generated from band ratios 960 cm^{-1} (PO_4^{-3})/1,460 cm^{-1} (CH_2 wagging, amide II). In this image, intact dentin is dark red while demineralized dentin is blue.

A color representation of the K-means cluster analysis, corresponding to the same mapping zone shown in **Figure 3B**, is presented in **Figure 3C**. This technique was used to divide the scanned area into chemically different regions in successively increasing detail. The cluster analysis displayed two well-distinguished classes, and their multivariate maps were displayed in the overlay mode confirming the result from the univariate analysis, e.g., the demineralized dentin (in green) on the left and intact dentin (in red) on the right. The cluster centroid spectra from the two principal components are derived (**Figure 3D**), which denote the center of the mean of the clusters. For each point of analysis, all spectra described for each cluster were averaged to obtain the mean cluster spectrum. The Raman spectral features of ID associated with dentin mineral are phosphate (PO_4^{-3}) and carbonate (CO_3^{-2}) at 960 cm^{-1} and 1,070 cm^{-1}, respectively. These mineral-derived bands diminished in the demineralized dentin spectra, where spectral features assigned to dentin collagen became obvious, such as 1,003 cm^{-1} (C-C in phenyl group), 1,667 cm^{-1} (*C* = O, amide I), 1,460 cm^{-1} (CH_2 wagging, amide II), and doublet bands from 1,215 to 1,310 cm^{-1} (N-H, amide III) (**Figure 3D**).

The representative Raman images of peptide-functionalized adhesive-infiltrated demineralized dentin (P-AIDD) specimens are shown in **Figure 4**. For ease of comparison, **Figure 4** is presented in a manner similar to **Figure 3**. Two-dimensional XY Raman imaging is acquired from the scan area shown in the light micrograph (**Figure 4A**). The micro-Raman mineral map (**Figure 4B**) is generated from band ratios 960 cm^{-1} (PO_4^{-3})/1,460 cm^{-1} (CH_2 wagging, amide II) and in this image, intact dentin is dark red while peptide-functionalized adhesive-infiltrated demineralized dentin is blue. **Figure 4C** is the K-means clustering map (DCA) of the Raman profile of the same scan area. With the assistance of the cluster analysis, a false color-image of the substrate, on the basis of similar spectral features, was produced. As the cluster centroids are essentially means of the cluster score for the elements of the cluster, ID and three regions on the left could be identified and examined for each cluster (**Figure 4C**).

In addition to the collagen features, the Raman spectral features associated with methacrylate-based adhesive appeared in these three regions, such as 605 cm^{-1} (C-COO),853 cm^{-1} (ν CH_2),1,084 cm^{-1} (ν C-C), 1,450 cm^{-1} (CH def), 1,608 cm^{-1} (phenyl), 1,635 cm^{-1} (ν *C* = C), and 1,710 cm^{-1} (ν *C* = O). The band intensity of 1,635 cm^{-1} (ν *C* = C) is quite weak indicating the infiltrated adhesive was polymerized well, i.e., high degree of monomer-to-polymer conversion. The spectral features associated with adhesive contributed less in the two small regions on the far left, thus these two small regions are identified as partially infiltrated demineralized dentin (P-PIDD). As a reference, Raman spectra of peptide-functionalized adhesive and co-polymerizable hydroxyapatite binding peptide (MMES-KGGG_HABP) are shown in **Supplementary Figure 1**. Raman spectra of intact dentin, demineralized dentin and peptide-functionalized adhesive-infiltrated demineralized dentin are shown in **Supplementary Figure 2**. Spectra acquired from calcium phosphate standards, i.e., hydroxyapatite, α-tricalcium phosphate, β-tricalcium phosphate, and amorphous calcium phosphate are shown in **Supplementary Figure 4**.

Raman images of the specimens following treatment with the remineralization protocol are presented in **Figure 5**. Analyses of representative peptide-functionalized-adhesive-infiltrated regions (P-AIDD) and control demineralized dentin specimens are presented in **Figures 5A,B**, respectively. The micro-Raman mineral map of a representative P-AIDD specimen (**Figure 5Aa1**) shows mineral throughout the area represented by peptide-functionalized-adhesive-infiltrated regions and extending into the intact dentin region. Following treatment with the remineralization protocol, the P-AIDD specimen demonstrated a layer of peptide-mediated mineral with distinct spectral features associated with ν1 phosphate band at 960 cm^{-1} (**Figure 5Aa4**). In contrast, there is a distinct absence of the characteristic band associated with mineral (960 cm^{-1}) in the control demineralized dentin specimen after the remineralization protocol (**Figure 5b1**). The cluster analysis verifies this result (**Figure 5b2**) showing the DD region (in green) and ID (in red). The visible images of the control demineralized dentin samples

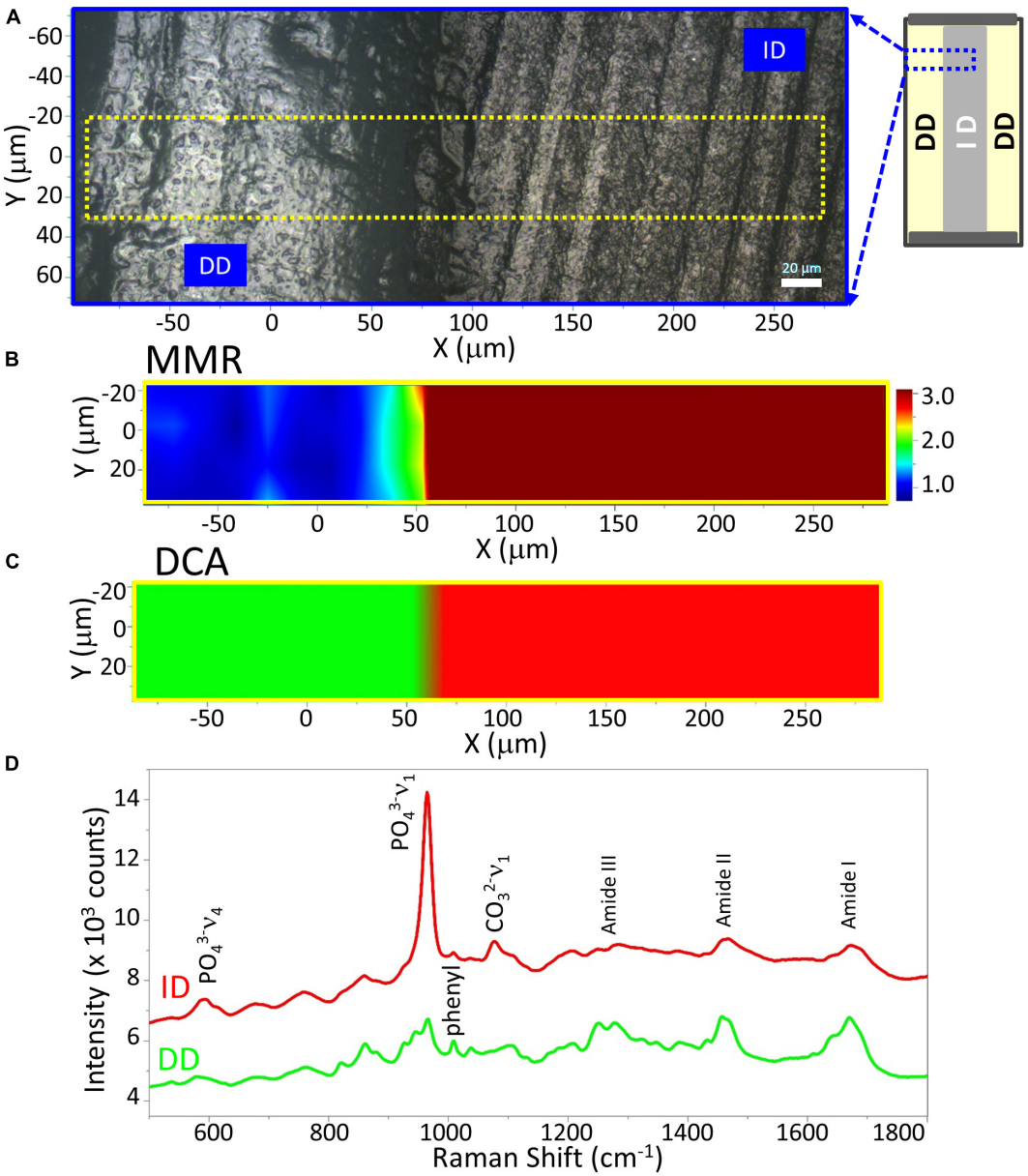

FIGURE 3 | Raman analysis of a representative demineralized dentin disc (control). **(A)** Light micrograph marked with a X-Y scan area. Scan bar is 20 μm. **(B)** μ-Raman mineral map (MMR) of the X-Y scan area. Blue represents the lowest ratio, while red represents the highest. **(C)** K-means clustering map (DCA) of the Raman profile of the same scan area. Two distinguished classes are identified, e.g., intact dentin (ID) and demineralized dentin (DD) region. **(D)** μ-Raman spectra of two classes, corresponding to ID and DD regions.

show very few hydroxyapatite crystals (white deposits) within the demineralized dentin region (**Figure 5b3**).

The cluster analysis provides further information about the peptide-mediated mineral in the P-AIDD specimen. Quantification of mineral content, crystallinity, and adhesive infiltration in the different dentin samples before and after treatment with the remineralization protocol, are summarized in **Figure 5C**. The calculated mineral content for ID (**Figure 3D**) and DD specimens is used as a reference. The MMR values were ∼8.7 for ID, and 1.3 for DD (as base line), whereas the MMR values for the new peptide-mediated minerals are about 3∼4. The relative crystallinities of the new peptide-mediated minerals are different from that of intact dentin, with their FWHM much larger than that of intact dentin ($p < 0.05$). Using FWHM as a measure of crystallinity, the different sample components can be ordered, e.g., ID > remineral on P-AIDD > remineral on P-PIDD specimen. The carbonate content of the new peptide-mediated remineralized dentin presented as GMC is also larger than that of intact dentin ($p < 0.05$), indicating the reverse order for the carbonate substitution for phosphate, e.g., ID < remineral

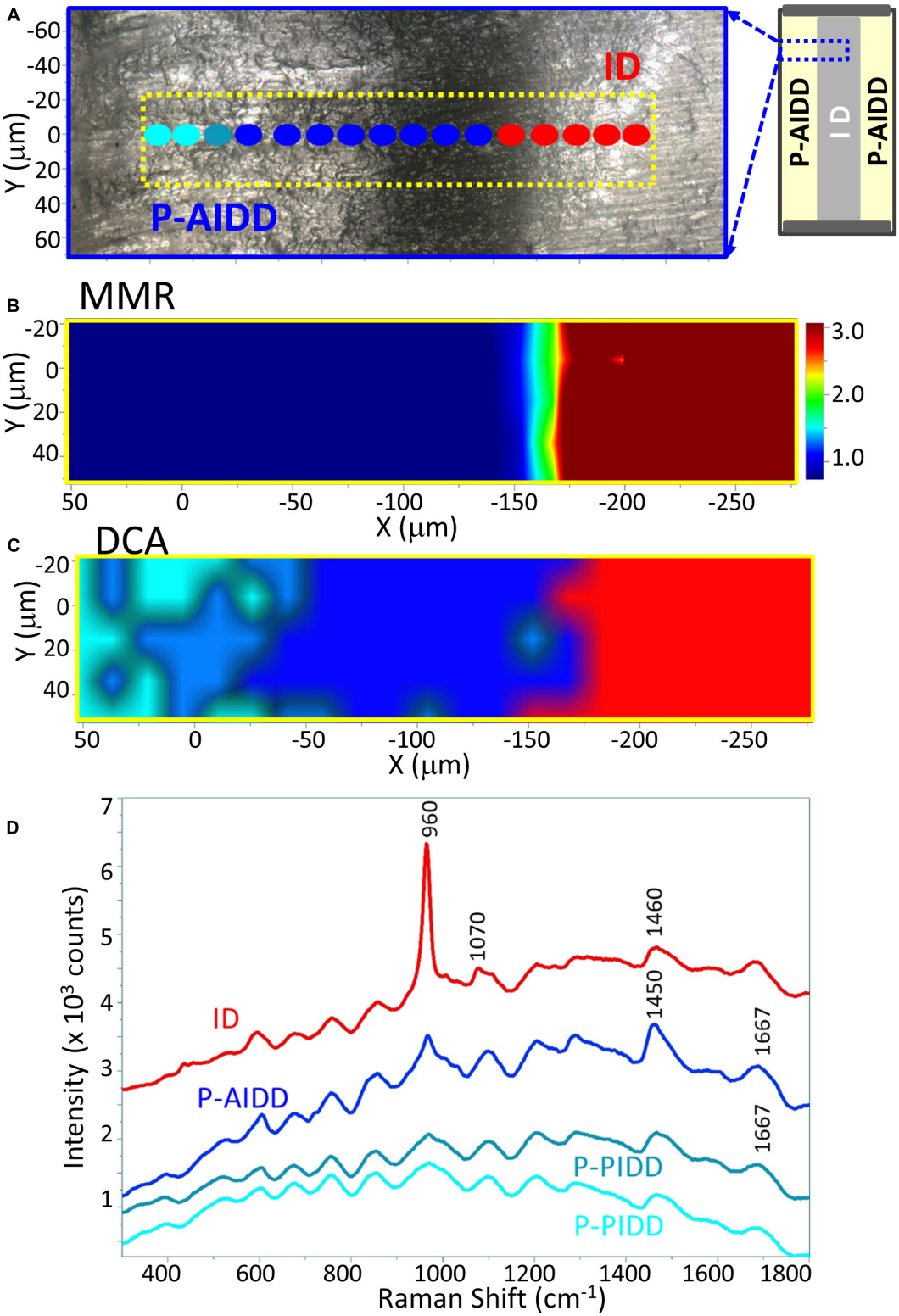

FIGURE 4 | Raman analysis of a representative peptide-functionalized adhesive-infiltrated demineralized dentin (P-AIDD) specimen. **(A)** Light micrograph marked with a X-Y scan area, **(B)** μ-Raman mineral map (MMR) of the X-Y scan area. **(C)** K-means clustering map (DCA) of the Raman profile of the same scan area. Four classes are identified, including intact dentin (ID), peptide-functionalized adhesive-infiltrated demineralized dentin (P-AIDD) and two peptide-functionalized partially-infiltrated demineralized dentin (P-PIDD) regions with similar spectral features. **(D)** Raman spectra from the four classes.

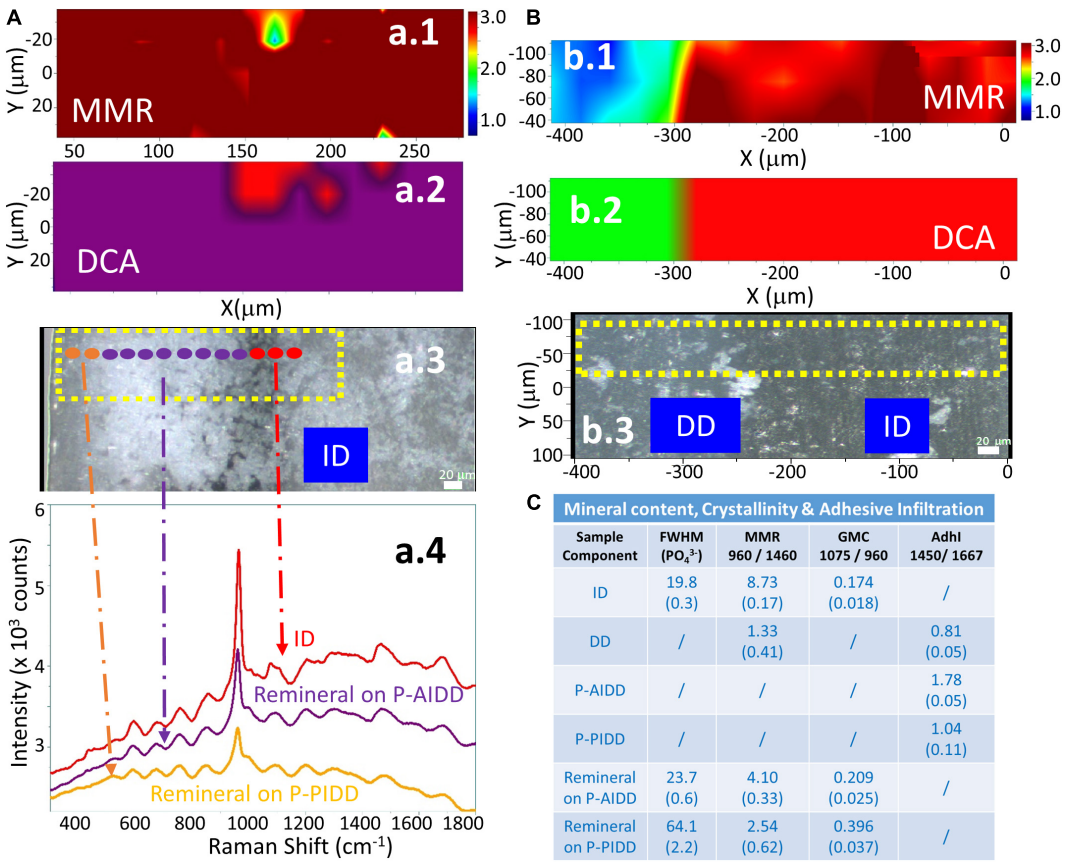

C

Mineral content, Crystallinity & Adhesive Infiltration				
Sample Component	FWHM (PO_4^{3-})	MMR 960 / 1460	GMC 1075 / 960	AdhI 1450/ 1667
ID	19.8 (0.3)	8.73 (0.17)	0.174 (0.018)	/
DD	/	1.33 (0.41)	/	0.81 (0.05)
P-AIDD	/	/	/	1.78 (0.05)
P-PIDD	/	/	/	1.04 (0.11)
Remineral on P-AIDD	23.7 (0.6)	4.10 (0.33)	0.209 (0.025)	/
Remineral on P-PIDD	64.1 (2.2)	2.54 (0.62)	0.396 (0.037)	/

FIGURE 5 | RAMAN analysis of a representative peptide-functionalized adhesive-infiltrated demineralized dentin (P-AIDD) specimen after remineralization **(A)** and a control demineralized dentin (DD) specimen after remineralization protocol **(B)**. (a.1,b.1) μ-Raman mineral map (MMR) of the X-Y scan area. Blue represents the lowest ratio, while red represents the highest. (a.2,b.2) K-means clustering map (DCA) of the Raman profile of the same sample. (a.3,b.3) Visible images of the scanned areas. Scale bar is 20 μm. (a.4) Raman spectra of principal components (PCs) from the DCA. **(C)** Summary of the Raman spectral features related to quantification of mineral content, crystallinity, and adhesive infiltration to the dentin samples before and after remineralization.

on P-AIDD < remineral on P-PIDD specimen. The adhesive infiltration calculated from band ratio 1,450/1,667 verified that P-PIDD has less adhesive contribution (∼1.0), compared to that of P-AIDD (∼1.8).

Atomic Force Microscopy

The collagen model specimens with presence of peptides were used to simulate the interface between demineralized dentin collagen and co-polymerizable HABP, i.e., MAHABP. **Figure 6** shows early stages of peptide-mediated mineralization on the model specimens. The collagen fibrils are presented in **Figures 6A,B** with scattered mineral particles after 20 min peptide-mediated mineralization initiated. Mineral growth extended throughout collagen network after 40 min (**Figures 6C,D**). Subtle differences are spotted in the mineral growth between the HABP and co-polymerizable HABP, i.e., MAHABP. While collagen network could still be observed in the presence of HABP, MAHABP resulted in large mineral island formations. The Raman spectra of the mineral produced with collagen: MAHABP after 20 min was obtained and compared with that of later stage mineral (**Figure 6E**). Based on the spectral analysis, the early-stage mineral has less mineral concentration, larger FWHM (960 cm^{-1}) and higher carbonate content. The $\nu1$ phosphate band shifted to a higher position at later stage of mineralization as seen in **Figure 6E**.

DISCUSSION

Conventional Raman Spectroscopy and Its Limitations

Overlapping features were observed in the spectra of the peptide-functionalized adhesive, intact dentin, demineralized dentin, and peptide-functionalized adhesive-infiltrated demineralized dentin (**Supplementary Figures 1**, **2**). For instance, the CH_2 wagging (1,460 cm^{-1}) deformation bands in demineralized dentin collagen (generally assigned to proteins, lipids and carbon hydrates) overlap with the peak at 1,450 cm^{-1} (assigned to the C-H group of methacrylate-based adhesive). Due to the overlapping spectral bands, univariate analysis, such as mapping of peak areas of specific functional groups or band ratio values, do not always accurately identify the location

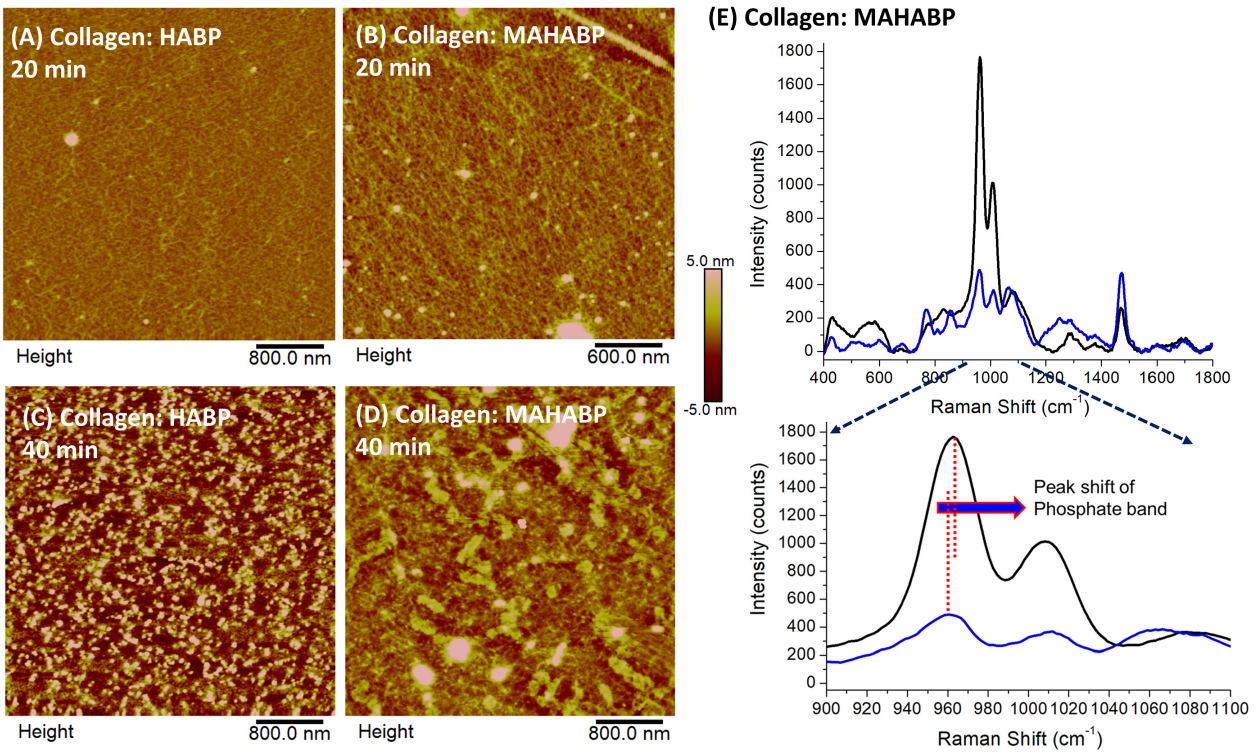

FIGURE 6 | AFM images of peptide-functionalized collagen model surfaces after alkaline phosphatase mediated mineralization and their Raman spectra. **(A)** Collagen: HABP after 20 min; **(B)** collagen: MAHABP after 20 min **(C)** collagen: HABP after 40 min; **(D)** collagen:MAHABP after 40 min **(E)** Raman spectra of the minerals grown on the MAHABP-functionalized collagen model surfaces at 20 min and longer mineralization.

and concentration of the functional group. Unanticipated components may be completely overlooked after data processing using univariate analysis.

In addition to the challenges associated with overlapping spectral bands, the non-uniform coverage of new peptide-mediated minerals on the surface of the experimental specimens may directly influence the point-to-point reproducibility of the recorded spectra. On a point-to-point basis, the spectral differences are often subtle, but they are key to differentiating composition and crystallinity. Faced with these challenges, the simplified peak area calculations with univariate analysis offered limited information—quantified relationships could not be determined using these calculations. The challenges associated with these specimens also made discriminating between species very difficult. Multivariate analysis tools were required to track subtle differences in these complex, heterogeneous samples.

Insights Gained Through Combined Chemometric Analysis

Divisive clustering analysis (DCA) was selected for this study to separate the group of spectra into clusters with clear similarities, i.e., similarities within each cluster and distinctions between the clusters. The biochemical content of each cluster, e.g., the mineral and organic components of the adhesive/collagen hybrid, was analyzed using the average cluster spectra. These multivariate analyses confirmed the differences in the spectral composition. Separation of chemical spectra distinct to each chemical constituent is inherent in the algorithm, thus digital subtraction of spectra with overlapping features is not needed—digital subtraction can obscure subtle differences. The cluster analyses revealed detailed differences in the P-AIDD specimen (**Figure 4C**), where, four different components, i.e., ID, P-AIDD and two P-PIDD regions correspond to the four clusters that were created. All spectra for each cluster were averaged to obtain the mean cluster spectrum, for each point of analysis (**Figure 4D**).

Different levels of the C-H bond (at 1,450 cm^{-1}) associated with adhesive were noted at the DCA centroids associated with P-AIDD and the two P-PIDD regions. These differences were not visible following univariate analyses (**Figure 4B**). Indeed, after cluster analysis of the area as a whole and over the full spectral range, each principal component represents one or two chemical constituents in the specimen that are uncorrelated with other constituents (**Figure 4C**). This means that the spectra are classified using a systematic approach, which directly offers information about the distribution of components in the specimen, as opposed to univariate methods that involve a more trial-and-error procedure along with the necessity for *a priori* knowledge of the specimen.

Mineral Content

The additional insights gained through this chemometrics analysis include the relative mineral content, carbonate content

and the mineral crystallinities. This information was revealed in the average cluster spectra. Crystal formation was not encountered in the control group after the remineralization protocol, and their mineral-to-matrix ratio (MMR) values did not change, being 1.3 as base line ($p > 0.05$). The existence of new peptide-mediated mineral following treatment with the remineralization protocol is a crucial finding with the peptide-functionalized adhesive-infiltrated demineralized dentin (P-AIDD) samples. The mineral crystals suggest that the peptide-functionalized adhesive is responsive to environmental stimuli, in this case mineralization buffer.

Crystallinity

Vibrational spectroscopic techniques such as FTIR and Raman, are used intensively to determine crystal phases of mineralized materials (Toledano et al., 2012). The band width, i.e., full-width-half-maximum (FWHM) and Raman shift of ν1 phosphate band are used to indicate the structural differences in mineral. In general, the narrower the spectra peak width, the higher the degree of mineral crystallinity (Karan et al., 2009).

The PO_4 band in spectra of the new peptide-mediated mineral in the P-AIDD region of the sample is narrower and more resolved than the PO_4 band in the P-PIDD region (**Figures 5a3**, C). This difference suggests less structural variation in bond distances and angles in the peptide-mediated mineral in the P-AIDD region (Schwartz et al., 2012). This effect shows a higher degree of crystallinity of the new mineral in the P-AIDD region as compared to the new peptide-mediated mineral in the P-PIDD region. This was probably due to less incorporation of peptide-functionalized adhesive in the P-PIDD region compared to that in the P-AIDD region. These differences support the potential of tailoring the peptide-functionalized adhesive to the tissue interface.

Raman shift of ν1 phosphate band center usually identifies the classification of a crystal feature. This ν1 phosphate band of normal dentin and bone is usually located at 950–960 cm^{-1} and this band could be shifted to a position close to 970 cm^{-1} for β-tricalcium phosphate (β-TCP) (Penel et al., 2005). In the fractured specimen, the ν1 phosphate band of intact dentin was located at 964 cm^{-1}. Investigators reported that in the micro-damaged and fractured regions of mineralized tissue, the ν1 phosphate band shifted to a higher wavenumber (963 and 965 cm^{-1}, respectively) than the ν1 phosphate band in carbonated hydroxyapatite associated with tooth or bone (959 cm^{-1}) (Dooley et al., 2009). The Raman shift of ν1 phosphate band center for the new peptide-mediated minerals in this study is very close to that for chemically synthesized hydroxyapatite (960 cm^{-1}) (Daculsi et al., 1987; Duke and Lindemuth, 1991).

Carbonate Content

Biological apatite is often calcium deficient with substantial amounts of carbonate occupying the phosphate position in the hydroxyapatite structure (Zurick et al., 2013). Carbonated apatite is a precursor of hydroxyapatite. The ν1 carbonate band at ∼1,070 cm^{-1} in the Raman spectra is often used to measure the relative B-type carbonate content (Awonusi et al., 2007). Detailed analysis of the average cluster spectra data suggested that the new peptide-mediated mineral has relatively higher carbonate content (**Figure 5C**), and the carbonate content on the P-AIDD and P-PIDD regions are distinctly different. The FWHM of ν1 phosphate and the carbonate content are correlated, e.g., the higher the carbonate content in the mineral, the broader the ν1 phosphate band. This means lower mineral crystallinity yields wider phosphate band, which is mirrored by high carbonate substitution (i.e., increased carbonate-to-phosphate ratio) in the present study. The structural differences in the peptide-mediated mineral associated with the P-AIDD and P-PIDD provide evidence that the peptide-functionalized adhesive is responsive to environmental stimuli. These structural differences also support the potential of tailoring the peptide-functionalized adhesive to the tissue interface. The results support the potential of engineering the adhesive to promote peptide-mediated remineralization at the adhesive/dentin interface.

Defective Material/Tissue Interface and Our Bio-Enabled Approach to Address This Weakest Link

In our previous investigations, we used micro-scale structure/property measurements as a guide to develop an idealized microstructural representation of the hybrid layer (Wang and Spencer, 2003; Singh et al., 2015). The adhesive/collagen hybrid constructs were prepared using a hydrophobic dental adhesive and collagen matrix from demineralized bovine dentin. Time-dependent and rate-dependent mechanical behavior of this ideal adhesive/collagen hybrid was investigated under conditions that simulated the functional environment of the mouth. The results emphasized the complexity of the interfacial behavior. For example, the ideal adhesive/collagen hybrid experienced smaller and uniform stress due to constant material properties along the depth of the hybrid layer (Spencer and Misra, 2017), but the behavior depended on several factors including moisture content, adhesive characteristics, relative ratio of adhesive and collagen, loading level and loading rate. Fatigue was affected by both the material components and micro-structure (Singh et al., 2015).

The complex structure/property relationships that determine durability at the adhesive/dentin interface are magnified under clinical conditions. The adhesive seal to dentin is fragile and the fragility can be traced to defects such as pockets of resin-sparse collagen—this unprotected collagen is degraded by acids and enzymes. Bacteria and bacterial by-products infiltrate the resulting interfacial gaps, demineralize and decompose the tooth, and further erode the adhesive, leading to wider and deeper gaps that create an ideal environment for bacteria to proliferate. These activities lead ultimately to recurrent decay, hypersensitivity and pulpal inflammation (Van Meerbeek et al., 2005; Nedeljkovic et al., 2015, 2016; Spencer et al., 2019). The current investigation addresses this problem by using a peptide-functionalized adhesive to promote peptide-mediated remineralization of interfacial defects—defects that may be traced to resin-sparse pockets of collagen.

The remineralization experiment was initiated using enzyme-based assay mimicking biological systems by incorporating alkaline phosphatase enzyme. This enzyme-based mineralization offers control of the kinetics by controlling the phosphate ion release from the organic phosphate source cleaved by alkaline phosphatase. Dentin remineralization is driven by mineral growth within nucleation sites in preserved collagen fibrils (Bertassoni et al., 2011), however, the role of the collagen matrix in dentin remineralization is still controversial. It was reported that crystal apatites remaining on demineralized collagen fibrils can serve as nucleation templates or seeds (Zhang et al., 2003).

We propose that the remineralization observed with P-AIDD is a result of 2-phase sequence, i.e., binding to the exposed collagen fibers and crystal nucleation facilitated by the tethered mineral-forming peptide. The tethered mineral-forming peptide may offer preferential binding sites for ions (calcium, phosphate, fluoride, and hydroxyl ions), chelate ions and promotes mineralization through controlling kinetics. Overall the peptide conformation and available sites for chelated ions and their binding kinetics in the collagen network could serve as a template for peptide-assisted mineral formation.

The control demineralized dentin specimens treated with the remineralization protocol showed few, tiny, scattered mineral crystals, and the spectral features associated with mineral-derived bands were very weak. The diminished remineralizing effect might be linked to poor mineral precipitation of calcium and phosphate ions at the demineralized organic matrix (McKee et al., 2011).

Initial Mineralization at the Collagen Interface

Based on the early-stage mineralization study, mineral particles (50–300 nm) were detected by AFM after only 20 min reaction (**Figure 6**). The results suggest that mineral growth was quicker and more uniform with the co-polymerizable hydroxyapatite-binding peptide (MAHABP) on the collagen model specimens (**Figure 6B**). With longer mineralization time, e.g., 40 min, the mineral particles grow rapidly and start to form clusters (**Figures 6C,D**).

The broad and poorly resolved PO_4 spectral features suggest reduced atomic order, i.e., more structural variation in bond distances and angles, in the early-stage mineral (**Figure 6E**). The PO_4 band was narrower and better resolved after the longer mineralization reaction; these spectral results indicate a higher degree of crystallinity. The carbonate content also decreased after the longer mineralization reaction. The relationship between the crystallinity and carbonate content in this mineral maturation process is similar to the case of P-AIDD study.

Limitations and Next Steps

The dentin collagen matrix treated with the peptide-functionalized adhesive showed promising results in terms of delivering biologic cues direct at the adhesive/dentin interface. There are, however, limitations that require further investigation. Raman is a surface-sensitive technique and thus, mineral formation was demonstrated at the surface. Further research is needed to determine the depth of the remineralization reaction. In addition, the kinetics of nucleation, crystal formation, and time-resolved compositional changes must be determined. Based on initial light microscopic analysis, mineral crystals started to grow on the surface of P-AIDD specimens at about 24–30 h (unpublished results). In addition, the amount of co-polymerizable peptide used in the adhesive formulation could be a major factor for the remineralization reaction. In the current investigation, 10 mass% of co-polymerizable HABP was used. Future investigations should include detailed studies on the peptide mediated mineralization kinetics and determine the parameters affecting the kinetics under clinically relevant conditions.

The factors that led to the P-PIDD regions as the top layer of the peptide-functionalized-adhesive-infiltration demineralized dentin have not been resolved in this investigation. These studies should be extended to optimize the protocol. For example, these P-PIDD regions may be related to sample preparation, e.g., the air stream which was forced across the surface of the specimen may have dislodged the relatively hydrophilic, low viscosity adhesive. In addition, the surface layer of this hydrophilic resin may not have been adequately polymerized due to oxygen inhibition (Ruggeberg and Margeson, 1990). Under these circumstances, the unpolymerized monomer could be leached which would reduce infiltrated adhesive. The depth of P-PIDD region is about 50 μm which is close to the depth of oxygen inhibition layer reported in the literature (Ruggeberg and Margeson, 1990; Nunes et al., 2005).

Understanding Reactions at Interface and Knowledge-Based Engineering Biomaterials

Our prior work used a peptide-based approach to build an engineered fluorescent probe to label mineralized tissues (Yuca et al., 2011), developed a biomarker protein tag on the mineral forming peptide (Ye et al., 2017), and designed a biomimetic adhesive formulation using a combination of peptide and a ε-poly-lysine resin system (Xie et al., 2019). To address concerns associated with non-specific interaction, a peptide system capable to mediate mineralization, to incorporate a spacer sequence to retain active peptide conformation, and conjugated with a methacrylate-based monomer for copolymerization into dental adhesive polymer was designed and synthesized in the current work. This engineered peptide-based copolymer is a promising approach for a next generation adhesive to repair deficient dentin matrices and protect exposed collagen at the vulnerable adhesive/dentin interface.

CONCLUSION

For the first time, we introduce a combined Raman spectroscopy and chemometrics approach to investigate heterogeneous material/tissue interfaces where biological cues were provided to promote tissue mineralization of deficient dentin matrices. The approach correlates physical properties to analytical data by extracting important information hidden in the heterogeneous

interfaces. The adhesive/collagen hybrid served as a model of the heterogeneous adhesive/dentin interface that is formed during composite restoration. We extended our analyses to next generation adhesive design where remineralization of exposed collagen at the vulnerable adhesive/dentin interface was achieved using a stimuli-responsive engineered peptide-functionalized adhesive.

Analysis of these hybrid systems using Raman spectroscopy in combination with chemometrics revealed important structural details about the mineral content, crystallinity and carbonate content. The existence of new peptide-mediated mineral crystals is a crucial finding with the peptide-functionalized adhesive-infiltrated demineralized dentin (P-AIDD) samples. The peptide-mediated mineral crystals suggest that the peptide-functionalized adhesive is responsive to environmental stimuli, in this case mineralization buffer. There is a higher degree of crystallinity in the new mineral formed at the region of the specimen marked by complete infiltration with the peptide-functionalized adhesive as compared to partial infiltrate. These differences are also reflected in the carbonate content, i.e., the lower mineral crystallinity noted with partial infiltration is associated with increased carbonate-to-phosphate ratio. This was probably due to less incorporation of peptide-functionalized adhesive in the partially infiltrated demineralized dentin (P-PIDD) region compared to that in the adhesive-infiltrated demineralized dentin (P-AIDD) region. These differences support the response of the peptide-functionalized adhesive to environmental stimuli and the potential of tailoring the peptide-functionalized adhesive to the tissue interface.

Chemometrics-assisted confocal Raman spectroscopy provides more accurate information on the chemical composition and enhanced analyses of the mineral structure. Micro-Raman spectroscopy coupled with multivariate data analysis facilitated straightforward and efficient *in situ* structural characterization of these complex, heterogeneous material/tissue interfaces.

Overall, our results demonstrate that essential information hidden in the complex material/tissue interfaces, both structural and compositional information can be extracted using Raman spectroscopy combined with chemometrics. The insight provided by this data-driven approach can improve our understanding of phenomena that lead to failure at the biomaterial/tissue interface. This knowledge will enhance our ability to identify features within the interfacial micro-environment that should be harnessed to engineer biomaterials that will integrate with biological systems to promote tissue health and healing.

DATA AVAILABILITY STATEMENT

The original contributions presented in the study are included in the article/**Supplementary Material**, further inquiries can be directed to the corresponding author/s.

AUTHOR CONTRIBUTIONS

PS: concept development, experimental design, manuscript preparation and editing. QY: experimental design, data collection, data analysis, manuscript preparation, and editing. NK: protocol development, data collection, data analysis, and manuscript preparation. SW: data collection and data analysis. BB and AM: manuscript preparation and editing. CT: concept development, experimental design, protocol development, manuscript preparation, and editing. All authors contributed to the article and approved the submitted version.

FUNDING

Research reported in this publication was supported by the National Institute of Dental & Craniofacial Research of the National Institutes of Health under Award Number R01DE025476. The content is solely the responsibility of the authors and does not necessarily represent the official views of the National Institutes of Health. The research was also supported, in part, by a Research GO award from the University of Kansas.

SUPPLEMENTARY MATERIAL

The Supplementary Material for this article can be found online at: https://www.frontiersin.org/articles/10.3389/fmats.2021.681415/full#supplementary-material

REFERENCES

Abedin, F., Ye, Q., Good, H. J., Parthasarathy, R., and Spencer, P. (2014). Polymerization- and solvent-induced phase separation in hydrophilic-rich dentin adhesive mimic. *Acta Biomater.* 10, 3038–3047. doi: 10.1016/j.actbio.2014.03.001

Afrashtehfar, K. I., Emami, E., Ahmadi, M., Eilayyan, O., Abi-Nader, S., and Tamimi, F. (2017). Failure rate of single-unit restorations on posterior vital teeth: a systematic review. *J. Prosthet. Dent.* 117, 345–353.e8. doi: 10.1016/j.prosdent.2016.08.003

Awonusi, A., Morris, M. D., and Tecklenburg, M. M. (2007). Carbonate assignment and calibration in the Raman spectrum of apatite. *Calcif. Tissue Int.* 81, 46–52. doi: 10.1007/s00223-007-9034-0

Bacino, M., Girn, V., Nurrohman, H., Saeki, K., Marshall, S. J., Gower, L., et al. (2019). Integrating the PILP-mineralization process into a restorative dental treatment. *Dent. Mater.* 35, 53–63. doi: 10.1016/j.dental.2018.11.030

Bertassoni, L. E., Habelitz, S., Marshall, S. J., and Marshall, G. W. (2011). Mechanical recovery of dentin following remineralization in vitro–an indentation study. *J. Biomech.* 44, 176–181. doi: 10.1016/j.jbiomech.2010.09.005

Calvo, N. L., Maggio, R. M., and Kaufman, T. S. (2018). Chemometrics-assisted solid-state characterization of pharmaceutically relevant materials. Polymorphic substances. *J. Pharm. Biomed. Anal.* 147, 518–537. doi: 10.1016/j.jpba.2017.06.018

Chen, R., Jin, R., Li, X., Fang, X., Yuan, D., Chen, Z., et al. (2020). Biomimetic remineralization of artificial caries dentin lesion using Ca/P-PILP. *Dent. Mater.* 36, 1397–1406. doi: 10.1016/j.dental.2020.08.017

Daculsi, G., LeGeros, R. Z., Jean, A., and Kerebel, B. (1987). Possible physico-chemical processes in human dentin caries. *J. Dent. Res.* 66, 1356–1359.

Dina, N. E., Gherman, A. M. R., Chis, V., Sarbu, C., Wieser, A., Bauer, D., et al. (2018). Characterization of clinically relevant fungi via SERS fingerprinting assisted by novel chemometric models. *Anal. Chem.* 90, 2484–2492. doi: 10.1021/acs.analchem.7b03124

Dooley, K. A., McCormack, J., Fyhrie, D. P., and Morris, M. D. (2009). Stress mapping of undamaged, strained, and failed regions of bone using Raman spectroscopy. *J. Biomed. Opt.* 14:044018. doi: 10.1117/1.3184435

Duke, E. S., and Lindemuth, J. (1991). Variability of clinical dentin substrates. *Am. J. Dent.* 4, 241–246.

Eltahlah, D., Lynch, C. D., Chadwick, B. L., Blum, I. R., and Wilson, N. H. F. (2018). An update on the reasons for placement and replacement of direct restorations. *J. Dent.* 72, 1–7. doi: 10.1016/j.jdent.2018.03.001

Fang, C., Xin, G. Z., Wang, S. L., Wei, M. M., Wu, P., Dong, X. M., et al. (2020). Discovery and validation of peptide biomarkers for discrimination of *Dendrobium* species by label-free proteomics and chemometrics. *J. Pharm. Biomed. Anal.* 182:113118. doi: 10.1016/j.jpba.2020.113118

Ferracane, J. L. (2013). Resin-based composite performance: are there some things we can't predict? *Dent. Mater.* 29, 51–58. doi: 10.1016/j.dental.2012.06.013

Ferracane, J. L. (2017). Models of caries formation around dental composite restorations. *J. Dent. Res.* 96, 364–371. doi: 10.1177/0022034516683395

Garvin, J. (2021). *National Children's Dental Health Month Turns 80*. Ada, OK: ADA News.

Gungormus, M., Fong, H., Kim, I. W., Evans, J. S., Tamerler, C., and Sarikaya, M. (2008). Regulation of in vitro calcium phosphate mineralization by combinatorially selected hydroxyapatite-binding peptides. *Biomacromolecules* 9, 966–973. doi: 10.1021/bm701037x

Guo, X., Wang, Y., Spencer, P., Ye, Q., and Yao, X. (2008). Effects of water content and initiator composition on photopolymerization of a model BisGMA/HEMA resin. *Dent. Mater.* 24, 824–831. doi: 10.1016/j.denta1.2007.10.003

Karan, K., Yao, X., Xu, C., and Wang, Y. (2009). Chemical profile of the dentin substrate in non-carious cervical lesions. *Dent. Mater.* 25, 1205–1212. doi: 10.1016/j.dental.2009.04.006

Kermanshahi, S., Santerre, J. P., Cvitkovitch, D. G., and Finer, Y. (2010). Biodegradation of resin-dentin interfaces increases bacterial microleakage. *J. Dent. Res.* 89, 996–1001. doi: 10.1177/0022034510372885

Kontoyannis, C. G., Bouropoulos, N. C., and Koutsoukos, P. G. (1997). Urinary stone layer analysis of mineral components by Raman spectroscopy, IR spectroscopy, and X-ray powder diffraction: a comparative study. *Appl. Spectrosc.* 51, 1205–1209.

Kopperud, S. E., Espelid, I., Tveit, A. B., and Skudutyte-Rysstad, R. (2015). Risk factors for caries development on tooth surfaces adjacent to newly placed class II composites–a pragmatic, practice based study. *J. Dent.* 43, 1323–1329. doi: 10.1016/j.jdent.2015.08.013

Lemor, R. M. (1997). *Micro-Raman- and Infrared Absorption Studies on Human Dentin/Adhesive Interfaces.* Master of Science. Kansas, MO: University of Missouri.

Lin, K. F., He, S., Song, Y., Wang, C. M., Gao, Y., Li, J. Q., et al. (2016). Low-temperature additive manufacturing of biomimic three-dimensional hydroxyapatite/collagen scaffolds for bone regeneration. *ACS Appl. Mater. Interfaces* 8, 6905–6916. doi: 10.1021/acsami.6b00815

Liu, Y., Tjaderhane, L., Breschi, L., Mazzoni, A., Li, N., Mao, J., et al. (2011). Limitations in bonding to dentin and experimental strategies to prevent bond degradation. *J. Dent. Res.* 90, 953–968. doi: 10.1177/0022034510391799

Makvandi, P., Jamaledin, R., Jabbari, M., Nikfarjam, N., and Borzacchiello, A. (2018). Antibacterial quaternary ammonium compounds in dental materials: a systematic review. *Dent. Mater.* 34, 851–867. doi: 10.1016/j.dental.2018.03.014

McKee, M. D., Nakano, Y., Masica, D. L., Gray, J. J., Lemire, I., Heft, R., et al. (2011). Enzyme replacement therapy prevents dental defects in a model of hypophosphatasia. *J. Dent. Res.* 90, 470–476. doi: 10.1177/0022034510393517

Moussa, D. G., and Aparicio, C. (2019). Present and future of tissue engineering scaffolds for dentin-pulp complex regeneration. *J. Tissue Eng. Regen. Med.* 13, 58–75. doi: 10.1002/term.2769

National Center for Health Statistics (US) (2007). *Health, United States, 2007 With Chartbook on Trends in the Health of Americans,* Report No. 2007-1232. Hyattsville, MD: National Center for Health Statistics.

Nedeljkovic, I., De Munck, J., Slomka, V., Van Meerbeek, B., Teughels, W., and Van Landuyt, K. L. (2016). Lack of buffering by composites promotes shift to more cariogenic bacteria. *J. Dent. Res.* 95, 875–881. doi: 10.1177/0022034516647677

Nedeljkovic, I., Teughels, W., De Munck, J., Van Meerbeek, B., and Van Landuyt, K. L. (2015). Is secondary caries with composites a material-based problem? *Dent. Mater.* 31, E247–E277. doi: 10.1016/j.dental.2015.09.001

Nunes, T. G., Ceballos, L., Osorio, R., and Toledano, M. (2005). Spatially resolved photopolymerization kinetics and oxygen inhibition in dental adhesives. *Biomaterials* 26, 1809–1817.

Nurrohman, H., Saeki, K., Carneiro, K., Chien, Y. C., Djomehri, S., Ho, S. P., et al. (2016). Repair of dentin defects from DSPP knockout mice by PILP mineralization. *J. Mater. Res.* 31, 321–327. doi: 10.1557/jmr.2015.406

Ohsaki, K., Shibata, A., Yamashita, S., Oe, M., Wang, K. Q., Cui, P.-C., et al. (1995). Demonstrations of de- and remineralization mechanism as revealed in synthetic auditory ossicle (Apaceram) of rats by laser-Raman spectrometry. *Cell. Mol. Biol.* 41, 1155–1167.

Opdam, N., Frankenberger, R., and Magne, P. (2016). From 'direct versus indirect' toward an integrated restorative concept in the posterior dentition. *Oper. Dent.* 41, S27–S34. doi: 10.2341/15-126-LIT

Palmer, C. (2013). *Census Bureau Targets Unmet Need*. Available online at: ADA.News.ADA.org (accessed April 01, 2013).

Panseri, S., Montesi, M., Dozio, S. M., Savini, E., Tampieri, A., and Sandri, M. (2016). Biomimetic Scaffold with aligned microporosity designed for dentin regeneration. *Front. Bioeng. Biotechnol.* 4:48. doi: 10.3389/fbioe.2016.00048

Pashley, D. H., Tay, F. R., Breschi, L., Tjaderhane, L., Carvalho, R. M., Carrilho, M., et al. (2011). State of the art etch-and-rinse adhesives. *Dent. Mater.* 27, 1–16. doi: 10.1016/j.dental.2010.10.016

Paudel, A., Raijada, D., and Rantanen, J. (2015). Raman spectroscopy in pharmaceutical product design. *Adv. Drug Deliv. Rev.* 89, 3–20. doi: 10.1016/j.addr.2015.04.003

Penel, G., Delfosse, C., Descamps, M., and Leroy, G. (2005). Composition of bone and apatitic biomaterials as revealed by intravital Raman microspectroscopy. *Bone* 36, 893–901.

Pisapia, C., Jamme, F., Duponchel, L., and Menez, B. (2018). Tracking hidden organic carbon in rocks using chemometrics and hyperspectral imaging. *Sci. Rep.* 8:2396. doi: 10.1038/s41598-018-20890-4

Rebiere, H., Martin, M., Ghyselinck, C., Bonnet, P. A., and Brenier, C. (2018). Raman chemical imaging for spectroscopic screening and direct quantification of falsified drugs. *J. Pharm. Biomed. Anal.* 148, 316–323. doi: 10.1016/j.jpba.2017.10.005

Ruggeberg, F. A., and Margeson, D. H. (1990). The effect of oxygen inhibition on an unfilled/filled composite system. *J. Dent. Res.* 69, 1652–1658.

Saeki, K., Chien, Y. C., Nonomura, G., Chin, A. F., Habelitz, S., Gower, L. B., et al. (2017). Recovery after PILP remineralization of dentin lesions created with two cariogenic acids. *Arch. Oral Biol.* 82, 194–202. doi: 10.1016/j.archoralbio.2017.06.006

Salzer, R., Steiner, G., Mantsch, H. H., Mansfield, J., and Lewis, E. N. (2000). Infrared and Raman imaging of biological and biomimetic samples. *J. Anal. Chem.* 366, 712–726.

Saxena, N., Habelitz, S., Marshall, G. W., and Gower, L. B. (2019). Remineralization of demineralized dentin using a dual analog system. *Orthod. Craniofac. Res.* 22, 76–81. doi: 10.1111/ocr.12271

Schwartz, A. G., Pasteris, J. D., Genin, G. M., Daulton, T. L., and Thomopoulos, S. (2012). Mineral distributions at the developing tendon enthesis. *PLoS One* 7:e48630. doi: 10.1371/journal.pone.0048630

Schwendicke, F., Gostemeyer, G., Blunck, U., Paris, S., Hsu, L. Y., and Tu, Y. K. (2016). Directly placed restorative materials: review and network meta-analysis. *J. Dent. Res.* 95, 613–622. doi: 10.1177/0022034516631285

Singh, V., Misra, A., Parthasarathy, R., Ye, Q., and Spencer, P. (2015). Viscoelastic properties of collagen-adhesive composites under water-saturated and dry conditions. *J. Biomed. Mater. Res. A* 103, 646–657. doi: 10.1002/jbm.a.35204

Sinjab, F., Sicilia, G., Shipp, D. W., Marlow, M., and Notingher, I. (2017). Label-free raman hyperspectral imaging of single cells cultured on polymer substrates. *Appl. Spectrosc.* 71, 2595–2607. doi: 10.1177/0003702817715042

Song, L. Y., Ye, Q., Ge, X. P., Misra, A., and Spencer, P. (2016). Mimicking nature: self-strengthening properties in a dental adhesive. *Acta Biomater.* 35, 138–152. doi: 10.1016/j.actbio.2016.02.019

Song, L. Y., Ye, Q., Ge, X. P., Misra, A., Laurence, J. S., Berrie, C. L., et al. (2014). Synthesis and evaluation of novel dental monomer with branched carboxyl acid group. *J. Biomed. Mater. Res. Part B Appl. Biomater.* 102, 1473–1484. doi: 10.1002/Jbm.B.33126

Spencer, P., and Misra, A. (2017). *Material-Tissue Interfacial Phenomena: Contributions from Dental and Craniofacial Reconstructions*. Amsterdam: Elsevier Science.

Spencer, P., and Swafford, J. R. (1999). Unprotected protein at the dentin-adhesive interface. *Quintessence Int.* 30, 501–507.

Spencer, P., and Wang, Y. (2002). Adhesive phase separation at the dentin interface under wet bonding conditions. *J. Biomed. Mater. Res.* 62, 447–456.

Spencer, P., and Wang, Y. (2007). *Micro-Raman Spectroscopy: Principles and Applications in Dental Research*. London: Imperial College Press.

Spencer, P., Wang, Y., and Bohaty, B. (2006). Interfacial chemistry of moisture-aged class II composite restorations. *J. Biomed. Mater. Res. B Appl. Biomater.* 77, 234–240.

Spencer, P., Wang, Y., Walker, M. P., Wieliczka, D. M., and Swafford, J. R. (2000). Interfacial chemistry of the dentin/adhesive bond. *J. Dent. Res.* 79, 1458–1463.

Spencer, P., Ye, Q., Song, L., Parthasarathy, R., Boone, K., Misra, A., et al. (2019). Threats to adhesive/dentin interfacial integrity and next generation bio-enabled multifunctional adhesives. *J. Biomed. Mater. Res. B Appl. Biomater.* 107, 2673–2683. doi: 10.1002/jbm.b.34358

Stewart, C. A., and Finer, Y. (2019). Biostable, antidegradative and antimicrobial restorative systems based on host-biomaterials and microbial interactions. *Dent. Mater.* 35, 36–52. doi: 10.1016/j.dental.2018.09.013

Suzuki, M., Kato, H., and Wakumoto, S. (1991). Vibrational analysis by Raman spectroscopy of the interface between dental adhesive resin and dentin. *J. Dent. Res.* 70, 1092–1097.

Tjaderhane, L., Nascimento, F. D., Breschi, L., Mazzoni, A., Tersariol, I. L., Geraldeli, S., et al. (2013). Strategies to prevent hydrolytic degradation of the hybrid layer-a review. *Dent. Mater.* 29, 999–1011. doi: 10.1016/j.dental.2013.07.016

Toledano, M., Yamauti, M., Ruiz-Requena, M. E., and Osorio, R. (2012). A ZnO-doped adhesive reduced collagen degradation favouring dentine remineralization. *J. Dent.* 40, 756–765. doi: 10.1016/j.jdent.2012.05.007

Tsuda, H., Ruben, J., and Arends, J. (1996). Raman spectra of human dentin mineral. *Eur. J. Oral Sci.* 104, 123–131.

Van Meerbeek, B., Mohrbacher, H., Celis, J. P., Roos, J. R., Braem, M., Lambrechts, P., et al. (1993). Chemical characterization of the resin-dentin interface by micro-Raman spectroscopy. *J. Dent. Res.* 72, 1423–1428.

Van Meerbeek, B., Van Landuyt, K., De Munck, J., Hashimoto, M., Peumans, M., Lambrechts, P., et al. (2005). Technique-sensitivity of contemporary adhesives. *Dent. Mater. J.* 24, 1–13.

Wang, A., Han, J., Guo, L., Yu, J., and Zeng, P. (1994). Database of standard Raman spectra of minerals and related inorganic crystals. *Appl. Spectrosc.* 48, 959–968.

Wang, Y., and Spencer, P. (2002a). Analysis of acid-treated dentin smear debris and smear layers using confocal Raman microspectroscopy. *J. Biomed. Mater. Res.* 60, 300–308.

Wang, Y., and Spencer, P. (2002b). Quantifying adhesive penetration in adhesive/dentin interface using confocal Raman microspectroscopy. *J. Biomed. Mater. Res.* 59, 46–55.

Wang, Y., and Spencer, P. (2003). Hybridization efficiency of the adhesive dentin interface with wet bonding. *J. Dent. Res.* 82, 141–145.

Wang, Y., and Spencer, P. (2005). Interfacial chemistry of class II composite restoration: structure analysis. *J. Biomed. Mater. Res. A* 75, 580–587.

Wang, Y., Spencer, P., and Walker, M. P. (2007). Chemical profile of adhesive/caries-affected dentin interfaces using Raman microspectroscopy. *J. Biomed. Mater. Res. A* 81, 279–286.

Wang, Y., Spencer, P., and Yao, X. (2006). Micro-Raman imaging analysis of monomer/mineral distribution in intertubular region of adhesive/dentin interfaces. *J. Biomed. Optics* 11:024005.

WHO (2020). *Oral Health: Achieving Better Oral Health as Part of the Universal Health Coverage and Noncommunicable Disease Agendas Towards 2030*. Geneva: WHO.

Wieliczka, D. M., Kruger, M. B., and Spencer, P. (1997). Raman imaging of dental adhesive diffusion. *Appl. Spectrosc.* 51, 1593–1596.

Xie, S. X., Boone, K., VanOosten, S. K., Yuca, E., Song, L. Y., Ge, X. P., et al. (2019). Peptide mediated antimicrobial dental adhesive system. *Appl. Sci. Basel* 9:557. doi: 10.3390/a9030557

Xie, S.-X., Song, L., Yuca, E., Boone, K., Sarikaya, R., VanOosten, S. K., et al. (2020). Antimicrobial peptide–polymer conjugates for dentistry. *ACS Appl. Polym. Mater.* 2, 1134–1144. doi: 10.1021/acsapm.9b00921

Ye, Q., Park, J., Laurence, J. S., Parthasarathy, R., Misra, A., and Spencer, P. (2011). Ternary phase diagram of model dentin adhesive exposed to over-wet environments. *J. Dent. Res.* 90, 1434–1438. doi: 10.1177/0022034511423398

Ye, Q., Park, J., Topp, E., and Spencer, P. (2009). Effect of photoinitiators on the in vitro performance of a dentin adhesive exposed to simulated oral environment. *Dent. Mater.* 25, 452–458. doi: 10.1016/j.dental.2008.09.011

Ye, Q., Spencer, P., Yuca, E., and Tamerler, C. (2017). Engineered peptide repairs defective adhesive-dentin interface. *Macromol. Mater. Eng.* 302:1600487. doi: 10.1002/mame.201600487

Ye, Z., Zhu, X., Mutreja, I., Boda, S. K., Fischer, N. G., Zhang, A., et al. (2021). Biomimetic mineralized hybrid scaffolds with antimicrobial peptides. *Bioact. Mater.* 6, 2250–2260. doi: 10.1016/j.bioactmat.2020.12.029

Yuca, E., Karatas, A. Y., Seker, U. O., Gungormus, M., Dinler-Doganay, G., Sarikaya, M., et al. (2011). In vitro labeling of hydroxyapatite minerals by an engineered protein. *Biotechnol. Bioeng.* 108, 1021–1030. doi: 10.1002/bit.23041

Zhang, W., Liao, S. S., and Cui, F. Z. (2003). Hierarchical self-assembly of nano-fibrils in mineralized collagen. *Chem. Mater.* 15, 3221–3226. doi: 10.1021/cm030080g

Zurick, K. M., Qin, C., and Bernards, M. T. (2013). Mineralization induction effects of osteopontin, bone sialoprotein, and dentin phosphoprotein on a biomimetic collagen substrate. *J. Biomed. Mater. Res. A* 101, 1571–1581. doi: 10.1002/jbm.a.34462

Conflict of Interest: The authors declare that the research was conducted in the absence of any commercial or financial relationships that could be construed as a potential conflict of interest.

frontiers in Materials

ORIGINAL RESEARCH
published: 04 June 2021
doi: 10.3389/fmats.2021.670010

Polyblend Nanofibers to Regenerate Gingival Tissue: A Preliminary *In Vitro* Study

Elena Canciani[1†], Nicoletta Gagliano[2†], Francesca Paino[1], Evžen Amler[3,4,5,6], Radek Divin[3,4,6], Luca Denti[2], Dolaji Henin[1], Andrea Fiorati[7,8] and Claudia Dellavia[1]*

[1]Department of Biomedical, Surgical and Dental Sciences, Università degli Studi di Milano, Milan, Italy, [2]Department of Biomedical Sciences for Health, Università degli Studi di Milano, Milan, Italy, [3]Department of Tissue Engineering, Institute of Experimental Medicine of the Czech – Academy of Science, Prague 4, Czech Republic, [4]Institute of Biophysics, 2nd Faculty of Medicine, Charles University, Prague 5, Czech Republic, [5]Student Science s.r.o, Národních Hrdinů 279, Dolní Počernice, Prague, Czech Republic, [6]UCEEB, Czech Technical University, Bustehrad, Czech Republic, [7]Department of Chemistry, Materials and Chemical Engineering "G. Natta", Politecnico di Milano, Milano, Italy, [8]INSTM - Local Unit Politecnico di Milano, Milano, Italy

OPEN ACCESS

Edited by:
Fabricio Mezzomo Collares, Federal University of Rio Grande do Sul, Brazil

Reviewed by:
Gabriela Balbinot, Universidade Federal do Rio Grande do Sul, Brazil
Victor Pinheiro Feitosa, Faculdade Paulo Picanço, Brazil

***Correspondence:**
Elena Canciani
elena.canciani@unimi.it

†These authors have contributed equally to this work and share first authorship

Specialty section:
This article was submitted to Biomaterials, a section of the journal Frontiers in Materials

Received: *19 February 2021*
Accepted: *12 May 2021*
Published: *04 June 2021*

Citation:
Canciani E, Gagliano N, Paino F, Amler E, Divin R, Denti L, Henin D, Fiorati A and Dellavia C (2021) Polyblend Nanofibers to Regenerate Gingival Tissue: A Preliminary In Vitro *Study. Front. Mater. 8:670010. doi: 10.3389/fmats.2021.670010*

Aim: The regeneration of small periodontal defects has been considered an important divide and challenging issue for dental practitioners. The aim of this preliminary in vitro study was to analyze the effects of polycaprolactone (PCL) nanofibers enriched with hyaluronic acid and vitamin E vs. nude nanofibers on gingival fibroblasts activity, an innovative graft for periodontal soft tissue regeneration purposes.

Methods: Nanofibers were produced in PCL (NF) or PCL enriched with hyaluronic acid and vitamin E (NFE) by electrospinning technique. NF and NFE were stereologically and morphologically characterized by scanning electron microscope (SEM), and composition was analyzed by infrared spectroscopy. Human fibroblasts were obtained from one gingival tissue fragment (HGF) and then seeded on NF, NFE, and plastic (CT). Cell adhesion and morphology were evaluated using SEM at 24 h and cell viability after 24, 48, and 72 h by alamarBlue® assay. Gene expression for COL-I, LH2b, TIMP-1, PAX, and VNC was analyzed by real-time RT-PCR in samples run in triplicate and GAPDH was used as housekeeping gene. Slot blot analysis was performed and immunoreactive bands were revealed for MMP-1 and COL-I. YAP and p-YAP were analyzed by Western blot and membranes were reprobed by α-tubulin. Statistical analysis was performed.

Results: IR spectrum revealed the presence of PCL in NF and PCL and vitamin E and hyaluronic acid in NFE. At 24 h, HGF adhered on NF and NFE conserving fibroblast like morphology. At 72 h from seeding, statistically significant differences were found in proliferation of HGF cultured on NF compared to NFE. Expression of genes (LH2b, TIMP-1, and MMP-1) and proteins (COL-I) related to collagen turnover revealed a reduction of COL-1 secretion in cells cultured on NF and NFE compared to CT; however, NFE stimulated cross-linked collagen deposition. Mechanosensor genes (PAX, VNC, and YAP) were upregulated in HGF on NF while they were decreased in cells grown on NFE.

Conclusion: Preliminary data suggest that PCL-enriched nanofibers could represent a support to induce HGF proliferation, adhesion, collagen cross-linking, and to reduce collagen degradation, therefore favoring collagen deposition in gingival connective tissue.

Keywords: polycaprolactone, hyaluronic acid, vitamin E, nanofibers, oral soft tissues regeneration, gingival fibroblasts, collagen turnover

INTRODUCTION

Patients' aesthetic expectation and awareness about oral health have considerably increased in last years. The regeneration of small periodontal defects has been considered an important and challenging issue for dental practitioners (Hatayama et al., 2017; Rasperini et al., 2020). Periodontal plastic surgery is the gold standard for correcting the morphology of gingival defects. However, surgical interventions have shown to be unpredictable for long-term stability of the sites (Hägi et al., 2014).

Recently, numerous technologies and materials have been developed in order to promote periodontal soft tissue regeneration by means of three-dimensional (3D) supports that stimulate the biological process of the connective tissues (Botelho et al., 2017).

An ideal scaffold for connective tissue engineering, to stimulate cellular biological processes, should have several features: support cell growth by 3D topography mimicking extracellular matrix (ECM), have a high surface-to-volume ratio, have the presence of many interconnected pores for blood vessels passage, and have the possibility to be functionalized or to be composed by several materials.

Synthetic polymers, such as polycaprolactone (PCL), are largely used in several fields of regenerative medicine, including dentistry, to create bio-printed scaffolds for periodontal osseous defect treatment (Rasperini et al., 2015) and to produce nanofibers to stimulate human dental pulp–derived stem cells activity (Mohandesnezhad et al., 2020). Furthermore, PCL allows to produce miscible polyblend with natural polymers (Gunn et al., 2010) and substances.

Polyblend nanofibers represent an innovative biomimetic synthesized material in nanoscale with great potential to create 3D scaffolds for their physical, chemical, and morphological features. During the healing process and tissue regeneration, nanofibers provide mechanical support and structural guidance for cellular growth, exploiting properties of the native tissue and releasing chemical cues (Gunn et al., 2010; Amler et al., 2014). Thus, numerous are the advantages to design polyblend nanofibers. On one side, polyblending would allow to control physicochemical features such as morphology, wettability, formulation, mechanical strength, (Carter et al., 2016); on the other side, polyblending would allow to stimulate biological activity of cells, favoring cell attachment, proliferation, and differentiation (Beznoska et al., 2019).

In the literature, miscible polyblend PCL based have been recently tested to improve wound healing (Amler et al., 2014). Chanda et al., (2018) studied an electrospinned scaffold consisting of chitosan, PCL, and hyaluronic acid (HA) to enhance proliferation, growth, and migration of Vero cell. Further with the presence of HA, it aimed to mechanically stabilize the scaffold (Chanda et al., 2018). Kalantary et al., (2020) charged PCL/gelatin nanofibers with vitamin E to produce a device able to protect skin from ROS (reactive oxygen species) released after occupational skin exposure (Kalantary et al., 2020). The authors demonstrated that nanofibers containing vitamin E showed a higher viability compared to PCL/gelatin ones and significantly assisted human skin cells against *tert*-Butyl hydroperoxide (t-BHP)-induced oxidative stress (Kalantary et al., 2020). Although PCL nanofibers were previously studied, the behavior of gingival fibroblasts in contact with PCL nanofibers enriched with vitamins for tissue regeneration and wound healing has not yet been largely investigated.

Hyaluronic acid is a natural glycosaminoglycan, an essential molecule of the connective tissue of the oral mucosa and the skin, which plays a pivotal role in numerous processes such as wound healing (Alexander et al., 1980). HA is a well-known natural hydrogel. In fact, it is able to maintain ECM resilience and tissue hydration, to create temporary structure for deposition of ECM proteins, to trigger cell adhesion, proliferation, and migration. It was demonstrated that HA regulates vascular endothelial cell function (Mesa et al., 2002; Tammi et al., 2002; Litwiniuk et al., 2016; Canciani et al., 2021) giving beneficial effect when used in the treatment of diabetic wound ulcers (Chen et al., 1999; Voigt et al., 2012). HA is biocompatible, biodegradable, bacteriostatic, antioxidant, anti-edematous, and finally anti-inflammatory (Fraser et al., 1997; Pirnazar et al., 1999; Campo et al., 2012). HA is used in various fields of medicine and also in dentistry (Robert et al., 2015; Eliezer et al., 2019); a systematic review and meta-analyses reported that seems to favor periodontal healing after surgical procedures (Bertl et al., 2015).

Vitamin E is known to have a key role in the prevention of many pathogens thanks to its anti-inflammatory effects (Konieczka et al., 2019). It is therefore a pivotal nutrient in dermatological application (Thiele et al., 2005) because it seems to affect collagen turnover to improve wound healing (Hobson, 2016).

The aim of this preliminary *in vitro* study was to analyze the effects of PCL nanofibers enriched with HA and vitamin E (NFE) vs PCL nanofibers alone (NF) on the gingival fibroblast activity assessing morphology, viability, collagen turnover, and mechanosensing.

MATERIALS AND METHODS

Nanofibers Production and Characterization

Nanofibers tested in the experiment were produced in PCL or PCL enriched with HA and vitamin E.

NF was obtained from a solution of 14% (w/v) of PCL, with a molecular weight (MWPCL) of 45,000 Dalton (Sigma-Aldrich, MO, United States) dissolved in chloroform:ethanol (8:2) (Plencner et al., 2014). NFE were obtained as described above but adding to the solution of hyaluronic acid (HA) at 0.002% (Sigma-Aldrich, MO, United States) and vitamin E at 0.0014% (α-Tocopherol; Sigma, St. Louis, MO). The concentration of the enriching agents (HA and vitamin E) was chosen in accordance with our previous work (Canciani et al., 2021), also taking into account that higher concentrations of HA and vitamin E could cause structural defects in 3D nanofiber's structure. This emulsion was prepared and preserved from light due to the photosensitivity of the vitamin. Electrospinning was performed using a Nanospider TM device (Elmarco, Czech Republic) (Amler et al., 2014). A high-voltage source generated voltage of up to 56 kV, and the polymer solutions were connected to the high-voltage electrode. The electrospun nanofibers were deposited on a grounded collector electrode. The distance between the tip of the syringe needle and the collecting plate was 12 cm. For both NF and NFE, one sheet of 50 × 50 cm was produced. All electrospinning processes were performed at room temperature (RT; ~24°C) and a relative humidity of ~50%.

Characterization of NF and NFE samples was performed by means of attenuated total reflection Fourier transform infrared spectroscopy (ATR-FTIR). The ATR-FTIR spectra were recorded at T = 298 K, under nitrogen atmosphere, in a 550–4,000 cm^{-1} wavelength range using an Agilent Cary 640-IR infrared spectrometer (Agilent Technologies, Santa Clara, CA, United States) equipped with a single bounce ZnSe ATR accessory. All the spectra were collected in triplicate.

Mechanical properties of five 0.5 × 2 cm^2 pieces obtained from the produced sheets were preconditioned in PBS for 10 min, and these wet pieces were evaluated by a dynamic mechanical analyzer (DMA) (TA, Q800). The DMA strain rate was 0.02 min^{-1}; tensile test was performed with a preload of 1 mN at room temperature.

Biodegradability test was performed by a stereomicroscope (SZX Olympus instruments), leaving nanofibers for 28 days in a phosphate buffer saline (PBS) solution.

Morphological analysis was effectuated by scanning electron microscope (SEM) (Tescan Vega 3, Brno, Czech Republic) to verify the nanofiber's diameter and largest pore size by means of image analysis software (Vega3 SB, Tescan a.s). For both NF and NFE, three random 0.8 × 0.8 cm^2 pieces of the produced sheets were selected and three 80 × 80 μm^2 areas were analyzed on each piece. For each area, 5 measurements of largest pores and nanofiber's diameter were executed. Nanofiber's diameter distribution was obtained and the largest pore range was computed.

Cell Cultures of Primary Gingival Fibroblasts (HGF)

During molar extraction appointment, following local anesthesia, using articaine with epinephrine 1:100,000 (Pierrel Pharma S.P.A., Zurich), a surgical incision was performed to expose the impacted tooth in a female patient, 35 years old, and after the extraction, the flaps were sutured (Vycril 3/0). The patient was free from periodontal diseases, did not use hormonal contraceptives or hormonal replacement medications, and signed a consent form to participate in the experiment. The study was conducted in accordance with the ethical principles of the World Medical Association Declaration of Helsinki and the local Ethics Committee of Università degli Studi di Milano, Milan (29/18 of the 28 June 2018). Exceeded soft tissue biopsy was collected to obtain HGF.

Bioptical fragment was washed with sterile PBS and incubated in a solution of DMEM (Dulbecco's Modified Eagle Medium) and collagenase I 4 mg/ml (Millipore, United States). Cell suspension was filtered and plated in a T25 flask. Cells were cultured at 37°C in a 5% CO_2 humidified incubator in a DMEM containing 10% heat-inactivated fetal bovine serum (FBS) (GIBCO), supplemented by 100 U/mL penicillin (Invitrogen), 100 μg/mL streptomycin (GIBCO), 2.5 μg/mL amphoterycin B (Sigma), and adding ascorbic acid (200 μM) (Francetti et al., 2019).

For the analysis, cells were seeded on a plastic or on nanofibers in 6- or 24-well multi-well plates at the concentration of 1.5 × 10^4. HGF were used between the fourth and the fifth passage, approximately at 80% confluence, and molecular evaluations were performed in samples cultured for 72 h on NF, NFE. or on plastic (CT). Primary HGF were tested for viability and adhesion. Furthermore, genes and proteins expression related to collagen turnover and mechanotransduction pathways were also evaluated. Two replicate experiments for both NF and NFE were performed. In each experiment, a technical triplicate was applied and conducted at 37°C in a 5% CO_2 humidified incubator.

Viability Test by alamarBlue

To test cell viability, 7 × 10^3 cells were seeded on NF and NFE in 24-well multi-well plates. Cell viability was tested at 3 different time points (24, 48, and 72 h from seeding) using alamarBlue® (Thermo Fisher Scientific), a test that allows to determine a proliferation curve related to the metabolic cellular ability.

The color changing of the culture medium reveals an active cellular metabolism, and it was monitored and read by a spectrophotometer (Glo Max Discover, Promega Corporation, United States). For each group, a proliferation curve was created, and the % of cells proliferation was calculated in relation to CT proliferation, inserting the values in an algorithm, as described by the manufacturer's protocol.

Cell Adhesion and Morphology

Cell adhesion and morphological assessment of spreading of the cells on NF and NFE were evaluated after 24 h from seeding. Morphological analysis was performed on images acquired using SEM. In brief, the samples were fixed with 2.5% glutaraldehyde, postfixed in osmium tetroxide, dehydrated through an increasing scale of alcohol, infiltrated with hexamethyldisilane, and dried. Finally, the samples were mounted on stubs and coated with a thin layer of gold. The fields to analyze were acquired at a total

magnification until 1,000x by means of a Jeol Neoscope Electron Microscope (JCM-6000; Nikon, Tokyo, Japan). Cell morphology was analyzed, with particular attention to observe the presence of cytoplasmic extensions, functional orientation, and cell arrangement on the surface (Canciani et al., 2016).

Real-Time PCR

Cells were harvested and the total RNA was isolated (Tri Reagent, Sigma, Italy). One μg of total RNA was reverse transcribed in a 20 μL final volume of reaction mix (Bio-Rad, Segrate, Milan, Italy). mRNA levels for long type I collagen (COL-I), lysyl hydroxylase 2 (LH2b), and tissue inhibitor of matrix metalloproteinase 1 (TIMP-1) were analyzed by real-time RT-PCR in samples run in triplicate. Glyceraldehyde 3-phosphate dehydrogenase (GAPDH) was used as housekeeping gene to normalize the differences in the amount of total RNA in each sample. The primers sequences were the following: GAPDH: sense CCCTTCATTGACCTCAACTACATG, antisense TGG GATTTCCATTGATGACAAGC; LH2b: sense CCGGAAACA TTCCAAATGCTCAG, antisense GCCAGAGGTCATTGTTAT AATGGG; TIMP-1: sense GGCTTCTGGCATCCTGTTGTTG, antisense AAGGTGGTCTGGTTGACTTCTGG; PAX sense CAGCAGACACGCATCTCG, antisense GAGCTGCTCCCT GTCTTCC; VNC sense GGAGGTGATTAACCAGCCAAT, antisense AATGATGTCATTGCCCTTGC. Each sample was analyzed in triplicate in a Bioer LineGene 9600 thermal cycler (Bioer, Hangzhou, China). The cycle threshold (Ct) was determined and gene expression levels relative to that of GAPDH were calculated using the ΔC_T method.

Slot Blot

Slot blot analysis was performed in serum-free cell culture supernatants. Cell culture media protein content was determined by a standardized colorimetric assay (DC Protein Assay, Bio- Rad, Italy); 100 μg of total protein per sample in a final volume of 200 μL of Tris buffer saline (TBS) was spotted onto a nitrocellulose membrane in a Bio-Dot SF apparatus (Bio-Rad, Italy). Membranes were blocked for 1 h with 5% skimmed milk in TBST (TBS containing 0.05% Tween-20), pH 8, and incubated for 1 h at room temperature in a monoclonal antibody to COL-I (1:1,000 in TBST) (Sigma-Aldrich, Milan, Italy) and MMP-1 (1 μg/ml in TBST, Millipore, Milan, Italy). After washing, membranes were incubated in HRP-conjugated rabbit anti-mouse serum (1:6,000 in TBST to detect COL-I; 1:20,000 in TBST to detect MMP-1) (Sigma, Italy) for 1 h. Immunoreactive bands were revealed by the Opti-4CN substrate or Amplified Opti-4CN substrate (Bio-Rad, Italy) and scanned densitometrically (UVBand, Eppendorf, Italy).

Western Blot

Whole cell lysates were prepared in a lysis buffer (Tris-HCl 50 mM pH 7.6, 150 mM NaCl, 1% Triton X-100, 5 mM EDTA, and 1% sodium dodecyl sulphate), proteases inhibitors, and 1 mM sodium orthovanadate. Lysates were incubated in ice for 30 min and centrifuged at 14,000×*g* for 10 min at 4°C. Cell lysates (30 μg of total proteins) were run on 10% SDS–polyacrylamide gel, separated under reducing and denaturing conditions at 80 V according to Laemmli, and transferred at 90 V for 90 min to a nitrocellulose membrane in 0.025 M Tris, 192 mM glycine, and 20% methanol, pH 8.3. Membranes were incubated with YAP (1:1,000 dilution, D8H1X, Rabbit mAb, Cell Signaling) or p-YAP (S109) (1: 1,000 dilution, D3I6D Rabbit mAb, Cell Signaling). After the incubation with a horseradish peroxidase (HRP)-conjugated goat anti-rabbit antibody (1:20,000 dilution, Cell Signaling), immunoreactive bands were revealed using the Amplified Opti-4CN (Bio-Rad).

Membranes were reprobed by monoclonal antibody to α-tubulin (1:2,000 dilution, Sigma-Aldrich) to confirm equal loading.

Statistical Analysis

Descriptive analysis was performed and mean and standard deviation (SD) of the values obtained from the two experimental technical triplicates were computed for both NF and NFE samples in all performed tests. A nonparametric statistical analysis by Wilcoxon rank-sum test was used to compare the results of the mechanical characterization of NF and NFE, and a p value < 0.05 was considered significant (GraphPad Software Inc., San Diego).

Comparisons between NF and NFE mean values were performed at each time point of the viability test by means of paired t-test with a level of significance of $p < 0.05$ (GraphPad Software Inc., San Diego, CA 92108, United States). Differences associated with p values lower than 5% were to be considered statistically significant.

RESULTS

Nanofibers Characterization

In **Figure 1** are reported the ATR-FTIR spectra of the specimens (NFE and NF) and of the corresponding enriching agents (HA and vitamin E). As expected, the spectra of the unloaded nanofibers samples (NF) show only signals which can be attributed to the PCL used as starting materials (Primpke et al., 2018). The enriched specimens (NFE) possess ATR-FTIR spectra which are composed mainly of the signals of PCL; however, the presence of a breaded peak at about 3,400 cm^{-1}, typical of O–H stretching vibrations, the broadening of the signal at 1,176 cm^{-1}, and the growth of the peak at 1,103 cm^{-1} suggest the proper loading of HA and vitamin E in the samples NFE. (**Figure 1A**). HA presence influences the spectrum from 500 to 700 cm^{-1} by increasing the values in NFE compared with NF as illustrated in figure B (**Figure 1B**). Furthermore, considering vitamin E, a peak around 3,008 cm^{-1} was observed, thus confirming its incorporation in NFE sample (**Figure 1C**). NF showed a higher but not statistically significant stress at break than NFE (1.47 ± 0.34 MPa vs 1.06 ± 0.25 MPa, $p > 0.05$). In contrast, deformation at break was significantly higher in NF than in NFE (31.52 ± 5.08% vs. 14.11 ± 4.64%, $p < 0.01$). Strain resulted statistically significant between NF and NFE for p value < 0.01.

Biodegradability observation showed that after 28 days the nanofibers had maintained their structure.

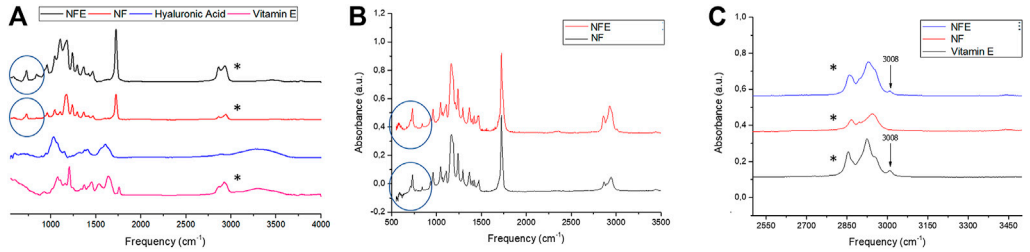

FIGURE 1 | Panel shows **(A)** ATR-FTIR spectra of samples NFE, NF, and of vitamin E and hyaluronic acid. **(B)** Spectra highlights hyaluronic acid peak (blue circles) and **(C)** the peak relative to vitamin E (black asterisks).

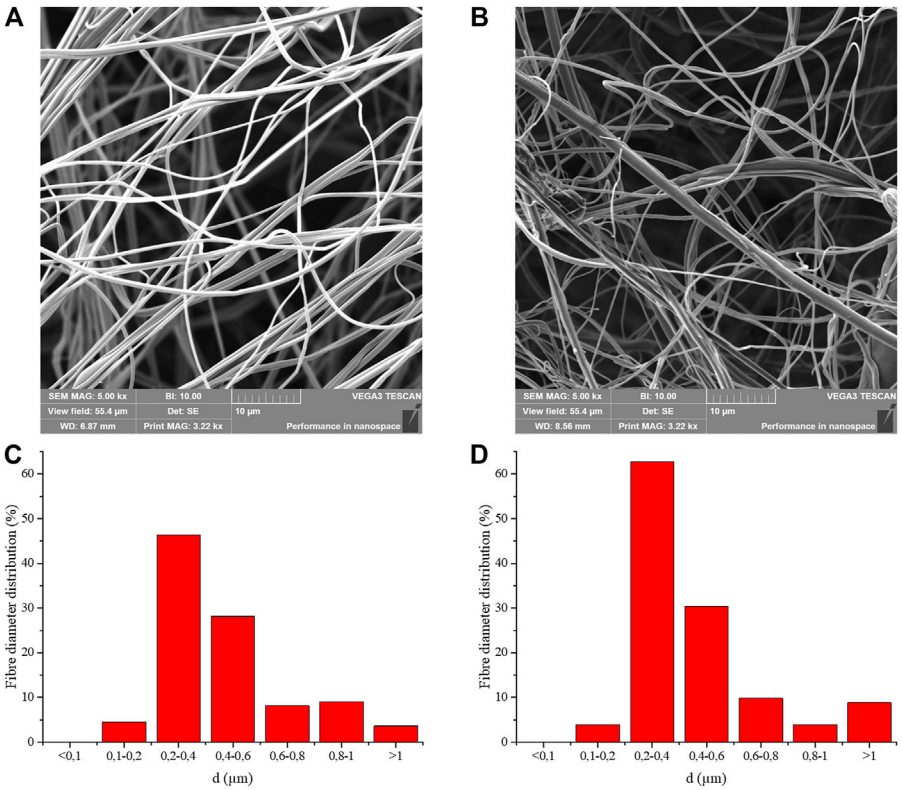

FIGURE 2 | Micrographs at SEM of the three-dimensional structure of NF **(A)** and NFE **(B)**, showing the width of the pores among fibers and fibers organization. SEM observation revealed that NFE appeared more swollen than NF. Nanofiber's diameter distributions are reported for NF **(C)** and NFE **(D)** samples.

NF and NFE morphology was assessed by SEM (**Figures 2A**,**B**) showing the typical organization of nanofibers in a mesh characterized by fibers of different dimension size and interconnection. Fiber's diameters presented a Gaussian-like distribution with a prevalent percentage of fibers in the range between 0.2 and 0.4 µm for both groups (**Figures 2C,D**). In NFE, the encapsulation of HA and vitamin E determined a shift of the distribution toward larger diameters (**Figure 2D**).

Due to difficulty in measuring the space of an irregular mesh on a bidimensional SEM image, the distance between the farthest nanofibers was calculated in the largest pores. In NF, the largest distance calculated was 86.98 ± 25.60 µm (**Figure 2A**), while in NFE, it was 31.66 ± 7.97 µm (**Figure 2B**).

Fibroblasts Morphology and Adhesion on NF and NFE

After seeding, HGF grew in adhesion on nanofibers. HGF morphological features were evaluated by SEM (**Figure 3**). One day after seeding, fibroblasts were housed on the surface of NF (**Figure 3A**) and NFE (**Figure 3B**).

HGF showed cytoplasmic protrusions extending on nanofibers used as rails (**Figure 3A**) and becoming in contact.

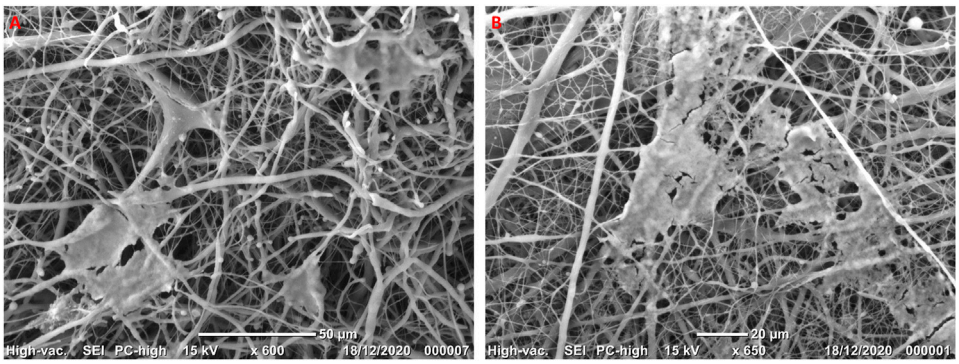

FIGURE 3 | Representative micrographs at SEM showing HGF cultured on NF **(A)** and NFE **(B)** highlighting the three-dimensional structure of nanofibers and cells that seem to be interconnected.

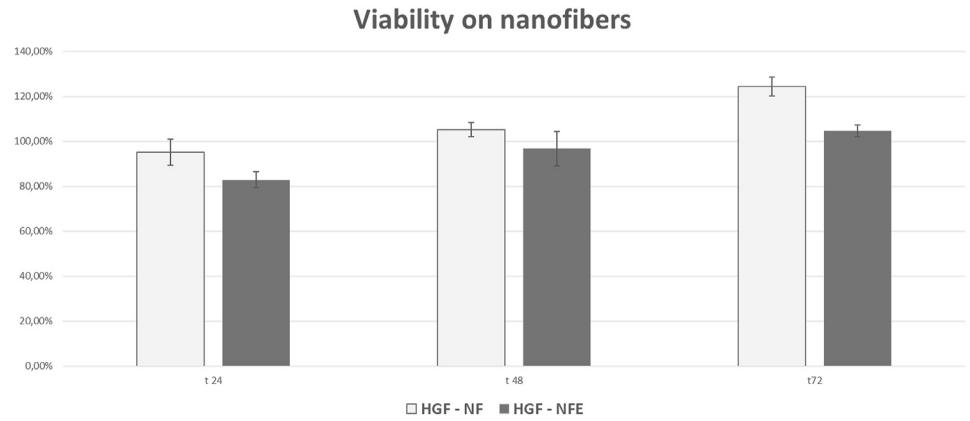

FIGURE 4 | Bar graphs showing cell viability and proliferation of HGF expressed as a % relative to CT (considered as the 100%). At all the considered time points and experimental conditions, cell viability was higher than 80%, suggesting that nanofibers do not elicit any evident cytotoxicity.

Moreover, they were arranged rolling up or reclining on nanofibers, in particular on NF samples. On the other hand, when cells grew on NFE, they extended across the pores creating bridges to build a network to cover the nanofibers mesh surface (**Figure 3B**).

Viability of HGF on NF and NFE

AlamarBlue® test evaluation at early time points revealed that the metabolism of HGF was not affected by NF and NFE. A trend of viability reduction was observed at 24 and 48 h after seeding in all experimental groups, considering 100% the viability reference of the CT. At 72 h from seeding, HGF cultured both on NF and NFE showed values over control threshold (**Figure 4**).

Expression of Genes and Proteins Related to Collagen Turnover

Type I collagen (COL-I) mRNA levels were increased in cells grown on nanofibers (+45% vs CT), while a strong downregulation was evident in fibroblasts cultured on NFE (−66%) (**Figure 5A**). COL-I protein levels secreted by HGF in cell culture supernatants were assessed by slot blot. COL-I protein levels revealed that the secretion of COL-I was reduced in cells cultured on NF (−39% vs CT) and on NFE (−75%) (**Figures 5B,C**).

Newly synthetized collagen undergoes maturation by covalent cross-linking after hydroxylation of amino acids such as lysine. Collagen maturation was assessed by analyzing the mRNA levels for LH2b by real-time PCR. LH2b mRNA levels showed a different pattern of expression in all experimental conditions. In fact, LH2b resulted downregulated and upregulated, respectively, in HGF cultured on NF and NFE, compared to CT (**Figure 5D**). The LH2b mRNA/COL-I mRNA and LH2b mRNA/COL-I protein ratio shows a strong increase in cells grown on NFE (**Figure 5E**), pointing to an increased collagen cross-linking in this experimental condition.

Interstitial collagen degradation was assessed by slot blot analysis of MMP-1 levels in cell culture supernatants. Our data show that MMP-1 levels were similar in supernatants of

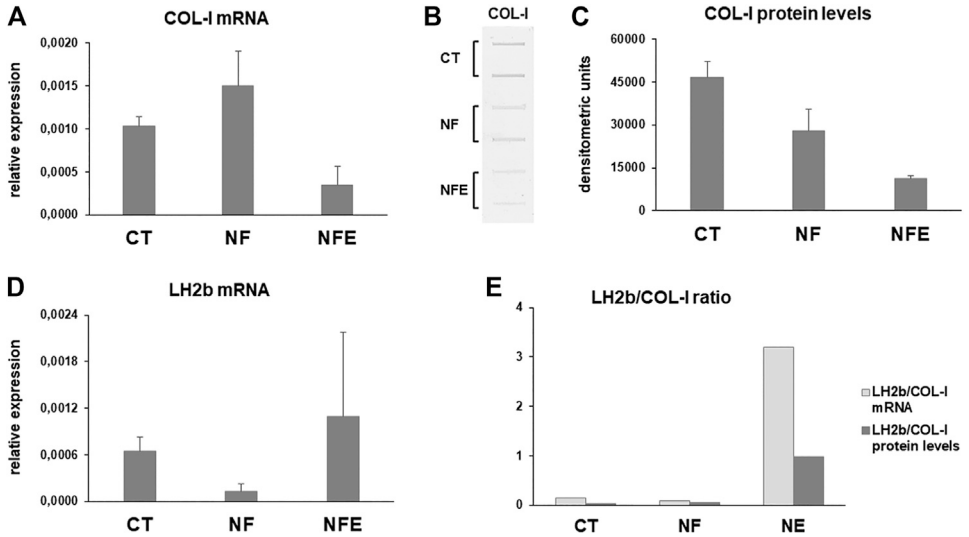

FIGURE 5 | (A) Bar graphs showing COL-I mRNA levels in HGF cultured on NF and NFE. **(B)** Representative slot blot and bar graphs showing COL-I protein levels **(C)** secreted in cell culture supernatant of HGF cultured on NF and NFE assayed by slot blot after densitometric scanning of immunoreactive bands in the considered experimental conditions. Data are expressed as mean ± SD of two independent experiments. **(D)** mRNA levels for long lysyl hydroxylase 2 (LH2b) in CT and cells grown on NF and NFE. Data were normalized on GAPDH gene expression and are expressed as mean ± SD for at least two independent experiments. **(E)** Bar graphs showing the LH2b mRNA/COL-I mRNA and LH2b mRNA/COL-I protein ratio in the different experimental conditions.

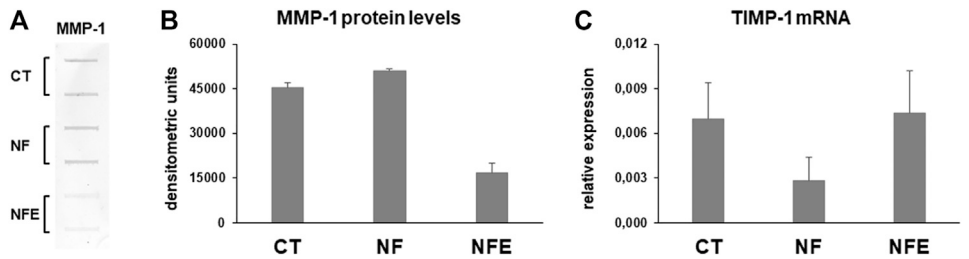

FIGURE 6 | (A) Representative slot blot for MMP-1 levels assayed by slot blot in serum-free cell supernatants of HGF cultured in the considered experimental settings. **(B)** Bar graphs showing MMP-1 protein levels after densitometric analysis of immunoreactive bands. Data are expressed as mean ± SD for at least two independent experiments. **(C)** Bar graphs showing TIMP-1 gene expression after normalization on GAPDH mRNA levels. Data are expressed as mean ± SD for at least two independent experiments.

HGF on NF and CT but were downregulated when cells are grown on NFE (**Figures 6A**,**B**). Gene expression analysis for TIMP-1 mRNA revealed that its expression was decreased in cells grown on NF but was unchanged in cells cultured on NFE (**Figure 6C**).

Expression of PAX, VNC, and YAP as Mechanosensors

To better understand whether NF exert any mechanical effect on collagen turnover pathways, we analyzed the expression of mechanosensors such as PAX, VCN, and YAP. PAX and VCN are components of the adhesion plaque and also act as mechanosensors. Their mRNA levels were tended to be upregulated in HGF on NF, while they were decreased in cells grown on NFE (**Figures 7A**,**B**).

Yes-associated protein (YAP) is a mechanosensor that can be inactivated by phosphorylation, leading to cytoplasmic translocation. YAP and p-YAP were analyzed by Western blot. YAP and p-YAP resulted similarly expressed in cell lysates obtained from CT and HGF on NF. By contrast, a strong downregulation was evident in fibroblasts grown on NFE (**Figures 7C–G**).

DISCUSSION

To date, dental practitioners still have to face a challenging issue to restore a proper morphology of the oral soft tissue due to periodontal disease.

The development of new technologies and devices may help in the regeneration of the oral soft tissues, thus allowing to obtain a physiologically stable masticatory apparatus and to reach an

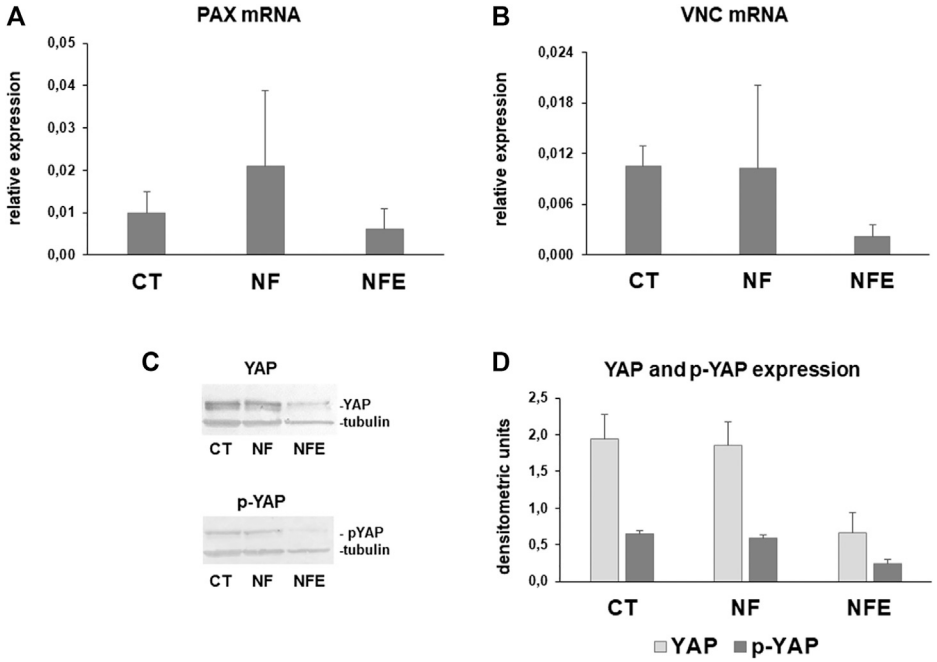

FIGURE 7 | Bar graphs showing PAX **(A)** and VNC **(B)** mRNA levels in HGF after normalization on GAPDH gene expression. Data are means for at least two independent experiments. **(C)** Representative Western blot for YAP and inactive phosphorylated p-YAP **(D)**. Bar graphs showing YAP and p-YAP assayed by Western blot in whole cell lysates after densitometric analysis of immunoreactive bands. Data are mean ± SD for at least two independent experiments.

optimal aesthetic. An emerging and increasingly widespread innovation in dentistry is the use of nanotechnologies for oral tissue regeneration (Ahadian et al., 2020; Bonilla-Represa et al., 2020; Mohandesnezhad et al., 2020).

In the current preliminary study, the authors were interested in evaluating the biological activity of primary HGF fibroblasts obtained from one patient on polyblend nanofibers exhibiting two key characteristics: they have a texture similar to the native ECM (Seo-Jin et al., 2016) and they can be loaded with compounds that stimulate resident cells (Bhattarai et al., 2018).

Several studies proposed the use of nanofibers to regenerate (Gunn et al., 2010; Chanda et al., 2018) or deliver substances and compounds (Amler et al., 2014; Ahadian et al., 2020) in different tissues (Wang et al., 2017; Beznoska et al., 2019); however, only few preliminary published articles are available in oral fields (Bonilla-Represa et al., 2020; Mohandesnezhad et al., 2020).

Due to their biological properties, in this study, we charged nanofibers with HA and vitamin E in order to characterize their impact on HGF metabolism and the possible effect on ECM deposition turnover.

The concentration of HA and vitamin E used in this study allowed to obtain nanofibers with a stable fibrillar structure organized in an irregular mesh, similar to the architecture of the extracellular matrix. The addition of these molecules determined the increase of the fiber's diameter with a consequent reduction of the pore dimensions, and a trend of reduction about mechanical properties was observed. In particular, NFE presented a significant reduction of the strain value compared to NF.

Due to these characteristics, polyblend nanofibers are supposed to be able to guide cells during their adhesion and proliferation, to bind water and therefore increase the volume *in situ*, and to act as a reserve of substances able to influence the quality of the ECM in accordance with the literature (Gunn et al., 2010).

All these features could be exploited to improve aesthetics and function in clinical procedures such as ridge augmentation (Dellavia et al., 2014).

In order to understand whether polyblend PCL nanofibers are a suitable device for HGF, this *in vitro* preliminary study analyzed HGF phenotype. For this purpose, in line with future clinical application, proliferation, adhesion, and collagen turnover pathways were evaluated. In fact, collagen is the main component of the gingival dense irregular connective tissue. Our results show that HGF were able to proliferate and adhere when cultured on both NF and NFE. However, SEM analysis revealed a different behavior of HGF between the two experimental groups. In fact, NF seemed to favor cell motility toward fibers, while cells grown on NFE seemed to be in closer contact and to form interconnecting bridges. These preliminary results suggested that NF and NFE likely affect cell adhesion and migration at a different extent and further experiments will be performed to analyze this effect.

We focused on collagen turnover pathways since COL-I is the main component of gingival connective tissue ECM. Its content is finely regulated by a balanced turnover controlled by HGF at the level of collagen synthesis, maturation, and degradation. Collagen turnover, therefore, is pivotal in influencing gingival connective tissue homeostasis. Our results show a nonsynchronous regulation of COL-I at the gene and protein expression in

fibroblasts cultured on NF, likely due to translational or posttranslational regulation mechanisms. By contrast, both COL-I mRNA and protein levels were decreased in cells grown on NFE compared to CT and NF. This finding suggests a reduced COL-I secretion induced by NFE. However, to predict the ability of fibroblasts to increase COL-I deposition in the gingival connective tissue, collagen maturation played by LH2b should also be considered. In fact, posttranslational hydroxylation of collagen by LH is a key mechanism of collagen maturation and ECM stability and, therefore, strongly influences collagen content. We analyzed LH2b gene expression since this is the major form expressed in all tissues. Moreover, LH2b is generally over-expressed in fibrotic processes and is responsible for the over-hydroxylation of the COL telopeptides, forming COL pyridinoline cross-links and, thus, contributing to unwanted COL accumulation. The LH2b mRNA/COL-I mRNA ratio indicates the gene expression of LH2b relative to COL-I and, therefore, is considered as an indicator of the susceptibility of collagen to undergo hydroxylation (Silver et al., 2000; Walker et al., 2005). Our results show that LH2b is downregulated by NF, while a very evident increase is induced in cells cultured on NFE. This finding suggests that NFE seem able to stimulate COL-I maturation by cross-linking to improve its stability and, therefore, favoring its deposition.

Collagen content is determined by the finely regulated dynamic balance between its synthesis and degradation by MMPs. Interstitial collagen breakdown is played by MMP-1, that cleaves the native triple helix of interstitial collagens into characteristic 3/4- and 1/4-collagen degradation fragments, also known as gelatins (Sakai et al., 1967), that can be further degraded to complete digestion by less specific proteinases such as MMP-2 (Sakai et al., 1967; Woessner et al., 1991).

MMP-1 is regulated at the posttranslational level by TIMP-1, the main inhibitor of MMP-1, that binds MMP-1 in a 1:1 stoichiometric ratio and inhibits its activation and activity (Murphy et al., 1994; Brew et al., 2001). Our results show that MMP-1 is similarly expressed in cell culture supernatants from CT and cells cultured on NF but it was strongly downregulated by NFE. This finding leads to the hypothesis that NFE are likely able to decrease COL-I degradation, and moreover, due to a higher cross-linking, they could favor COL-I accumulation in gingival connective tissue. This hypothesis is strengthened by the analysis of TIMP-1 mRNA levels that are highly expressed in HGF cultured on NF, therefore suggesting a further inhibition of COL-I degradation by NFE. These preliminary results suggest that HA in NFE could exert a role in influencing collagen degradation and are consistent with previously reported data showing that in HA cultures of fibroblasts a different collagen turnover pattern was observed when compared to collagen or collagen–fibrin cultures, mainly associated to a decrease in collagen synthesis (Chopin-Doroteo et al., 2018).

Mechanotransduction is the ability of cells to translate mechanical stimuli into biochemical signals that can influence gene expression, cell morphology, and cell fate. Mechanotransduction allows cells to respond to external forces and timely adapt their activity in ECM by remodeling (Jansen et al., 2015). To better understand whether nanofibers could exert any mechanical effect on HGF collagen turnover pathways, we analyzed the expression of mechanosensors such as PAX, VCN, and YAP in HGF cultured on NF and NFE. In particular, YAP acts as a mechanosensor whose activity is primarily regulated by the substrate on which cells adhere by phosphorylation, leading to protein inactivation and cytoplasmic translocation (Dupont et al., 2005; Totaro et al., 2018). Our preliminary data suggest a different effect induced by NF and NFE on collagen turnover pathways in HGF. Since ECM remodeling and homeostasis in connective tissues are influenced also by mechanical stimuli and fibroblasts are mechanoresponsive cells, we were interested in understanding if HGF cultured on NF or NFE are differently influenced in sensing mechanical signals and convert them into biological responses (Burridge et al., 2016; Wang et al., 2012). For this purpose, we analyzed the expression of key mechanosensors. mRNA levels for PAX and VNC resulted in expressed at a lower extent in cells cultured on NFE, suggesting that HA could be able to reduce the mechanoresponsive response of HGF. This hypothesis is consistent with YAP and p-YAP pattern. In fact, they resulted similarly expressed in CT and in cells cultured on NF, while a strong downregulation was induced by NFE. These preliminary findings seem to suggest that NF nanofibers do not affect the response to mechanical response of HGF, while the presence of HA used to charge the NFE nanofibers downregulated PAX and VNC mRNA levels as well as YAP and p-YAP expression. To explain this effect, we can hypothesize that HA interaction with its CD44 receptor could likely modulate fibroblast adhesion to the substrate, thus influencing fibroblast behavior (Price et al., 2005).

Considered as a whole, these preliminary data show that NF and NFE elicit a different effect on HGF. NF seem to favor COL-I degradation by reducing TIMP-1 mRNA levels and, therefore, MMP-1 inhibition. Moreover, LH2b mRNA levels are also downregulated, pointing to a less cross-linked collagen. Since a not evident mechanical response is triggered by NF on fibroblasts, we can hypothesize that these effects induced by NF on HGF are not primarily based on a mechanical response. Conversely, NFE seem to exert an opposite effect compared to NF. In fact, they favor collagen cross-linking and inhibit collagen degradation, thus favoring its deposition. This effect seems to be related to a reduced mechanical stimulation exerted by HA on HGF. However, the current preliminary results were obtained in only one sample, thus needing further experiments to confirm our hypothesis and to understand if the effect of HA used to charge the NFE involves other alternative mechanisms different from the mechanotransduction.

CONCLUSION

Considered as a whole, these preliminary *in vitro* findings suggest that PCL-enriched nanofibers (NFE) could represent a device to enhance HGF proliferation and biosynthetic phenotype, likely favoring collagen deposition in the gingival connective tissue. However, further experiments are needed to confirm these results and the mechanism responsible of NFE biological activity on a higher number of samples, in order to understand if NFE could represent the basis to build a new biomaterial for oral soft tissue regeneration.

DATA AVAILABILITY STATEMENT

The data that support the findings of this study are available from the corresponding author upon reasonable request.

AUTHOR CONTRIBUTIONS

All the Authors contributed to conception and design of the study. EC and EA formulated and synthesized nanofibers. RD and AF characterized nanofibers. EC, FP, and DH performed morphological andin vitro study. NG and LD performed gene and protein expression analysis. NG and EC wrote the first draft of the manuscript. DH and LD wrote sections of the manuscript. CD coordinated the project. All authors contributed to manuscript revision, read, and approved the submitted version.

ACKNOWLEDGMENTS

The Authors thank Dr. Kralovic Martin, Ing. Petr Novotný and Dr. Giuseppe Bitti, researchers at UCEEB, Czech Technical University, Trinecka 1024, 273 43 Bustehrad, Czech Republic, and Prof. Lina Altomare, Politecnico di Milano, for their precious contribution.

REFERENCES

Ahadian, S., Finbloom, J. A., Mofidfar, M., Diltemiz, S. E., Nasrollahi, F., Davoodi, E., et al. (2020). Micro and Nanoscale Technologies in Oral Drug Delivery. *Adv. Drug Deliv. Rev.* 157, 37–62. doi:10.1016/j.addr.2020.07.012

Alexander, S. A., and Donoff, R. B. (1980). The Glycosaminoglycans of Open Wounds. *J. Surg. Res.* 29, 422–429. doi:10.1016/0022-4804(80)90055-4

Amler, E., Filová, E., Buzgo, M., Prosecká, E., Rampichová, M., Nečas, A., et al. (2014). Functionalized Nanofibers as Drug-Delivery Systems for Osteochondral Regeneration. *Nanomedicine* 9, 1083–1094. doi:10.2217/nnm.14.57

Bertl, K., Bruckmann, C., Isberg, P.-E., Klinge, B., Gotfredsen, K., and Stavropoulos, A. (2015). Hyaluronan in Non-surgical and Surgical Periodontal Therapy: a Systematic Review. *J. Clin. Periodontol.* 42, 236–246. doi:10.1111/jcpe.12371

Beznoska, J., Uhlík, J., Kestlerová, A., Královič, M., Divín, R., Fedačko, J., et al. (2019). PVA and PCL Nanofibers Are Suitable for Tissue Covering and Regeneration. *Physiol. Res.* 68, S501–S508. doi:10.33549/physiolres.934389

Bhattarai, R., Bachu, R., Boddu, S., and Bhaduri, S. (2018). Biomedical Applications of Electrospun Nanofibers: Drug and Nanoparticle Delivery. *Pharmaceutics* 11, 5. doi:10.3390/pharmaceutics11010005

Bonilla-Represa, V., Abalos-Labruzzi, C., Herrera-Martinez, M., and Guerrero-Pérez, M. O. (2020). Nanomaterials in Dentistry: State of the Art and Future Challenges. *Nanomaterials* 10, 1770. doi:10.3390/nano10091770

Botelho, J., Cavacas, M. A., Machado, V., and Mendes, J. J. (2017). Dental Stem Cells: Recent Progresses in Tissue Engineering and Regenerative Medicine. *Ann. Med.* 49, 644–651. doi:10.1080/07853890.2017.1347705

Brew, K., Dinakarpandian, D., and Nagase, H. (2001). Tissue Inhibitors of Metalloproteinases: Evolution, Structure and Function. *Biochim. Biophys. Acta* 1477, 267–283. doi:10.1016/s0167-4838(99)0027910.1016/s0167-4838(99)00279-4

Burridge, K., and Guilluy, C. (2016). Focal Adhesions, Stress Fibers and Mechanical Tension. *Exp. Cel. Res.* 343, 14–20. doi:10.1016/j.yexcr.2015.10.029

Campo, G. M., Avenoso, A., D'Ascola, A., Prestipino, V., Scuruchi, M., Nastasi, G., et al. (2012). Inhibition of Hyaluronan Synthesis Reduced Inflammatory Response in Mouse Synovial Fibroblasts Subjected to Collagen-Induced Arthritis. *Arch. Biochem. Biophys.* 518, 42–52. doi:10.1016/j.abb.2011.12.005

Canciani, E., Dellavia, C., Ferreira, L. M., Giannasi, C., Carmagnola, D., Carrassi, A., et al. (2016). Human Adipose-Derived Stem Cells on Rapid Prototyped Three-Dimensional Hydroxyapatite/Beta-Tricalcium Phosphate Scaffold. *J. Craniofac. Surg.* 27, 727–732. doi:10.1097/SCS.0000000000002567

Canciani, E., Sirello, R., Pellegrini, G., Henin, D., Perrotta, M., Toma, M., et al. (2021). Effects of Vitamin and Amino Acid-Enriched Hyaluronic Acid Gel on the Healing of Oral Mucosa: *In Vivo* and *In Vitro* Study. *Medicina* 57, 285. doi:10.3390/medicina57030285

Carter, P., Rahman, S. M., and Bhattarai, N. (2016). Facile Fabrication of Aloe Vera Containing PCL Nanofibers for Barrier Membrane Application. *J. Biomater. Sci. Polym. Edition* 27, 692–708. doi:10.1080/09205063.2016.1152857

Chanda, A., Adhikari, J., Ghosh, A., Chowdhury, S. R., Thomas, S., Datta, P., et al. (2018). Electrospun Chitosan/polycaprolactone-Hyaluronic Acid Bilayered Scaffold for Potential Wound Healing Applications. *Int. J. Biol. Macromolecules* 116, 774–785. doi:10.1016/j.ijbiomac.2018.05.099

Chen, W. Y. J., and Abatangelo, G. (1999). Functions of Hyaluronan in Wound Repair. *Wound Repair Regen.* 7, 79–89. doi:10.1046/j.1524-475x.1999.00079.x

Chopin-Doroteo, M., Salgado-Curiel, R. M., Pérez-González, J., Marín-Santibáñez, B. M., and Krötzsch, E. (2018). Fibroblast Populated Collagen Lattices Exhibit Opposite Biophysical Conditions by Fibrin or Hyaluronic Acid Supplementation. *J. Mech. Behav. Biomed. Mater.* 82, 310–319. doi:10.1016/j.jmbbm.2018.03.042

Dellavia, C., Ricci, G., Pettinari, L., Allievi, C., Grizzi, F., and Gagliano, N. (2014). Human Palatal and Tuberosity Mucosa as Donor Sites for ridge Augmentation. *Int. J. Periodontics Restorative Dent.* 34, 179–186. doi:10.11607/prd.1929

Dupont, S., Morsut, L., Aragona, M., Enzo, E., Giulitti, S., Cordenonsi, M., et al. (2011). Role of YAP/TAZ in Mechanotransduction. *Nature* 474, 179–183. doi:10.1038/nature10137

Eliezer, M., Sculean, A., Miron, R. J., Nemcovsky, C., Weinberg, E., Weinreb, M., et al. (2019). Hyaluronic Acid Slows Down Collagen Membrane Degradation in Uncontrolled Diabetic Rats. *J. Periodont Res.* 54, 644–652. doi:10.1111/jre.12665

Francetti, L., Dellavia, C., Corbella, S., Cavalli, N., Moscheni, C., Canciani, E., et al. (2019). Morphological and Molecular Characterization of Human Gingival Tissue Overlying Multiple Oral Exostoses. *Case Rep. Dentistry* 2019, 1–10. doi:10.1155/2019/3231759

Fraser, J. R. E., Laurent, T. C., and Laurent, U. B. G. (1997). Hyaluronan: its Nature, Distribution, Functions and Turnover. *J. Intern. Med.* 242, 27–33. doi:10.1046/j.1365-2796.1997.00170.x

Gunn, J., and Zhang, M. (2010). Polyblend Nanofibers for Biomedical Applications: Perspectives and Challenges. *Trends Biotechnol.* 28, 189–197. doi:10.1016/j.tibtech.2009.12.006

Hägi, T. T., Laugisch, O., Ivanovic, A., and Sculean, A. (2014). Regenerative Periodontal Therapy. *Quintessence Int.* 45, 185–192. doi:10.3290/j.qi.a31203

Hatayama, T., Nakada, A., Nakamura, H., Mariko, W., Tsujimoto, G., and Nakamura, T. (2017). Regeneration of Gingival Tissue Using *In Situ* Tissue Engineering with Collagen Scaffold. *Oral Surg. Oral Med. Oral Pathol. Oral Radiol.* 124, 348–354. doi:10.1016/j.oooo.2017.05.471

Hobson, R. (2016). Vitamin E and Wound Healing: an Evidence-Based Review. *Int. Wound J.* 13, 331–335. doi:10.1111/iwj.12295

Jansen, K. A., Donato, D. M., Balcioglu, H. E., SchmidtDanen, T. E. H., Danen, E. H. J., and Koenderink, G. H. (2015). A Guide to Mechanobiology: where Biology and Physics Meet. *Biochim. Biophys. Acta (Bba) - Mol. Cel Res.* 1853, 3043–3052. doi:10.1016/j.bbamcr.2015.05.007

Kalantary, S., Golbabaei, F., Latifi, M., Shokrgozar, M. A., and Yaseri, M. (2020). Feasibility of Using Vitamin E-Loaded Poly(ε-caprolactone)/Gelatin Nanofibrous Mat to Prevent Oxidative Stress in Skin. *J. Nanosci. Nanotechnol.* 20, 3554–3562. doi:10.1166/jnn.2020.17486

Konieczka, P., Barszcz, M., Kowalczyk, P., Szlis, M., and Jankowski, J. (2019). The Potential of Acetylsalicylic Acid and Vitamin E in Modulating Inflammatory Cascades in Chickens under Lipopolysaccharide-Induced Inflammation. *Vet. Res.* 50, 65. doi:10.1186/s13567-019-0685-4

Litwiniuk, M., Krejner, A., Speyrer, M. S., Gauto, A. R., and Grzela, T. (2016). Hyaluronic Acid in Inflammation and Tissue Regeneration. *Wounds* 28, 78–88. doi:10.37473/dac/10.1101/2020.06.02.20120733

Mesa, F. L., Aneiros, J., Cabrera, A., Bravo, M., Caballero, T., Revelles, F., et al. (2002). Antiproliferative Effect of Topic Hyaluronic Acid Gel. Study in Gingival Biopsies of Patients with Periodontal Disease. *Histol. Histopathol.* 17, 747–753. doi:10.14670/HH-17.747

Mohandesnezhad, S., Pilehvar-Soltanahmadi, Y., Alizadeh, E., Goodarzi, A., Davaran, S., Khatamian, M., et al. (2020). *In Vitro* evaluation of Zeolite-nHA Blended PCL/PLA Nanofibers for Dental Tissue Engineering. *Mater. Chem. Phys.* 252, 123152. doi:10.1016/j.matchemphys.2020.123152

Murphy, G., Willenbrock, F., Crabbe, T., O'Shea, M., Ward, R., Atkinson, S., et al. (1994). Regulation of Matrix Metalloproteinase Activity. *Ann. NY Acad. Sci.* 732, 31–41. doi:10.1111/j.1749-6632.1994.tb24722.x

Pirnazar, P., Wolinsky, L., Nachnani, S., Haake, S., Pilloni, A., and Bernard, G. W. (1999). Bacteriostatic Effects of Hyaluronic Acid. *J. Periodontol.* 70, 370–374. doi:10.1902/jop.1999.70.4.370

Plencner, M., East, B., Litvinec, A., Buzgo, M., Tonar, Z., Otahal, M., et al. (2014). Abdominal Closure Reinforcement by Using Polypropylene Mesh Functionalized with Poly-□-Caprolactone Nanofibers and Growth Factors for Prevention of Incisional Hernia Formation. *Ijn* 9, 3263–3277. doi:10.2147/IJN.S63095

Price, R. D., Myers, S., Leigh, I. M., and Navsaria, H. A. (2005). The Role of Hyaluronic Acid in Wound Healing. *Am. J. Clin. Dermatol.* 6, 393–402. doi:10.2165/00128071-200506060-00006

Primpke, S., Wirth, M., Lorenz, C., and Gerdts, G. (2018). Reference Database Design for the Automated Analysis of Microplastic Samples Based on Fourier Transform Infrared (FTIR) Spectroscopy. *Anal. Bioanal. Chem.* 410, 5131–5141. doi:10.1007/s00216-018-1156-x

Rasperini, G., Pilipchuk, S. P., Flanagan, C. L., Park, C. H., Pagni, G., Hollister, S. J., et al. (2015). 3D-printed Bioresorbable Scaffold for Periodontal Repair. *J. Dent. Res.* 94, 153S–157S. doi:10.1177/0022034515588303

Rasperini, G., Tavelli, L., Barootchi, S., McGuire, M. K., Zucchelli, G., Pagni, G., et al. (2020). Interproximal Attachment Gain: The challenge of Periodontal Regeneration. *J. Periodontol.* 2020, 1–16. doi:10.1002/JPER.20-0587

Robert, L. (2015). Hyaluronan, a Truly "Youthful" Polysaccharide. Its Medical Applications. *Pathologie Biologie* 63, 32–34. doi:10.1016/j.patbio.2014.05.019

Sakai, T., and Gross, J. (1967). Some Properties of the Products of Reaction of Tadpole Collagenase with Collagen*. *Biochemistry* 6, 518–528. doi:10.1021/bi00854a021

Seo, S.-J., Kim, H.-W., and Lee, J.-H. (2016). Electrospun Nanofibers Applications in Dentistry. *J. Nanomater.*, 2016, 1, 7. doi:10.1155/2016/5931946

Silver, F. H., Christiansen, D., Snowhill, P. B., Chen, Y., and Landis, W. J. (2000). The Role of mineral in the Storage of Elastic Energy in turkey Tendons. *Biomacromolecules* 1, 180–185. doi:10.1021/bm9900139

Tammi, M. I., Day, A. J., and Turley, E. A. (2002). Hyaluronan and Homeostasis: a Balancing Act. *J. Biol. Chem.* 277, 4581–4584. doi:10.1074/jbc.R100037200

Thiele, J. J., Hsieh, S. N., and Ekanayake-Mudiyanselage, S. (2005). Vitamin E: Critical Review of its Current Use in Cosmetic and Clinical Dermatology. *Dermatol. Surg.* 31, 805–813. doi:10.1111/j.1524-4725.2005.31724

Totaro, A., Panciera, T., and Piccolo, S. (2018). YAP/TAZ Upstream Signals and Downstream Responses. *Nat. Cel Biol.* 20, 888–899. doi:10.1038/s41556-018-0142-z

Voigt, J., and Driver, V. R. (2012). Hyaluronic Acid Derivatives and Their Healing Effect on burns, Epithelial Surgical Wounds, and Chronic Wounds: A Systematic Review and Meta-Analysis of Randomized Controlled Trials. *Wound Repair Regen.* 20, 317–331. doi:10.1111/j.1524-475X.2012.00777.x

Walker, L., Overstreet, M., and Yeowell, H. (2005). Tissue-specific Expression and Regulation of the Alternatively-Spliced Forms of Lysyl Hydroxylase 2 (LH2) in Human Kidney Cells and Skin Fibroblasts. *Matrix Biol.* 23, 515–523. doi:10.1016/j.matbio.2004.11.002

Wang, J. H.-C., Guo, Q., and Li, B. (2012). Tendon Biomechanics and Mechanobiology-A Minireview of Basic Concepts and Recent Advancements. *J. Hand Ther.* 25, 133–141. doi:10.1016/j.jht.2011.07.004

Wang, M., Roy, A. K., and Webster, T. J. (2017). Development of Chitosan/Poly(Vinyl Alcohol) Electrospun Nanofibers for Infection Related Wound Healing. *Front. Physiol.* 7, 683. doi:10.3389/fphys.2016.00683

Woessner, J. F. (1991). Matrix Metalloproteinases and Their Inhibitors in Connective Tissue Remodeling. *FASEB j.* 5, 2145–2154. doi:10.1096/fasebj.5.8.1850705

Conflict of Interest: The authors declare that the research was conducted in the absence of any commercial or financial relationships that could be considered as a potential conflict of interest.

Advantages of publishing in Frontiers

OPEN ACCESS
Articles are free to read for greatest visibility and readership

FAST PUBLICATION
Around 90 days from submission to decision

HIGH QUALITY PEER-REVIEW
Rigorous, collaborative, and constructive peer-review

TRANSPARENT PEER-REVIEW
Editors and reviewers acknowledged by name on published articles

Frontiers
Avenue du Tribunal-Fédéral 34
1005 Lausanne | Switzerland

Visit us: www.frontiersin.org
Contact us: frontiersin.org/about/contact

REPRODUCIBILITY OF RESEARCH
Support open data and methods to enhance research reproducibility

DIGITAL PUBLISHING
Articles designed for optimal readership across devices

FOLLOW US
@frontiersin

IMPACT METRICS
Advanced article metrics track visibility across digital media

EXTENSIVE PROMOTION
Marketing and promotion of impactful research

LOOP RESEARCH NETWORK
Our network increases your article's readership